INFORMATION TO USERS

REHABILITATION OF NONDUCTILE REINFORCED

CONCRETE BUILDINGS USING STEEL SYSTEMS

By

Hamdy Mohamed Abou-Elfath

A Thesis

Submitted to the School of Graduate Studies

in Partial Fulfilment of the Requirements

for the degree

Doctor of Philosophy

McMaster University

REHABILITATION OF NONDUCTILE REINFORCED

CONCRETE BUILDINGS USING STEEL SYSTEMS

DOCTOR OF PHILOSOPHY (1998)   McMaster University
(Civil Engineering)   Hamilton, Ontario, Canada

TITLE: Rehabilitation of Nonductile Reinforced Concrete Buildings
                Using Steel Systems

AUTHOR: Hamdy Mohamed Abou-Elfath, B.Sc. (Alexandria University)
                                          M.Sc. (Alexandria University)

SUPERVISORS: Dr. A. Ghobarah and Dr. T.S. Aziz

NUMBER OF PAGES: xxii, 323

ABSTRACT

Many of the existing reinforced concrete (RC) structures performed poorly during recent earthquakes. Most of these structures were designed for gravity loads only with inadequate lateral load resistance. Several of the construction details in existing gravity load designed buildings do not conform to current code requirements for seismic design and may lead to nonductile inelastic behaviour.

The objective of this research program is to investigate the use of steel systems for the rehabilitation of existing nonductile RC buildings. The study is limited to low-and medium-rise frame buildings. A beam-column element capable of representing the behaviour of nonductile RC frame members is developed. The model is capable of representing the strength decay of nonductile RC members and the effects of the axial force on the yield moment and the deformation capacities of the member at peak strength. A procedure for evaluating the damage to nonductile RC structures following an earthquake is developed. The damage procedure depends on calculating the deterioration of the building stiffness and lateral load carrying capacity due to the application of the earthquake loading. The building stiffness and lateral load carrying capacity before and after the application of the earthquake loading were determined by conducting a pushover analysis.

Two nonductile RC buildings, three- and nine-stories, representing low-and medium-rise existing nonductile structures, were analyzed using various ground motion records. The seismic behaviour of the nonductile buildings when rehabilitated using various structural steel

systems was determined. The investigated steel systems include the addition of concentric X-bracing, eccentric bracing and attached steel frames. The effectiveness of the various steel systems in rehabilitating the three- and nine-story buildings were examined.

The effect of the distribution of the steel bracing along the height and along the bays of the RC frames on the seismic performance of the rehabilitated building was studied. A simplified approach was proposed for selecting the proper brace distribution. The seismic performance of the nonductile three-story building when using well designed eccentric bracing rehabilitation was compared with the performance of the building when using concentric bracing. The relationship between the deformation capacity of the rehabilitated building and the link deformation angle was evaluated. The distribution of the link strength along the building height was investigated. The seismic performance of the rehabilitated nine-story building was evaluated when using both flexible and stiff steel frames.

ACKNOWLEDGEMENT

To my parents

TABLE OF CONTENTS

LIST OF FIGURES

LIST OF TABLES

CHAPTER 1

INTRODUCTION

1.1 OVERVIEW

Existing Reinforced Concrete (RC) buildings include some newly designed and constructed structures according to modern seismic design provisions and many buildings constructed before the advent of earthquake regulations using gravity load design procedures. Several of the construction details in existing gravity load designed buildings do not conform to current code requirements for seismic design and detailing. Many of these buildings did not perform well during recent earthquakes due to the inadequate lateral load resistance and the nonductile inelastic behaviour. Severe damage to nonductile RC buildings was observed during earthquakes such as the 1985 Mexico City earthquake, the 1989 Loma-Prieta earthquake, the 1994 Northridge earthquake and the 1995 Hanshin-Awaji (Kobe) earthquake. It is now well recognized that existing nonductile RC buildings may pose serious risk to the society in seismic regions and that the issue of seismic rehabilitation should be addressed.

Different rehabilitation systems have been used to upgrade the seismic performance of existing RC structures. The two main approaches for structural rehabilitation of existing structures are to add new structural elements such as steel bracing and shear walls or to selectively strengthen the deficient structural elements of the building such as encasing the columns using steel or RC jackets and jacketing of the beam-column joints. Strengthening of the structural elements eliminates the brittle failure modes of these elements and therefore

1

enhances the overall ductility of the rehabilitated structure.

In the current study, rehabilitation of the nonductile RC buildings by adding new steel systems to the exterior frames is addressed. Steel systems were used in Mexico city, Japan and other places for rehabilitating of nonductile RC buildings (Canales and Briseno de la Vega, 1992; Mitchell and Dandurand, 1988; Kawamata and Masaki, 1980; Nateghi and Shahbazian, 1992). The steel systems that can be used to rehabilitate RC buildings include diagonal steel bracing inserted in the RC frame openings, attached steel frames or trusses and steel plate shear walls.

1.2 NONDUCTILE RC BUILDINGS

Several of the construction details in gravity load designed RC buildings may result in nonductile behaviour. Deficient reinforcement details that were in common use are shown in figure 1.1 (Ghobarah, 1998) and can be summarized as follows:

1   Column lap splices are located at potential plastic hinge regions with only 20 bar diameter lap length which may result in decreased strength and ductility as a result of bond failure. A common practice for rectangular column design involved the use of 9.5 mm grade 300 MPa ties spaced 304.8 mm (# 3 grade 40 ties @ 12") as the typical transverse reinforcement regardless of the column section dimensions. The transverse reinforcement provides inadequate confinement and clamping action to the lap splice to prevent splitting . The anchorage of the lapped bars may degrade rapidly due to the splitting action under reversing cyclic loads.

2   The bottom beam reinforcement has insufficient anchorage length embedded in the

beam-column joint. Typically at least 1/4 of the positive reinforcement is embedded 150 mm into the joint. Under the effect of gravity loads only, the beam ends will be subjected to negative moments (beam top reinforcement is in tension). Lateral seismic forces will cause positive beam end moments and may lead to pullout of the beam bottom reinforcement from the joint .

3   Beam-column joints may have been designed with little or no transverse reinforcement which may lead to inadequate joint shear capacity. Gravity loads in the RC frame buildings produce low levels of shear forces on the beam-column joints, however under the effect of seismic loading much higher shear demands are introduced into the joints which may cause joint failure.

In addition to the previously mentioned deficient reinforcement details, gravity load designed buildings may have columns with moment capacities insufficient to develop a desirable strong column-weak beam plastic mechanism. This will lead to the development of plastic hinges in the columns with the possibility of forming a soft story plastic mechanism.

1.3 REHABILITATION OF RC BUILDINGS USING STEEL SYSTEMS

The steel system rehabilitation technique was first used in Japan (Badoux, 1987). In some cases, the steel systems were used to upgrade the seismic capacity of existing structures, while in other cases they were part of the repair process of buildings damaged in an earthquake. The steel systems used in rehabilitating RC buildings include; a) steel bracing inserted in the frame openings as shown in figure 1.2 (Mitchell and Dandurand, 1988); b) steel trusses or frames attached to the building exterior as shown in figures 1.3 and 1.4; c) steel

plate shear walls (Yamamoto and Aoyama, 1987); and d) the addition of prestressed steel cables (Miranda, 1991).

In the current study, only the use of steel bracing inserted in the frame openings and steel frames attached to the building exterior frames for rehabilitating RC buildings is investigated. Examples of brace patterns which are used in rehabilitating RC buildings include X-bracing, V-bracing and inverted V-bracing. Architecturally, the steel bracing allows for the construction of door and window openings within the braced bays.

Steel trusses, braced steel frames and moment resisting steel frames have been used to strengthen RC buildings in Mexico city following the 1985 Mexico earthquake (Canales and Briseno de la Vega, 1992; Mitchell and Dandurand, 1988). The original RC frame and the attached steel system represent a dual system. The stiffness and strength characteristics of both the RC frame and the attached steel system play an important role in determining the overall performance of the rehabilitated frame.

The connections between the steel system and the RC frame are important since they are required to transfer the loads between the two lateral load resisting systems. Connections have been developed (figure 1.5) to join the steel elements to the existing RC frames (Kawamata and Masaki, 1980; Sugano, 1989; Canales and Briseno de la Vega, 1992). These connections may use adhesive anchors (bolts anchored in drilled holes in the concrete using adhesive resins) or mechanical anchors. Figure 1.6 shows the details of a connection between RC frame and steel bracing members inserted in the frame opening (Maheri and Sahebi, 1995). Figure 1.7 (Mitchell and Dandurand, 1987) shows the details of a connection between RC frame and an external truss system. In this connection, the diagonal steel members were

welded to a 12 mm thick steel plate. The steel plate was connected to the RC members using grouted anchors. Figure 1.8 shows the connection of a steel X-bracing system inserted in the openings of RC frame (Nateghi, 1994). In this connection, the bracing members are welded to a 10 mm gusset plate. The gusset plate is welded to 10 mm steel plates surrounding the RC column.

The connection details shown in figures 1.2 and 1.6 attempt to reduce the eccentricity effects. Tests conducted by Goel and Masri (1994) and Maheri and Sahebi (1995) indicated the possibility of transferring the brace loading to the corner of the RC frames without producing local damage in the concrete members.

Rehabilitation of RC buildings using steel systems offers some advantages which include the possibility of accommodating openings. The weight of the steel system is relatively small by comparison with the case of using RC shear walls. In case of an external steel system, most of the construction work can be performed on the exterior of the building and therefore disruption during construction is minimized. The main disadvantage of the steel system is its initial and continued maintenance cost. In some countries, steel is imported as compared with locally available concrete materials. Skilled labour is needed to connect the steel systems to the existing RC structure. Following the construction of the steel system, continuous maintenance is needed especially for the external members exposed to the weather.

1.4 EXPERIMENTAL RESEARCH

Much of the experimental research on seismic rehabilitation of RC frames using steel systems has been conducted in Japan. Most of these experimental studies have been carried out on a reduced scale, one bay, single story frames using various rehabilitation techniques. Sugano (1989) reported that in general, steel systems significantly improved the strength and the stiffness of the tested RC portal frames (figure 1.9). The diagonal X-bracing systems exhibits higher strength than other steel bracing configurations. Yamamoto and Umemura (1992) developed a steel rehabilitation system shown in figure 1.10 that consist of steel braces with peripheral steel frame. The steel braces are welded to the peripheral steel frame which is attached to the existing RC frame through mortar fill. Stud bolts are welded along the steel frame and adhesive anchors are installed along the existing RC frame before filling mortar. This steel system was capable of improving both the strength and the ductility of the existing RC frame. However, it should be noted that the construction is much more complicated than in the case of using diagonal steel braces connected only to the corners of the RC frame.

Jones (1985) conducted an experimental study in which a RC frame model was rehabilitated using a steel truss system and was subjected to cyclic lateral loading. The steel system was connected to the RC members using epoxy grouted dowels. The study showed that the lateral strength of the braced frame reached about six times the determined strength of the original RC frame. The diagonal steel members experienced buckling in compression and yielding in tension. However, a connection weld failed during the test.

Goel and Lee (1990) conducted a cyclic load test on a two-thirds scale model of RC frame rehabilitated using inverted V-bracing. Horizontal and vertical steel members

(collectors) were added along the RC beams and columns. The rehabilitated frame showed significant improvement in strength and stiffness.

Goel and Masri (1994) conducted an experimental study on seismic strengthening of a two-bay, two-story RC slab-column frames using steel bracing. Inverted V-bracing members were inserted into the RC frame openings. The bracing members were tube sections with clear width-thickness ratio of 14 and an effective slenderness ratio of 61. Vertical steel collectors were provided to the RC frame by means of four steel angles wrapped to each of the RC columns and tied together using batten plates. Because the model frame had no beams, the RC slabs were strengthened using horizontal steel collectors to provide beam action. The test result indicated that the rehabilitation technique provides a significant increase in stiffness and strength to the RC frame with stable hysteretic response. Buckling and yielding of the steel bracing members were observed during the test.

Maheri and Sahebi (1995) investigated the use of X-steel bracing in RC framed structures. Experimental investigation was conducted on a number of single-bay, one-story model frames. Each of the diagonal braces consisted of two equal angles. At the connection between the bracing member and the RC frame, the bracing member was welded to a gusset plate which itself was welded to steel angles pre-casted at the corner of the frame. No steel collectors were provided to the concrete members of the frame. The test results indicate a considerable increase in the in-plane strength of the frame due to steel bracing. Maheri and Sahebi concluded that with proper connection between the brace and the RC frame, the steel bracing could be a viable alternative or supplement to shear walls in concrete framed buildings in seismic areas.

Steel bracing incorporating energy dissipating devices was used for rehabilitating existing RC structures. This system have shown to be capable of providing structures with considerable added damping to reduce deformation due to earthquake loading (Su and Hanson, 1990).

Reported experimental research on the use of steel systems as a rehabilitation technique for RC frames has focused on using concentric steel bracing. Although concentric bracing provides the RC frame with the required strength and stiffness, it exhibits rapid stiffness and strength deteriorations due to repeated buckling of the brace members. In eccentrically braced frames, forces are transferred to the brace members through bending and shear forces developed in steel links. The applicability of using eccentric bracing, inserted in the RC frame openings, for rehabilitating nonductile RC buildings needs to be investigated.

1.5 ANALYTICAL RESEARCH

Badoux (1987) presented an analytical study on a simple structural subassemblage simulating an interior column of a laterally loaded braced frame. The subassemblage response was studied under the effect of a static cyclic loading. In this study, RC members were modeled using a simplified one component flexural model. The interaction between the axial force and bending moment was neglected. The study showed that the inelastic buckling of the braces detrimentally influences the cyclic behaviour of the braced frame.

Miranda (1991) conducted an analytical study on the seismic performance of a three-story RC building rehabilitated using pre-tensioned steel rods. The interaction between axial forces and moments of the frame columns was neglected. The study showed that the pre-

tensioned steel rods provided the building with adequate strength and stiffness that kept the building in the elastic range when subjected to seismic loads.

Pincheira and Jirsa (1995) studied the seismic performance of nonductile RC frames. The frames were rehabilitated using pre-tensioned steel rods and X-steel bracing. The study showed that the steel brace significantly improved the seismic performance of the RC frames. The RC frame members were modeled using a one component model with two nonlinear springs attached at the element ends. The nonductile behaviour resulting from reinforcement pull out was taken into consideration by producing a negative slope in the constitutive moment-rotation relationships of the nonlinear springs. The study neglected the interaction between the moments and the axial forces and the P-Δ effect. Pincheira and Jirsa (1995) concluded that steel bracing significantly enhanced the seismic performance of the rehabilitated buildings.

Bouadi et al.(1994) studied the seismic behaviour of RC buildings with short columns and deep beams rehabilitated using eccentrically braced steel frames. The rehabilitation steel system was attached to the building exterior. The results indicated that the steel system resulted in reduced deformation and increased stiffness and strength. The study did not address the comparative behaviour of the eccentrically and concentrically braced steel frames rehabilitation systems.

1.6 MOTIVATION

The number of reported analytical studies to investigate the seismic performance of nonductile RC frames rehabilitated using steel systems is small. The applicability of using

eccentric bracing inserted in the frame openings as a rehabilitation scheme for nonductile RC buildings needs to be investigated. The models used for representing the behaviour of RC members may not reflect the actual nonductile behaviour observed in existing structures. In addition, the used models were not verified experimentally. Important factors that are known to influence the behaviour were neglected in the analysis such as the P-Δ effect and the interaction of the axial force with both moment and deformation capacities of the RC members. Seismic damage evaluation of the rehabilitated RC buildings in terms of damage indices needs to be addressed as it provides means by which different rehabilitation options may be compared.

Experimental studies on nonductile RC members with deficient details have been conducted by Pessiki et al. (1990), Aycardi et al. (1992), Lynn et al. (1994), Aboutaha and Jirsa (1996) and Ghobarah et al. (1997). The results of these studies demonstrated the need for new modelling approaches that are capable of representing the strength, ultimate deformation capacities, and the softening behaviour of nonductile RC members.

1.7 OBJECTIVE

The objective of this research program is to develop the tools for the analysis of the seismic performance of existing nonductile RC buildings rehabilitated using steel systems. The study is limited to low-and medium-rise frame buildings. The behaviour of different structures strengthened using various rehabilitation schemes is evaluated. The rehabilitation schemes considered are limited to concentric X-steel bracing, eccentric steel bracing and attached steel frames.

1.8 SCOPE

To achieve the study objective, development is needed in modelling the nonductile behaviour of existing RC buildings and evaluating the seismic damage in terms of damage indices. The seismic behaviour of the nonductile buildings rehabilitated using various steel systems was determined. The research program included the following six phases.

1   A beam-column element capable of representing the behaviour characteristics of nonductile RC frame members is developed. The model is capable of representing the strength softening of nonductile RC members and the effects of the axial force on the yield moment and the deformation capacities of the member at peak strength.

2   A procedure for evaluating the seismic damage of nonductile RC structures is developed.

3   Examples of the analysis applicability to two RC buildings, three and nine-stories, representing existing low-and medium-rise nonductile structures, are carried out. The seismic response of the buildings is evaluated in terms of deformations and damage indices using ground motion records which cover a wide range of duration and frequency contents. A simplified approach for evaluating the seismic performance of nonductile RC frame structures is proposed.

4   The seismic performance of the nonductile three-story RC building is evaluated when rehabilitated using concentric X-bracing. The effect of the brace distribution along the height and along the frame bays including the P-Δ effect is investigated.

5   The use of eccentric bracing as a rehabilitation scheme for the nonductile three- story RC building is evaluated.

6   The developed analytical models are applied to the case of a nonductile nine-story RC

building rehabilitated using steel systems.

1.9 THESIS ORGANIZATION

The reminder of the thesis is organized in seven chapters. Chapter 2 includes the development of the analytical model for predicting the seismic performance of nonductile buildings. A proposed damage evaluation approach is presented in Chapter 3. Chapter 4 deals with the seismic performance evaluation of the three and nine story nonductile buildings. A simplified seismic performance evaluation approach was also presented in Chapter 4. The seismic performance of the three-story building when rehabilitated using concentric X-bracing is introduced in Chapter 5. Chapter 6 contains an evaluation of the seismic performance of the three-story building when rehabilitated using eccentric bracing inserted in the frame openings. The seismic performance of the nonductile nine-story building when rehabilitated using steel bracing and attached steel frames is investigated in Chapter 7. Chapter 8 summarizes the findings, conclusions and recommendations of the research.
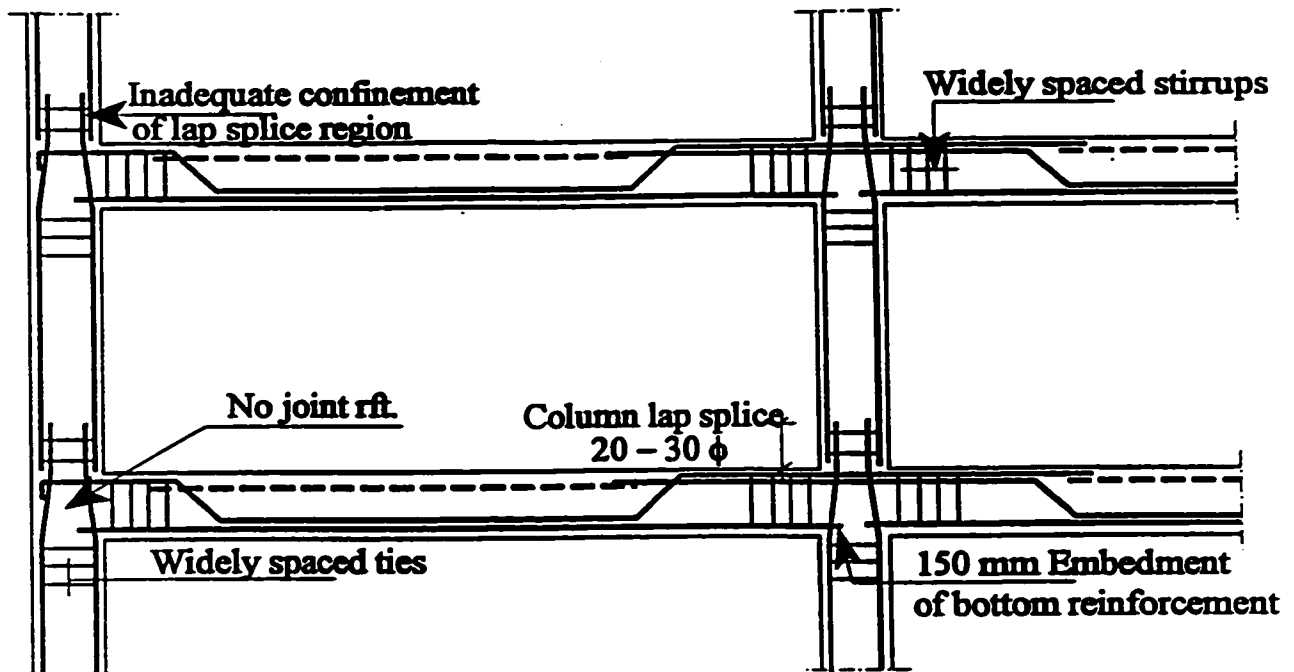
Figure 1.1 Nonductile reinforcement details in gravity load designed buildings
(Ghobarah, 1998)
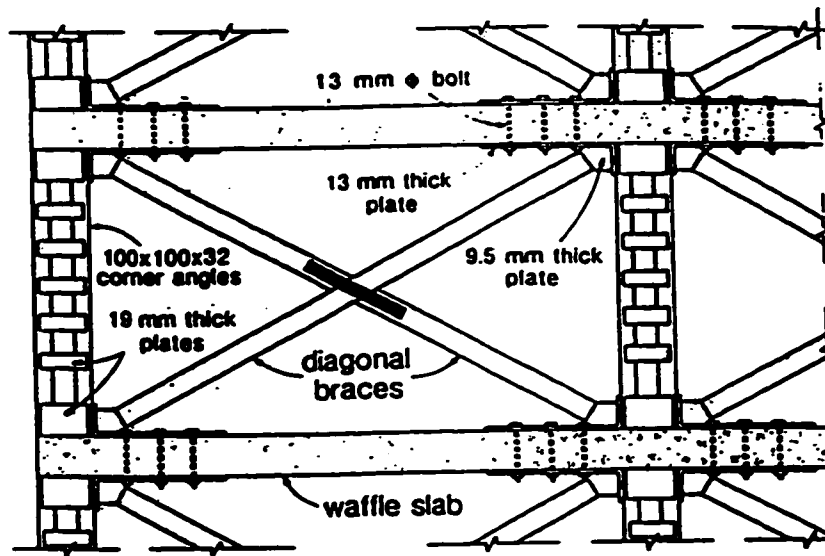
Figure 1.2 Steel bracing inserted in the RC frame openings
(Mitchell and Dandurand, 1988)
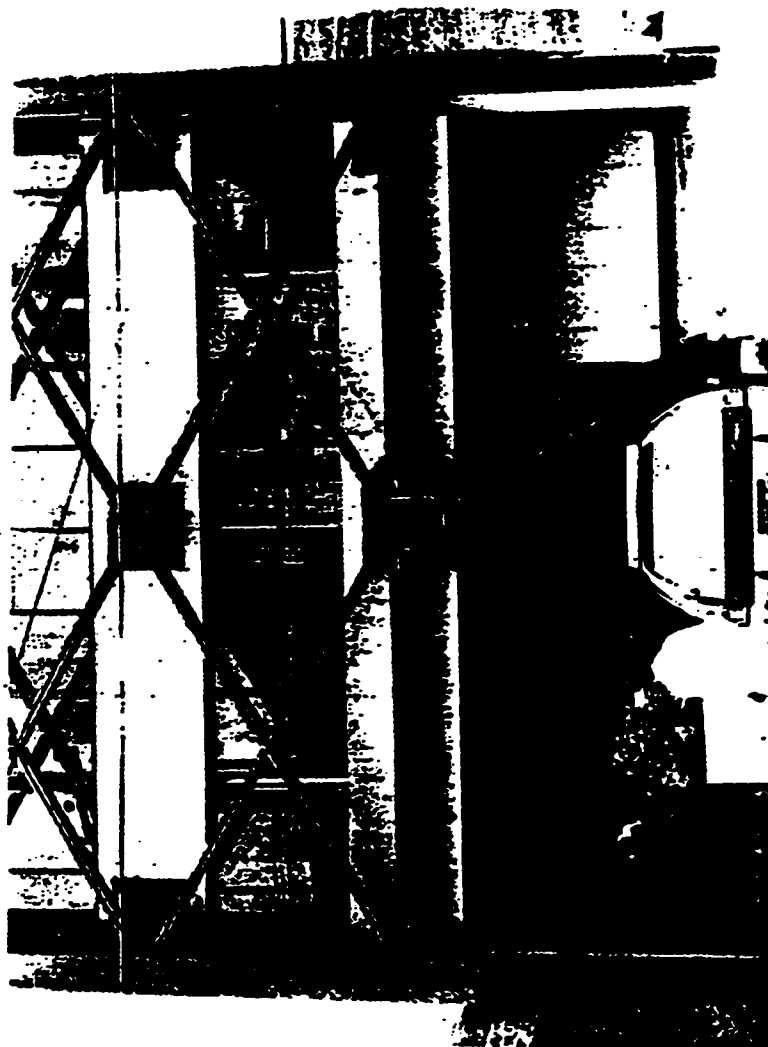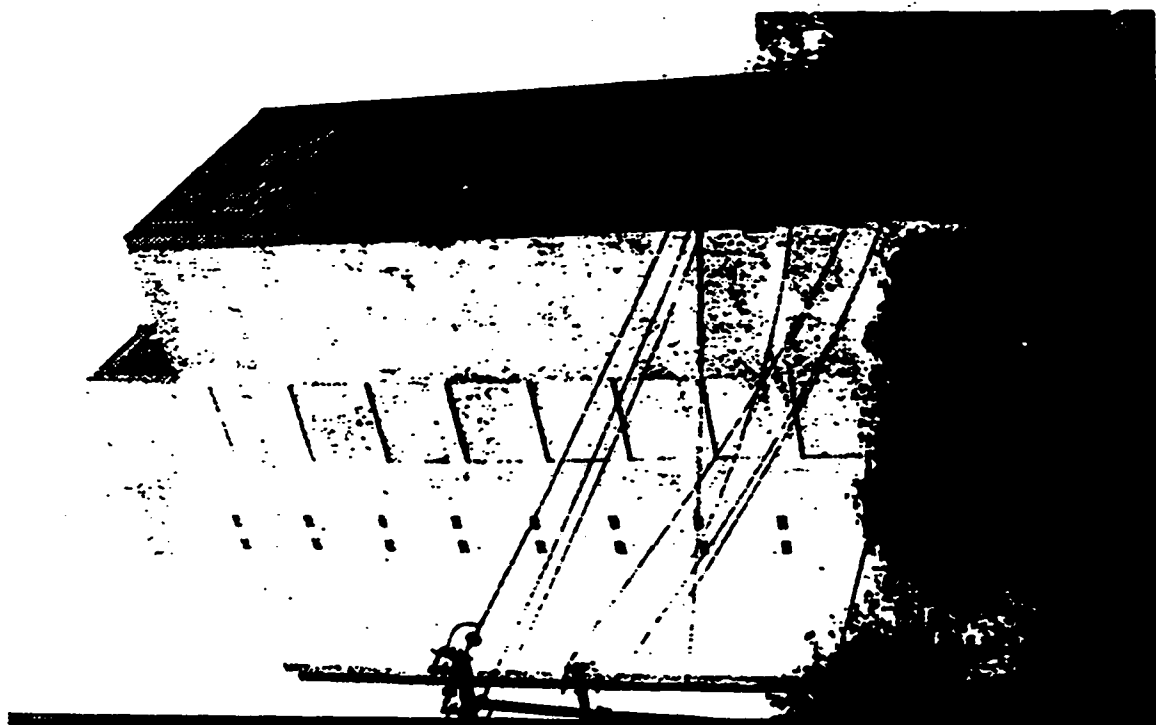
Figure 1.3 Durango 49, Mexico City; steel bracing retrofitting (Badoux, 1987)

14
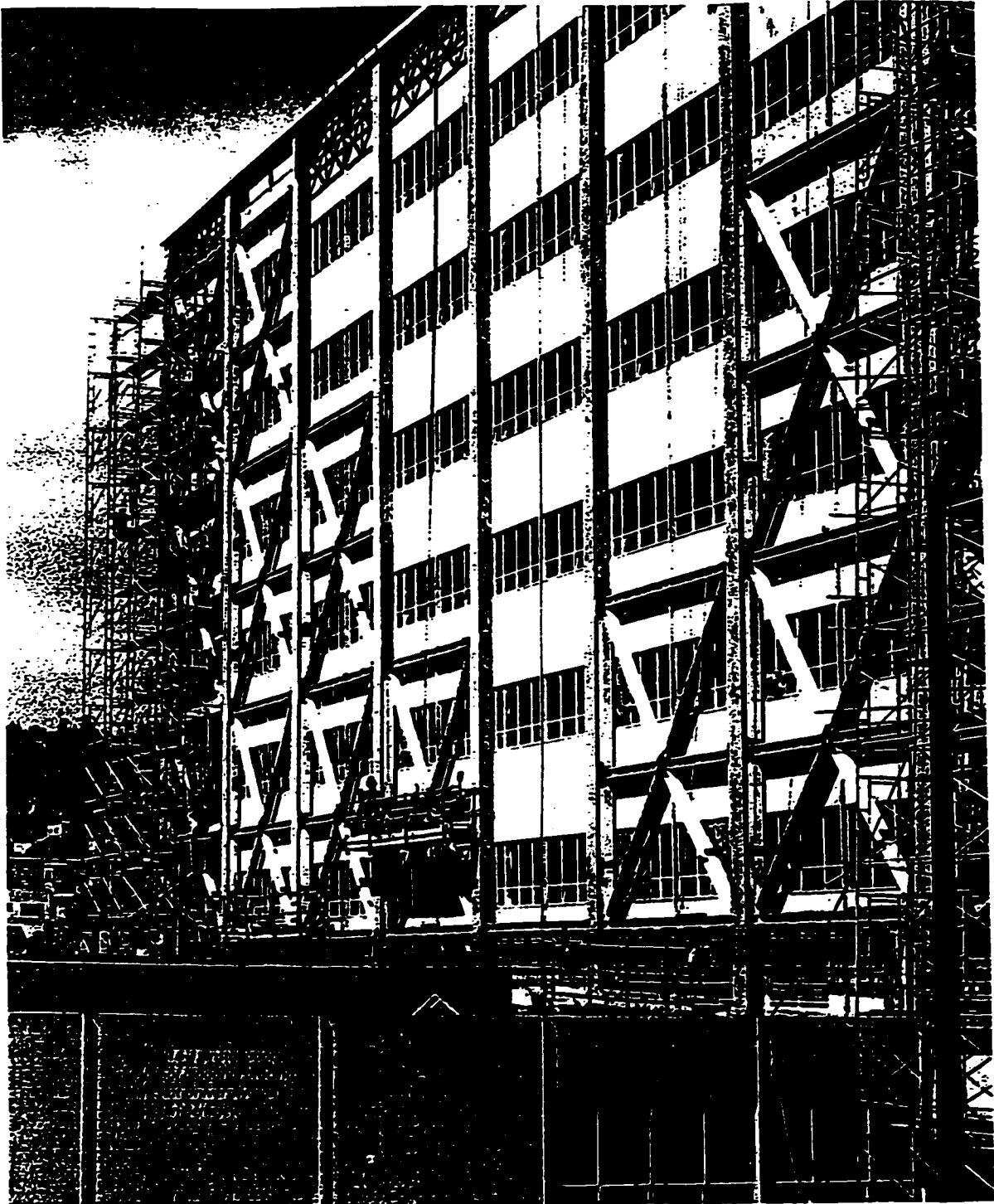
Figure 1.4 Retrofitting of university hall in Berkeley, California using steel system
(EERI, HF-96, 1996)
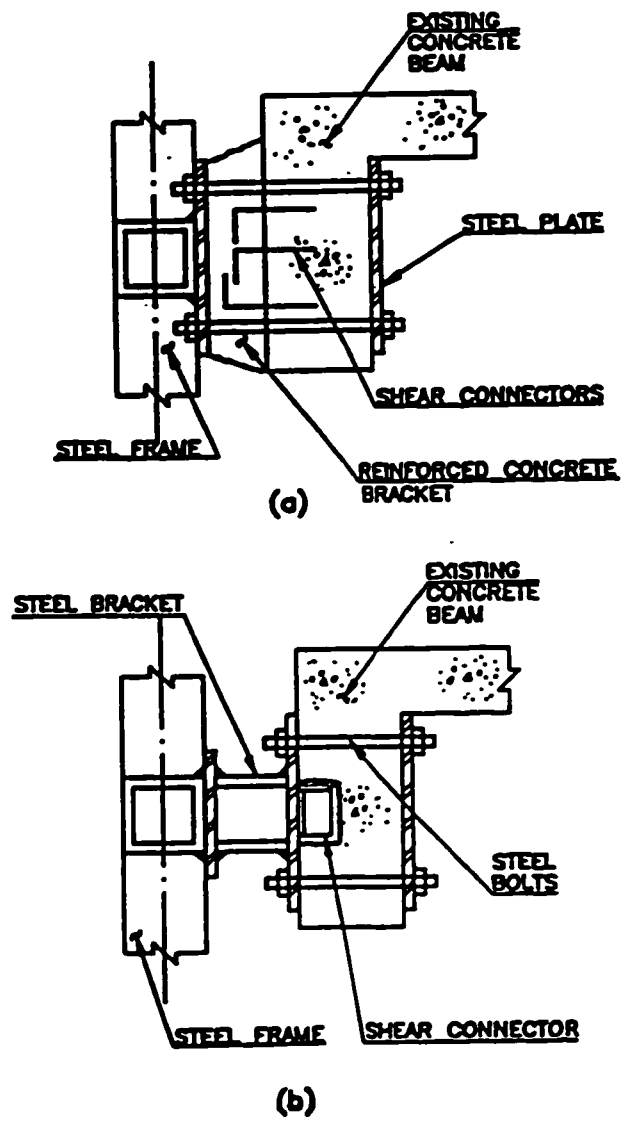
Figure 1.5 Details of a connection between RC frame and a steel frame
(Canales and Briseno de la Vega, 1992)
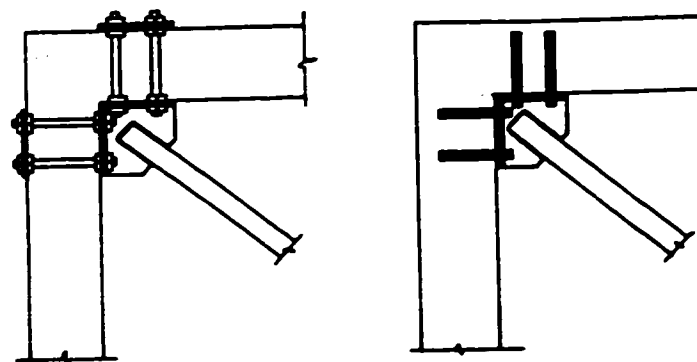
(a) The anchors are fixed
in the RC member by
bearing on a steel plate

(b) The anchors are fixed in the
RC member by means of wedging
action or adhesive resins

Figure 1.6 Details of a connection between a reinforced concrete frame and steel bracing
members (Maheri and Sahebi, 1995)
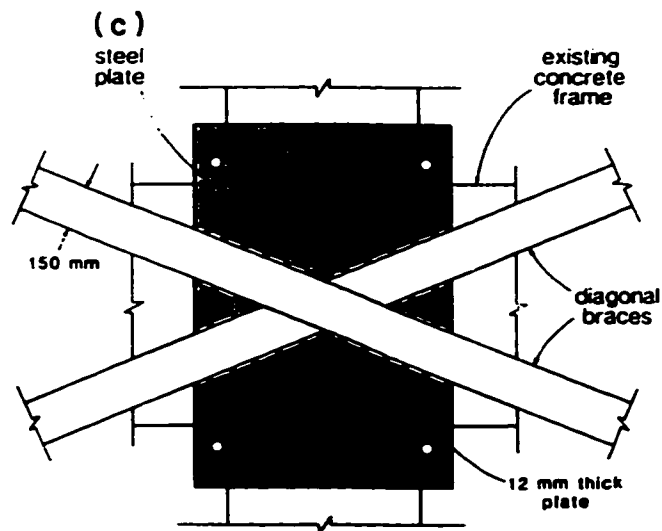
Figure 1.7 Details of a connection between RC frame and an external truss system.
(Mitchell and Dandurand, 1987)
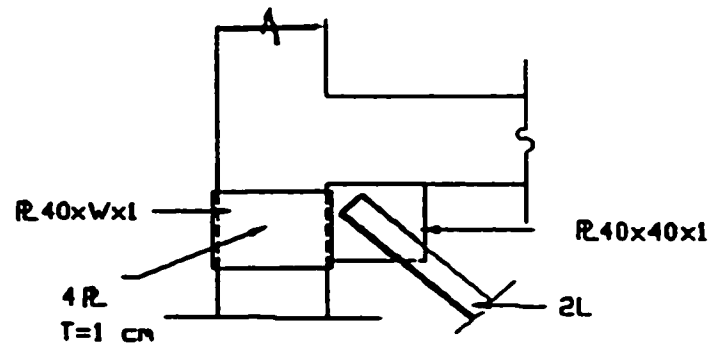
Figure 1.8 Connection details of steel X-bracing system inserted in the openings of RC frame (Nateghi, 1994)
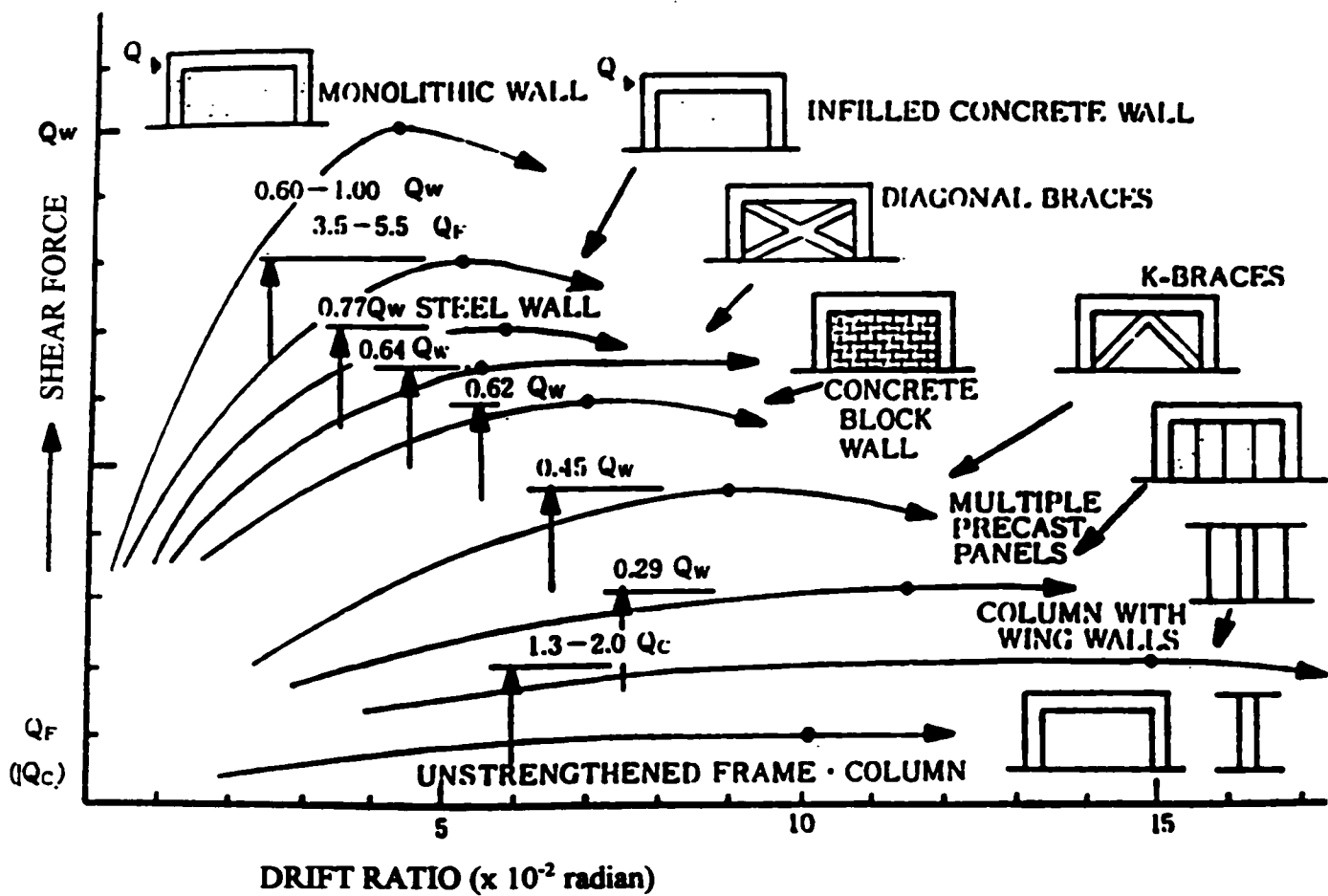
Figure 1.9 Experimental results on the seismic retrofitting of RC frames (Sugano, 1989)
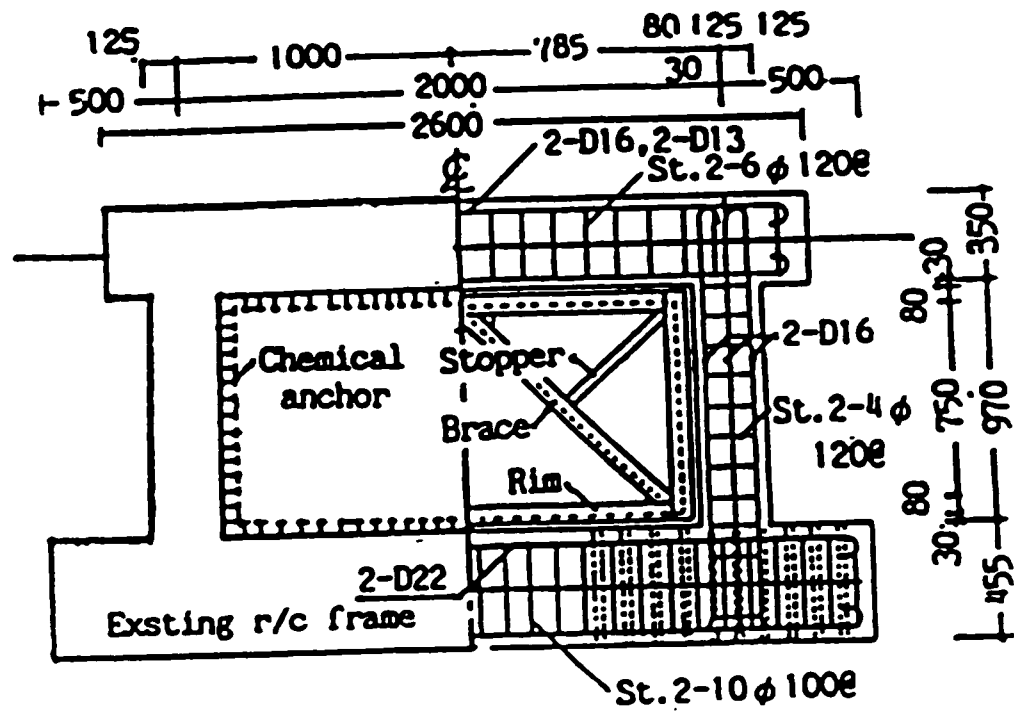
Outline of specimen [V-1]

Figure 1.10 Retrofitting details of a single-story, one bay RC frame
(Yamamoto and Umemura, 1992)

CHAPTER 2

MODELLING OF NONDUCTILE REINFORCED CONCRETE FRAMES

2.1 INTRODUCTION

To rehabilitate nonductile reinforced concrete (RC) frame buildings, it is necessary to establish the behaviour of these structures under seismic loading. Such behaviour is complex because of the different possible modes of failure due to the various design and reinforcement detailing deficiencies in the frame members. Modelling of the RC members in nonductile frames should consider the effects of deficient reinforcement details on the behaviour of these members. The main aspects to consider in component modelling are:

- Anchorage failure of the column lap-splice or beam bottom reinforcement may decrease the moment capacities of these regions below the reinforcement yield levels. The early anchorage failure will reduce the shear demand and the possibility of shear failure of the joint. For simplicity the joint shear model is not included in this study. Detailed discussion of joint behaviour is presented in section 2.6.

- The deformation capacities of the frame members at peak resistance are dependent on the mode of failure of the frame members. Deformation capacities of members can be estimated based on experimental data.

- Strength softening or strength decay (Otani, 1980) is used to define the reduction in the component strength capacity under cyclic loading after reaching the ultimate strength limit. It results from typical deterioration modes such as pullout of steel

reinforcement or concrete splitting, buckling of steel in compression and shear failure in the plastic hinge regions. These deterioration modes often happen as a result of lack of confinement by lateral reinforcement or due to insufficient development length of steel reinforcement. Modelling of softening behaviour of nonductile members is needed in order to take into account the effect of the post peak strength behaviour of one or more members on the behaviour of the frame as a whole. It is also important in the assessment of the vulnerability of the frame to collapse by predicting its performance to failure.

Phenomenological global models offer an attractive alternative to micro modelling both in the ease of computation and in the flexibility of modelling. It is possible to calibrate the model to represent a behaviour pattern established by test data. The ability of a global model to capture the overall behaviour pattern makes it suitable for modelling of reinforced concrete structures. Takeda et al.(1970), Roufaiel and Meyer (1987) and Park et al. (1987) developed phenomenological global models of RC members that are suitable for members designed according to current seismic codes and are expected to exhibit ductile behaviour. However, softening of nonductile members after reaching a specified ultimate capacity with an associated level of deformation can not be represented by these models. This is because these models do not distinguish between the behaviour of the RC members in the pre-peak and post-peak strength ranges of deformation. In addition, the calculations of the moment and the deformation capacities of the members using these models are based on flexural behaviour which may not be the case in nonductile members. Miramontes et al. (1996)

developed a phenomenological beam model that produce a quick deterioration in behaviour after reaching an ultimate point to allow for the member to lose its strength. For nonductile components the degree of softening may not be rapid and will differ depending on the mode of failure. For this reason, there is a need for simple and reliable strength softening model that is capable of predicting different modes of failure of nonductile members.

In this chapter, a beam-column element capable of representing the behaviour of nonductile members is developed. The element models the strength softening (decay) behaviour of these members past the ultimate capacity and up to the collapse of the structure.

2.2 THE BEAM-COLUMN ELEMENT

In the development of the beam-column element and in modelling of the concrete building, the reinforced concrete floors are assumed as rigid diaphragms in their own plane with out-of-plane flexibility. Accordingly, the building is considered as a series of planar frames connected at each floor level by the rigid diaphragms. The response of the planar frames is evaluated using two-dimensional analysis. The frame members are assumed to have sufficient shear capacity such that shear failure of the frame members before reaching flexural yielding is excluded. For a wide range of existing structures, column shear strength capacity is found to be adequate for the earthquake demands (Pessiki et al., 1990; Bracci et al., 1992 and Aycardi et al., 1992).

For well designed ductile RC members subjected to seismic loads, softening occurs at a late stage of the loading routine with rapid rate as a result of the previously accumulated damage. On the other hand, in nonductile members, softening occurs early and affects most

of the member response history due to a deterioration mode. There are several hysteretic global models of RC frame members which provide both stiffness and strength deteriorations. These models provide for the drop in strength (strength deterioration) when cycling to the same displacement level. However, at higher deformation levels, the original inelastic moment-curvature envelope will be eventually resumed without a defined ultimate strength limit.

An inelastic single component element was developed to model beams and columns of RC frames. The essential characteristics of the hysteretic behaviour of nonductile RC members including stiffness degradation, pinching and softening, are explicitly taken into account. The element is implemented in the general-purpose program DRAIN-2DX (Prakash and Powell, 1993). In the hysteretic moment-curvature relationship of the element, the ultimate moment and the corresponding curvature are specified and the softening behaviour of the member in the post-peak strength range is represented using a strength softening parameter. It is assumed that the specified curvature at peak moment is independent of the cyclic history experienced in the pre-ultimate strength zone. This assumption is especially realistic for nonductile members, where the deformation at peak strength is relatively small and the hardening branch occupies a small portion of the member response. It is expected that the effect of cyclic damage in the pre-ultimate strength zone on the deformation at peak strength will be small and can be neglected. The following subsections contain detailed description of both the hysteretic and the flexibility models used in the element.

2.2.1 Hysteretic Modelling of the Moment-Curvature Relationship

A phenomenological hysteretic model was developed in which a non-symmetric bilinear curve is utilized in conjunction with four control parameters to produce the effects of stiffness degradation, pinching, strength deterioration and softening after reaching an ultimate strength point. The consideration of a bilinear envelope (based on neglecting the concrete tensile strength) instead of a trilinear one (based on concrete cracking and steel yielding) is realistic in the case of existing nonductile RC buildings. The reason is that over the years these buildings may have been subjected to high dead loads, live loads, wind loads, and possibly to minor earthquakes. The initial flexural stiffness of a cross section in this type of buildings is expected to be closer to the damaged or cracked stiffness based on neglecting the concrete tensile strength. For RC sections subjected to early bond failure before the steel reaches its yield stress, the elastic stiffness is reduced using a reduction factor suggested by Kang-Ning Li (1992) to account for the bond slip deformation.

The proposed hysteretic rules for the moment-curvature relationship at the ends of an RC member are shown in figure 2.1. The stiffness degradation is introduced by setting a common point on the initial envelope curve, and assuming that the unloading lines aim at this point until they reach the horizontal axis as shown in figure 2.1a. The parameter "γ" that specifies the degree of stiffness degradation is the same as the stiffness degradation parameter proposed by Park et al. (1987). A typical value of γ ranges from 1.0 to 10.0, where a value of 1.0 gives high stiffness degradation and a value of 10.0 gives negligible stiffness degradation.

The pinching effect is introduced in the loops as shown in figure 2.1b by the control

parameter α proposed by Chung et al. (1987). The reloading branch is subdivided into two segments. The first segment aims at the crack closing point (ϕ_x, M_x) and the second segment starts from (ϕ_x, M_x) and aims at (ϕ_a, M_a). The parameter α governs the position of the crack closing point. The value of α may vary between 0.0 which leads to high pinching and 1.0 which signifies no pinching effect.

The strength deterioration is introduced in the loops by specifying the point at which the reloading branch is aiming. This point is different from the point at which unloading started in the previous cycle. A control parameter β governs the strength deterioration (Park et al., 1987). Figure 2.1c and the following equation describe the procedure:

$$\phi_a^* = \phi_a + \beta \frac{\Delta E}{M_y}$$ (2.1)

where ΔE is the incremental dissipated energy and ϕ_a^* is the curvature of the new targeted point. Introducing this parameter results in a reduced strength at the maximum attained deformation level ϕ_a. However, with increasing the deformation beyond ϕ_a, the strength increases until reaching the original moment-curvature envelope at point (ϕ_a^*, M_a^*). A typical value of β ranges between 0.0 and 0.2, where a value of 0.0 signifies no strength deterioration.

It is proposed to include the softening behaviour in the post-peak strength range as in the model illustrated by figure 2.1d by using an additional softening parameter η such that:

$$M_s = M_u (1 - \eta \lambda)$$ (2.2)

where M_u is the ultimate moment, M_s is the reduced moment capacity, while λ is a ductility

factor defined as:

$$\lambda = \frac{\phi_a - \phi_u}{\phi_y} \qquad (2.3)$$

where ϕ_u is the curvature at maximum moment, ϕ_a is the maximum curvature reached ($|\phi_a|$ > $|\phi_u|$) and ϕ_y is the curvature at yield. The value of η ranges from 0.0 to 0.5, where a value of 0.5 signifies rapid strength softening after the ultimate point, and 0.0 signifies no softening. A residual moment M_r can also be specified if desired. This means that the bending moment capacity will not be less than M_r. The strength softening hysteretic relationship shown in figure 2.1d is introduced in the DRAIN-2DX program in the form of a series of horizontal M_u branches and vertical ($\eta \lambda M_u$) drops which eliminates the problem of negative stiffness.

During earthquakes, reinforced concrete members are expected to experience substantial variations in axial forces. A tensile axial force tends to reduce the member flexural capacity. On the other hand, a compressive force up to balanced condition tends to increase the flexural capacity of the reinforced concrete member. Continuous variation in the level of the axial force in a member will affect its yield level due to the interaction between the applied moment and the axial force. An idealized axial force-moment interaction diagram is used in the development of the element in order to update the yield moments until yielding is reached in both directions of the hysteretic curve. The interaction diagram is similar to the one used for the RC beam-column model of the DRAIN-2DX program (Prakash and Powell, 1993). The effect of the axial load on ductility is taken into account. Figure 2.2 shows the interaction between the axial force and the curvature corresponding to a specified maximum concrete strain for a typical reinforced concrete section. The analysis of the cross section was

performed using a fibre approach, in which the concrete area is divided into a small number of fibres and the steel areas are identified separately. Material laws were used to describe the concrete and steel stress-strain relationships. The figure shows that the ductility of the RC member decreases when it is subjected to an increasing compressive axial force. In the current study, the effect of the axial force on the deformation capacity of the RC member at peak strength is taken into account using an interaction diagram between the instantaneous axial force (gravity loads plus dynamic effects) and the curvature at peak strength. Linear variation between the curvature at peak strength and axial load has been assumed as shown in figure 2.2. The curvature at peak strength at the axial load of the balanced section is considered equal to the curvature at yield. The curvatures at peak strength corresponding to zero axial load and half of the axial load of the balanced cross section are specified in the input data.

2.2.2 Flexibility Model

The inelastic deformation of reinforced concrete frame members subjected to lateral loads is considered to be concentrated at the member ends. Different approaches can be used to generate the total stiffness matrix of the frame member from the known stiffness at the member ends. A concentrated plastic hinge approach was adopted in the current study. In this approach, the RC members are modelled using two inelastic rotational springs attached to the ends of a linear elastic element. The properties of the rotational springs can be calculated from the previously defined moment-curvature relationships at the member end sections. The basic assumption in this approach is that the RC member is bent in double curvature with the contraflexure point at the middle of the member. The initial elastic stiffness

of the rotational spring is assumed to be a large number since the elastic deformation of the member is accounted for in the linear elastic element. The inelastic stiffness of the rotational spring can be calculated by equating the deflection at the contraflexure points of the actual and the idealized members. The deflection of the actual member at the contraflexure point can be calculated by integrating the curvature twice along the member length as:

$$\delta^a = \frac{M_y L^2}{2 \, EI} [1 - \frac{M_y^2}{3 \, M^2}] + \frac{M_y L^2}{2 \, EIP} [\frac{2 \, M}{3 \, M_y} + \frac{M_y^2}{3 \, M^2} - 1] \qquad (2.4)$$

where δ^a is the deflection at the contraflexure point of the actual member, M is the maximum moment at the end of the member ($|M| > |M_y|$), EI and EIP are the elastic and inelastic slopes of the (M-ϕ) diagram and L is the member length. The deflection at the contraflexure point of the idealized member (δ^i) can be calculated as:

$$\delta^i = \frac{M L^2}{3 \, EI} + \frac{(M - M_y) L}{S_p} \qquad (2.5)$$

The inelastic stiffness of the rotational spring (S_p) can be calculated from equations 2.4 and 2.5 as follows:

$$S_p = \frac{\rho - 1}{L \, [\frac{1}{EIP} - \frac{1}{EI}] \, [\frac{\rho}{3} + \frac{1}{6 \, \rho^2} - 0.5]} \quad , \qquad \rho = \frac{M}{M_y} \qquad (2.6)$$

The parameter ρ is calculated by considering $M=M_u$. The hysteretic rules which govern the moment-rotation curve are the same as those applied to the moment-curvature relationship.

The curvature at maximum moment ϕ_u is transformed into rotation at maximum moment (θ_u) using the following formula:

$$\theta_u = \frac{(\phi_u - \phi_y) \, EIP}{S_p} \tag{2.7}$$

Substituting S_p from equation 2.6 into equation 2.7, then:

$$\theta_u = \frac{M_y \, L}{6} \, [\frac{1}{EIP} - \frac{1}{EI}] \, [2 \, (\chi - 1) \, (\frac{EIP}{EI}) + \frac{1}{(1 + \frac{EIP}{EI}(\chi - 1))^2} - 1],$$

$$\chi = \frac{\phi_u}{\phi_y} \tag{2.8}$$

The beam-column element has six global degrees of freedom which can be transformed into four local flexural degrees of freedom. It also has two additional rotational degrees of freedom of the two springs, but these additional rotations are condensed out at the element level, and do not appear as structure degrees of freedom. The member flexural flexibility matrix in local coordinate can be written as:

$$F = \begin{bmatrix} f_{11} + \dfrac{1}{S_1} & f_{12} \\ f_{21} & f_{22} + \dfrac{1}{S_2} \end{bmatrix} \tag{2.9}$$

where, S_1 and S_2 are the stiffness of the rotational springs and f_{11}, f_{22}, f_{12}, f_{21} are the flexibility coefficients of the linear elastic element. The flexibility matrix can be inverted to form the member stiffness matrix in local coordinates.

2.3 COLUMN END WITH A LAP SPLICE

The behaviour of the column ends with lap splices can be classified into two categories. In the first category, the anchorage capacity between the steel bars and the concrete is not sufficient to develop bar yielding while in the second category the anchorage capacity is sufficient to develop bar yielding. The determination of the moment and deformation capacities as well as the model parameters in the two cases will be discussed separately.

2.3.1 Anchorage failure before bar yielding

In this case, an early splitting bond failure between steel bars and concrete is expected to develop before the steel reaches its yield stress. The tensile splitting cracks develop parallel to the axis of the bars due to the radial component of the lug-bearing forces causing premature splitting bond failure. The moment capacity of the section can be calculated using the steel stress at the onset of the anchorage failure. The deformation capacity at peak strength can be estimated to correspond to the curvature of the cross section at the onset of the anchorage failure. This means that no plastic slip is assumed to develop after the onset of the splitting cracks. The equation proposed by Priestley and Seible (1991) can be used to determine the maximum stress that may develop in the steel bar prior to anchorage failure:

$$ f_s = \frac{2 f_t \, l_s \, (s + 4 d_b + 4c)}{\pi \, d_b^2} \quad , \quad f_t = 0.332 \sqrt{f_c'} \tag{2.10} $$

where f_t is the tensile strength of concrete in MPa, s is the bar spacing, d_b is the bar diameter,

l_s is the lap splice length, c is the cover depth and f_c' is the concrete compressive strength in MPa.

The proposed model parameters applicable to this case are shown in table 2.1. The model prediction is compared with the experimental results of a column specimen FC1 (Aboutaha and Jirsa, 1996), as shown in figure 2.3. The dimensions, reinforcement details and material strengths of this column are listed in table 2.2.

2.3.2 Bar yielding before anchorage failure

When the anchorage capacity is sufficient to develop bar yielding, the deformation capacity at peak strength of the column ends with lap splices will be limited by the strain at which the concrete cover begins to spall. This is true if the splice region has insufficient transverse reinforcement to provide clamping action to the lap splice to prevent splitting which is the case in gravity load designed RC buildings. A common past practice for rectangular column design involved the use of grade 40 (300 MPa), 9.5 mm (#3) ties at 304.8 mm (12") spacing as typical transverse reinforcement. These ties are often anchored by 90° hooks. As a result, the transverse reinforcement provides inadequate confinement to the lap splice to prevent splitting. The anchorage of the lapped bars will degrade once the concrete cover is damaged under seismic load. The capacity of the concrete cover can be measured in terms of the concrete strain at the extreme compression fibre of the member ends. The maximum strain of the unconfined concrete is in the range of 0.003 to 0.008 depending on the properties of the concrete. In the current study, a maximum concrete strain of 0.0035 is adopted as a limit to the deformation capacity at peak strength of the spliced ends. The

model parameters proposed in this case are shown in table 2.1. The analytical behaviour was compared with the results of experimental studies conducted by Ghobarah et al., (1997), Aycardi et al. (1992) and Lynn et al. (1994), as shown in figures 2.4 to 2.6. The dimensions, reinforcement details and material strengths of these columns are listed in table 2.2.

2.4 COLUMN END WITH CONTINUOUS STEEL

The behaviour of the column end with continuous reinforcement is expected to be more ductile than the behaviour of column end with a lap splice. However, the deformation capacity at peak strength and the rate of strength softening at these ends will depend on the mode of failure. Possible failure modes are shear failure in the plastic hinge region due to concrete damage or buckling of the longitudinal reinforcement because of the wide spacing between the ties. The type of failure depends on the column dimensions and the longitudinal steel ratio. Shear failure was excluded in the current study.

Tests conducted on columns with continuous reinforcement (Aycardi et al., 1992; and Lynn et al., 1994) are shown in figures 2.7 and 2.8. The dimensions, reinforcement details and material strengths of these columns are listed in table 2.2. The parameters proposed for this case are shown in table 2.1. Deformation capacities at peak strength corresponding to concrete strain of 0.006 were found to be in good agreement with the experimental results. The concrete strain at peak strength in case of column ends with continuous reinforcement is higher than that of column ends with lap splices due to the absence of the anchorage failure of the column bars.

2.5 BEAM BEHAVIOUR

The behaviour of beams in a nonductile RC frame is affected by the insufficient development length of the bottom longitudinal steel. The mode of failure that characterizes bond failure of the beam bottom reinforcement is different from that of the column lap splice. The beam bottom reinforcement is anchored in the beam-column joint where a large mass of concrete surrounds the reinforcement. The bond failure often occurs by bar pullout due to shearing off of the concrete keys between the lugs (Eligehausen et al., 1983). The anchorage capacity of a steel bar can be estimated in terms of average bond stress along the embedment length (L_d) given as:

$$f_s = \frac{u_u \, \pi \, d_b \, L_d}{A_b}$$

(2.11)

where, u_u is the average bond stress at peak resistance, f_s is the steel stress at anchorage failure, d_b is the bar diameter, and A_b is the bar cross section area. The ultimate bond stress for embedded bars in well confined concrete is taken as $u_u=1.8\sqrt{f_c'}$ (MPa) (Robins and Standish, 1984).

The bond slip is often initiated once the cross section at the beam-column interface is cracked in positive bending. Before cracking of this section, the concrete will carry most of the tensile stress and the stress in the bars will be low. Once the concrete cracks at the interface, the tensile force will be redistributed to the bars. Figure 2.9 shows the effect of pullout of bottom beam reinforcement on the moment-rotation relationship. The moment M_1 is the cracking moment in positive bending, θ_1 is the corresponding rotation. The ultimate

moment capacity of the beam in positive bending M_2, is calculated using the steel stress at anchorage failure. The corresponding rotation at ultimate capacity of the beam end in positive bending is θ_2. The value of θ_2 is calculated using the local bond-slip model proposed by Eligehausen et al. (1983), shown in figure 2.10, as well as the bond stress distribution model proposed by Alsiwat and Saatcioglu (1992). It is assumed that the bond stress distribution is uniform and equal to u_x along the embedment length of the bar at bond failure. The bar slip at peak resistance can be calculated by summing the slip δ_{s2} shown in figure 2.10 and the extension in the steel bar assuming linear variation of steel strain along the embedment length of the steel bar. The associated rotation θ_2 is calculated by dividing the slip at peak resistance over the distance between the bottom bars and the neutral axis of the beam cross section. The position of the neutral axis can be calculated from equilibrium of forces at the cross section. The deformation capacity at peak strength of the beam in negative bending is assumed to correspond to a concrete strain of 0.0035. The model parameters proposed for beams in nonductile reinforced concrete frames are shown in table 2.1. The analytical prediction was compared with the results of an experimental study of beam-column subassembly conducted by Biddah et al. (1997). The analytical prediction was found in good agreement with the experimental results, as shown in figure 2.11.

2.6 BEAM-COLUMN JOINTS

Seismic loads on reinforced concrete frames produce high shear forces in the beam-column joints. In some cases, the joint shear capacity may be inadequate and this will lead to a brittle failure of the joint. The early anchorage failure of the positive reinforcement in

beams will reduce the shear demand and the possibility of shear failure of the joint. Tests conducted by Pessiki et al. (1990) indicated that the beam-column joints without transverse reinforcement failed in the specimens with continuous beam reinforcement through the joints. However, for the specimens with 150 mm embedded beam bottom reinforcement, only minor cracking was visible in the joints at peak resistance of the specimens. In the current study, it is assumed that the beam-column joints are rigid, and that all the inelastic deformation will be concentrated at the member ends.

2.7 STRENGTH SOFTENING EFFECT

The effect of the strength softening behaviour on the cyclic response of nonductile frames is evaluated in this section. A 3-story RC office building was selected to represent existing non-ductile RC buildings. The frame is gravity load designed according to the 1963 ACI code. Typical floor plan and elevation of the office building are shown in figure 2.12. Details of column and beam cross sections of the building are shown in figure 2.13. Nonductile critical regions in the building include: (1) beam bottom longitudinal reinforcement embedded 150 mm into the beam-column joint; (2) widely spaced (300 mm) transverse reinforcement in beams and columns; (3) column lap splices of 20 bar diameter length located just above the floor level.

A static cyclic inelastic analysis is performed on an interior three-bay frame. The P-Δ effect is considered in the analysis. The lateral load applied to the frame is a triangular load with maximum load at the roof. The frame is subjected to eight displacement cycles with increasing amplitude. Figure 2.14 shows the variation of the base shear coefficient with the

roof displacement of the frame with and without modelling the strength softening. The base shear is normalized by the dead weight acting on the frame. The story drift ratios corresponding to a roof drift ratio of 1.0% reached approximately 1.84%, 0.88% and 0.31% for the first, second and third story, respectively. The distribution of the story drift ratios indicates the formation of a soft story mechanism in the first story of the frame. Figure 2.14 indicates that the ability of the model to represent the softening behaviour provides a more realistic response than when softening is not included in the model.

The seismic behaviour of the interior frame is studied using scaled versions of the S00E component of the acceleration time history recorded at El Centro during the 1940 Imperial Valley earthquake. The dynamic analysis is carried out using a time step increment of 0.005 second and Rayleigh damping which is defined to achieve 2.0% viscous damping in the first two natural modes of the frame. Figure 2.15 shows the roof drift variation with the peak ground acceleration (PGA) of the earthquake with and without modelling the strength softening. The roof drift ratios of the frame at PGA level of 0.40 g are approximately 1.2 % and 1.4 % with and without modelling the strength softening, respectively. The corresponding drift ratios of the first story are approximately 2.18% and 2.88%, respectively. Figure 2.16 represents the maximum story drift ratios reached during the dynamic analysis. As expected, the effect of strength softening dominates the behaviour past the ultimate strength reached at roof drift ratio of approximately 0.9 (figure 2.15). The collapse of the frame under the effect of gravity and seismic loads occurred in the softening model when the PGA level reached 0.42 g. The collapse occurs due to the frame lateral instability under the effect of gravity and seismic loads. This is determined by checking the lateral displacement

of the frame and the progress of inelastic action and hinging of members of the frame to ensure that structural instability is taking place and not numerical instability. Figure 2.17 shows the effect of the strength softening on the base shear coefficient at PGA level of 0.40 g. Without strength softening, the dotted line indicates that the base shear coefficient is overestimated due to underestimated drift and P -Δ effect.

2.8 SIMPLIFIED PROCEDURE FOR SEISMIC PERFORMANCE EVALUATION OF NONDUCTILE BUILDINGS

In section 2.7 the seismic performance of the three-story building was evaluated using dynamic inelastic time-history analysis. The inelastic dynamic time-history approach is difficult to use in practical applications because of the time and effort required to perform and interpret its results. Moreover, in reliability evaluation of building structures under seismic excitation, repeated analyses of the response of the (MDOF) systems in the inelastic range are often required and the computations can become excessive. The computational effort can be significantly reduced when simplified procedures that can predict the expected building performance when subjected to ground motion records with reasonable accuracy are used.

A simple approach for evaluating the seismic performance of structures is to relate the building performance parameters to the elastic spectral force level of an equivalent linear elastic SDOF model along with using force reduction factors for inelastic systems (e.g., Riddell et al., 1979; and Krawinkler, 1991). Although, such approach provides simple and convenient means for analysis and design of MDOF systems, the accuracy is inherently limited because of basic differences between the dynamics of an inelastic MDOF system and linear elastic SDOF system as well as the effects of the strong ground motion duration of

earthquakes.

A simplified approach for evaluating the seismic performance of building structures with improved accuracy, relies on creating an equivalent inelastic SDOF system. This approach was applied successfully to the analysis of ductile concrete and steel structures (Collins and Foutch, 1995; Han and Wen, 1997). It is based on obtaining a nonlinear force-displacement relationship of the equivalent SDOF system from a static pushover analysis of the MDOF structure and then performing an inelastic dynamic analysis to obtain an estimate of the peak response parameters of the MDOF system. This methodology is applied to the analysis of the seismic response of nonductile reinforced concrete buildings with the objective of accounting for the differences between ductile and nonductile building behaviours. These differences arise from the strength softening behaviour in the post peak strength range and the characteristics of the developed plastic mechanism under the effect of the earthquake loading.

In the formulation of the simplified approach, the strength softening behaviour was included in the hysteretic force-displacement relationship of the SDOF model. A simple procedure was used to estimate the story drift ratio using the lateral displacement profile of the static pushover analysis as well as the roof drift ratio obtained from the SDOF analysis. Evaluating the seismic performance of nonductile structures using the formulated simplified approach will be carried out in Chapter 4.

2.8.1 Equations of the Equivalent Single-Degree-of-Freedom model

The equations of motion of a multi-degree of freedom frame structure subjected to

horizontal ground motion can be written as:

$$[M]\{\ddot{u}\} + [C]\{\dot{u}\} + \{F\} = - [M]\{1\}\ddot{u}_g \qquad (2.12)$$

where, $[M]$ is a diagonal mass matrix, $[C]$ is the damping matrix, $\{u\}$ is the lateral displacement vector, $\{F\}$ is the resisting force vector, $\{1\}$ is a unit vector and $\ddot{u}_g$ is the ground motion acceleration.

The SDOF model is required to represent the displacement response of the MDOF structure at some selected "significant" point. In the current study, the roof level was selected as the "significant" point in the structure with roof displacement response of $u_r(t)$.

To develop an equivalent SDOF model, assumptions are made regarding the lateral displacement profile of the structure, $\{u\}$, and the resisting lateral force vector, $\{F\}$. The lateral displacement vector $\{u\}$ in equation 2.12 can be approximated as, $\{u\} = \{\Psi\}u_r(t)$, where $\{\Psi\}$ is an assumed lateral displacement profile of the structure which is assumed to remain constant during the response and is normalized such that the component of $\{\Psi\}$ corresponding to the roof displacement is unity. The resisting lateral force vector $\{F\}$ in equation 2.12 is approximated as, $\{F\} = V\{S\}$, where $\{S\}$ is an assumed lateral force profile of the structure that remains constant during response and is normalized such that it corresponds to a base shear of unity, and V is a function of time scale factor that physically represents the base shear coefficient.

The vector $\{\Psi\}$ can be chosen based on the results of a static pushover analysis of the MDOF system. The pushover analysis can be carried out using the lateral force distribution $\{S\}$. When the structure behaviour is dominated by the first mode response, the lateral force

distribution {S} can be approximated as an inverted triangular distribution (maximum value at the roof level). Substituting {F} and {u} by V{S} and {Ψ}u$_r$(t) in equation 2.12 yields:

$$[M]\{\Psi\}\ddot{u}_r + [C]\{\Psi\}\dot{u}_r + V\{S\} = -[M]\{l\}\ddot{u}g \qquad (2.13)$$

To reduce the matrix equation 2.13 to a single equation, both sides of the equation can be pre-multiplied by {Ψ}^{T} to get:

$$M^* \ddot{u} + C^* \dot{u} + V^* = -L^* \ddot{u}_g \qquad (2.14)$$

where, $M^* = \{\Psi\}^T [M]\{\Psi\}$, $C^* = \{\Psi\}^T [C]\{\Psi\}$, $V^* = V\{\Psi\}^T \{S\}$, and $L^* = \{\Psi\}^T [M]\{l\}$.

Equation 2.14 can be interpreted as the equation of motion for a SDOF system and is consistent with the SDOF equation derived by Anderson (1989) and Collins and Foutch (1995).

2.8.2 Selecting the lateral force profile vector

A selection of the lateral force profile vector of the structure is needed for the formulation of the SDOF analysis. The distribution of the lateral force will affect the force-displacement relationship obtained from the pushover analysis. The distribution of the resisting lateral force during the structure dynamic response is dependent on the characteristics of the mode shapes of the structure and the characteristics of the ground motion. Moreover, this distribution is expected to change during the structure response as a result of the inelastic behaviour. Krawinkler (1996) concluded that no single lateral load profile can capture the variations in local demands expected in a design earthquake. He

reported that there are two lateral load profiles that may bound the inertia force distribution during an earthquake. The first one is uniform load profile (story forces proportional to story mass) which magnifies the relative importance of story shear forces compared to overturning moments. The other could be the design load profile used in present codes. In the current study, the approximate analysis of the nonductile buildings was performed using two lateral load profiles. The first is a uniform distributed lateral loading and the second is the lateral load distribution suggested by the National Building Code of Canada (NBCC, 1995). The accuracy of the approximate analysis results was evaluated in the two cases of lateral load distributions.

2.8.3 Estimating the lateral displacement profile vector $\{\Psi\}$

The accuracy of the SDOF model depends on the proper selection of the lateral displacement profile vector $\{\Psi\}$. The main problem in selecting $\{\Psi\}$ is that the lateral displacement profile of the structure is not constant during the response as a result of the structure inelastic behaviour. The lateral displacement profile of the structure is approximated using two lateral displacement profile vectors $\{\Psi_o\}$ and $\{\Psi_1\}$ which results in two different SDOF systems representing the MDOF structure. The first SDOF system is for representing the elastic behaviour of the structure and is applicable up to 0.5% roof drift ratio, which represents approximately the yield displacement limit of both the three and nine-story buildings. The corresponding lateral displacement profile vector, $\{\Psi_o\}$, is selected as the initial displacement profile of the structure calculated in the first loading increment of the pushover analysis where the structure response is in the elastic range. The second SDOF system is for

representing the inelastic behaviour of the structure and is applicable when the roof drift ratio is greater than 0.5%. The corresponding lateral displacement profile vector, $\{\Psi_1\}$, is selected as the displacement profile from the pushover analysis at 1.0 % roof drift. The selection of 1.0 % roof drift is arbitrary, however, it represents an approximate intermediate value between the yield limit and the collapse limit of nonductile buildings.

2.8.4 Approximate Estimation of the Maximum Story Drift Ratio

The described SDOF model is capable of predicting approximate estimations of the structure roof drift ratio. The maximum story drift ratio of the structure can not be predicted directly from the SDOF results. A simple procedure is proposed for the estimation of the maximum story drift ratio using the lateral displacement profile vectors $\{\Psi_o\}$ and $\{\Psi_1\}$ as well as the roof drift obtained from the SDOF results. The maximum story drift is assumed equal to (w .u_r), where u_r is the roof drift obtained from the SDOF results and w is calculated as follows:

1. For roof drift ratio up to 0.5%, w is considered as the maximum story drift from the initial lateral displacement profile vector $\{\Psi_o\}$.

2. For roof drift ratio greater than 1.0 %, w is considered as the maximum story drift from the lateral displacement profile vector $\{\Psi_1\}$.

3. For roof drift ratio between 0.5 % and 1.0 %, w is obtained by interpolation using the two values calculated in steps (1) and (2).

2.9 SUMMARY

A phenomenological model is proposed for representing the strength softening behaviour of nonductile reinforced concrete frame members based on component tests. The main characteristic of the developed element is its ability to represent the drop in the strength of nonductile RC members after reaching the ultimate strength level. Moment and deformation capacities of the frame members were estimated taking into consideration the effect of the various deficient details in nonductile components. The analytical predictions are compared with experimental measurements of the response of members of nonductile frames.

The developed model was applied to study the seismic response of a 3-story nonductile frame. The response calculated using the softening model is compared with the prediction using traditional models that do not represent the strength softening of the frame members. The results indicate that neglecting the strength softening when modelling nonductile frames will lead to underestimation of the displacements. An important advantage of the softening model is its ability to represent the behaviour of the structure past its ultimate strength up to failure and to predict its failure mode.

A simplified approach for evaluating the seismic performance of nonductile building structures was presented. The approach relies on creating an equivalent inelastic SDOF system with nonlinear force-displacement relationships obtained form a static pushover analysis of the MDOF structure. An approximate estimate of the peak response parameters of the MDOF system can be obtained by performing an inelastic dynamic analysis to the SDOF system. The strength softening behaviour in the hysteretic force-displacement relationship of the SDOF model was included in the simplified analysis.

Table 2.1 Model parameters

Case	Pinching α	Stiffness degradation γ	Strength deterioration β	Strength softening η	Ultimate concrete strain
Column end with lap splice (Bond failure before bar yielding)	0.75	1	0.1	0.3	—
Column end with lap splice (Bar yielding before bond failure)	0.7 5	1	0.1	0.1	0.0035
Column end with continuous steel	1	2	0.1	0.15	0.006
Beams	0.75	2	0.1	0.1	0.0035

Table 2.2 Experimental data for the column specimens

Test	d/b	L/d	ψ %	ρ %	r %	L_s/d_s	f_y MPa	f_c' MPa
Ghobarah et al., 1997 (column S1)	0.8	5	0.52	0.36	6.5	37.5	437	24.8
Aycardi et al., 1992 (specimen 1)	1	5	1	0.75	39	26.7	448	23.4
Aycardi et al., 1992 (specimen 2)	1	5	1	0.75	30	no splice	448	30
Lynn et al., 1994 (column 2)	1	3	2	0.16	10	no splice	300	21
Lynn et al., 1994 (column 4)	1	3	2	0.16	10	20	300	21
Aboutaha and Jirsa, 1996 (column FC1)	0.5	6	1.9	0.21	0	24	414	19.7

d= Cross section depth b=Cross section width L = Column length (Cantilever)
L_s= Splice length ψ= Longitudinal steel ratio d_s= Longitudinal steel diameter
ρ= Lateral steel ratio f_y=Steel yield stress f_c'= Concrete compressive strength
r=P/ (f_c' d b) P=Axial load

(a) Modelling of stiffness degradation

(b) Modelling of pinching

(c) Modelling of strength deterioration

(d) Modelling of softening
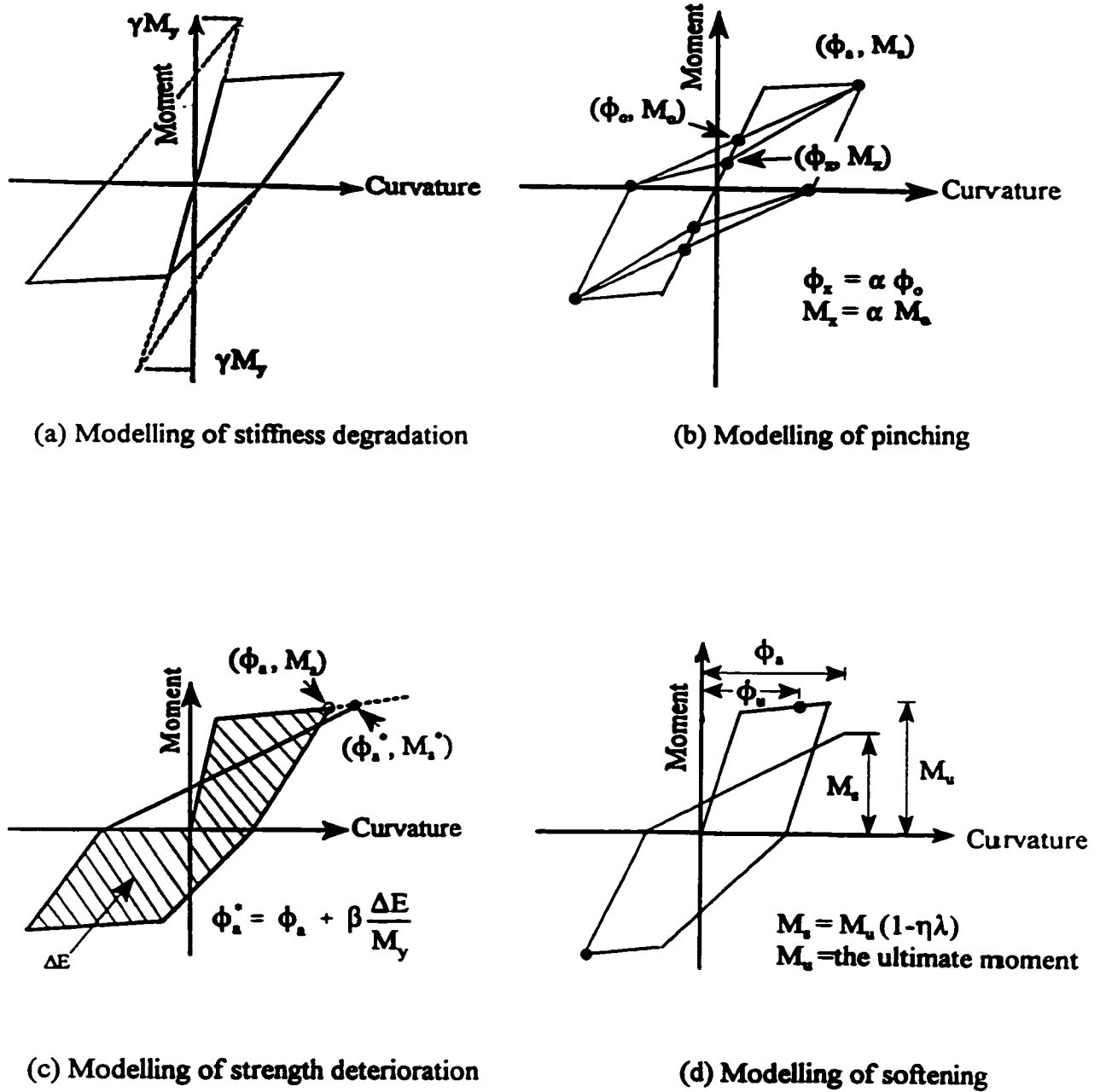
Figure 2.1 Hysteretic modelling of the moment-curvature relationship
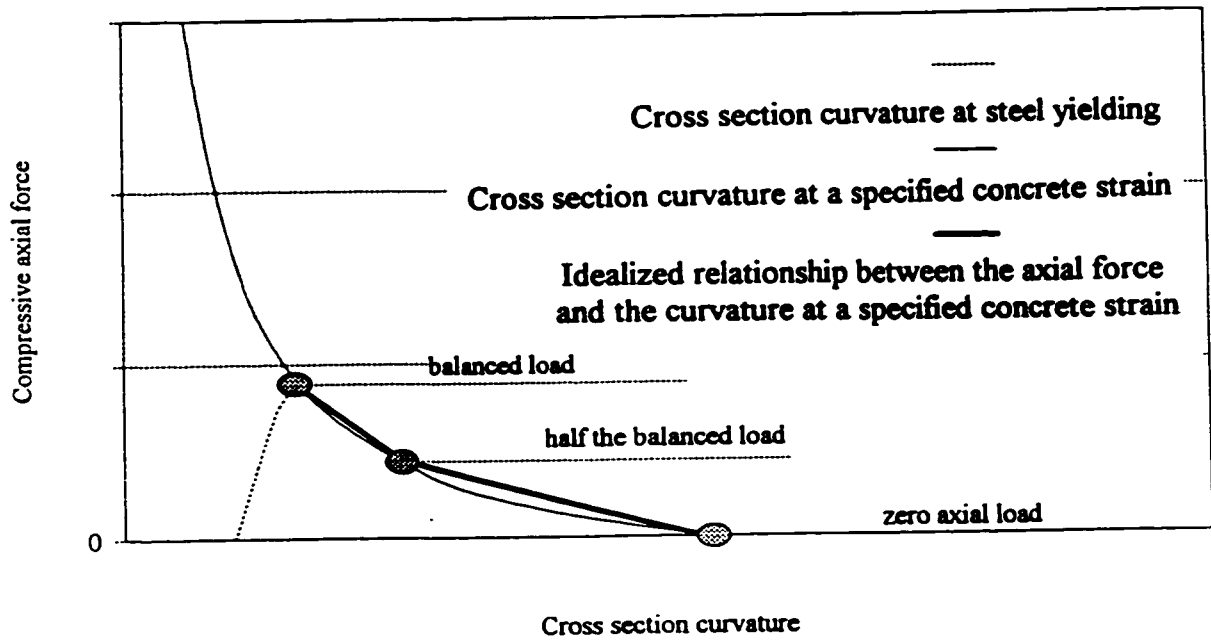
Figure 2.2 Interaction between the axial forces and the curvatures for typical RC section
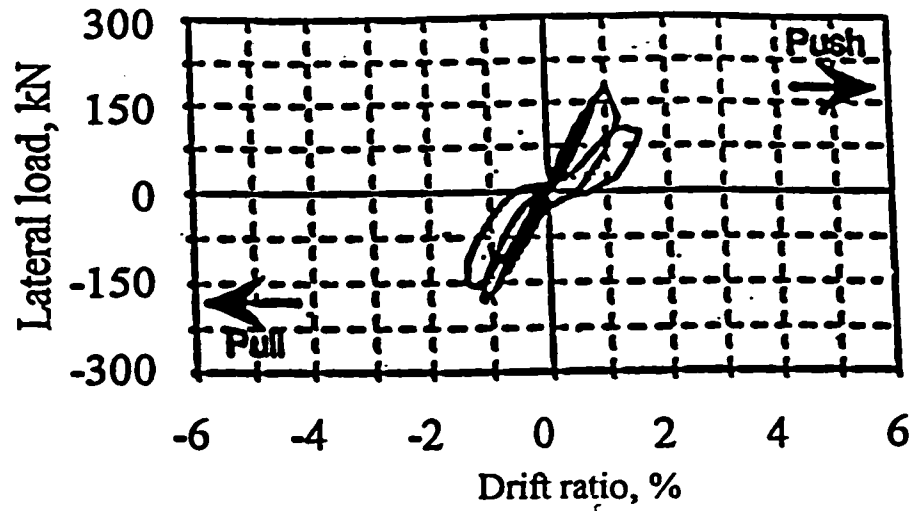
(a) Experimental-column FC1 (Aboutaha and Jirsa, 1996)
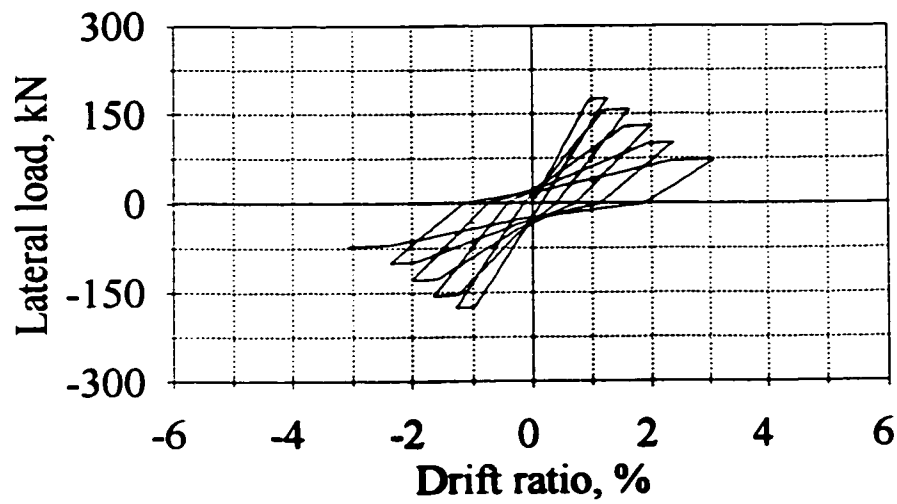
(b) Proposed model

Figure 2.3 Experimental and Analytical comparison of load-displacement relationship
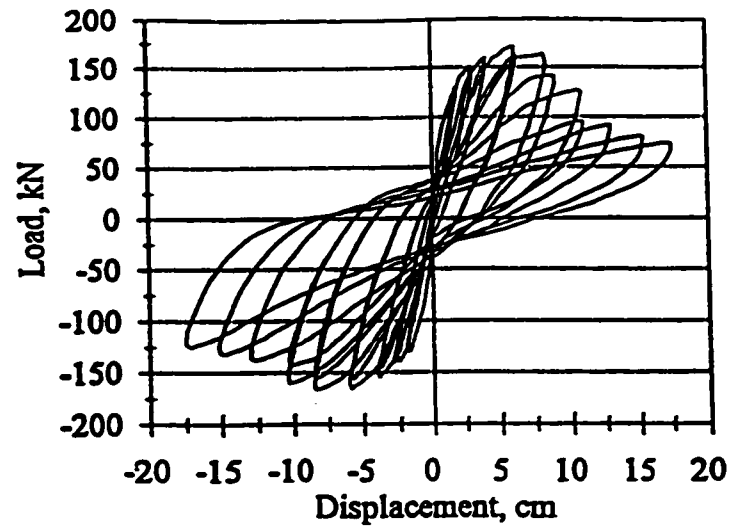
(a) Experimental-specimen 1 (Ghobarah et al., 1997)
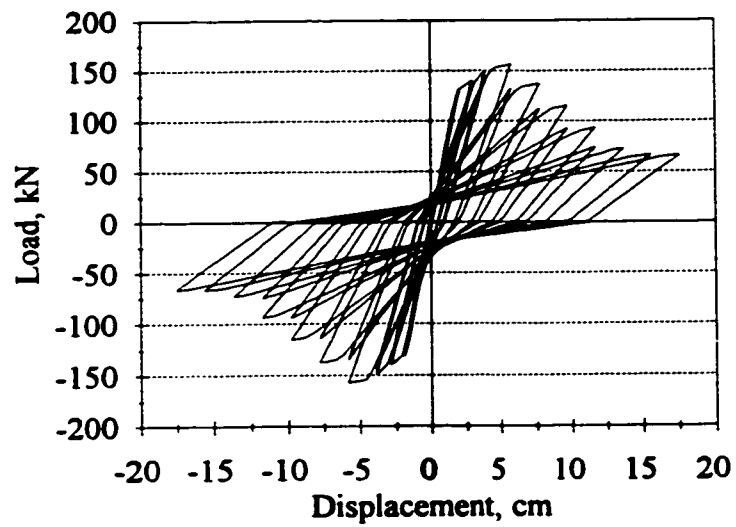
(b) Proposed model

Figure 2.4 Experimental and Analytical comparison of load-displacement relationship
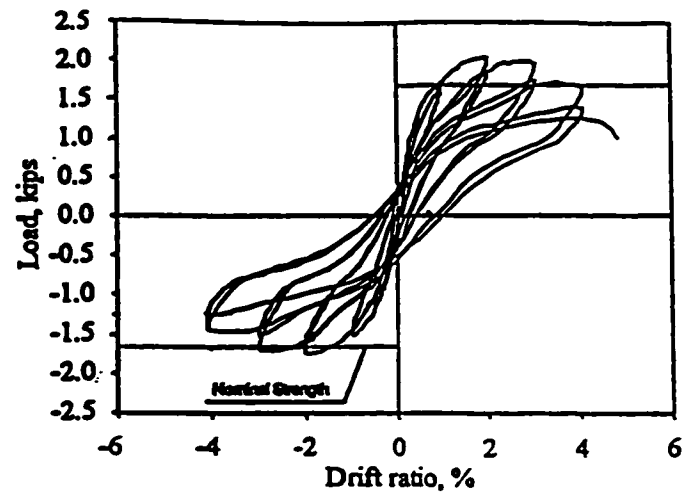
(a) Experimental-specimen 1 (Aycardi et al., 1992)
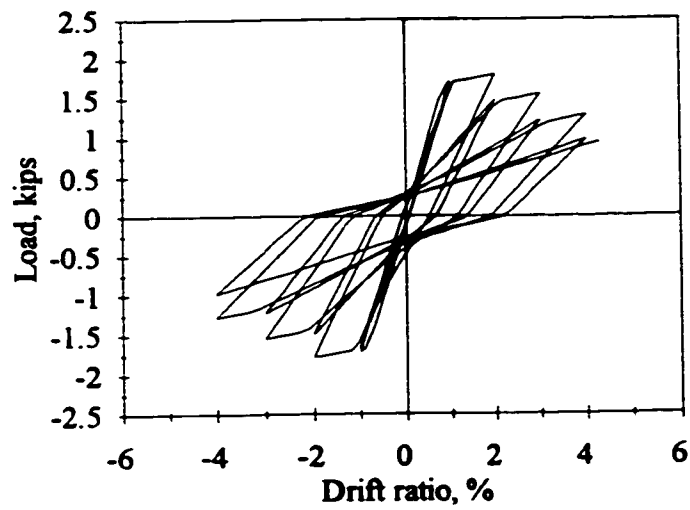
(b) Proposed model

Figure 2.5 Experimental and Analytical comparison of load-displacement relationship
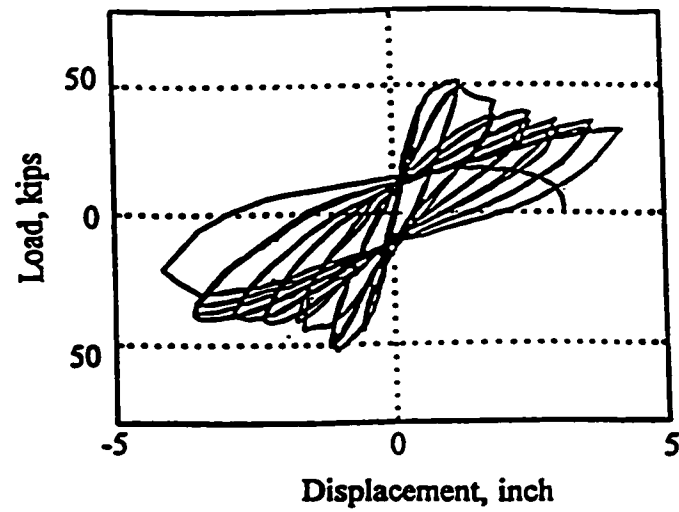
(a) Experimental-column 4 (Lynn et al., 1994)
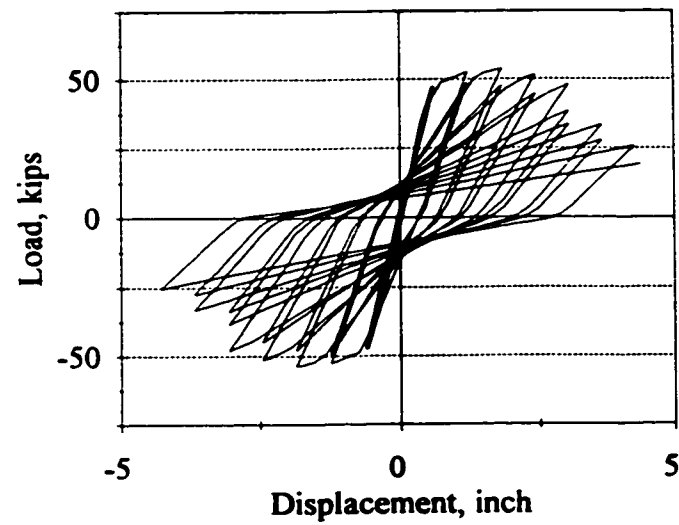
(b) Proposed model

Figure 2.6 Experimental and Analytical comparison of load-displacement relationship
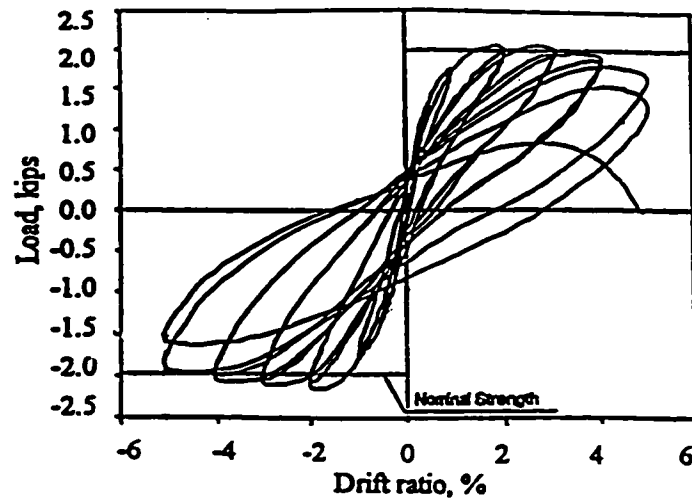
(a) Experimental-specimen 2 (Aycardi et al., 1992)
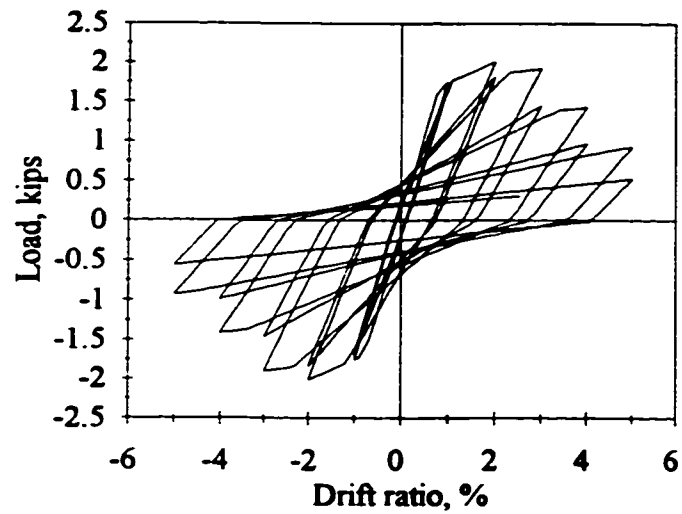
(b) Proposed model

Figure 2.7 Experimental and Analytical comparison of load-displacement relationship
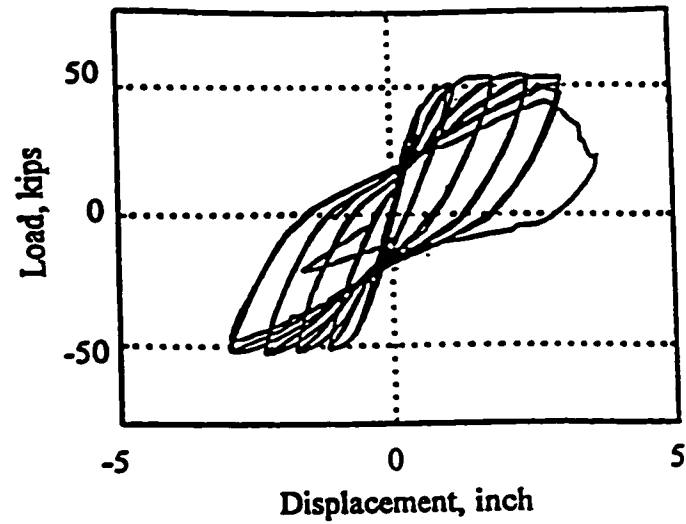
(a) Experimental-column 2 (Lynn et al., 1994)
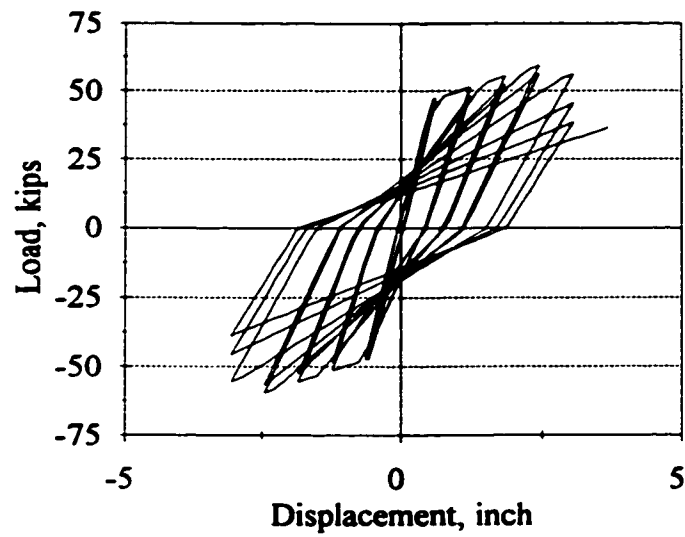
(b) Proposed model

Figure 2.8 Experimental and Analytical comparison of load-displacement relationship
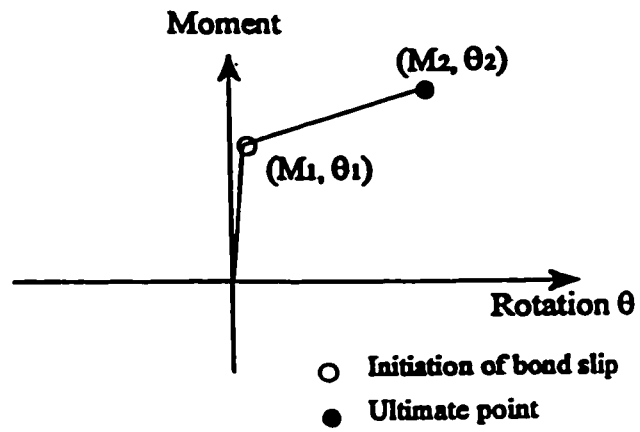
Figure 2.9 Effect of bond slip on the moment-rotation relationship
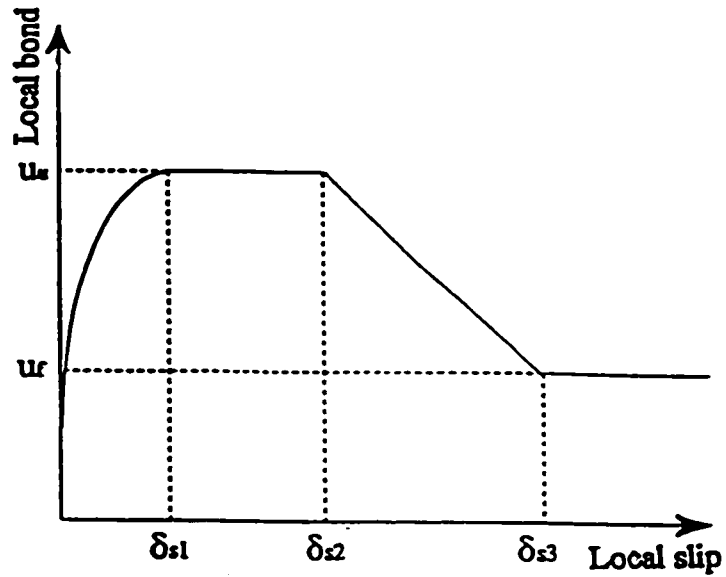
Figure 2.10 Local bond-slip model (Eligehausen et al., 1983)
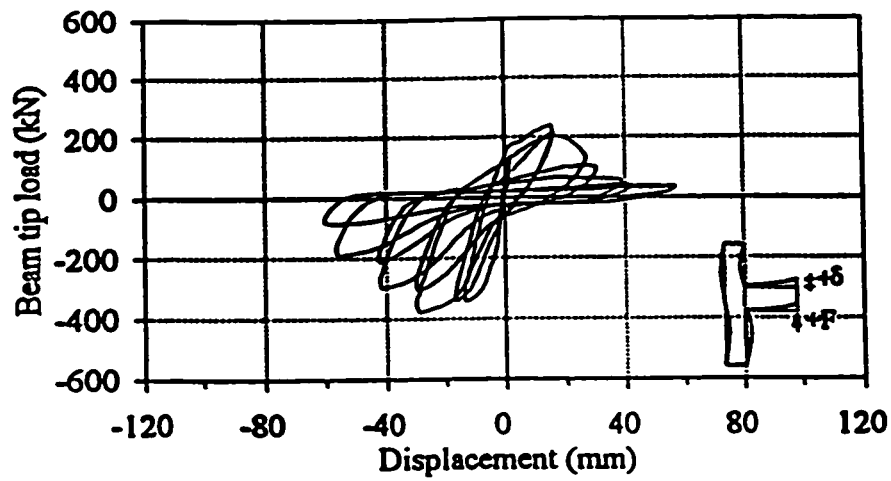
(a) Experimental-specimen J4 (Biddah et al., 1997)
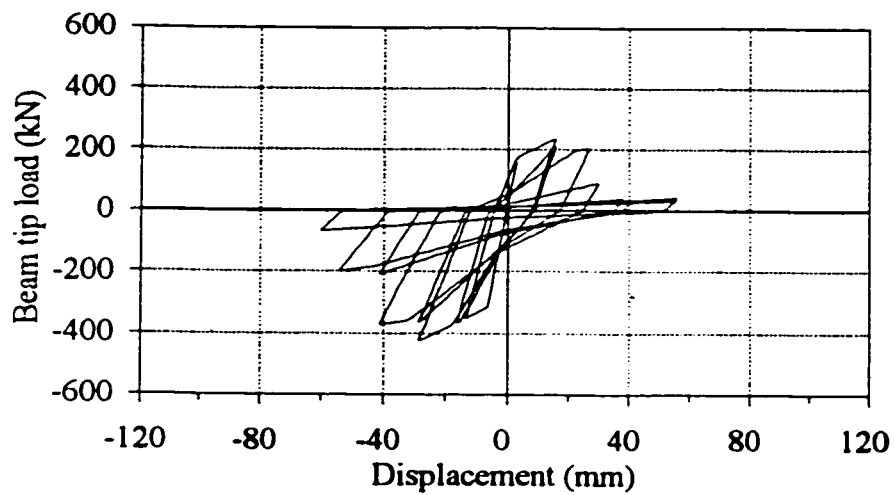
(b) Proposed model

Figure 2.11 Experimental and analytical comparison of load-displacement relationship
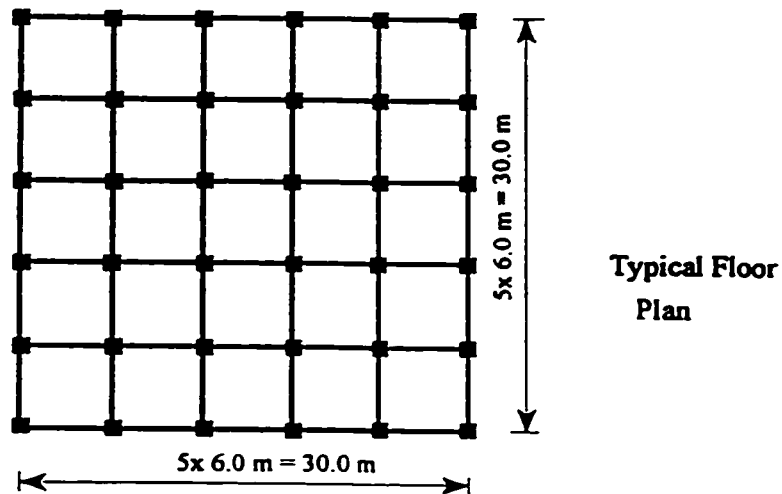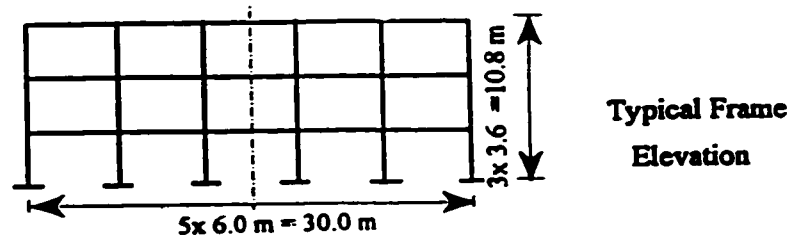
Figure 2.12 Dimensions of the 3-story office building
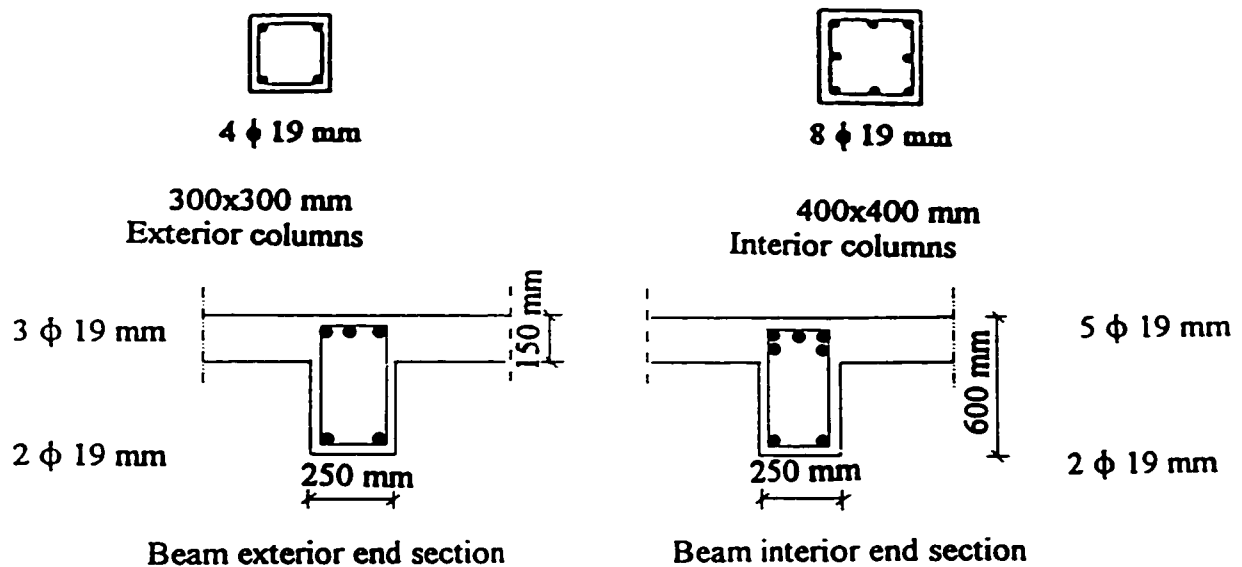
Figure 2.13 Details of columns and beams
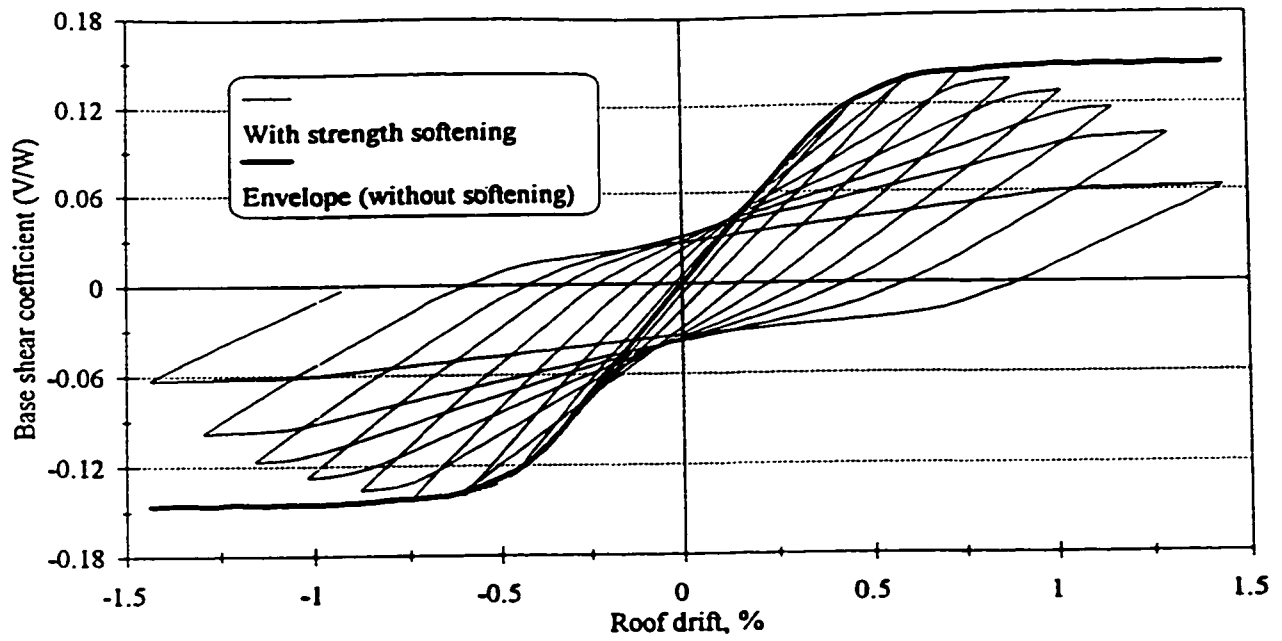
Figure 2.14 Static cyclic behaviour of the frame
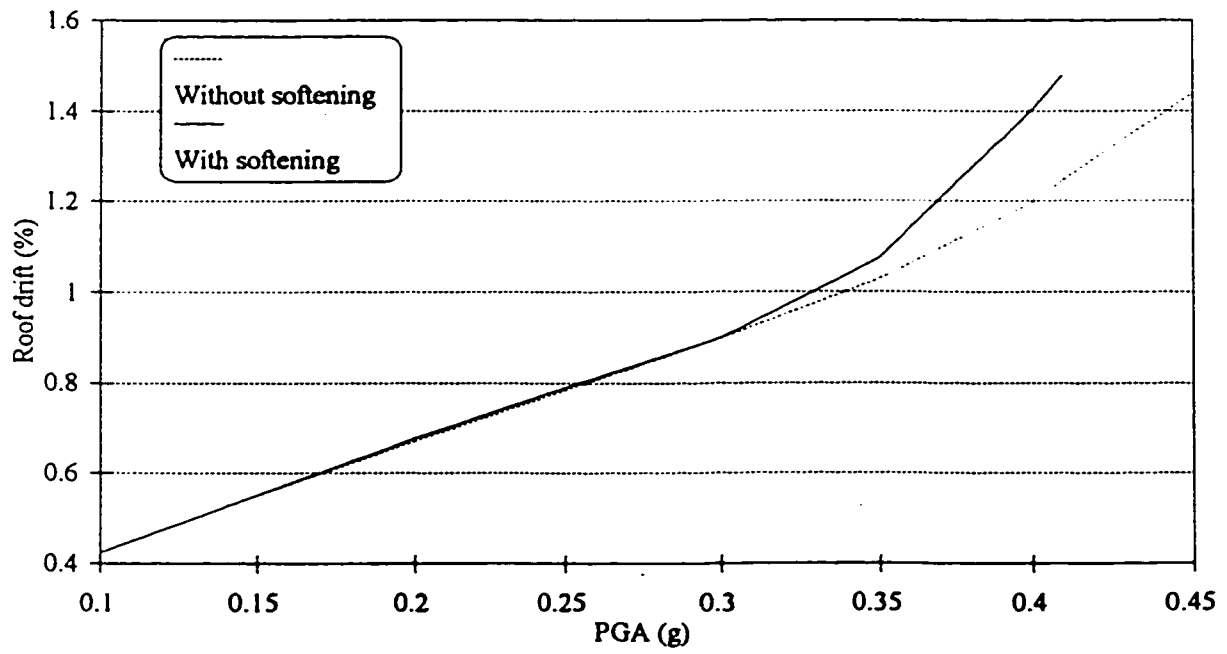
Figure 2.15 Effect of softening on the roof drift
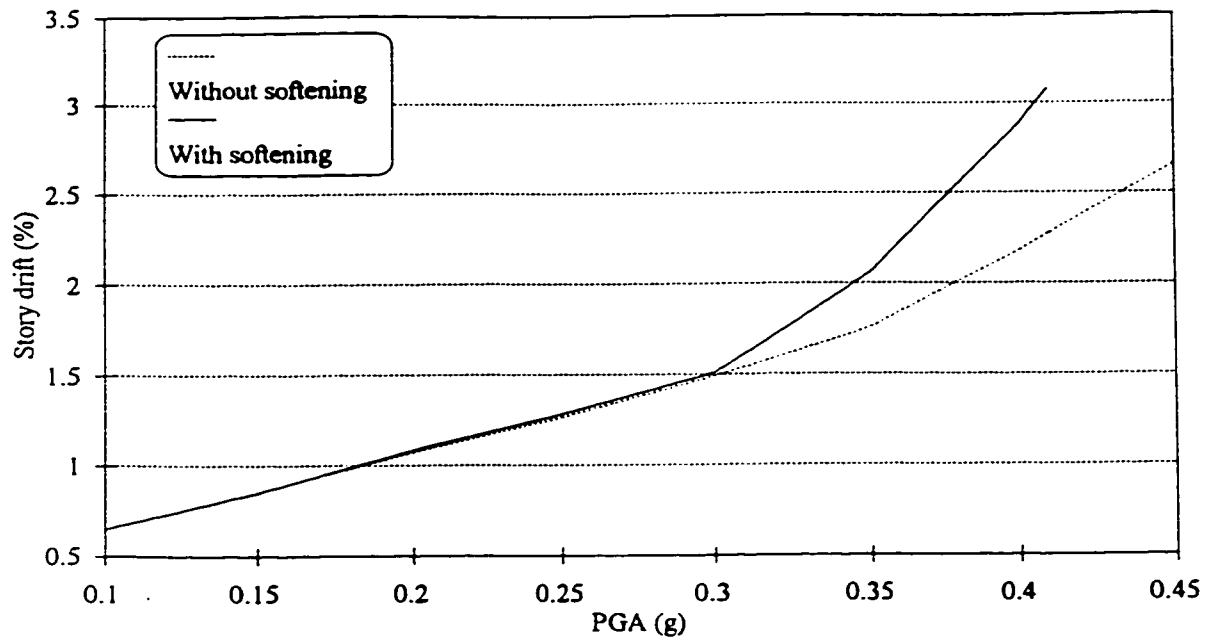
Figure 2.16 Effect of softening on the story drift
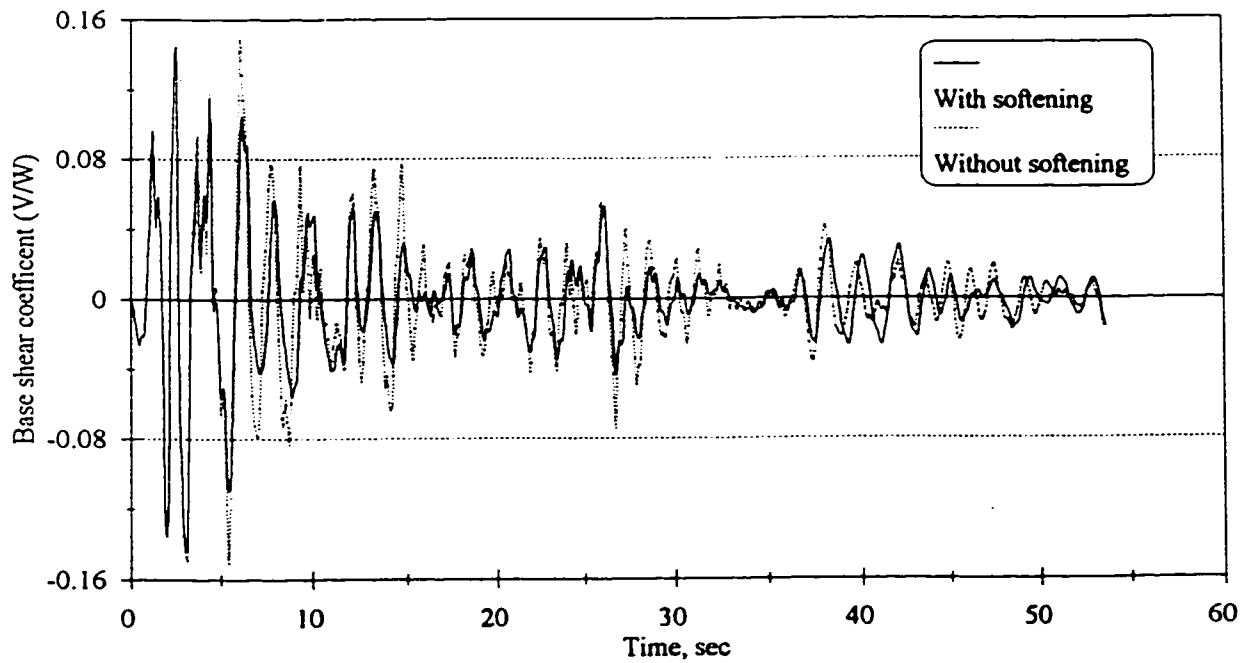
Figure 2.17 Effect of softening on the base shear

CHAPTER 3

SEISMIC DAMAGE EVALUATION

3.1 INTRODUCTION

The objective of seismic analysis of existing nonductile reinforced concrete buildings is to assess their lateral load resisting capacity and to evaluate their damage state when subjected to an earthquake loading. This analysis forms the basis for the rehabilitation decisions. Damage indices may be used to describe the amount of potential damage of structures. They represent valuable design tools since they provide means by which different design or retrofit options can be compared.

Several damage models have been proposed to quantify the level of damage to structures due to an earthquake. Indices may be evaluated locally for an element, by measuring local response parameters of the flexural plastic hinges, e.g., maximum curvature, maximum rotation, and the dissipated energy. Global damage indices for the various stories and for the whole building are calculated by summing of the local indices by a weighing procedure or by considering changes in the structure's global response parameters.

The applicability of available damage indices in measuring seismic damage of nonductile existing structures is questionable. Most of the indices are derived on the basis of an assumed ductile behaviour which is characteristic of properly seismically designed components. The seismic behaviour of existing nonductile structures is characterized by strength softening in the post-peak range. Strength softening of nonductile members in the

58

post peak range occurs early and occupies most of the member time history response. It results from typical deterioration modes such as pullout of steel reinforcement, concrete splitting, buckling of steel in compression and shear failure in the plastic hinge regions. There is a need for developing damage models that are suitable for evaluating the seismic damage of existing nonductile buildings. In this chapter a procedure for evaluating the damage to nonductile RC structures following an earthquake is developed. The damage procedure is based on evaluating the deterioration of the building stiffness and lateral load carrying capacity due to the application of the earthquake loading. The building stiffness and lateral load carrying capacity before and after the application of the earthquake loading were determined using a pushover analysis.

3.2 REVIEW OF AVAILABLE DAMAGE MODELS

Available damage models may be classified into two main types. The first type is damage models that are formulated locally, using the hysteretic characteristics of a particular member or cross section. In this case, global damage indices for the entire structure are calculated by integrating the local indices using a weighing procedure. The second type is global damage indices for the whole building that are calculated by considering changes in the structure global parameters, e.g., story drift and fundamental period. The two types will be discussed in details in the following subsections.

3.2.1 Local Damage Models

Several local damage models have been reported in the literature. Martin et al.

(1997) provided a comparison between some of the available local damage models. They concluded that all the studied local indices did not provide good performance when used for evaluating damage in shear-dominated RC elements.

Local damage models may be categorized into two main groups. The first group includes damage models that account only for maximum deformation, while the second group includes damage models that account for maximum deformation and cumulative damage. Examples of damage indices that are based on Maximum deformation include, the Ductility Ratio (DR) and the Modified Stiffness Ratio (MSR). The Ductility Ratio (DR) is defined as the ratio of maximum deformation to the yield deformation. It has been applied extensively in seismic analysis to evaluate the capacity of structures undergoing inelastic deformation and in developing inelastic response spectra (Newmark and Rosenblueth, 1971). It is assumed that failure occurs when the ductility demand exceeds the structural ductility capacity. The ductility capacity of an element is the ratio of the ultimate deformation under monotonic static load to the yield deformation.

The Modified Stiffness Ratio (Roufaiel and Meyer, 1987) can be defined as:

$$MSR = \frac{k_f}{k_m} \cdot \frac{(k_m - k_0)}{(k_f - k_0)} \tag{3.1}$$

where k_f and k_m are the secant stiffnesses at failure and at maximum deformation, respectively. The initial stiffness is termed k_0. The value of the damage index will vary between zero and one and is dependent on the magnitude of the maximum deformation and the deformation at failure. The deformation at failure is usually calculated as the ultimate deformation under

monotonic static load.

The Ductility Ratio (DR) and the Modified Stiffness Ratio (MSR) are considered unsatisfactory as damage indices because they can not account for the duration of the ground motion. Experimental evidence on the behaviour of nonductile components indicates that repeated cycles at the same ductility level will cause deterioration in both the stiffness and strength and therefore will increase the damage level. Such effects are ignored when using the Ductility Ratio (DR) and the Modified Stiffness Ratio (MSR) as damage indices.

An example of the damage models that account for maximum deformation and cumulative damage is the damage index proposed by Park and Ang (1985). The index is defined as:

$$D = \frac{\delta_m}{\delta_u} + \frac{\beta \int dE}{F_y \, \delta_u} \tag{3.2}$$

where δ_m is the maximum displacement response, δ_u is the ultimate deformation capacity under monotonic loading, F_y is the yield strength, dE is the incremental dissipated energy and β is a non-negative constant. The first term in equation 3.2 accounts for damage based on the ductility ratio, while the second term accounts for the cumulative damage as a result of the loading cycles based on the principle of low cycle fatigue of metal structures.

This type of damage model may be appropriate for the case of ductile structural components that do not exhibit significant deterioration in response due to repeated loading cycles and will be subjected to a rapid loss of strength after reaching their failure deformation at a late stage of the response. The application of this type of damage models for the case of

nonductile structural components that exhibit deterioration in response due to repeated cycles at the same ductility level is not appropriate (Krawinkler, 1987). For nonductile components, it is more appropriate to define damage in terms of the loss in strength.

Global damage index for the entire building or for a particular story provides means by which different designs or retrofit options can be compared. Global damage indices are obtained by integrating the local damage indices of the various building elements. A procedure proposed by Park and Ang (1985) to integrate the local damage indices depends on calculating a weighted average of the local damage indices of a particular story or the entire building. The weighing factor for an element is taken as the dissipated hysteretic energy by such element. Considering for example the frame shown in figure 3.1, where the cases (a) and (b) represent two sequential damage states during an earthquake analysis. Global damage indices for the two damage states can be calculated as; $D^a = d_1^a$ and $D^b = (d_1^b.E_1^b + d_2^b.E_2^b)/(E_1^b + E_2^b)$, where d_i^j and E_i^j are, respectively, the local damage index and the dissipated hysteretic energy of element i at damage state j. D^j is the corresponding global damage index.

When using the averaging procedure for calculating the global damage indices, inaccurate results may be obtained because of two reasons. First, in the case where (d_1^b, E_1^b) are slightly larger than (d_1^a, E_1^a) and (d_2^b, E_2^b) are fractions of (d_1^b, E_1^b), the calculation may yield ($D^a > D^b$). This is an incorrect result because case (b) is a later stage of loading and should have more damage than case (a). Second, the procedure neglects the relative importance of each element to the lateral stability of the entire structure. The damage procedure does not distinguish between a column and a beam. Kappos (1997) reported that

there is a difficulty in the appropriate definition of a global damage index for the entire

structure. He concluded that in some cases, the global damage index for the entire structure

can not be expressed simply as a weighted average of member indices.

3.2.2 Global Damage Models Based on the Global Response Parameters or the Dynamic Characteristics of the Structure

Global damage indices can be calculated directly from the global response parameters

or the dynamic characteristics of the structure. Two types of global damage indices are

discussed. The first damage index is the Interstory Drift ratio (ID) and the second index is

the Final Softening index (FS) proposed by DiPasquale and Cakmak (1988) which is

calculated using the natural fundamental period of the structure.

3.2.2.1 Interstory drift ratio

The Interstory Drift ratio (ID) is the ratio of the maximum relative displacement

between two stories to the story height. It is used as criteria for evaluating the damage level

to structural and nonstructural components after an earthquake. In the case of reinforced

concrete nonductile buildings, the interstory drift ratio is not a reliable measure of damage for

the following reasons:

- The interstory drift ratio does not account for the effects of cumulative damage due

  to repeated inelastic deformation with constant displacement amplitude. Experimental

  studies demonstrated that nonductile components are expected to suffer from

  significant damage due to repeated inelastic deformation.

- The interstory drift ratio does not account for the differences in the plastic deformation capacities (or the ductility class) of the structural systems. For example, the damage level corresponding to a 1.0% interstory drift ratio in a nonductile structure is expected to be much higher than that of a ductile building.

- The interstory drift capacity of a nonductile building is dependent on the deformation capacities of the plastic hinges of the developed plastic mechanism. Existing nonductile reinforced concrete buildings are characterized by a wide variation in the deformation capacities of the plastic hinges of the building members (beams or columns) or even whether the plastic hinge is located at the bottom or top end of the column. Moreover, changes may exist in the deformation capacities of the plastic hinges of the building columns from floor to floor depending on the level of axial forces. The variation in deformation capacities of the elements will cause a significant variation in the interstory drift capacity of the building. This is particularly evident in the case where a change in the characteristics of the developed plastic mechanism occurs as a result of adding a rehabilitation system to the building. It should be noted that such wide variation in the level of deformation capacities of the building elements is not expected to occur in ductile reinforced concrete buildings detailed according to current seismic codes.

3.2.2.2 Damage indices based on the vibrational parameters

A global damage index, known as "Final Softening" (FS) has been developed by Dipasquale and Cakmak (1988). The damage index is defined as:

$$FS = 1 - \frac{T_0^2}{T_{final}^2} \tag{3.3}$$

where T_0 and T_{final} are the building fundamental natural periods before and after the application of the dynamic loading, respectively. The fundamental period of the building is dependent on both the fundamental modal stiffness and the fundamental modal mass.

The final softening index is related to the global stiffness deterioration of the building and it has the advantage of avoiding the averaging procedure. In addition, the index has the advantage that the actual measurements of the fundamental period can be made before and after the earthquake. The final softening index can not be used to determine the deterioration in the building load carrying capacity or quantify the damage to the various stories.

The final softening index is limited to the case where the fundamental mode shape does not change significantly after seismic damage. Changes in the fundamental mode shape will cause a corresponding change in the modal mass leading to a final softening index that is no longer representative of the global stiffness deterioration.

3.3 PROPOSED DAMAGE EVALUATION APPROACH

The proposed damage evaluation approach provides indices for measuring damage to the various stories and to the whole building. The damage evaluation approach is based on measuring the stiffness degradation and strength deterioration for structures. Damage indices of the various stories and the whole building can be calculated as a percentage loss in stiffness or in the load carrying capacity due to the application of the dynamic load.

To calculate the damage indices that represent the deterioration in the stiffness or in the load carrying capacity, two pushover analyses are conducted on the building. The first pushover analysis is carried out before the application of the dynamic load, while the second pushover analysis is carried out after the application of the dynamic load, removing the inertia and damping force effects and bringing the building to the unloaded static state. Typical relationships between the lateral load and the roof (or story) drift before and after the dynamic load application are shown in Figure 3.2. A damage index that represents the deterioration of the building stiffness (D_g) is calculated as:

$$D_g = 1 - \frac{K_{final}}{K_o} \qquad (3.4)$$

where K_o and K_{final} represent the slopes of the lateral load-roof drift relationships in the linear range of deformation before and after the dynamic load application, respectively. In the current study, the values of K_o and K_{final} are considered as the secant stiffnesses at roof drift ratio of 0.25%, before the structure undergoes significant inelastic deformation. Similarly, a damage index, D_i, can be calculated from the lateral load-i^{th} story drift relationships before and after the dynamic load application to measure the stiffness deterioration of the ith story as follows:

$$D_i = 1 - \frac{K^i_{final}}{K^i_o} \qquad (3.5)$$

where K^i_o and K^i_{final} represent the slopes of the lateral load-i^{th} story drift relationships in the

linear range of deformation before and after the dynamic load application, respectively.

Another damage index (D_g^*) that measures the load carrying capacity deterioration of the whole building due to the dynamic load application can also be calculated from the two pushover analyses. This index is defined as:

$$D_g^* = 1 - \frac{F_{final}}{F_o} \tag{3.6}$$

where F_o and F_{final} are the initial and the final lateral load carrying capacities of the building as determined from the pushover analyses before and after the dynamic load application as shown in Figure 3.2. The calculation of the damage index (D_g^*) requires the use of beam-column models that account for the strength softening behaviour of nonductile reinforced concrete members after reaching their ultimate strength levels.

The values of the proposed damage indices representing the stiffness degradation and the lateral load carrying capacity deterioration of a particular story or the entire building as given by equations 3.4 to 3.6, vary between zero and one. A value of one for the index represents collapse. However, in practical terms failure of the building may be defined at a lower damage index corresponding to a certain percentage loss of the lateral load carrying capacity. The Damage indices (D_i) are useful in determining the distribution of damage among the various stories.

The advantage of the proposed damage indices is that they represent an actual measure of the deterioration of the stiffness and load carrying capacity of a story or the total building. These damage indices are obtained without the need for an averaging or weighing

procedure to integrate the effect of the building elements. The effect of the ground motion duration was taken into consideration as the repeated cycles will cause deterioration in stiffness and strength of the building elements and therefore will cause a corresponding increase in the damage level.

3.4 CHARACTERISTICS OF THE DEVELOPED DAMAGE INDICES

The applicability of the damage indices D_s and D_s^* for evaluating the seismic damage of a structure is dependent on the models used for representing the structure behaviour. Nonductile models such as the model developed in Chapter 2 are used for representing the behaviour of RC components that are not seismically designed and in which a number of brittle failure modes may be experienced in the process of inelastic deformation. In this type of models, cyclic loading is expected to cause significant stiffness deterioration and strength softening. The strength softening of nonductile members in the post peak range usually occupies most of the member time history response. Damage in this type of model can be defined as the deterioration levels in the stiffness or the strength magnitudes using the developed damage indices D_s and D_s^*. The two indices measure the deterioration in two different properties of the structure and provide sufficient information for assessing the damage to nonductile structures due to the application of earthquake loading.

On the other hand, ductile models are used for representing the behaviour of well designed RC components according to current seismic codes in which brittle failure modes are prevented through proper design and detailing of individual members. Examples of this type of model include the models developed by Takeda et al.(1970), Roufaiel and Meyer

(1987) and Park et al. (1987). Most of the available damage models are derived for ductile models as pointed out in section 3.2. Strength softening is not represented in these models. For ductile behaviour, it is assumed that strength softening will occur at a late stage of response with rapid rate as a result of the previously accumulated damage and that failure in this type of behaviour can be considered to be associated with the onset of the strength softening (Krawinkler, 1987). The damage index D_e^* is not applicable for the case of ductile behaviour and is not similar to other damage models derived on the basis of an assumed ductile behaviour. It is only limited to the structural components that exhibit deterioration in strength due to cyclic loading. On the other hand, the stiffness-based damage index D_k can be used in damage evaluation of both ductile and nonductile RC components as both exhibit stiffness deterioration under the effect of cyclic lateral loading. There is a similarity between the damage index D_k and the final softening index proposed by Dipasquale and Cakmak (1988). This similarity arises due to the strong relationship between the structure stiffness and fundamental period.

3.5 EFFECT OF THE LATERAL LOAD DISTRIBUTION

The lateral load carrying capacity and stiffness of the nonductile building as calculated from the pushover analysis are dependent on the distribution of the applied lateral load used in the analysis. When the structure behaviour is dominated by the first mode response, the pushover analysis can be conducted using an increasing inverted triangular lateral load. For multi story structures, the appropriate criteria for selecting the lateral load distribution is to obtain a shear force distribution along the building height that is as close as possible to the

shear distribution caused by the earthquake loading. This criterion is difficult to apply accurately and therefore a certain level of approximation is required. Recently, adaptive lateral load patterns were utilized in the pushover analysis to follow more closely the time variant distribution of the inertia forces. Krawinkler (1996) reviewed the available adaptive load patterns. He concluded that none of the available adaptive patterns have proven to be universally applicable.

In order to evaluate the effect of the lateral load distribution used in the pushover analysis on the proposed damage indices, two nonductile reinforced concrete frames with different heights are analyzed. The two interior frames are from two reinforced concrete office buildings that are designed to represent existing non-ductile reinforced concrete buildings. The buildings are three and nine stories representing low to moderate height nonductile buildings. They are designed for gravity loads only according to the 1963 ACI code (ACI 318-63). Detailed description of the three-story building is presented in section 2.7 while the nine story building is discussed in section 4.2.

Three types of applied lateral loads are considered: a) a uniformly distributed lateral load along the frame height; b) an inverted triangular code-type lateral loading; c) a concentrated load at the roof level. A lateral load with shear force distribution along the building height similar to the shear distribution caused by the earthquake loading at maximum response in the linear elastic range was also considered. The selected lateral load distributions give a wide variation of shear force distribution along the building height. The frame members were modelled using the beam-column model presented in Chapter 2. The dynamic analyses of the nonductile frames were carried out using a time step increment of 0.005

second and viscous-damping which was defined to achieve 2.0% damping in the first two

natural modes of the frames. The P-Δ effect was considered in the analysis. The results of

the three story and the nine story buildings are discussed separately in the following

subsections.

3.5.1 Response of the three-story building

The three story building was subjected to scaled versions of El Centro, Mexico City

and Nahanni ground motion records. Detailed information regarding these ground motion

records is summarized in Chapter 4. Figures 3.3 and 3.4 show the lateral load-roof drift

relationships of the three-story frame before and after the application of El Centro earthquake

(PGA=0.3 g). In the DRAIN-2DX program, the final pushover analysis is conducted after

removing the inertia and damping force effects and bringing the building to the unloaded static

state. Figures 3.5 and 3.6 show the relationships between the PGA level of El Centro

earthquake and the damage indices D_g and D_g^*, respectively. The different cases of lateral

load distribution are plotted on the figures. Figures 3.7 and 3.8 represent the damage indices

variation with the PGA of the Mexico earthquake. The results obtained when applying the

Nahanni earthquake are shown in figures 3.9 and 3.10. Figures 3.3 and 3.4 indicate that the

lateral load distribution has a significant effect on the magnitude of the lateral load carrying

capacity and stiffness of the nonductile frame. However, figures 3.5 to 3.10 indicate that in,

general, the distribution of the applied lateral load has a smaller effect on the values of the

damage indices D_g and D_g^* in the case of the three story frame. This is because the damage

index is the ratio of two values from two pushover analyses calculated using the same

approximate load distribution. For example, in the case of El Centro earthquake at PGA= 0.4 g, the values of D_g^* calculated by the concentrated, inverted triangular and uniform lateral load distributions show differences of approximately 9.0%, 2.0% and 0.0%, respectively, from the value calculated by the lateral load with shear force distribution similar to the shear distribution caused by the earthquake loading. The corresponding values of D_g calculated by the concentrated, inverted triangular and uniform lateral load distributions show differences of approximately 11.0%, 4.0% and 0.0%, respectively, from the value calculated by the lateral load with shear force distribution similar to the shear distribution caused by the earthquake loading.

It is concluded from the response of the three-story building that both the uniform and the inverted triangular lateral load distributions give values of damage indices approximately equal to the values calculated using the earthquake lateral loading although the shear force distribution, lateral load carrying capacity and the stiffness of the frame are significantly different in the two cases of load distribution. The calculated damage indices are not very sensitive to whether a uniform or inverted triangular lateral load distribution is used to perform the pushover analysis in the case of the three-story building.

3.5.2 Response of the nine-story building

The seismic Analysis of the nine story frame was carried out using scaled versions of the San Fernando, Mexico and Long Beach earthquakes. The Mexico earthquake was used before in the analysis of the three story building. The other two records, San Fernando and Long Beach, are used in the analysis of the nine story building as they represent low

frequency content records. Detailed information regarding these ground motion records is summarized in Chapter 4. Figure 3.11 shows the lateral load-roof drift relationships of the frame before the application of the dynamic loads for the three cases of lateral load distributions. Figure 3.12 shows the lateral load-roof drift relationships of the frame after the applications of San Fernando earthquake with (PGA=0.3 g). Figures 3.13 and 3.14 represent the relationships between the PGA level of the San Fernando earthquake and the damage indices D_g and D_g^*, respectively. The predicted response to the Mexico City earthquake is shown in figures 3.15 and 3.16, while for the Long Beach earthquake is shown in figures 3.17 and 3.18. Figures 3.11 and 3.12 show the significant effect of the lateral load distribution on the magnitude of the lateral load carrying capacity and stiffness of the nonductile frame. Figures 3.13 to 3.18 show that the damage indices calculated using both the uniform and the inverted triangular lateral load distributions are approximately equal to the values calculated from the earthquake lateral loading. Damage indices calculated in the case of the concentrated lateral load are slightly smaller in magnitude than those calculated due to the other lateral load distributions.

The predicted shear force distribution along the frame height in the linear elastic analysis range at maximum response of the San Fernando, Mexico and Long Beach earthquakes are shown in figures 3.19, 3.20 and 3.21, respectively, along with the shear distributions in the frame due to the three lateral load distributions. The figures indicate that the shear force distribution due to the inverted triangular lateral loading represented an upper limit of the shear distribution along the frame height. The shear force distribution of the uniform lateral loading tended to underestimate those of the earthquakes. Both the uniform

and the inverted triangular lateral load distributions give values of damage indices approximately equal to the values calculated using the earthquake lateral loading. Selecting either lateral load distribution to perform the pushover analysis in the case of the nine story building results in reliable damage values.

3.6 RELATIONSHIP BETWEEN D_ϵ AND THE FINAL SOFTENING INDEX

There is a similarity between the damage index D_ϵ and the final softening index proposed by DiPasquale and Cakmak (1988). This similarity is due to the fact that the fundamental period of the structure is dependent on the structure stiffness. A comparison was performed between the damage index D_ϵ and the final softening index defined by equation 3.3 for the cases of the three-and nine-story frames using several earthquakes. Figures 3.22, 3.23 and 3.24 show the relationships between D_ϵ and the final softening index for the three-story frame in the case of El Centro, Mexico and Nahanni ground motions, respectively. Figures 3.25, 3.26 and 3.27 show the relationship between D_ϵ and the final softening index for the nine-story frame in the case of San Fernando, Mexico and Long Beach ground motions, respectively.

In the case of the three story frame the final softening index approaches the D_ϵ at some points and slightly underestimates it at others. In the case of the nine story frame, the final softening index significantly underestimates the value of D_ϵ. The results suggest that the final softening index does not properly represent the deterioration of the building stiffness. The predicted trend of the final softening index may be because of the following reasons:

First, in the case of reinforced concrete buildings that are damaged due to an

earthquake loading, it is expected that the building stiffness will be dependent on the loading direction. The final fundamental period used in calculating the final softening index is determined after the application of the last increment of the earthquake loading with no control over the loading direction. This will lead to some randomness in the calculated instantaneous stiffness of the structure at the final step of the earthquake loading. In the case of the damage index D_p two different final stiffnesses are calculated using two final pushover analyses (e.g, from right to left and from left to right). Each of the final pushover analyses is performed after removing the inertia and damping force effects and bringing the frame to a static state. The smaller stiffness is used in calculating the stiffness index D_s.

Second, the time windows for the calculations of the fundamental period and the pushover stiffness are different. The fundamental period is calculated at an instant using the tangent stiffness of the structure at the end of the dynamic load. While in the case of D_p the pushover stiffness is calculated using a wider time window representing the pushover loading time from point "o" to point "a" as indicated on the pushover plot shown in figure 3.4. A wider time window provides much more reliability in determining a representative value of the building stiffness, especially when the calculations are performed on the damaged structure suffering from residual deformations and forces after the application of the dynamic load. It was observed during the analysis of some cases that the instantaneous stiffness of the damaged structure at the first loading increment of the pushover is higher than the stiffness calculated after the application of few loading increments. This is attributed to the fact that the element residual forces which result from the dynamic loading affect the element pushover stiffness. Figure 3.28 represents two different cases of the moment-rotation relationship of

the structure plastic hinges. In case I of figure 3.28, the residual moment and the pushover loading are in the same direction, while in case II, the residual moment and the pushover loading are in opposite directions. In general, when pushing a structure laterally after the application of the earthquake loading, it is expected that some of the plastic hinges of the structure are similar to case II of figure 3.28, especially when the structure is affected by the higher modes of vibrations. Figure 3.29 shows the expected force-displacement relationship from the pushover analysis. The instantaneous stiffness of the structure at the first loading increment is higher than the stiffness calculated at other loading increments in the linear range of the force-displacement relationship. This explains why the final softening index tends to be lower than the damage index D_k. The instantaneous stiffness of the structure at the first loading increment will be influenced by the residual forces and can not be considered as a representative value of the building stiffness, especially when the calculations are performed on a damaged structure after the application of the earthquake loading. The approach considered in calculating the pushover stiffness in the current study provides a reliable representation of the building stiffness. In case of the nine-story building the effect of the residual forces will be more pronounced due to the effect of higher modes of vibrations.

Third, the calculations of the final softening index may be affected by the changes in the fundamental mode shape due to inelastic response. These changes will cause a corresponding change in the modal mass leading to a final softening index that is no longer representative of the global stiffness deterioration.

3.7 RELATIONSHIP BETWEEN D_g^* AND STORY DRIFT

The use of story drift as a measure of seismic damage may not be appropriate in case of nonductile reinforced concrete building structures. Existing nonductile buildings are characterized by a wide variation in the deformation capacities of the plastic hinge regions of the building members and therefore significant variation in the story drift capacities of nonductile reinforced concrete buildings are expected to occur depending on the experienced mode of failure.

The relationships between the story drift ratio and the damage index D_g^* were evaluated for the three-and the nine-story frames. Figures 3.30 and 3.31 represent the relationships between the story drift ratio and the damage index D_g^* due to the application of San Fernando and Mexico earthquakes, respectively. Both the three-and the nine-story frame responses are included in each figure. The results shown in the figures indicate that the relationship between the story drift and the damage index is dependent on the building height. Different buildings with different heights may experience different modes of failures leading to significant variation in the story drift capacities corresponding to a certain level of damage. The nine-story frame exhibited higher story drift capacities as compared to the response of the three-story frame. The results presented in figures 3.30 and 3.31 indicate also that for a specific structure, the relationship between the story drift ratio and the damage index is earthquake dependent. Different earthquakes will have different frequency contents and different strong ground motion durations and this will lead to different relationships between the story drift and the damage index.

3.8 STORY DRIFT VARIATION

To evaluate the variation of plastic deformation along the building height under the effect of earthquake loading, a plastic mechanism parameter "v" is proposed to measure the variation in the story drift ratios corresponding to a certain roof drift. This parameter is useful in comparing the plastic mechanisms of buildings with different heights or retrofit options. In the current study, a 1.0 % roof drift ratio is considered in calculating the parameter "v". The selection of the specified roof drift is somewhat arbitrary, however, the 1.0 % roof drift ratio is assumed to represent an approximate intermediate value between the yield limit and the collapse limit of nonductile buildings. Collins and Foutch (1995) analyzed several buildings and used a 1.0 % roof drift ratio in obtaining an approximate estimate of the lateral displacement profile of the building in the inelastic deformation range. The proposed plastic mechanism parameter "v" is defined by the empirical relationship:

$$v = \frac{\sum_{i=1}^{i=n} |(S_i - 1.0)|}{2\,(n-1)} \qquad (3.7)$$

where S_i is the story drift ratio of the ith story multiplied by 100 and n is the total number of stories (n >1). The building stories are assumed to have equal heights, therefore, the average value of the story drift ratios of all the building stories will be equal to the roof drift ratio.

The nomirator of equation 3.7 represents the summation of the absolute differences between the story drift ratios and the average story drift ratio and it ranges theoretically between zero and 2(n-1). The denominator of the equation was chosen to make the value of the parameter v ranges between zero and 1. The case when v equals zero represents equal

story drift ratios for all the building stories. In this case, the necessary overall displacement ductility can be developed with relatively small story drift demand. The development of such plastic mechanism in building structures will lead to a relatively lower deformation and damage levels under the effect of the earthquake loading. On the other hand, the case when v equals 1 indicates that one story is the only source of the overall building deformation. In this case, the necessary overall displacement ductility is developed with relatively high story drift demand, leading to the development of relatively higher deformation and damage levels under the effect of the earthquake loading. In general, it can be expected that the lower the value of v, the better is the distribution of the story drift ratios of the nonductile building under the effect of lateral loading.

3.9 SUMMARY

The application of available damage models in the case of nonductile reinforced concrete components was evaluated. The damage models, either fail to account for duration of the ground motion or they were found to be based on an assumed ductile behaviour. It was found that the average procedure for integrating local damage indices of the building elements may yield inaccurate results.

A new procedure for evaluating the seismic damage of existing nonductile buildings was proposed. Damage indices for the various stories and the entire building are calculated as a percentage loss in stiffness or in the load carrying capacity due to the application of the dynamic load. The approach involves using the results of two pushover analyses; before and after the application of the earthquake loading.

It was found that the variation in the damage indices calculated from pushover analyses with different load distributions, is relatively small. The results indicate that using an inverted triangular loading or a uniform lateral load distribution will yield approximately equal values of the damage indices although the shear force distribution, lateral load carrying capacity and the stiffness of the frame are significantly different in the two cases of lateral load distributions.

In the case of the three-story frame the final softening index approaches the D_s at some points and underestimates it at others. In the case of the nine-story frame the final softening index significantly underestimates the damage of the frame as determined by the proposed approach. This was attributed to different reasons which include, the effect of the residual forces on the structure stiffness, the changes in the fundamental mode shape due to inelastic response and the randomness in the calculated instantaneous stiffness of the structure at the final step of the earthquake loading. The results suggested that the final softening index may not properly represent the deterioration of the building stiffness.

A parameter v was proposed for evaluating the plastic mechanism of building structures under the effect of lateral loading. The parameter v measures the uniformity of the distribution of the story drift ratios corresponding to a roof drift ratio of 1.0 % due to the application of lateral loading. The lower the value of v, the more desirable is the developed plastic mechanism of the building.

$[d_1^a, E_1^a]$

Plastic hinge

$[d_1^b, E_1^b]$ $[d_2^b, E_2^b]$

Plastic hinges
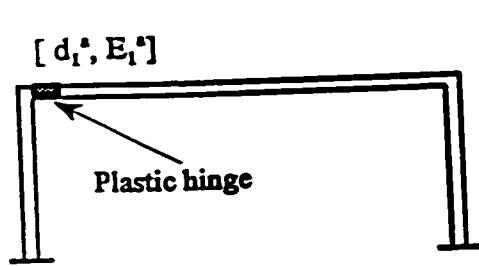
d_1^a is the local damage index

E_1^a is the dissipated hysteretic energy
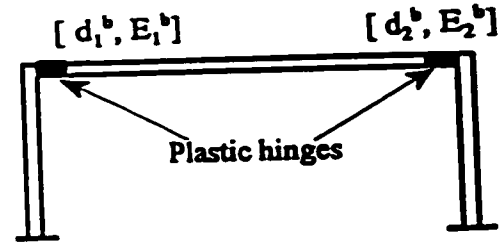
d_1^b, d_2^b are the local damage indices

E_1^b, E_2^b are the dissipated hysteretic energy

(a)

(b)

Figure 3.1 Two sequential damage states during an earthquake analysis

Lateral load

F_o

F_{final}

Before the earthquake

After the earthquake

K_{final}

K_o 0.25 %
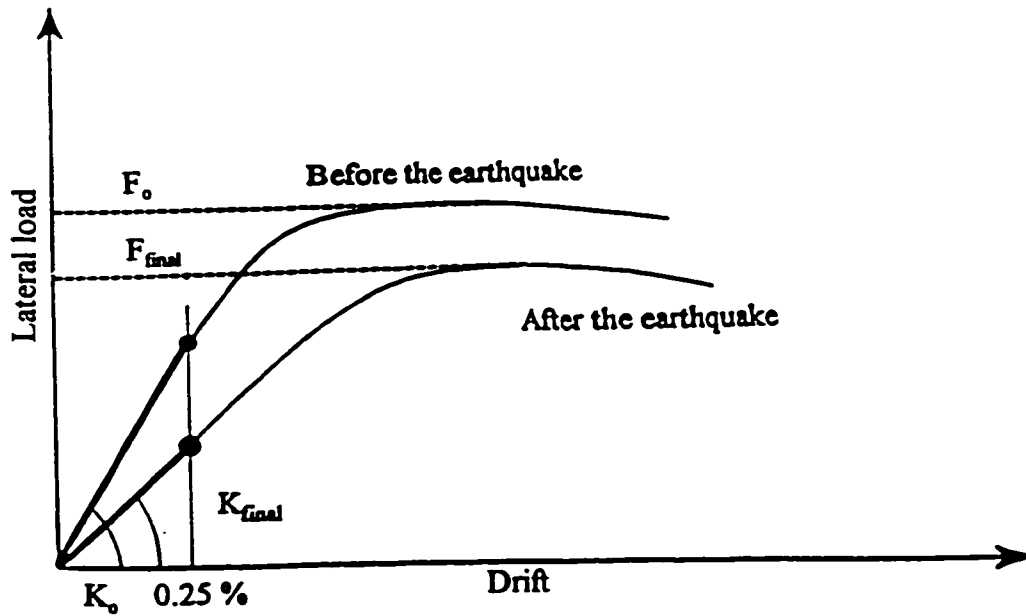
Drift

Figure 3.2 Typical relationships between the lateral load and the roof (or maximum story) drift ratio
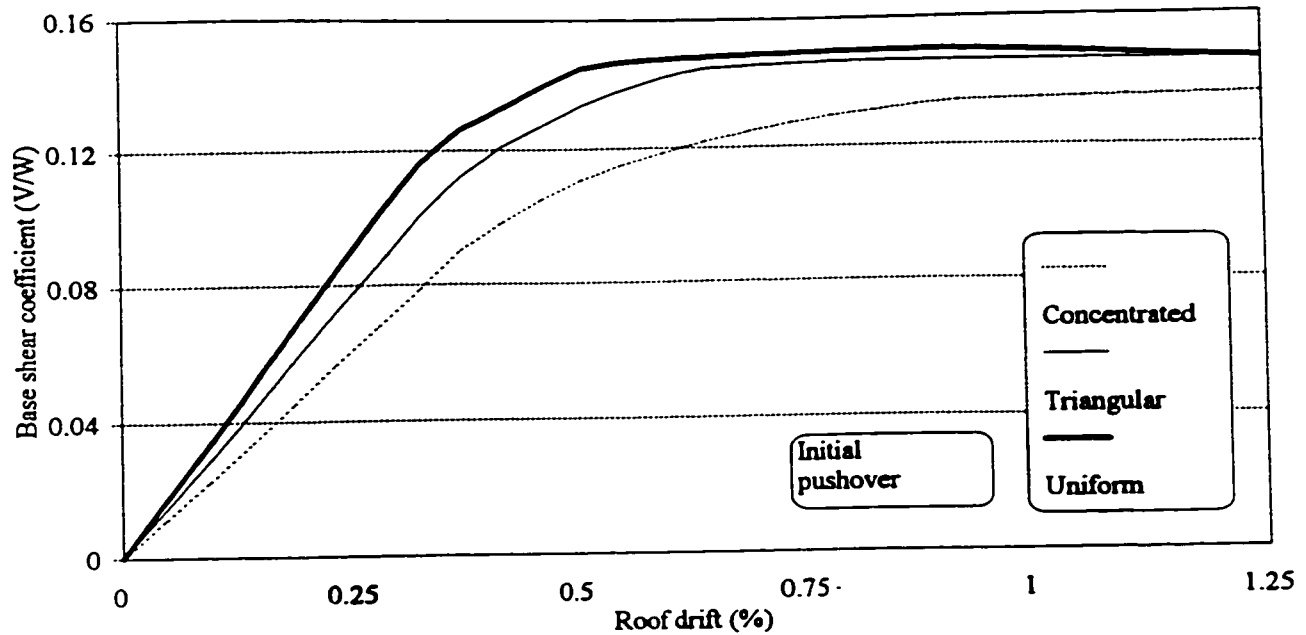
Figure 3.3 Lateral load-roof drift relationships of the three-story frame before the application of the dynamic loads using different lateral load distributions
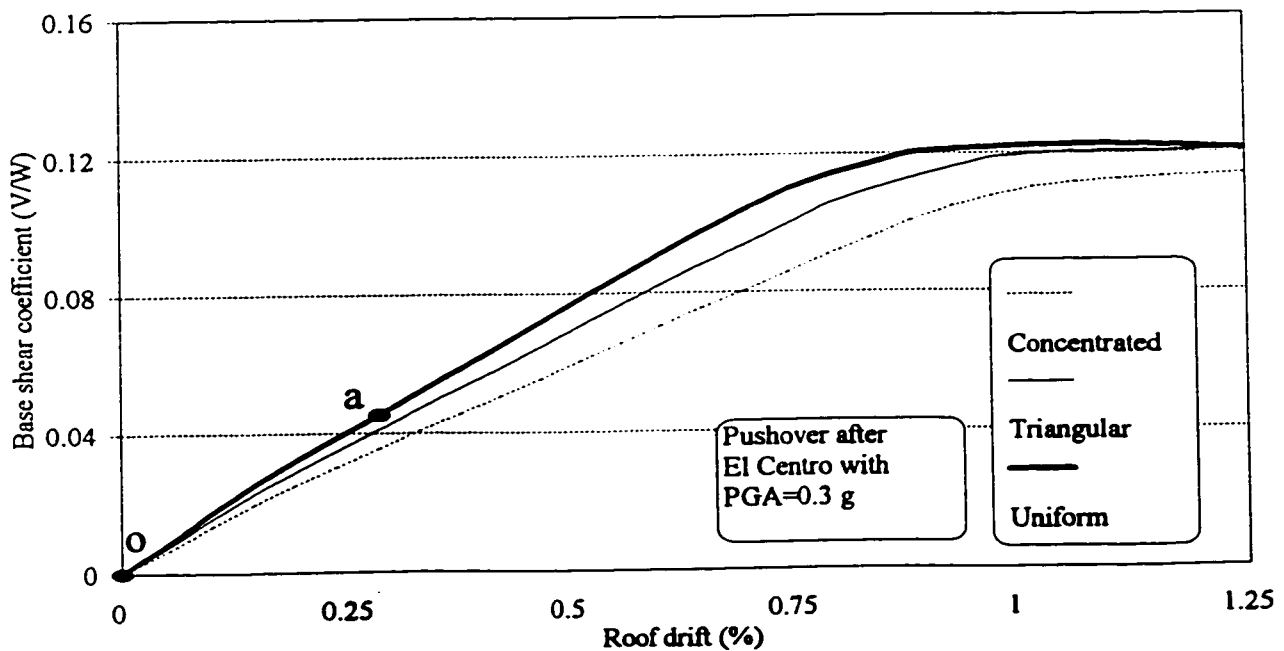
Figure 3.4 Lateral load-roof drift relationships of the three-story frame after the application of El Centro earthquake (PGA=0.3g)
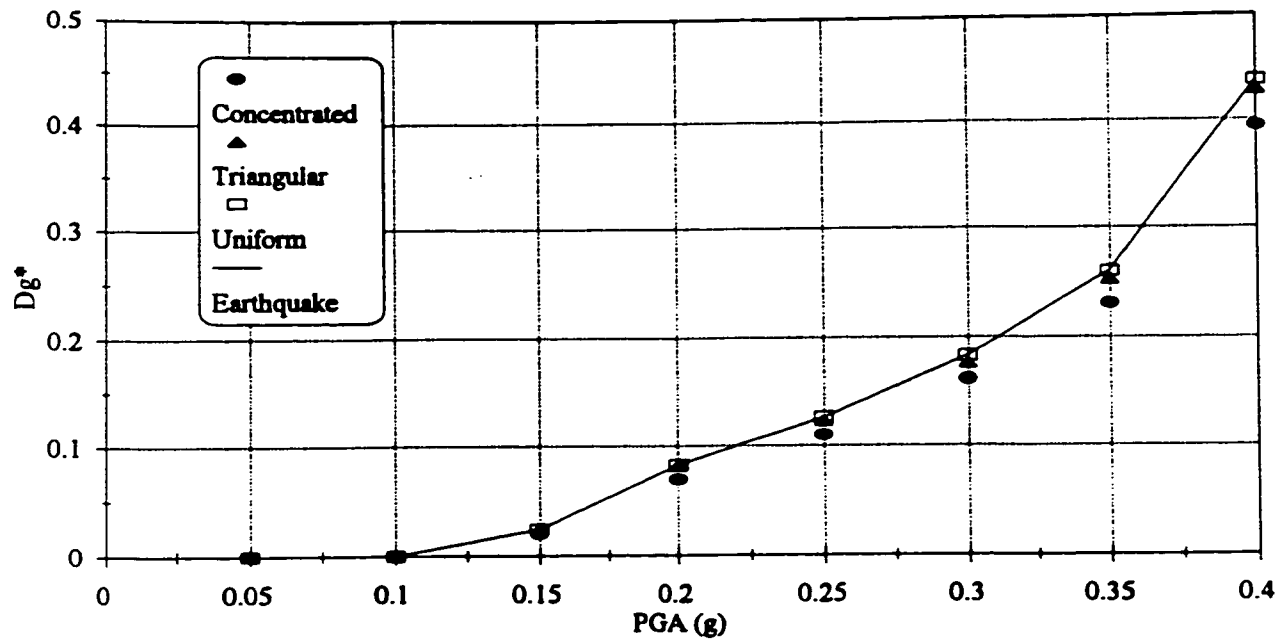
Figure 3.5 Relationships between the PGA level of El Centro earthquake and the damage index D_g^* for the three-story frame
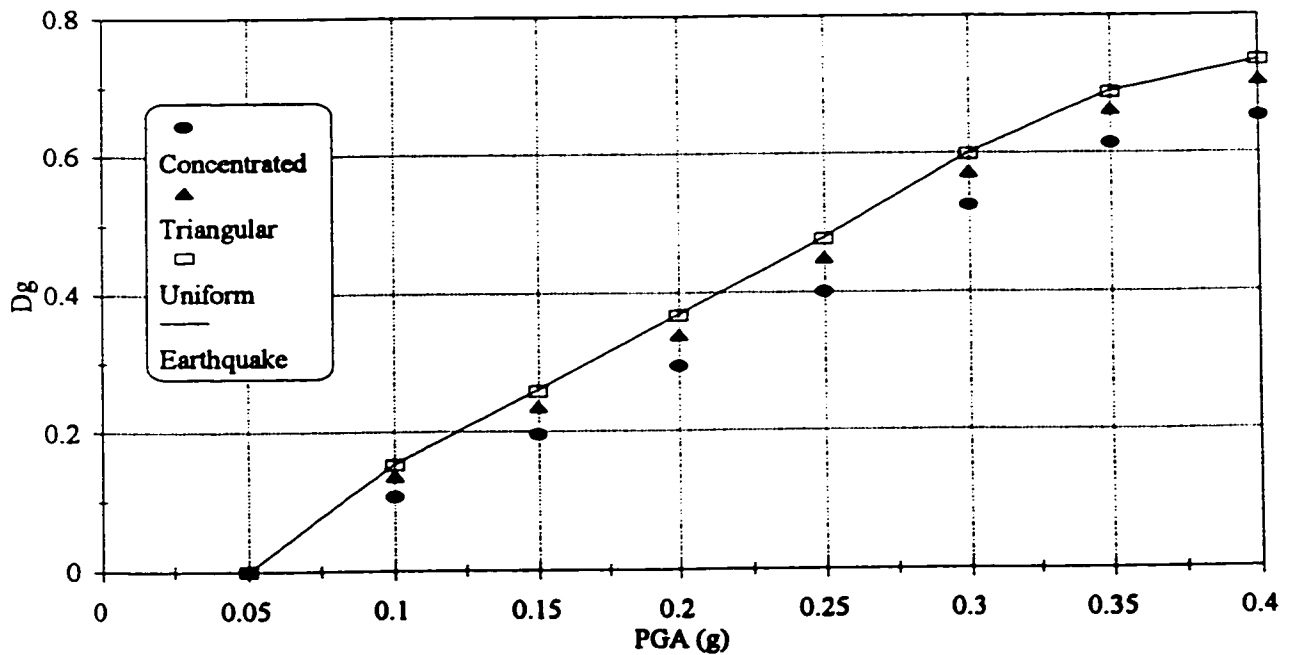
Figure 3.6 Relationships between the PGA level of El Centro earthquake and the damage index D_g for the three-story frame
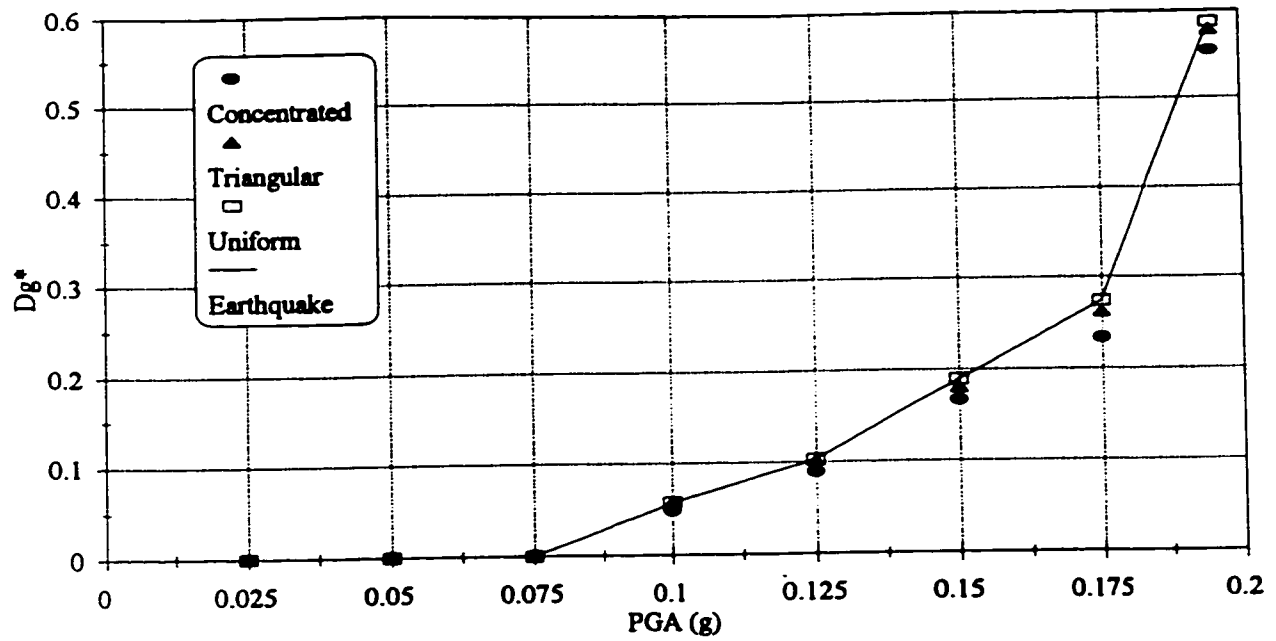
Figure 3.7 Relationships between the PGA level of Mexico earthquake and the damage index D_g^* for the three-story frame
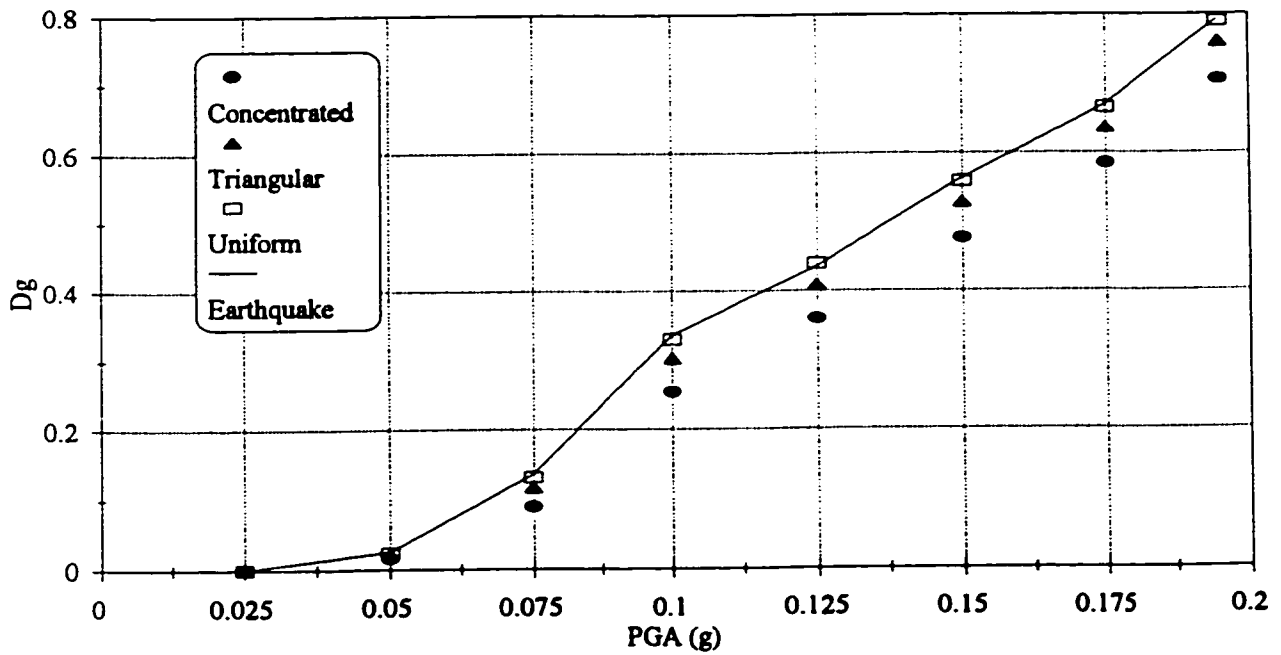
Figure 3.8 Relationships between the PGA level of Mexico earthquake and the damage index D_g for the three-story frame
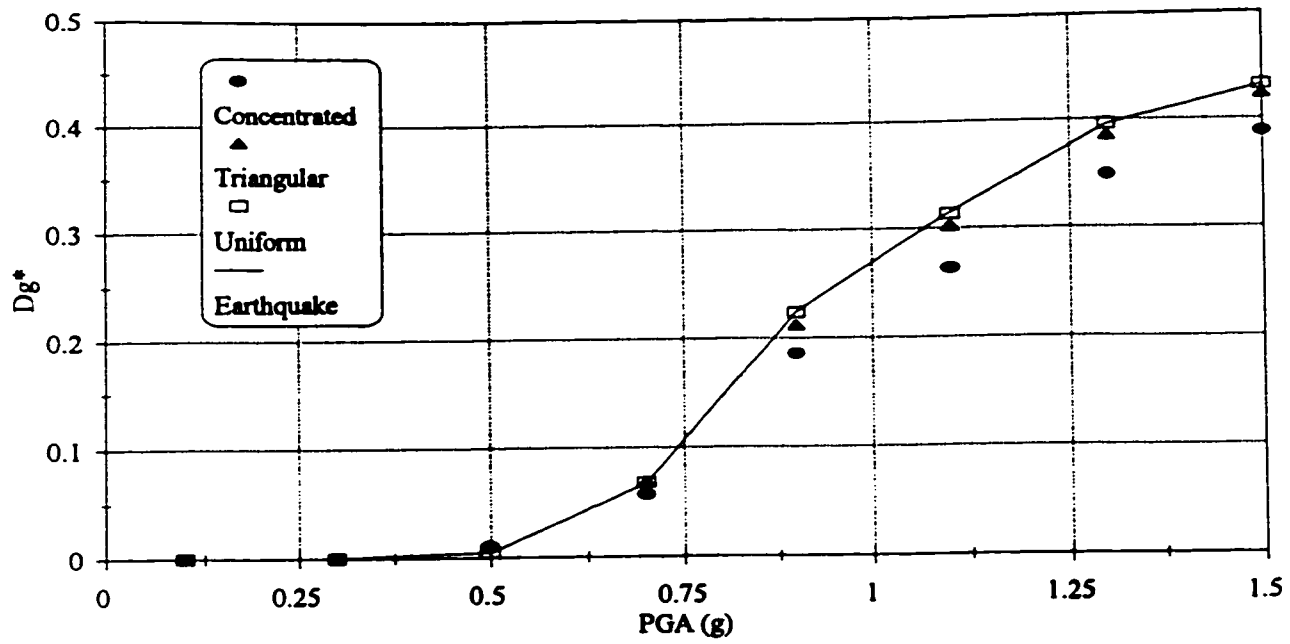
Figure 3.9 Relationships between the PGA level of Nahanni earthquake and the damage index D_g^* for the three-story frame
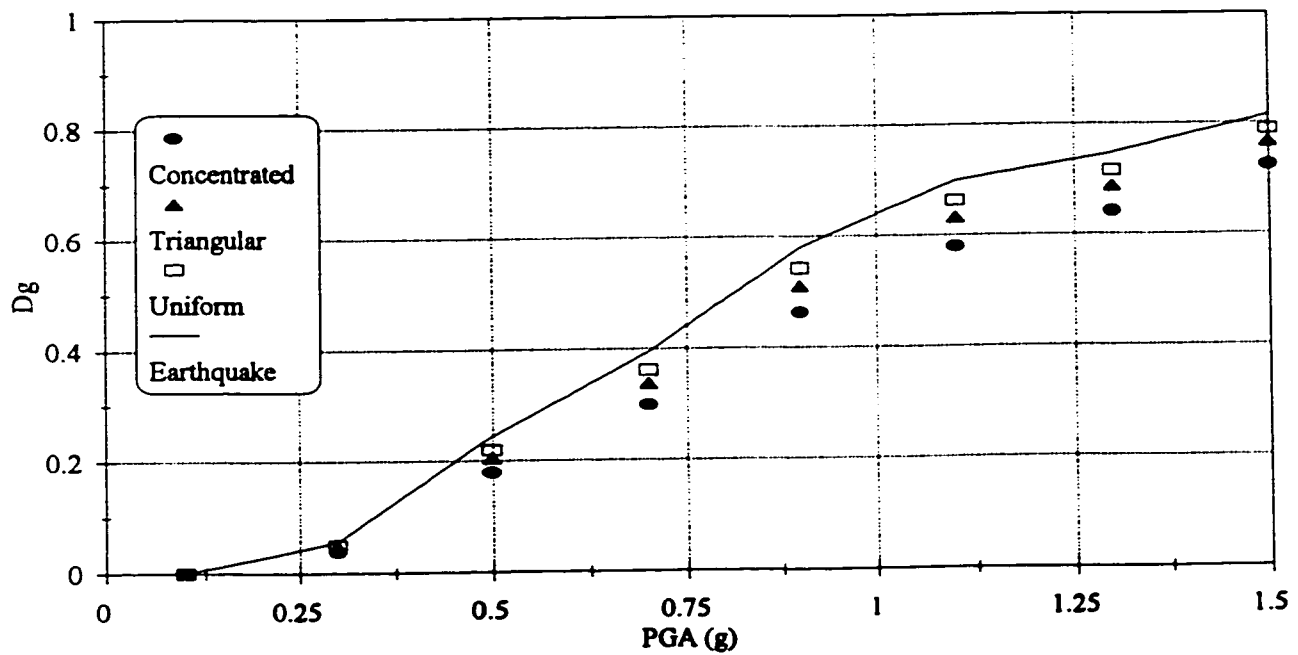
Figure 3.10 Relationships between the PGA level of Nahanni earthquake and the damage index D_g for the three-story frame
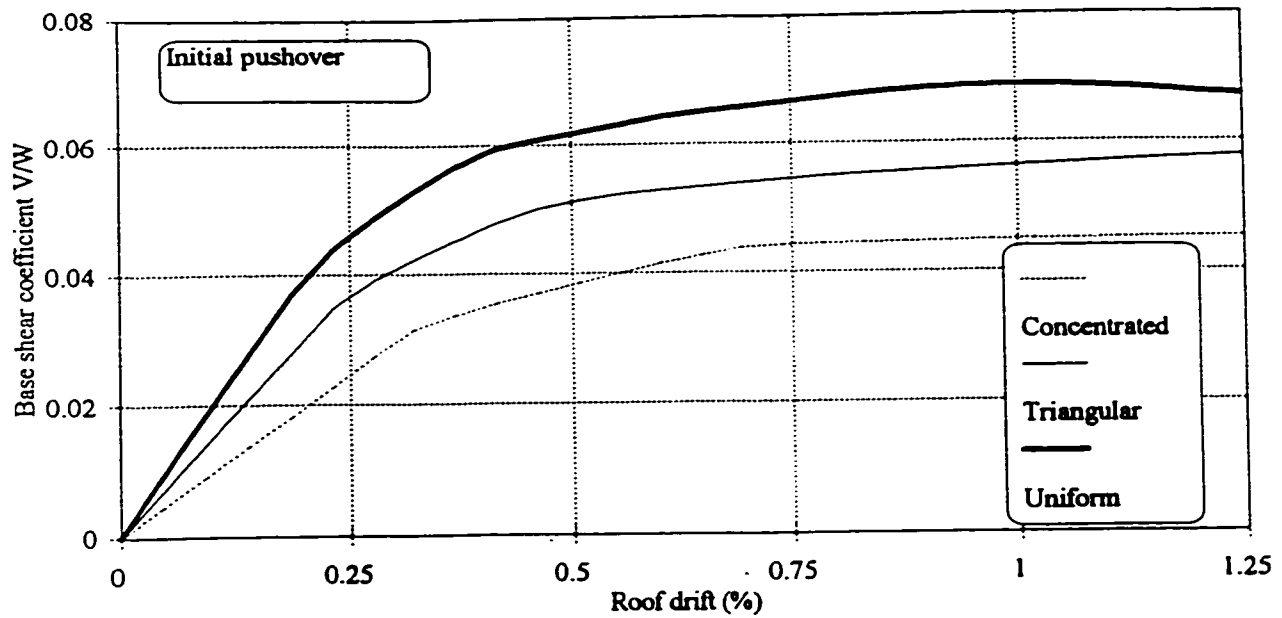
Figure 3.11 Lateral load-roof drift relationships of the nine-story frame before the application of the dynamic loads using different lateral load distributions
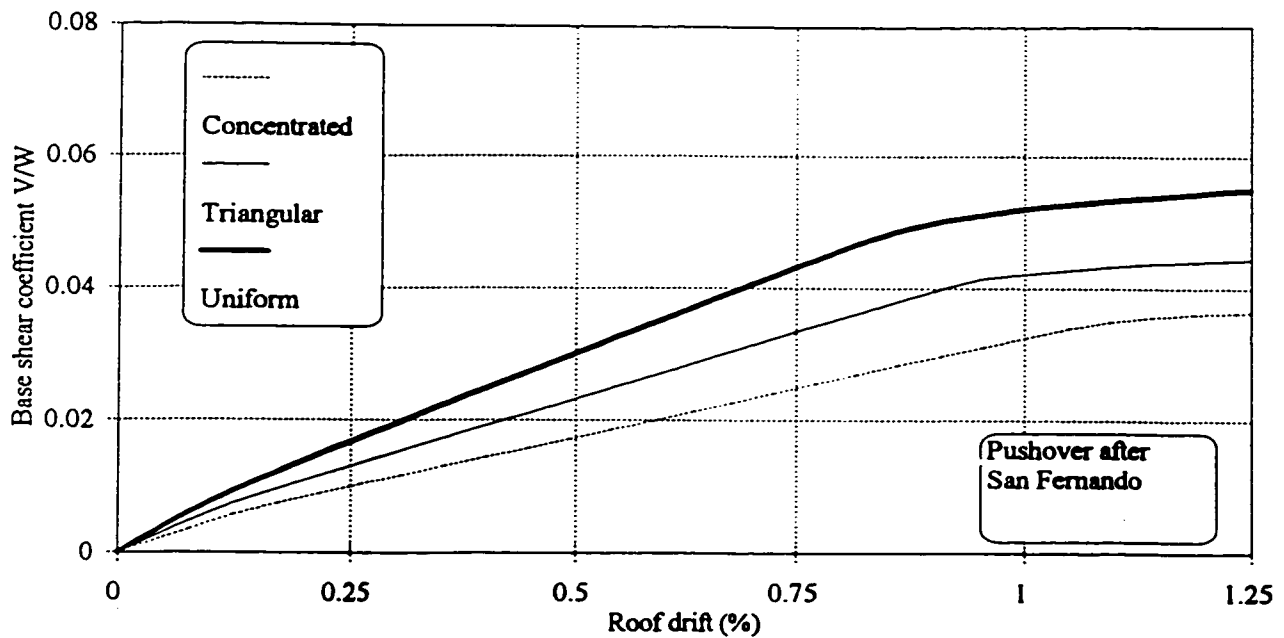
Figure 3.12 Lateral load-roof drift relationships of the nine-story frame after the application of San Fernando earthquake (PGA=0.3g)
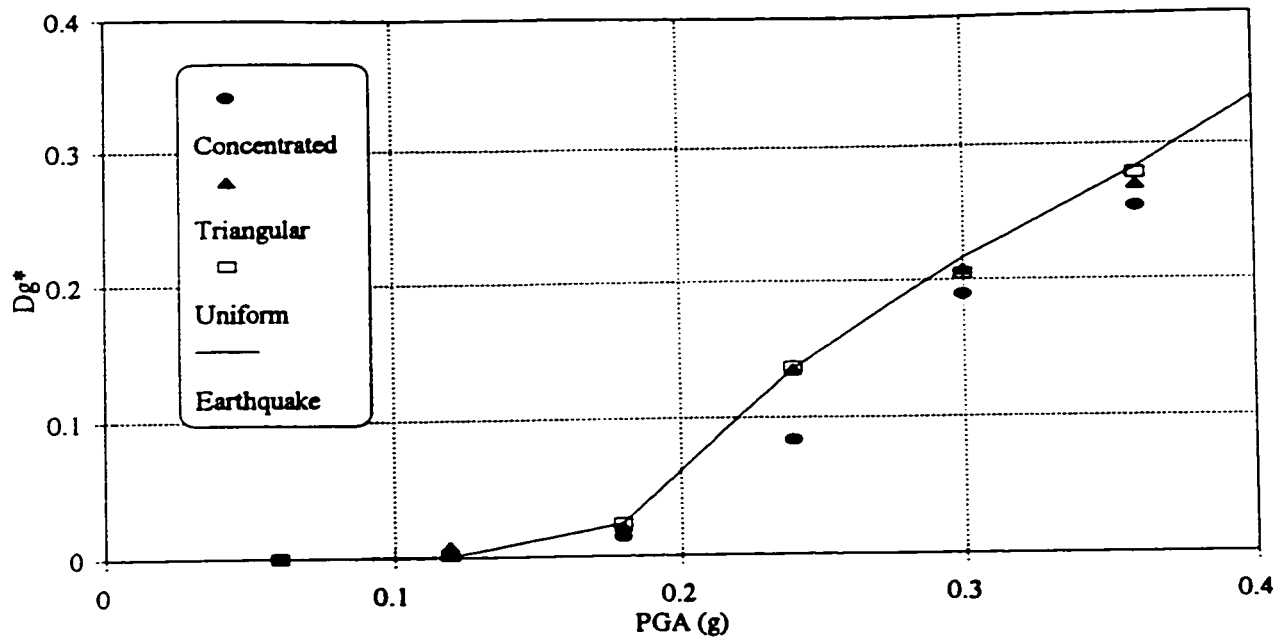
Figure 3.13 Relationships between the PGA level of San Fernando earthquake and the damage index D_g^* for the nine-story frame
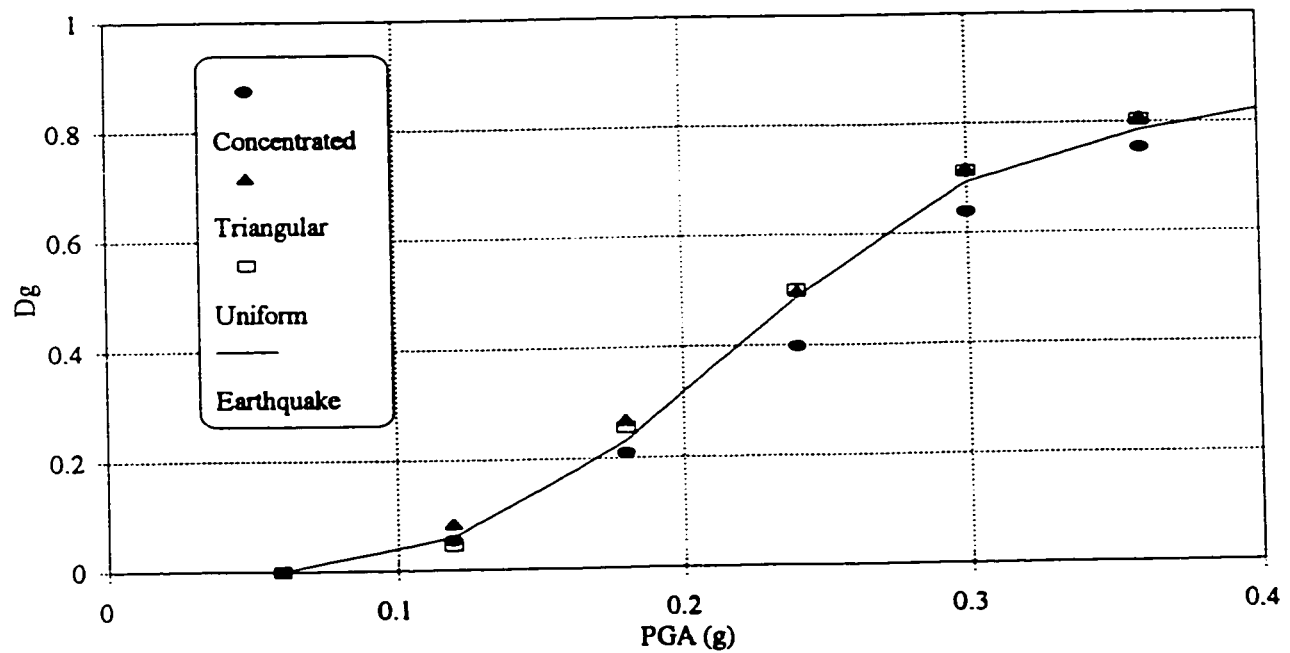
Figure 3.14 Relationships between the PGA level of San Fernando earthquake and the damage index D_g for the nine-story frame
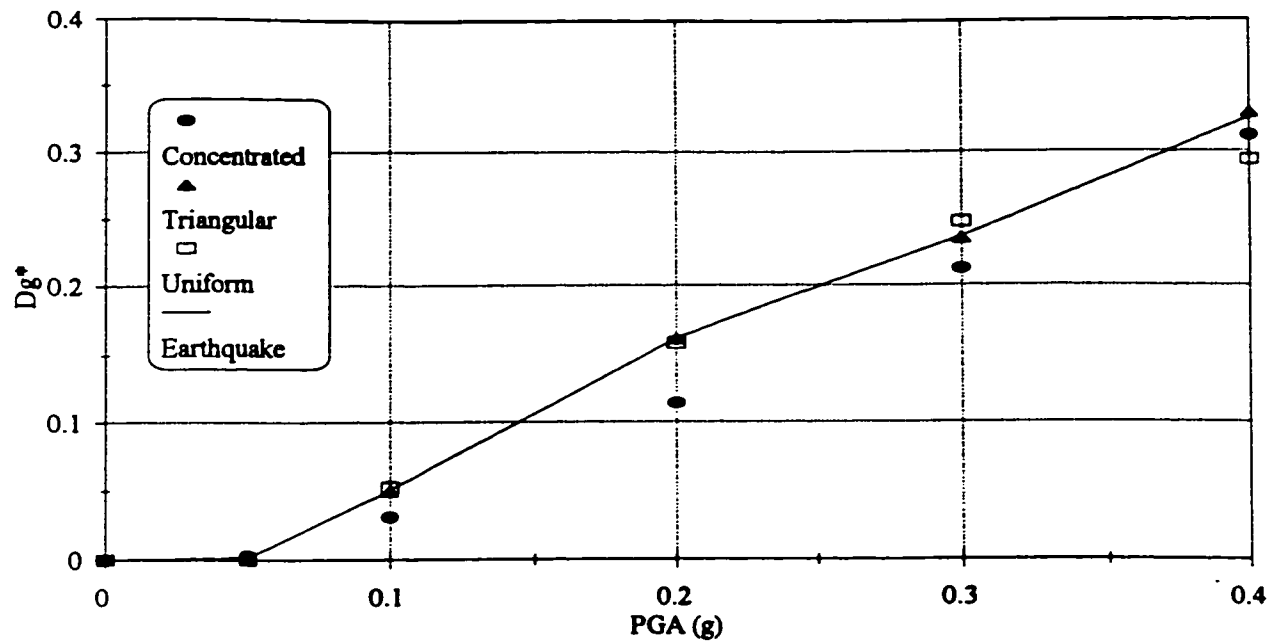
Figure 3.15 Relationships between the PGA level of Mexico earthquake and the damage index D_g^* for the nine-story frame
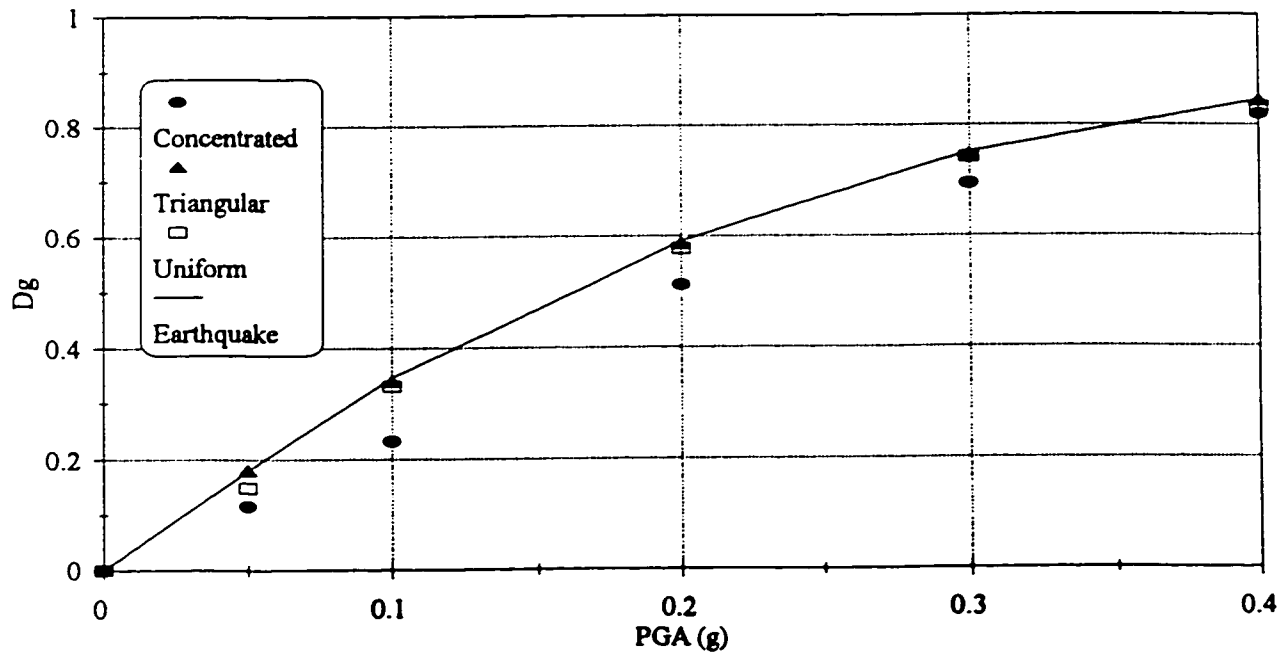
Figure 3.16 Relationships between the PGA level of Mexico earthquake and the damage index D_g for the nine-story frame
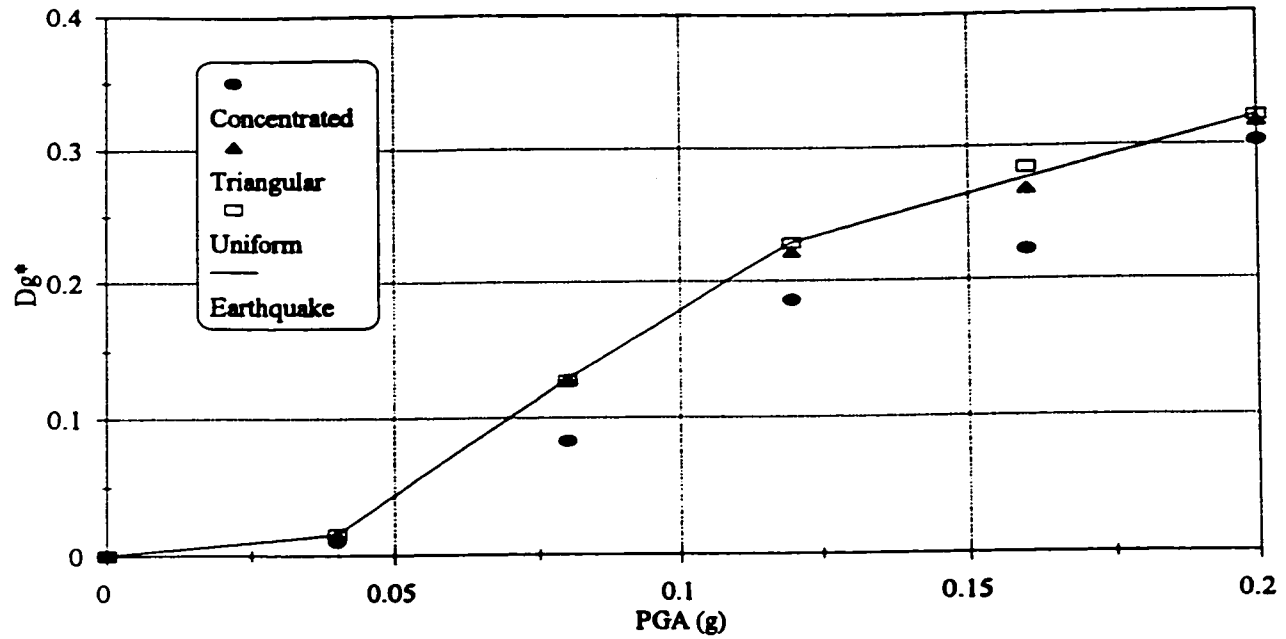
Figure 3.17 Relationships between the PGA level of Long Beach earthquake and the damage index D_g^* for the nine-story frame
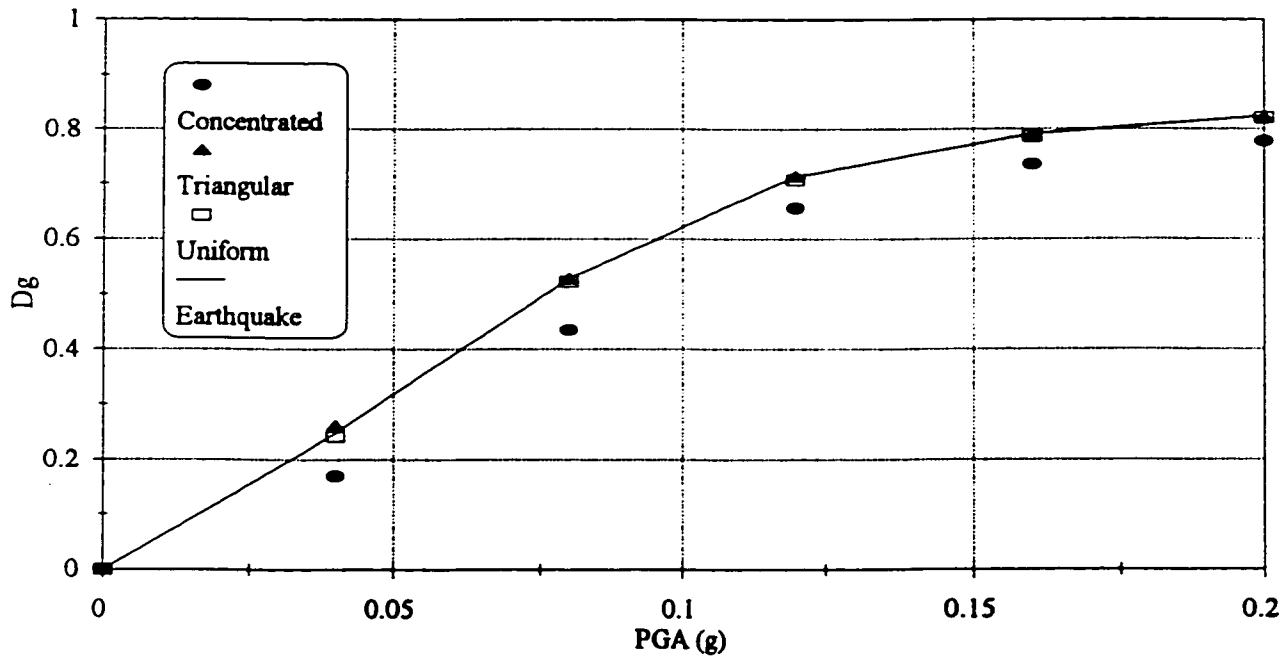
Figure 3.18 Relationships between the PGA level of Long Beach earthquake and the damage index D_g for the nine-story frame
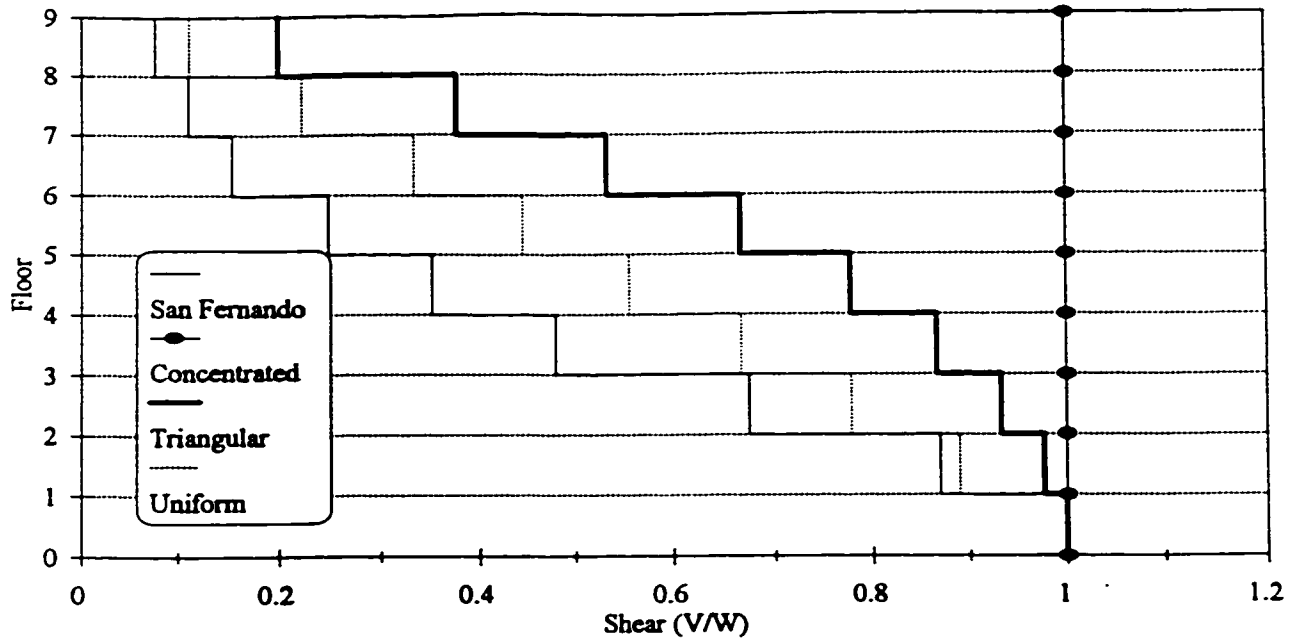
Figure 3.19 The shear force distribution along the nine-story frame height at maximum response of San Fernando earthquake as well as when using the three lateral load distribution cases
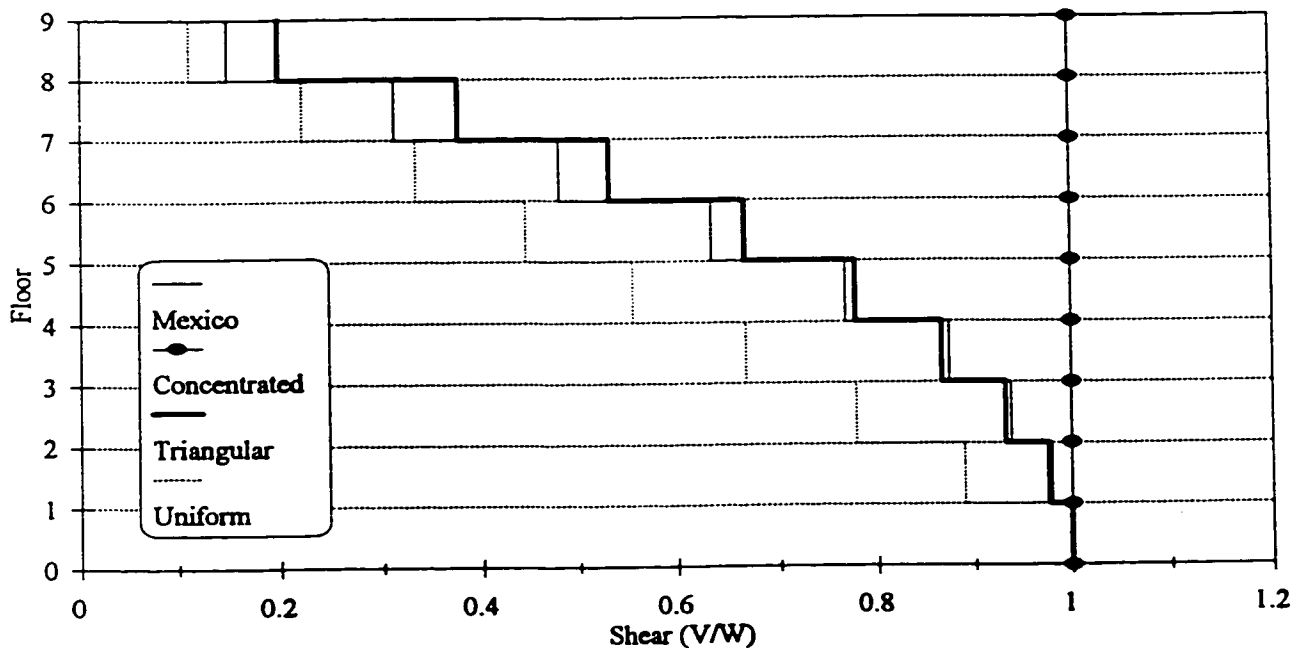
Figure 3.20 The shear force distribution along the nine-story frame height at maximum response of Mexico earthquake as well as when using the three lateral load distribution cases
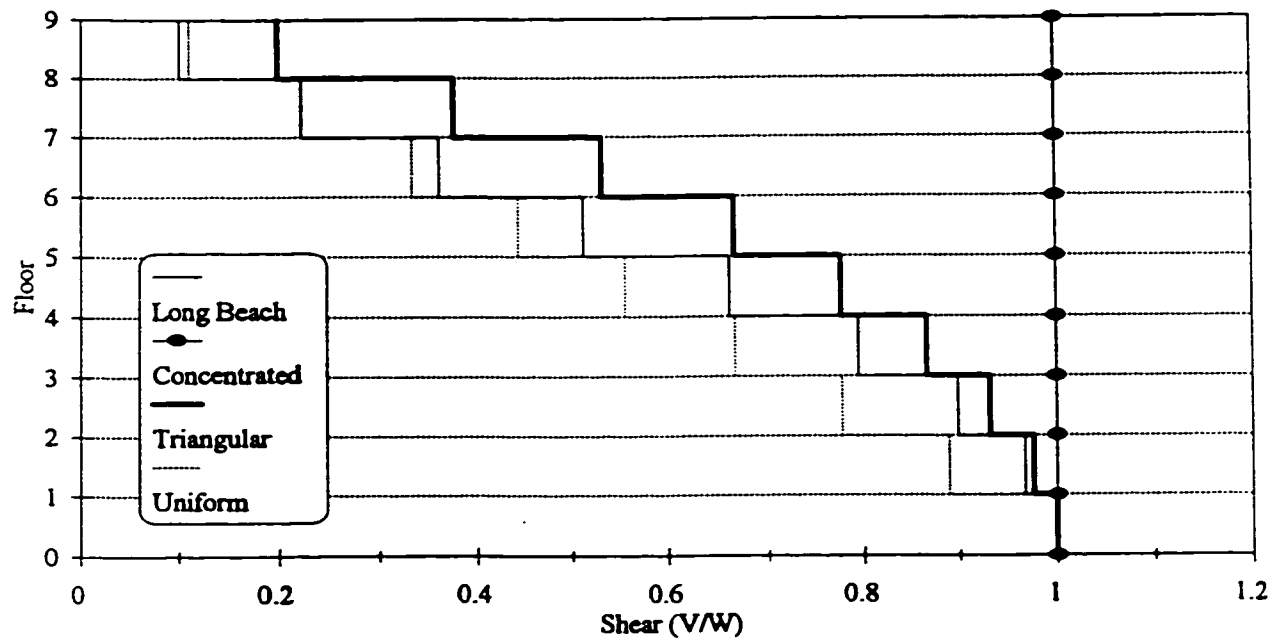
Figure 3.21 The shear force distribution along the nine-story frame height at maximum response of Long Beach earthquake as well as when using the three lateral load distribution cases
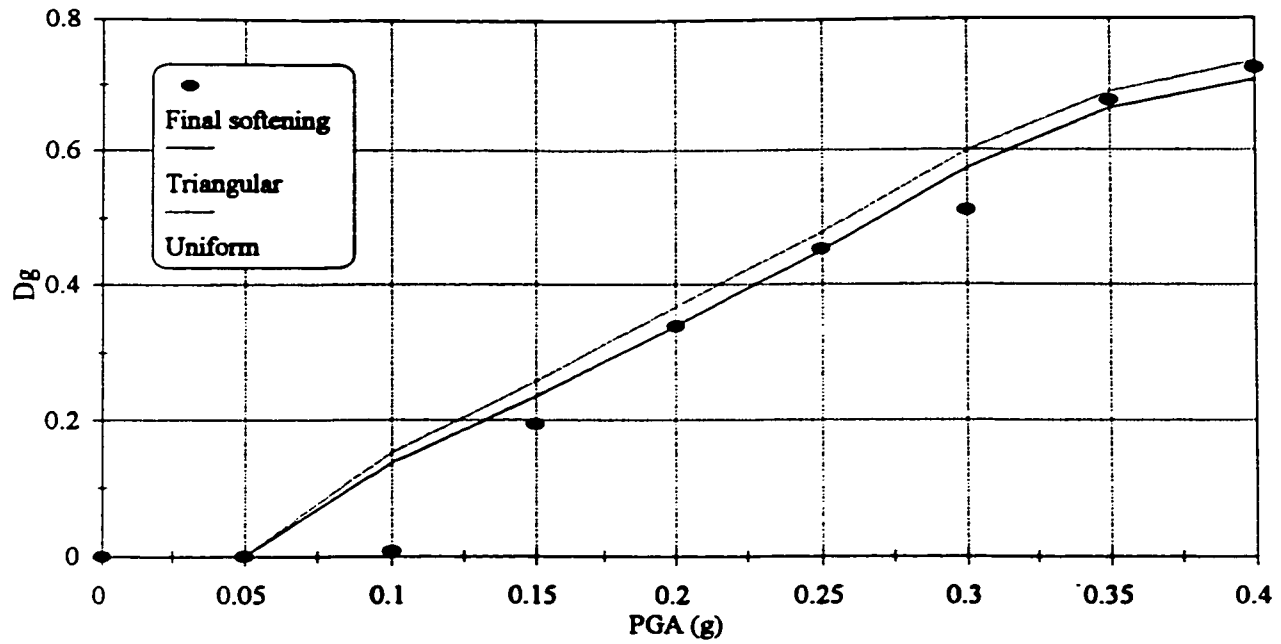
Figure 3.22 Variations of the damage index D_g and the final softening index with the PGA level of El Centro earthquake for the case of the three-story frame
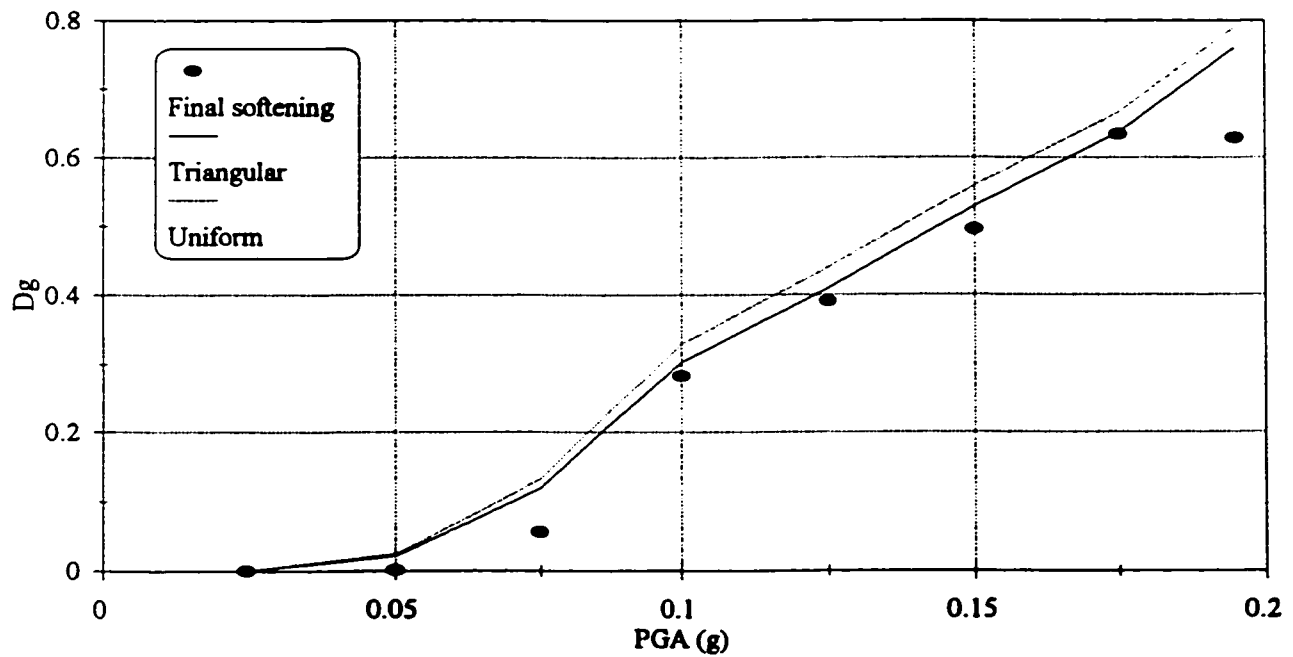
Figure 3.23 Variations of the damage index D_g and the final softening index with the PGA level of Mexico earthquake for the case of the three-story frame
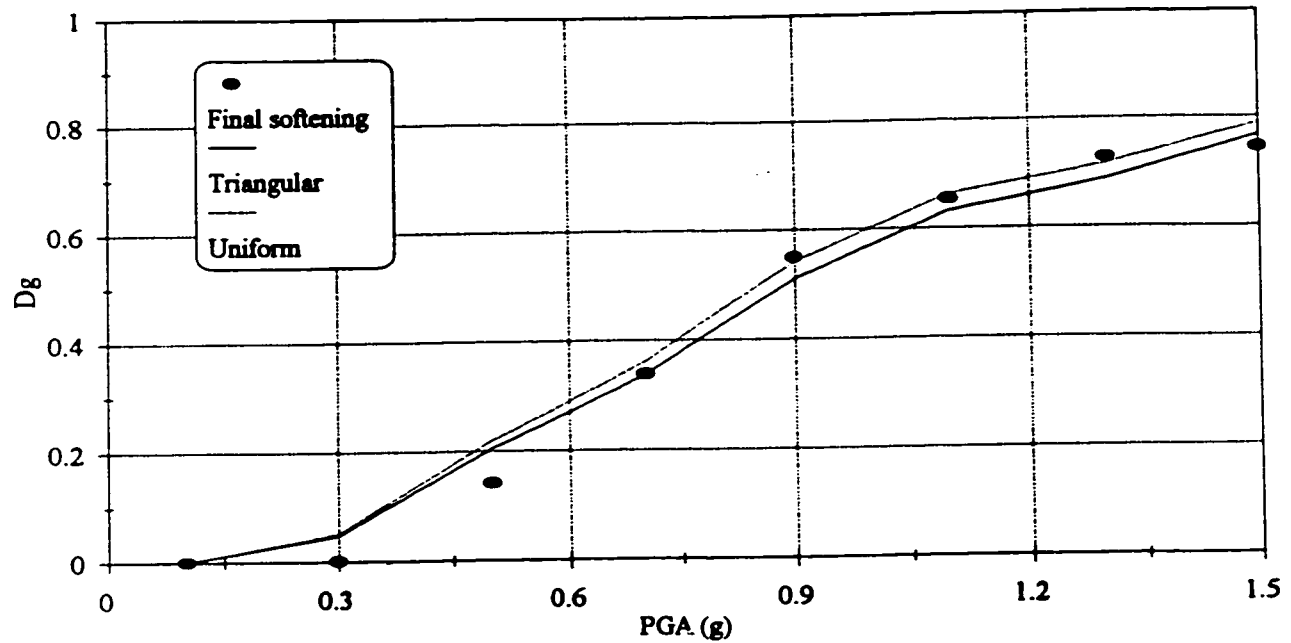
Figure 3.24 Variations of the damage index D_g and the final softening index with the PGA level of Nahanni earthquake for the case of the three-story frame
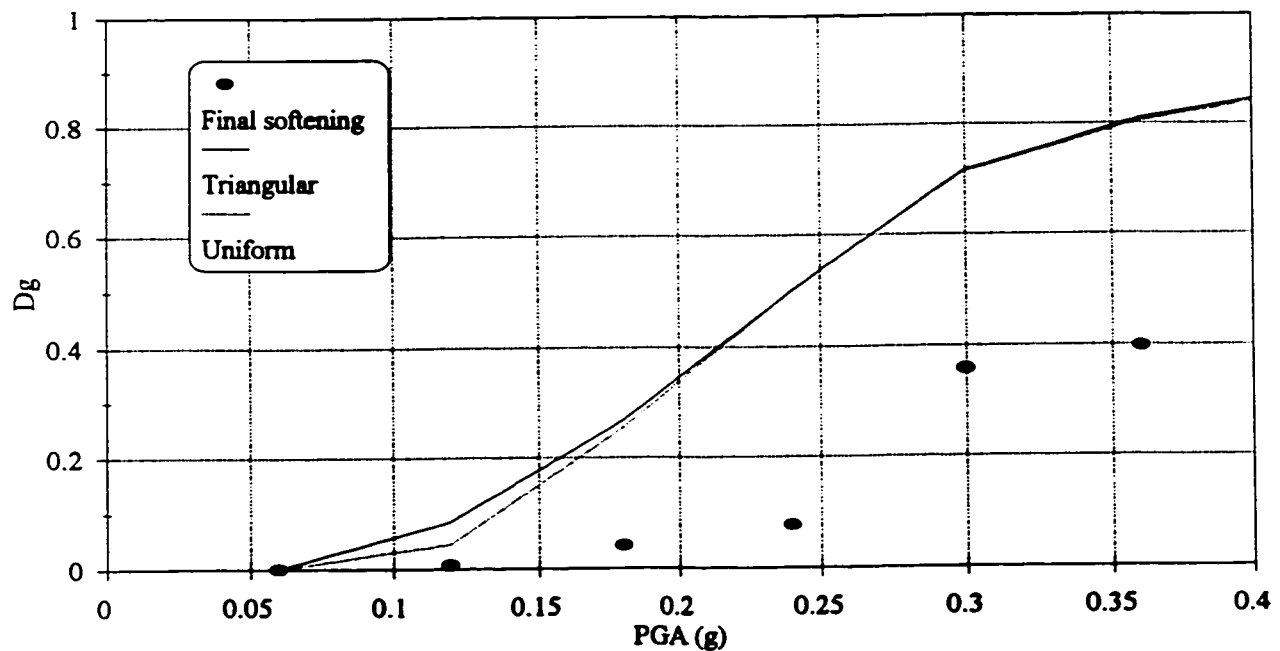
Figure 3.25 Variations of the damage index D_g and the final softening index with the PGA level of San Fernando earthquake for the case of the nine-story frame
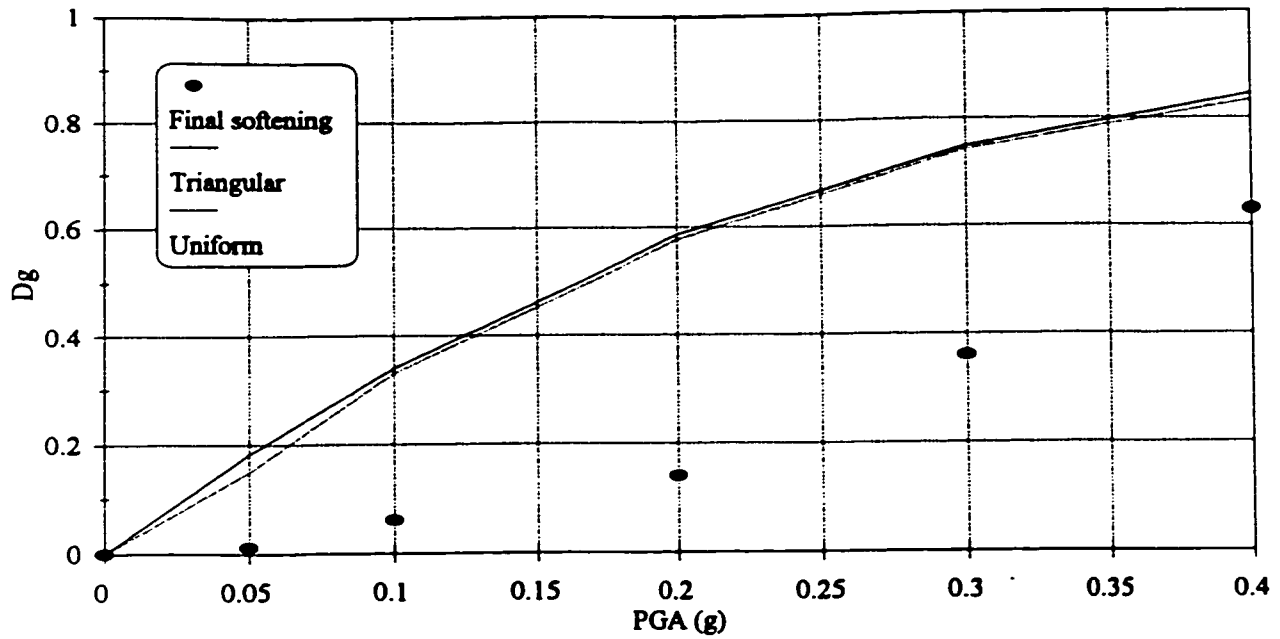
Figure 3.26 Variations of the damage index D_g and the final softening index with the PGA level of Mexico earthquake for the case of the nine-story frame
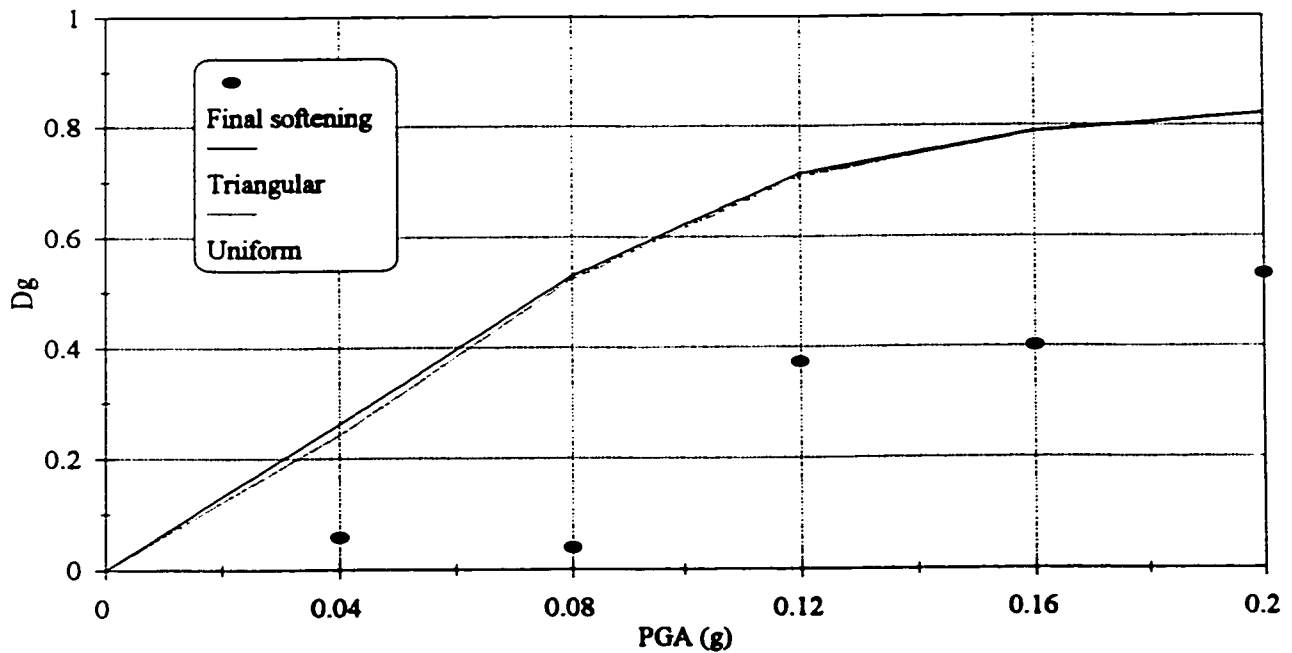
Figure 3.27 Variations of the damage index D_g and the final softening index with the PGA level of Long Beach earthquake for the case of the nine-story frame

Moment

Final pushover
loading

a

Residual Force

Rotation

Point "a" represents the response at
the end of the dynamic load

Moment

Final pushover
loading

a

Residual Force

Rotation

Point "a" represents the response at
the end of the dynamic load
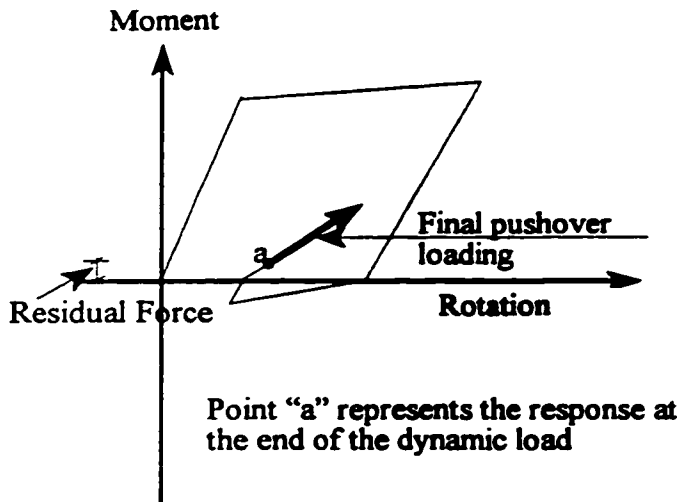
Case I: The residual force and the pushover
loading are in the same direction
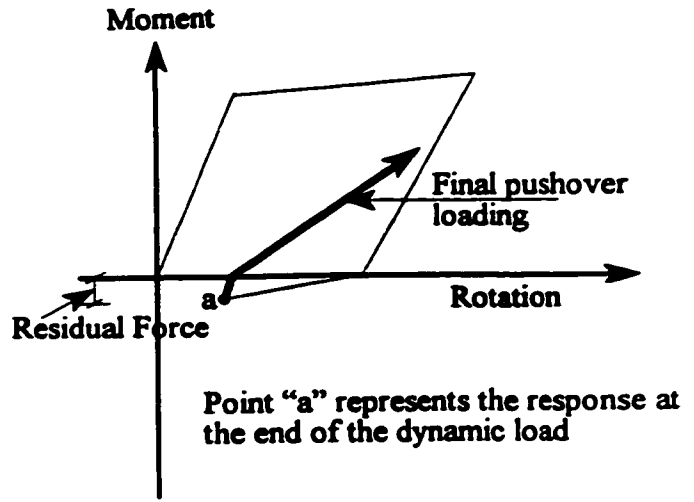
Case II: The residual force and the pushover
loading are in opposite directions

Figure 3.28 Effect of the residual moments in the plastic hinges on the developed stiffness

Force

Displacement
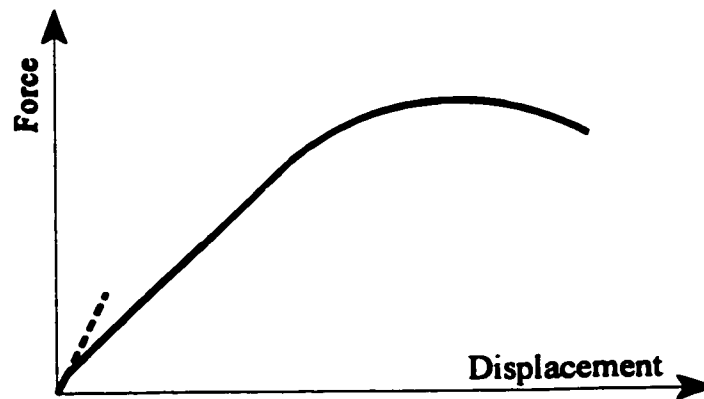
Figure 3.29 Effect of the residual forces on the structure stiffness
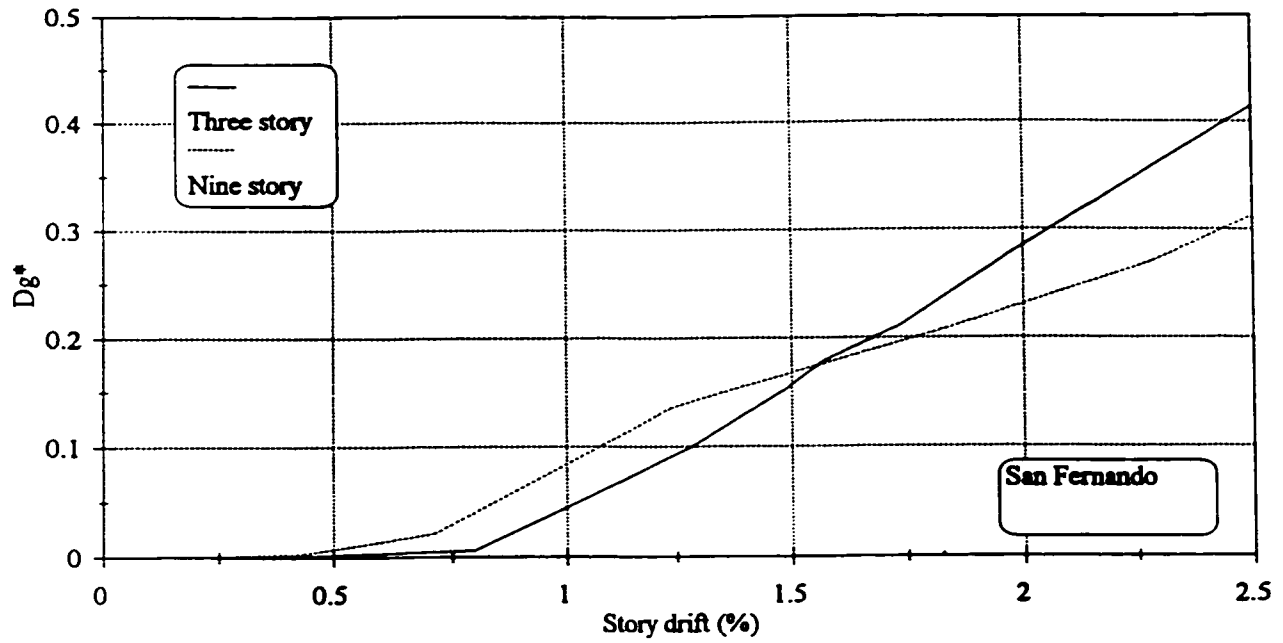
Figure 3.30 Relationships between the story drift and the damage index D_g^* due to the application of San Fernando earthquake
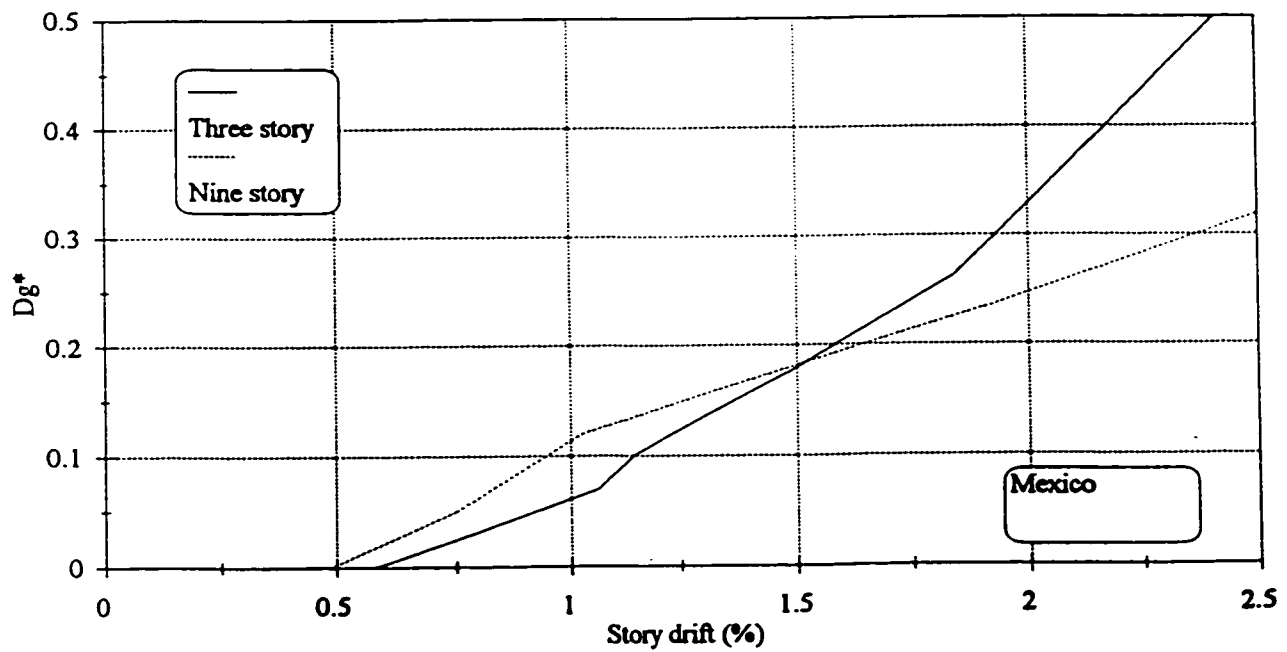
Figure 3.31 Relationships between the story drift and the damage index D_g^* due to the application of Mexico earthquake

CHAPTER 4

PERFORMANCE EVALUATION OF NONDUCTILE BUILDINGS

4.1 INTRODUCTION

Two reinforced concrete buildings, three-and nine-stories, were selected to represent existing nonductile structures that were designed according to early codes. The seismic response of the buildings was evaluated in terms of deformations and damage. The buildings were considered as a series of planar frames connected at each floor level by a rigid diaphragm, therefore, only 2D analysis was performed. The beams and columns were modelled using the beam-column model described in Chapter 2. The effect of the geometric nonlinearity (P-Δ) was considered in the analysis.

The building seismic performance parameters were obtained using twelve ground motion records with different characteristics. The selected records covered a wide range of frequency content and strong ground motion durations. The free vibration characteristics of the buildings were determined and the correlation between the building seismic performance parameters and the PGA level of the earthquake records was investigated. The relationships between deformation and damage for the two buildings were evaluated. The seismic performance of the buildings was determined using the simplified seismic performance evaluation approach presented in Chapter 2. The accuracy of the simplified approach in predicting the seismic performance parameters of nonductile reinforced concrete structures was evaluated.

4.2 SELECTED NONDUCTILE BUILDINGS

The selected buildings are three-and nine-stories and were gravity load designed according to the 1963 ACI code (ACI 318-63). The design concrete strength is 21 MPa and the design steel yield strength is 300 MPa. Various factors are expected to affect the concrete compressive strength of the nonductile building over time. Concrete aging will cause a compressive strength increase, however, environmental stressors may attack the integrity of the concrete with or independent of operating, environmental and accidental loads, causing the strength to degrade over time (Mori and Ellingwood, 1993). In the current study, it is assumed that the current concrete compressive strength of the building is equal to the original strength. The design live load for the building is taken as 2.4 kN/m^2 which is typical for an office building. Typical floor plan and elevation of the nine-story office building are shown in figure 4.1. Figure 4.2 shows the cross section details of the beams and columns of the nine-story building. The details of the building members are similar to those of the nonductile building designed by Biddah (1997). The building mass due to the dead weight of all structural and nonstructural elements is equal to 567,200 kg/floor. The three-story building was designed according to the same code provisions. The exterior columns are 300x300 mm reinforced using 4ϕ19 mm bars and the interior columns are 400x400 mm reinforced using 8ϕ19 mm bars. The exterior and interior beam sections are as shown in figure 4.2 for a typical floor. The steel reinforcement details in the buildings include: (1) beam bottom longitudinal reinforcement embedded 150 (mm) into the beam-column joint for anchorage; (2) widely spaced (300 mm) transverse reinforcement in beams and columns; (3) column lap splices of 20 bar diameter length located just above the floor level.

4.3 SELECTION OF THE GROUND MOTION RECORDS

Earthquake ground motions may be categorized based on parameters such as the peak ground acceleration (PGA), the peak ground velocity (PGV), frequency content and the duration of the strong ground motion. The ratio of PGA in (g) to the PGV in (m/sec.), commonly referred to as (A/V) ratio, can be considered as a simple qualitative measure of the frequency content of the ground motion. High (A/V) records represent high frequency content, while low (A/V) records indicate low frequency content.

Twelve ground motion records are selected for use in the current study. The criteria used in this selection is to cover a wide range of ground motion durations and frequency content represented by the (A/V) ratio. The durations of the ground motions were calculated using the method proposed by Trifunac and Brady (1973). Information concerning these ground motion records is summarized in table 4.1.

4.4 SEISMIC PERFORMANCE OF THE THREE-STORY BUILDING

The seismic performance of the three-story nonductile building was studied using scaled versions of the selected twelve ground motion records listed in table 4.1. The free vibration characteristics of the building are obtained and the correlation between the building seismic performance parameters and the PGA level of the earthquake records was investigated. The relationships between deformations and the levels of damage indices were presented. The dynamic analyses of the building were performed using a time step increment of 0.005 second and Rayleigh damping which was defined to achieve 2.0% viscous damping in the first two natural modes of the building.

4.4.1 Free Vibration Characteristics and the Elastic Spectral Forces

A free vibration analysis was carried out to determine the free vibration characteristics of the existing three-story building. The results are summarized in table 4.2. The fundamental period of the building was calculated as 0.99 second. Table 4.3 summarizes the elastic spectral forces (equivalent to the elastic base shear coefficients) for all the earthquake records corresponding to the fundamental period of the building. The elastic spectral force is considered as one of the main parameters that characterize ground motions and their effects on the structures. In general, the lateral seismic design force for a structure as considered in current seismic design provisions is the elastic spectral force divided by a force reduction factor to account for the inelastic behaviour of the structure. Table 4.3 shows that on average, records with low (A/V) ratios cause the greatest elastic spectral forces, while records with high (A/V) cause the smallest elastic spectral forces on the structure.

4.4.2 Seismic Analysis Results

An inelastic dynamic analysis was carried out for the three-story building using the selected twelve ground motion records. The seismic analysis results are summarized in table 4.4. The table presents the global seismic response parameters of the three-story building for each of the ground motion records when scaled to different PGA levels. The PGA scale factors of each of the ground motion records were selected to produce various levels of the building response, including severe inelastic deformation. The maximum level of the PGA of each of the records shown in table 4.4 is very close to the level that causes the structure collapse. For example, the collapse of the three-story building under the effect of El Centro

record occurred when the PGA level reached 0.42 g. The collapse occurs due to the frame lateral instability under the effect of gravity and seismic loads.

Table 4.5 summarizes the distributions of the story drift and the stiffness-based damage indices D_i of the various stories due to the application of different ground motion records. The results shown in the table indicate that the seismic loading causes a soft story plastic mechanism to form in the first story, leading to the concentration of relatively high levels of deformation and damage in the first story members. The deformation and damage of the third story were relatively small and the deformation remains within the elastic range.

The first, second and third story drift ratios corresponding to 1.0 % roof drift ratio of the nonductile three-story building when subjected to a static pushover analysis are 1.86, 0.84 and 0.3 %. The corresponding value of v is equal to 0.43. For seismically well designed buildings, v is expected to be lower than the value calculated for the nonductile building. The distribution of the story shear for the three-story building when subjected to the highest PGA levels of the various ground motion records before the structure collapse, are presented in table 4.6. The base shear coefficient of the three-story building ranges from 0.15 to 0.16.

4.4.3 Variation of the Building Performance Parameters With the PGA Level

The relationships between the PGA level and the building seismic performance parameters due to the application of the twelve ground motion records are presented in figures 4.3 to 4.6. These figures show the relationships between the PGA level and the mean and mean plus standard deviation of the roof drift ratio, story drift ratio, strength based damage index D_s^* and the stiffness based damage index D_g, respectively. At PGA level of

0.35 g, the means of the roof drift ratio, story drift ratio, damage index D_g^* and the damage index D_g reached approximately 1.2 %, 2.3 %, 0.4 and 0.65. The standard deviations in the roof drift ratio and the story drift ratio reached about 47% and 68 % from the mean values, respectively. The large difference between the mean and mean plus standard deviation indicates that the inelastic response of the structure is heavily dependent on the specific characteristics of the ground motion record.

4.4.4 Building Damage

The relationships between the building deformation and the level of damage indices are presented in figures 4.7 to 4.10. Figures 4.7 and 4.8 show the roof drift-D_g^* and the maximum story drift-D_g^* relationships, respectively. Figures 4.9 and 4.10 represent the roof drift-D_g and the maximum story drift-D_g relationships, respectively. The standard deviations at 1.0 % roof drift ratio in the strength based damage index D_g^* and the stiffness based damage index D_g are approximately 27.0 % and 7.0 %, respectively. At a 2.5% story drift ratio, the standard deviations in the damage indices D_g^* and D_g are approximately 14.0 % and 7.0 %, respectively. The results indicate the high variation of the damage index D_g^* as compared to that of the damage index D_g. This means that the strength based damage index D_g^* is more sensitive to the differences in the strong ground motion duration of the earthquakes than the stiffness based damage index D_g.

The maximum theoretical value of the damage indices is 1.0 which represents the collapse of the structure. The analysis of the three-story building was terminated at PGA levels close to the levels that cause the building collapse. The ratios between the maximum

PGA levels reached in the analysis and those at the building collapse are greater than 90% for most of the earthquake records. At the maximum PGA levels considered in the analysis, the average values of the strength based damage index D_s^* and the stiffness based damage index D_g are 0.58 and 0.74, respectively. Damage to the building was attributed to column hinging in the first and second stories and beam hinging due to pullout of the bottom reinforcement and yielding of the top reinforcement.

4.5 SEISMIC RESPONSE OF THE NINE-STORY BUILDING

The seismic performance of the nine-story building was evaluated using scaled versions of the twelve ground motion records. The free vibration characteristics of the building were obtained. The correlation between the building seismic performance parameters and the PGA level of the earthquake records was investigated. The relationships between deformation and the level of damage indices were studied.

4.5.1 Free Vibration Characteristics

The results of the free vibration analysis of the nine-story building are presented in table 4.2. The elastic spectral forces of the earthquake records corresponding to the fundamental period of the building are presented in table 4.3. The table shows that on average, records with low (A/V) ratio caused the largest elastic spectral forces while records with high (A/V) ratio caused the smallest elastic spectral forces. This trend is similar to the case of the three-story building. In general, the seismic demand for the nine-story building is lower than that for the three-story building. This is attributed to the long fundamental

period of the nine-story building.

4.5.2 Seismic Analysis Results

The seismic analysis results of the nine-story nonductile building are presented in tables 4.7. The table shows the global performance parameters of the building for each of the ground motion records when scaled to different PGA levels.

Tables 4.8 and 4.9 summarize the distribution of the story drift and the damage indices D_i of the various stories due to the application of the different ground motion records, respectively. The results indicate that the story drift ratios of the nine-story building are more uniformly distributed than in the case of the three-story building. The value of v calculated for the nine-story building is equal to 0.30 which is lower than that of the three-story building (v=0.43). The participation of several of the building stories in the overall inelastic deformation as well as the value of the parameter v give an indication of the uniformity in the developed plastic mechanism of the nine-story building. Examination of the plastic hinging sequence indicates that the plastic mechanism of the nine-story building is close to that of a beam hinging type.

The distribution of the maximum story shear of the nonductile nine-story building when subjected to the maximum PGA levels of the various ground motion records is presented in table 4.10. The maximum base shear coefficient of the nine-story building ranges from 0.072 to 0.115. The nine-story building exhibited significantly lower levels of base shear coefficient as compared to the three-story building. This is attributed in part to the increase in the nine-story building weight along with the small corresponding change in the base shear

capacity. The floor beams of the nine-story building have the same details and dimensions as those of the three-story building.

4.5.3 Variation of the Building Performance Parameters With the PGA Level

Figures 4.11 to 4.14, show the relationships of the mean and the mean plus standard deviation values of the roof drift ratio, the story drift ratio and the damage indices D_g^* and D_g with the PGA level, respectively. The figures indicate that the nine-story building sustained higher PGA level than the three-story building. This behaviour is expected because of the lower seismic demand for the nine-story building as compared to that of the three-story building as discussed in subsection 4.5.1.

The standard deviations in the PGA-roof drift ratio relationship reached about 60% which indicates the poor correlation between the PGA level and the building seismic performance parameters as in the case of the three-story building. This means that the building inelastic seismic performance is strongly dependent on the specific record characteristics. For meaningful statistical analysis with reduced standard deviation, a large number of records should be used.

4.5.4 Building Damage

The relationships between the building deformations and the level of damage indices are presented in figures 4.15 to 4.18. Figures 4.15 and 4.16 represent the roof drift-D_g^* and the story drift-D_g^* relationships, respectively. Figures 4.17 and 4.18 represent the roof drift-D_g and the story drift-D_g relationships, respectively. The deviations in figures 4.15 to 4.18

indicate that the relationship between the deformation and damage is dependent on the specific record characteristics. Different earthquakes with different frequency contents and different durations cause different damage at a specific deformation level. Comparing figures 4.15 to 4.18 with the damage-deformation relationships of the three-story building shown in figures 4.7 to 4.10 indicates that the deformation-damage relationships are dependent on the building height. Different buildings with different heights may experience different modes of failures leading to significant variation in the experienced damage corresponding to a certain deformation level.

The distribution of the story damage indices for the nine-story building summarized in table 4.9 indicates that the third and fourth stories of the building experienced higher level of damage as compared to the other building stories. This observation is true for most of the selected twelve ground motion records. The level of damage of the top three stories was relatively small. Damage to the nine-story building was attributed mainly to hinging of the column base as well as beam hinging due to pullout of the bottom reinforcement and yielding of the top reinforcement.

4.6 BEHAVIOUR CHARACTERISTICS OF LOW AND MEDIUM-RISE NONDUCTILE BUILDINGS

The analysis results obtained in sections 4.4 and 4.5 indicated that the low-rise nonductile building suffered from a soft story plastic mechanism under the effect of lateral load leading to the concentration of damage in the first story of the building. The behaviour of this type of structure will be influenced by the performance of the columns of the soft story.

On the other hand, medium-rise buildings have stronger columns in the bottom stories than in the case of low-rise buildings, while there is no significant changes in the beam strengths. This will lead to the development of a plastic mechanism close to that of a beam hinging type. The development of such plastic mechanism will lead to the participation of several of the building stories in the overall inelastic deformation and therefore improve the overall building ductility. The damage experienced at specific deformation level is expected to be lower than that of low-rise buildings with soft story mechanism.

4.7 RESPONSE OF THE THREE-STORY BUILDING USING THE SIMPLIFIED PROCEDURE

The simplified dynamic analysis of the three-story building was carried out using two different SDOF systems (elastic and inelastic). The dynamic analysis was carried out using the twelve ground motion records described in section 4.3. The PGA scale factors are the same as those used in the inelastic dynamic analysis of the three-story building. The damping ratio used in the equivalent SDOF models was taken as 2.0%. The force-displacement relationships of the three-story building were obtained by performing a static pushover analysis using uniform and code lateral load distributions.

For the elastic SDOF model, the lateral displacement profile vector, $\{\Psi_o\}$, is determined in the first loading increment of the pushover analysis. The properties of the model are calculated as follows:

(i) case of code lateral load distribution

$$\{\Psi_o\}^T = \{0.39, 0.76, 1.0\}$$

$$\{S\}^T = \{0.155, 0.310, 0.535\}$$

$M^* = \{\Psi\}^T [M]\{\Psi\} = 1.73$ x (story mass) $= 981,256$ kg

$L^* = \{\Psi\}^T [M]\{I\} = 2.15$ x (story mass) $= 1,219,480$ kg

$V^* = V\{\Psi\}^T \{S\} = 0.83V$ (4.1)

(ii) case of uniform lateral load distribution

$\{\Psi_o\}^T = \{0.45, 0.81, 1.0\}$

$\{S\}^T = \{1/3, 1/3, 1/3\}$

$M^* = \{\Psi\}^T [M]\{\Psi\} = 1.86$ x (story mass) $= 1,054,992$ kg

$L^* = \{\Psi\}^T [M]\{I\} = 2.26$ x (story mass) $= 1,281,872$ kg

$V^* = V\{\Psi\}^T \{S\} = 0.75V$ (4.2)

The matrix [M] is diagonal and all its components are equal to the story mass. The base shear coefficient V is obtained from lateral force-roof displacement relationship of the building as determined from the static pushover analysis. The hysteretic parameters of the force-displacement relationship of the SDOF model were selected to obtain the same cyclic response as that of the MDOF system under the effect of lateral loading.

For the inelastic SDOF model, the lateral displacement profile vector, $\{\Psi_1\}$, is determined from the pushover analysis at 1.0 % roof drift ratio. The properties of the model are calculated as follows:

(i) case of the code lateral load distribution

$\{\Psi_1\}^T = \{0.56, 0.88, 1.0\}$

$\{S\}^T = \{0.155, 0.310, 0.535\}$

$M^* = 2.09$ x (story mass) $= 1,185,448$ kg

$L^* = 2.44$ x (story mass) $= 1,383,968$ kg

$$V^{*} = 0.89V \tag{4.3}$$

(ii) case of uniform lateral load distribution

$$\{\Psi_1\}^T = \{0.72, 0.92, 1.0\}$$

$$\{S\}^T = \{1/3, 1/3, 1/3\}$$

$$M^{*} = 2.36 \times (\text{story mass}) = 1{,}338{,}592 \text{ kg}$$

$$L^{*} = 2.64 \times (\text{story mass}) = 1{,}497{,}408 \text{ kg}$$

$$V^{*} = 0.88V \tag{4.4}$$

A comparison between the predictions of the simplified evaluation approach and those of the MDOF model are shown in figures 4.19 to 4.22 for the case the code lateral loading. The figures represent the relationships between the predicted story drift ratio and four response factors C_1, C_2, C_3 and C_4. The response factors are defined as:

$$C_1 = \frac{\text{roof drift of the SDOF system}}{\text{roof drift of the MDOF system}}, \qquad C_2 = \frac{\text{story drift of the SDOF system}}{\text{story drift of the MDOF system}}$$

$$C_3 = \frac{D_g^{*} \text{ of the SDOF system}}{D_g^{*} \text{ of the MDOF system}}, \qquad C_4 = \frac{D_g \text{ of the SDOF system}}{D_g \text{ of the MDOF system}} \tag{4.5}$$

In each plot, a dot represents a comparison of the calculated response parameter for a particular earthquake record. If the dot is above the horizontal line ($C_i = 1.0$), then the SDOF model over-predicts the MDOF response; if the dot is below the horizontal line ($C_i = 1.0$), then the SDOF model under-predicts the MDOF response. The mean and standard deviation of the four response factors C_1, C_2, C_3, C_4 are shown on figures 4.19 to 4.22. On average, the results indicate that the simplified approach slightly overestimated the building response parameters when using the code lateral loading. The mean and standard deviation of the

response factors C_1, C_2, C_3, C_4 in case of the uniform lateral load distribution are summarized in table 4.11. The results indicate that using the uniform lateral load distribution significantly overestimated the building maximum story drift and damage indices. For the case of the three story building, the predictions of the simplified approach in case of the code lateral loading have lower standard deviations than the predictions when using the uniform distributed lateral loading.

4.8 RESPONSE OF THE NINE-STORY BUILDING USING THE SIMPLIFIED PROCEDURE

The simplified equivalent SDOF dynamic analysis of the nine-story building was carried out using the same approach that was described in the case of the three-story building. The properties of the elastic SDOF model was calculated as follows:

(i) case of the code lateral load distribution

$\{\Psi_o\}^T = \{ 0.08, 0.20, 0.33, 0.46, 0.59, 0.71, 0.83, 0.93, 1.0\}$

$\{S\}^T = \{0.02, 0.04, 0.06, 0.08, 0.09, 0.11, 0.13, 0.15, 0.33\}$

$M^* = 3.78 \times (\text{story mass}) = 2,144,016$

$L^* = 5.13 \times (\text{story mass}) = 2,909,736 \text{ kg}$

$V^* = 0.77 \text{ V}$ \hfill (4.6)

(ii) case of uniform lateral load distribution

$\{\Psi_o\}^T = \{ 0.11, 0.27, 0.41, 0.56, 0.69, 0.80, 0.89, 0.96, 1.0\}$

$\{S\}^T = \{1/9, 1/9, 1/9, 1/9, 1/9, 1/9, 1/9, 1/9, 1/9\}$

$M^* = 4.41 \times (\text{story mass}) = 2,501,352$

$L^* = 5.70$ x (story mass) = 3,233,040 kg

$V^* = 0.63$ V (4.7)

The properties of the inelastic SDOF model was calculated as follows:

(i) case of the code lateral load distribution

$\{\Psi_1\}^T = \{0.08, 0.23, 0.42, 0.62, 0.77, 0.87, 0.93, 0.98, 1.0\}$

$\{S\}^T = \{0.02, 0.04, 0.06, 0.08, 0.09, 0.11, 0.13, 0.15, 0.33\}$

$M^* = 4.78$ x (story mass) = 2,711,216 kg

$L^* = 5.89$ x (story mass) = 3,340,808 kg

$V^* = 0.84$ V (4.8)

(ii) case of uniform lateral load distribution

$\{\Psi_1\}^T = \{0.12, 0.33, 0.56, 0.75, 0.87, 0.93, 0.96, 0.99, 1.0\}$

$\{S\}^T = \{1/9, 1/9, 1/9, 1/9, 1/9, 1/9, 1/9, 1/9, 1/9\}$

$M^* = 5.52$ x (story mass) = 3,130,944 kg

$L^* = 6.50$ x (story mass) = 3,686,800 kg

$V^* = 0.72$ V (4.9)

A comparison between the predictions of the simplified evaluation approach and those of the MDOF model is presented in figures 4.23 to 4.26 for the code lateral load distribution. The mean and standard deviation of the four response factors C_1, C_2, C_3, C_4 are shown on the figures. On average, the results indicate that the simplified approach with code lateral loading overestimated the roof drift ratio of the building and underestimated the story drift ratio and the damage indices. The mean and standard deviation of the response factors C_1, C_2, C_3, C_4 in case of the uniform and code lateral load distributions are summarized in

table 4.11. The mean and standard deviation levels of the response factors in case of uniform lateral load distribution are very close to those obtained when using the code lateral load distribution. Performing the simplified approach using uniform or code lateral loadings in case of the nine-story building will yield approximately the same results.

4.9 LIMITATIONS OF THE SIMPLIFIED APPROACH

The formulated simplified approach has the advantage of providing approximate predictions of the seismic performance of the MDOF nonductile buildings with significantly less computational effort. The approach is capable of accounting for the behaviour of nonductile buildings with soft story plastic mechanism. This was achieved in the calculations of the lateral displacement profile vector $\{\Psi\}$. The distribution of the lateral displacement has a significant effect on the properties of the SDOF model. The simplified approach also takes into account the effect of the P-Δ on seismic response of the structures. The limitations on the applicability of the simplified approach due to the assumptions made in the derivation are summarized as follows:

1.   The simplified approach was applied to nonductile buildings with number of stories up to nine. For higher buildings, the accuracy of the simplified approach is not expected to remain within the range obtained in the current study because of the contribution of the higher modes.

2.   The application of the simplified approach is limited to the case of buildings with equal story height and uniform distribution of mass along the building height.

3.   The simplified approach is incapable of predicting the level of PGA that causes the

structure collapse.

4.10 SUMMARY

Two nonductile RC buildings, three- and nine-stories, were selected to represent low- and medium-rise existing nonductile RC buildings. The seismic response of the buildings was evaluated using selected twelve ground motion records. The results of the dynamic analysis indicated the development of a soft story plastic mechanism in case of the three-story building. For the case of the nine-story building, the plastic mechanism was close to that of a beam hinging type which led to the participation of several of the building stories in the overall inelastic deformation.

The relationships between the mean values of the seismic performance parameters of the two nonductile buildings and the PGA level of the ground motion records were presented. In some cases, high standard deviations in the building performance parameters were observed which indicate that the response is dependent on the characteristics of the specific record used.

The simplified approach was applied for evaluating the seismic performance of the nonductile buildings. The results were found dependent on the lateral load distribution used in determining the structure static response. It was found that in general, the code lateral load distribution yields better results than the uniform load distribution. The application of the simplified approach is limited to the case of buildings with equal story height and uniform distribution of mass along the building height whose response is dominated by the first mode.

Table 4.1 Earthquake data and site information for the selected ground motions.

Rec. No.	Earthquake	Date	Epic. Dist., km	Site	Soil type	A (g)	V (m/s)	A/V	Dur. (s)
1	Parkfield, California	June 27, 1966	7	Temblor, No.2	Rock	0.27	0.15	1.86	5.62
2	Nahanni, Canada	Dec. 23, 1985	8	Site 1, Iverson	Rock	1.10	0.46	2.38	7.92
3	Imperial Valley, California	May 18, 1940	8	El Centro	Stiff Soil	0.35	0.33	1.04	24.42
4	Kern County, California	July 21, 1952	56	Taft Lincoln School Tunnel	Rock	0.18	0.18	1.01	28.86
5	San Fernando, California	Feb. 9, 1971	35	Hollywood Storage P.E. Lot	Stiff Soil	0.21	0.21	1.00	13.22
6	San Fernando, California	Feb. 9, 1971	41	234 Figueroa St., L.A.	Stiff Soil	0.20	0.17	1.19	11.28
7	Monte Negro, Yugoslavia	Apr. 15, 1979	17	Albatros Hotel, Ulcinj	Rock	0.17	0.19	0.88	12.22
8	Long Beach, California	Mar. 10, 1933	59	Subway Terminal, L.A.	Rock	0.10	0.24	0.41	23.98
9	Lower California	Dec. 30, 1934	58	El Centro	Stiff Soil	0.16	0.21	0.77	21.10
10	San Fernando, California	Feb. 9, 1971	40	2500 Wilshire Blvd., L.A.	Stiff Soil	0.10	0.19	0.52	11.66
11	Near E. Coast of Honshu, Japan	May 16, 1968	290	Muroran Harbor	Stiff Soil	0.23	0.33	0.68	33.38
12	Mexico	Sep. 19, 1985	135	Zihuatenejo, Guerrero Array	Rock	0.10	0.16	0.65	19.74

Table 4.2 Free vibration characteristics of the existing buildings

Building	First mode		Second mode	
	Period (sec.)	Modal mass*	Period (sec.)	Modal mass*
Three story	0.99	0.90	0.32	0.08
Nine story	2.26	0.79	0.79	0.11

* As a fraction of the building total mass

Table 4.3 Elastic spectral forces corresponding to the fundamental
periods of the existing buildings

Rec. No.	Earthquake (PGA=1.0 g)	Elastic spectral force (V/W)	
		Three story	Nine story
1	Parkfield, California	0.54	0.21
2	Nahanni, Canada	0.43	0.10
3	Imperial Valley, California	1.85	0.62
4	Kern County, California	1.09	0.40
5	San Fernando, California	1.33	0.45
6	San Fernando, California	1.04	0.44
7	Monte Negro, Yugoslavia	1.30	0.60
8	Long Beach, California	2.14	2.31
9	Lower California	1.41	0.41
10	San Fernando, California	3.61	0.68
11	Near E. Coast of Honshu, Japan	1.20	0.27
12	Mexico	2.31	1.52

Table 4.4 Global seismic response parameters of the three-story building

Record No.	Earthquake	PGA (g)	Roof drift ratio, %	Story drift ratio, %	D_g^*	D_g
1	Parkfield, California	0.22	0.33	0.40	0.00	0.00
		0.66	0.80	1.16	0.11	0.49
		1.10	1.61	2.91	0.49	0.73
2	Nahanni, Canada	0.34	0.47	0.57	0.00	0.08
		1.02	0.90	2.02	0.28	0.59
		1.70	1.35	2.76	0.52	0.79
3	Imperial Valley, California	0.08	0.40	0.56	0.00	0.07
		0.24	0.70	1.22	0.12	0.42
		0.40	1.38	2.61	0.43	0.71
4	Kern County, California	0.11	0.34	0.40	0.00	0.01
		0.33	0.91	1.30	0.16	0.56
		0.54	1.35	3.26	0.73	0.79
5	San Fernando, California	0.07	0.27	0.33	0.00	0.00
		0.21	0.69	1.04	0.08	0.36
		0.35	1.67	3.16	0.52	0.74
6	San Fernando, California	0.08	0.25	0.30	0.00	0.00
		0.24	0.54	0.80	0.02	0.24
		0.40	1.10	2.31	0.35	0.68
7	Monte Negro, Yugoslavia	0.09	0.34	0.42	0.00	0.01
		0.27	0.72	1.23	0.12	0.43
		0.45	1.26	3.00	0.76	0.77

Table 4.4 (continued) Global seismic response parameters of the three-story building

Record No.	Earthquake	PGA (g)	Roof drift ratio, %	Story drift ratio, %	D_s^*	D_s
8	Long Beach, California	0.04	0.20	0.26	0.00	0.00
		0.11	0.58	0.91	0.05	0.28
		0.16	1.30	3.19	0.71	0.67
9	Lower California	0.09	0.35	0.49	0.00	0.04
		0.27	0.95	1.60	0.19	0.55
		0.46	1.10	2.67	0.59	0.78
10	San Fernando, California	0.05	0.47	0.63	0.00	0.12
		0.15	0.86	1.74	0.21	0.56
		0.23	1.33	2.82	0.50	0.67
11	Near E. Coast of Honshu, Japan	0.10	0.40	0.52	0.00	0.06
		0.29	0.96	1.48	0.16	0.56
		0.48	1.47	2.59	0.39	0.73
12	Mexico	0.04	0.26	0.37	0.00	0.00
		0.12	0.65	1.08	0.08	0.38
		0.20	1.12	2.60	0.58	0.76

Table 4.5 Story drift ratios and story damage indices of the three-story building

Record No.	Earthquake	PGA (g)	Story drift ratios, %			Story damage indices (D_i)		
			First story	Second story	Third story	D_1	D_2	D_3
1	Parkfield, California	0.22	0.40	0.38	0.28	0.00	0.00	0.00
		0.66	1.16	0.87	0.78	0.58	0.40	0.43
		1.10	2.91	1.35	0.95	0.84	0.58	0.46
2	Nahanni, Canada	0.34	0.52	0.57	0.42	0.10	0.09	0.03
		1.02	2.02	0.81	0.50	0.76	0.27	0.08
		1.70	2.76	1.24	0.53	0.89	0.61	0.14
3	Imperial Valley, California	0.08	0.56	0.44	0.24	0.11	0.07	0.01
		0.24	1.22	0.77	0.45	0.60	0.27	0.04
		0.40	2.61	1.24	0.54	0.83	0.54	0.12
4	Kern County, California	0.11	0.40	0.38	0.26	0.01	0.01	0.00
		0.33	1.20	1.20	0.61	0.61	0.58	0.20
		0.54	3.26	1.65	0.80	0.87	0.72	0.20
5	San Fernando, California	0.07	0.33	0.30	0.21	0.00	0.00	0.00
		0.21	1.04	0.72	0.42	0.50	0.29	0.03
		0.35	3.16	1.75	0.44	0.84	0.65	0.15
6	San Fernando, California	0.08	0.30	0.28	0.21	0.00	0.00	0.00
		0.24	0.80	0.62	0.41	0.37	0.15	0.03
		0.40	2.31	1.03	0.44	0.82	0.50	0.07
7	Monte Negro, Yugoslavia	0.09	0.42	0.38	0.24	0.01	0.02	0.00
		0.27	1.23	0.67	0.36	0.61	0.24	0.03
		0.45	3.00	0.95	0.54	0.88	0.49	0.10

Table 4.5 (continued) Story drift ratios and story damage indices of the three-story building

Record No.	Earthquake	PGA (g)	Story drift ratios, %			Story damage indices (D_i)		
			First story	Second story	Third story	D_1	D_2	D_3
8	Long Beach, California	0.04	0.26	0.22	0.12	0.00	0.00	0.00
		0.11	0.91	0.60	0.31	0.42	0.19	0.03
		0.16	3.19	0.89	0.37	0.80	0.48	0.08
9	Lower California	0.09	0.49	0.40	0.26	0.06	0.05	0.01
		0.27	1.60	1.05	0.49	0.71	0.48	0.07
		0.46	2.67	1.08	0.44	0.89	0.50	0.06
10	San Fernando, California	0.05	0.63	0.52	0.28	0.20	0.09	0.01
		0.15	1.74	0.69	0.37	0.74	0.26	0.02
		0.23	2.82	1.06	0.36	0.82	0.42	0.05
11	Near E. Coast of Honshu, Japan	0.10	0.52	0.46	0.32	0.08	0.07	0.01
		0.29	1.48	1.21	0.54	0.69	0.53	0.11
		0.48	2.59	1.45	0.50	0.84	0.59	0.13
12	Mexico	0.04	0.37	0.29	0.18	0.00	0.00	0.00
		0.12	1.08	0.60	0.30	0.56	0.19	0.03
		0.20	2.60	0.86	0.36	0.88	0.52	0.08

Table 4.6 Story shear distribution of the three-story building

Record No.	Earthquake	PGA (g)	(Story shear) / (Building weight)		
			First story	Second story	Third story
1	Parkfield, California	1.10	0.152	0.135	0.141
2	Nahanni, Canada	1.70	0.151	0.138	0.113
3	Imperial Valley, California	0.40	0.149	0.137	0.113
4	Kern County, California	0.54	0.151	0.151	0.123
5	San Fernando, California	0.35	0.150	0.140	0.093
6	San Fernando, California	0.40	0.150	0.137	0.108
7	Monte Negro, Yugoslavia	0.45	0.155	0.137	0.114
8	Long Beach, California	0.16	0.151	0.130	0.079
9	Lower California	0.46	0.157	0.132	0.106
10	San Fernando, California	0.23	0.148	0.123	0.091
11	Near E. Coast of Honshu, Japan	0.48	0.149	0.138	0.111
12	Mexico	0.20	0.151	0.125	0.082

Table 4.7 Global seismic response parameters of the nine-story building

Record No.	Earthquake	PGA (g)	Roof drift ratio, %	Story drift ratio, %	D_s^*	D_s
1	Parkfield, California	0.35	0.29	0.57	0.01	0.24
		1.05	0.90	1.60	0.21	0.66
		1.75	1.23	2.33	0.31	0.85
2	Nahanni, Canada	0.60	0.30	0.78	0.01	0.17
		1.80	0.83	1.78	0.22	0.72
		3.00	1.33	2.64	0.40	0.81
3	Imperial Valley, California	0.15	0.46	0.69	0.02	0.30
		0.45	0.95	1.71	0.23	0.72
		0.75	1.92	3.37	0.55	0.77
4	Kern County, California	0.13	0.28	0.45	0.01	0.14
		0.39	0.72	1.37	0.22	0.56
		0.65	1.41	2.61	0.41	0.76
5	San Fernando, California	0.09	0.20	0.31	0.00	0.00
		0.26	0.62	1.36	0.15	0.55
		0.43	1.50	2.79	0.38	0.86
6	San Fernando, California	0.11	0.24	0.34	0.01	0.06
		0.33	1.02	2.04	0.22	0.70
		0.55	1.49	2.83	0.37	0.85
7	Monte Negro, Yugoslavia	0.15	0.44	0.83	0.05	0.37
		0.45	1.08	2.14	0.27	0.77
		0.75	1.47	2.71	0.56	0.82

Table 4.7 (continued) Global seismic response parameters of the nine-story building

Record No.	Earthquake	PGA (g)	Roof drift ratio, %	Story drift ratio, %	D_s^*	D_s
8	Long Beach, California	0.05	0.42	0.71	0.02	0.29
		0.15	1.06	2.30	0.24	0.77
		0.24	1.90	3.66	0.54	0.83
9	Lower California	0.20	0.30	0.62	0.03	0.28
		0.60	0.66	1.41	0.25	0.74
		1.00	1.65	3.14	0.56	0.79
10	San Fernando, California	0.08	0.25	0.41	0.01	0.09
		0.24	0.63	1.27	0.17	0.49
		0.40	1.75	2.94	0.50	0.83
11	Near E. Coast of Honshu, Japan	0.16	0.22	0.50	0.00	0.08
		0.48	0.62	1.14	0.17	0.64
		0.80	1.64	3.03	0.50	0.79
12	Mexico	0.09	0.40	0.69	0.03	0.30
		0.27	0.76	1.67	0.22	0.71
		0.45	1.77	3.26	0.49	0.84

Table 4.8 Story drift ratios of the nine-story building

Record No.	Earthquake	PGA (g)	Story drift ratios, %								
			1st	2nd	3rd	4th	5th	6th	7th	8th	9th
1	Parkfield, California	0.35	0.36	0.54	0.49	0.51	0.57	0.46	0.42	0.43	0.33
		1.05	0.83	1.38	1.60	1.56	1.15	0.90	0.72	0.85	0.58
		1.75	1.11	2.04	2.33	2.18	1.92	1.49	1.57	1.02	0.72
2	Nahanni, Canada	0.60	0.32	0.47	0.42	0.36	0.39	0.47	0.78	0.60	0.39
		1.80	0.91	1.51	1.78	1.61	1.22	0.92	1.16	0.85	0.74
		3.00	1.24	1.89	2.22	2.64	2.36	1.57	2.36	1.38	0.56
3	Imperial Valley, California	0.15	0.36	0.57	0.58	0.59	0.69	0.65	0.64	0.45	0.26
		0.45	0.65	1.29	1.65	1.71	1.54	1.12	1.09	0.66	0.58
		0.75	1.75	2.72	3.29	3.37	3.14	2.41	1.67	0.95	0.56
4	Kern County, California	0.13	0.30	0.45	0.38	0.35	0.35	0.33	0.39	0.36	0.26
		0.39	0.61	1.05	1.18	1.37	1.22	1.01	0.94	0.80	0.40
		0.65	0.95	1.93	2.40	2.61	2.51	2.09	1.41	0.70	0.50
5	San Fernando, California	0.09	0.20	0.26	0.24	0.26	0.24	0.24	0.31	0.29	0.17
		0.26	0.60	1.16	1.36	1.22	0.91	0.99	0.96	0.82	0.40
		0.43	0.99	1.97	2.50	2.79	2.48	2.00	1.46	0.91	0.37
6	San Fernando, California	0.11	0.23	0.34	0.32	0.32	0.31	0.29	0.31	0.25	0.17
		0.33	0.91	1.78	2.04	1.78	1.26	0.78	0.68	0.53	0.34
		0.55	1.14	2.28	2.83	2.78	2.34	1.58	0.93	0.57	0.46
7	Monte Negro, Yugoslavia	0.15	0.44	0.76	0.83	0.77	0.57	0.37	0.40	0.37	0.26
		0.45	1.04	1.91	2.14	2.08	1.77	1.09	0.75	0.71	0.45
		0.75	1.40	2.30	2.59	2.71	2.59	1.87	1.17	0.84	0.57

Table 4.8 (continued) Story drift ratios of the nine-story building

Record No.	Earthquake	PGA (g)	Story drift ratios, %								
			1st	2nd	3rd	4th	5th	6th	7th	8th	9th
8	Long Beach, California	0.05	0.35	0.61	0.69	0.71	0.54	0.35	0.37	0.29	0.16
		0.15	0.91	1.90	2.30	2.13	1.33	0.88	0.75	0.48	0.29
		0.24	1.19	2.56	3.38	3.66	3.36	2.30	1.33	0.59	0.35
9	Lower California	0.20	0.39	0.62	0.58	0.53	0.45	0.39	0.57	0.53	0.27
		0.60	0.61	1.02	1.29	1.41	1.34	1.20	0.92	0.83	0.39
		1.00	1.64	2.42	2.87	3.14	2.69	1.89	1.24	0.89	0.59
10	San Fernando, California	0.08	0.22	0.34	0.36	0.41	0.32	0.28	0.39	0.33	0.21
		0.24	0.50	0.79	0.86	1.03	1.27	1.27	1.01	0.73	0.34
		0.40	1.19	2.16	2.59	2.81	2.81	2.94	2.86	0.92	0.37
11	Near E. Coast of Honshu, Japan	0.16	0.32	0.43	0.32	0.30	0.30	0.33	0.50	0.38	0.24
		0.48	0.56	1.03	1.11	1.14	1.11	0.94	1.11	0.85	0.54
		0.80	1.65	2.60	3.03	2.93	2.19	1.58	1.35	0.97	0.68
12	Mexico	0.09	0.39	0.66	0.68	0.69	0.51	0.39	0.42	0.31	0.19
		0.27	0.79	1.37	1.52	1.67	1.29	0.75	0.63	0.53	0.39
		0.45	0.95	1.95	2.49	2.93	3.26	2.91	1.96	0.96	0.49

Table 4.9 Story damage indices of the nine-story building

Record No.	Earthquake	PGA (g)	1st	2nd	3rd	4th	5th	6th	7th	8th	9th
1	Parkfield, California	0.35	0.25	0.33	0.35	0.31	0.28	0.17	0.03	0.00	0.00
		1.05	0.66	0.75	0.79	0.76	0.69	0.47	0.13	0.15	0.13
		1.75	0.84	0.88	0.91	0.90	0.88	0.81	0.58	0.35	0.33
2	Nahanni, Canada	0.60	0.22	0.27	0.24	0.16	0.12	0.15	0.12	0.06	0.01
		1.80	0.73	0.80	0.83	0.80	0.71	0.51	0.29	0.15	0.16
		3.00	0.79	0.84	0.87	0.86	0.83	0.76	0.66	0.39	0.15
3	Imperial Valley, California	0.15	0.28	0.37	0.41	0.37	0.36	0.29	0.12	0.02	0.00
		0.45	0.63	0.75	0.80	0.79	0.78	0.74	0.56	0.13	0.08
		0.75	0.76	0.80	0.84	0.83	0.81	0.76	0.57	0.38	0.09
4	Kern County, California	0.13	0.23	0.29	0.25	0.13	0.07	0.03	0.01	0.00	0.00
		0.39	0.49	0.60	0.67	0.65	0.64	0.56	0.26	0.12	0.00
		0.65	0.70	0.80	0.85	0.84	0.80	0.69	0.40	0.12	0.03
5	San Fernando, California	0.09	0.00	0.00	0.00	0.00	0.00	0.00	0.00	0.00	0.00
		0.26	0.53	0.66	0.71	0.66	0.56	0.48	0.27	0.13	0.00
		0.43	0.82	0.88	0.91	0.91	0.90	0.86	0.64	0.28	0.03
6	San Fernando, California	0.11	0.10	0.14	0.12	0.05	0.01	0.00	0.00	0.00	0.00
		0.33	0.71	0.79	0.82	0.79	0.71	0.51	0.15	0.02	0.00
		0.55	0.83	0.88	0.91	0.90	0.89	0.83	0.60	0.13	0.03
7	Monte Negro, Yugoslavia	0.15	0.39	0.51	0.55	0.47	0.34	0.15	0.02	0.00	0.00
		0.45	0.76	0.82	0.85	0.84	0.82	0.72	0.36	0.07	0.01
		0.75	0.81	0.86	0.88	0.88	0.86	0.80	0.54	0.27	0.06

Table 4.9 (continued) Story damage indices of the nine-story building

Record No.	Earthquake	PGA (g)	Story damage indices (D_i)								
			1st	2nd	3rd	4th	5th	6th	7th	8th	9th
8	Long Beach, California	0.05	0.29	0.40	0.46	0.39	0.28	0.12	0.01	0.00	0.00
		0.15	0.76	0.84	0.87	0.85	0.79	0.61	0.18	0.02	0.00
		0.24	0.78	0.86	0.89	0.89	0.87	0.80	0.53	0.10	0.02
9	Lower California	0.20	0.35	0.44	0.46	0.37	0.23	0.13	0.04	0.02	0.00
		0.60	0.69	0.79	0.83	0.81	0.79	0.72	0.49	0.16	0.01
		1.00	0.78	0.82	0.85	0.84	0.82	0.78	0.61	0.25	0.19
10	San Fernando, California	0.08	0.09	0.16	0.20	0.15	0.06	0.01	0.00	0.00	0.00
		0.24	0.34	0.45	0.52	0.59	0.65	0.59	0.40	0.14	0.01
		0.40	0.77	0.84	0.87	0.86	0.86	0.86	0.82	0.34	0.04
11	Near E. Coast of Honshu, Japan	0.16	0.20	0.22	0.14	0.03	0.00	0.03	0.04	0.02	0.00
		0.48	0.60	0.71	0.75	0.73	0.71	0.61	0.37	0.20	0.08
		0.80	0.80	0.84	0.87	0.86	0.82	0.76	0.57	0.36	0.22
12	Mexico	0.09	0.33	0.44	0.47	0.40	0.30	0.16	0.03	0.00	0.00
		0.27	0.66	0.76	0.81	0.80	0.77	0.64	0.21	0.03	0.00
		0.45	0.78	0.85	0.88	0.89	0.89	0.87	0.73	0.34	0.05

Table 4.10 Story shear distribution of the nine-story building

Record No.	Earthquake	PGA (g)	(Story shear) / (Building weight)								
			1st	2nd	3rd	4th	5th	6th	7th	8th	9th
1	Parkfield, California	1.75	0.12	0.092	0.088	0.082	0.078	0.075	0.057	0.054	0.048
2	Nahanni, Canada	3.00	0.110	0.090	0.081	0.067	0.058	0.057	0.060	0.046	0.044
3	Imperial Valley, California	0.75	0.100	0.077	0.075	0.071	0.059	0.057	0.052	0.049	0.039
4	Kern County, California	0.65	0.080	0.068	0.069	0.072	0.071	0.055	0.047	0.044	0.037
5	San Fernando, California	0.43	0.073	0.065	0.057	0.057	0.051	0.052	0.052	0.044	0.032
6	San Fernando, California	0.55	0.076	0.066	0.058	0.057	0.052	0.053	0.048	0.044	0.039
7	Monte Negro, Yugoslavia	0.75	0.101	0.075	0.073	0.076	0.074	0.056	0.053	0.048	0.041
8	Long Beach, California	0.24	0.072	0.065	0.058	0.053	0.048	0.045	0.044	0.039	0.027
9	Lower California	1.00	0.114	0.086	0.088	0.086	0.077	0.069	0.054	0.049	0.042
10	San Fernando, California	0.40	0.090	0.069	0.060	0.056	0.059	0.058	0.054	0.043	0.028
11	Near E. Coast of Honshu	0.80	0.101	0.076	0.068	0.070	0.062	0.058	0.049	0.050	0.041
12	Mexico	0.45	0.089	0.074	0.069	0.056	0.058	0.055	0.048	0.045	0.034

Table 4.11 Mean and standard deviation of the repose factors of the simplified approach

Case	Item	Response factor			
		C_1	C_2	C_3	C_4
Three-story, Code loading	Mean	1.09	1.0	1.14	1.09
	St. deviation	0.12	0.15	0.25	0.17
Three-story, Uniform loading	Mean	1.05	1.16	1.42	1.29
	St. deviation	0.12	0.25	0.52	0.23
Nine-story, Code loading	Mean	1.08	0.86	0.89	0.96
	St. deviation	0.19	0.19	0.21	0.17
Nine-story, Uniform loading	Mean	1.06	0.97	0.88	0.99
	St. deviation	0.19	0.22	0.22	0.19

C. L.

Typical Frame
Elevation

9 x 3.6 m = 32.4 m

5x 6.0 m = 30.0 m

Typical Floor
Plan

5 x 6.0 m = 30.0 m

5x 6.0 m = 30.0 m
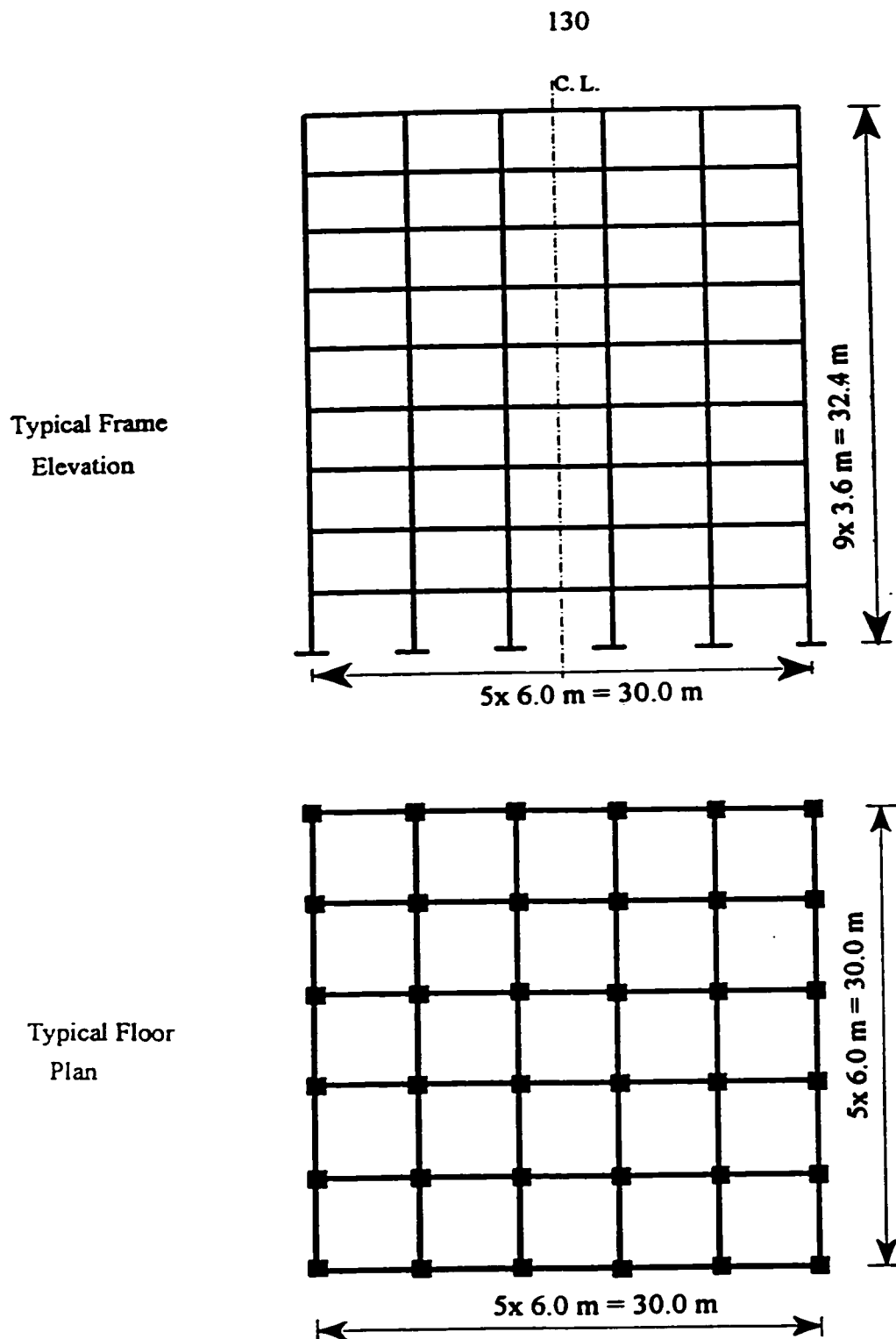
Figure 4.1 Overall dimensions of the nine-story building

4 φ 19 mm

300x300 mm
Exterior columns of
the top three stories

8 φ 19 mm

400x400 mm
Interior columns of
the top three stories

8 φ 19 mm

400x400 mm
Exterior columns of the
middle three stories

8 φ 22 mm

500x500 mm
Interior columns of the
middle three stories

8 φ 22 mm

500x500 mm
Exterior columns of the
bottom three stories

8 φ 25 mm

600x600 mm
Interior columns of the
bottom three stories

3 φ 19 mm   150 mm

2 φ 19 mm   250 mm

Beam exterior end section

5 φ 19 mm

600 mm   250 mm

2 φ 19 mm

Beam interior end section

Figure 4.2 Cross section details of the beams and columns of the nine-story building
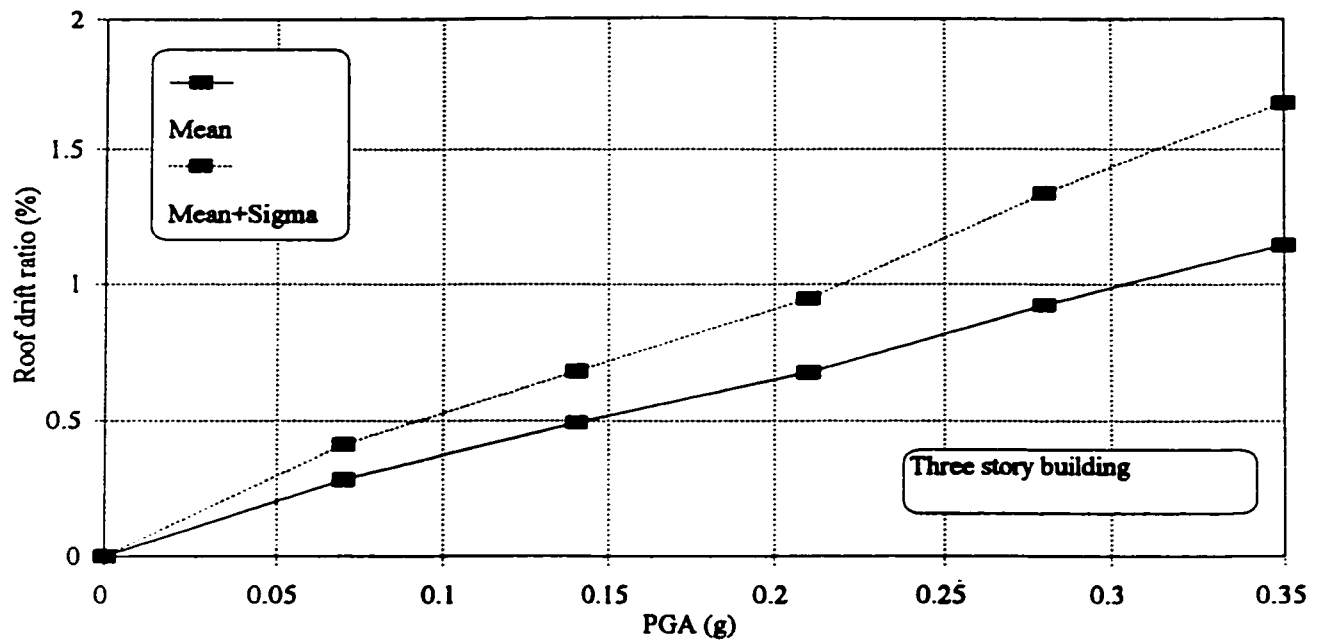
Figure 4.3 Relationship between the PGA and the roof drift ratio
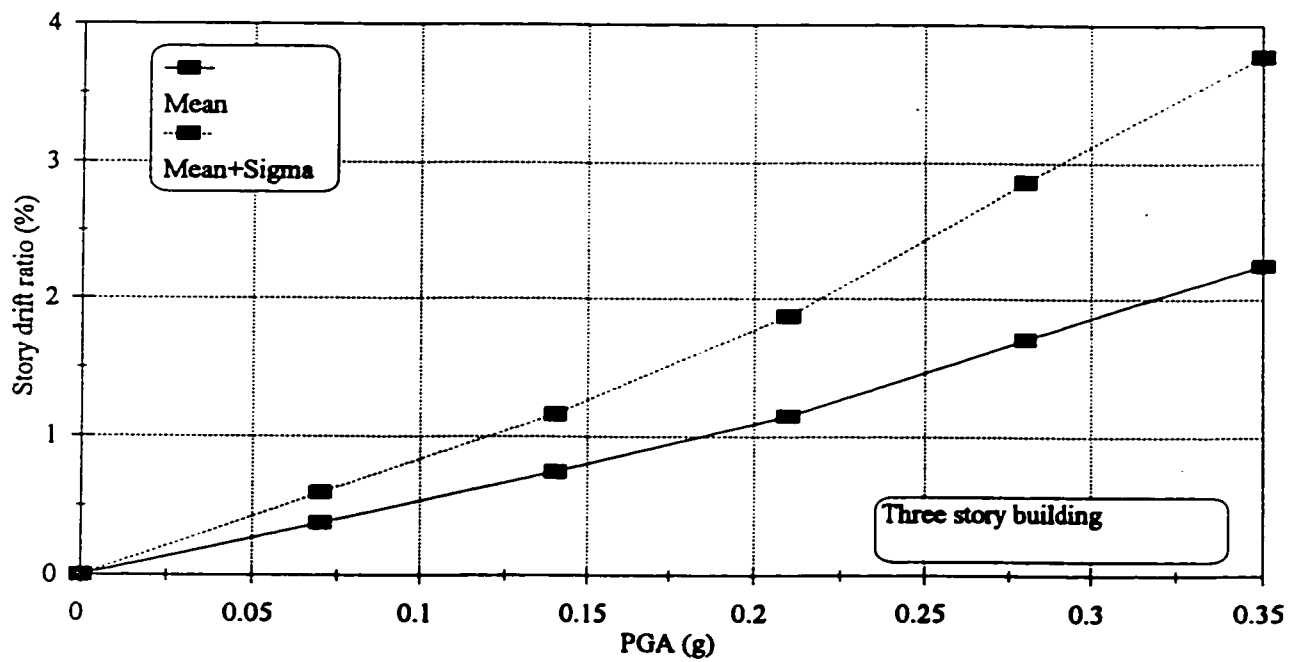
Figure 4.4 Relationship between the PGA and the story drift ratio
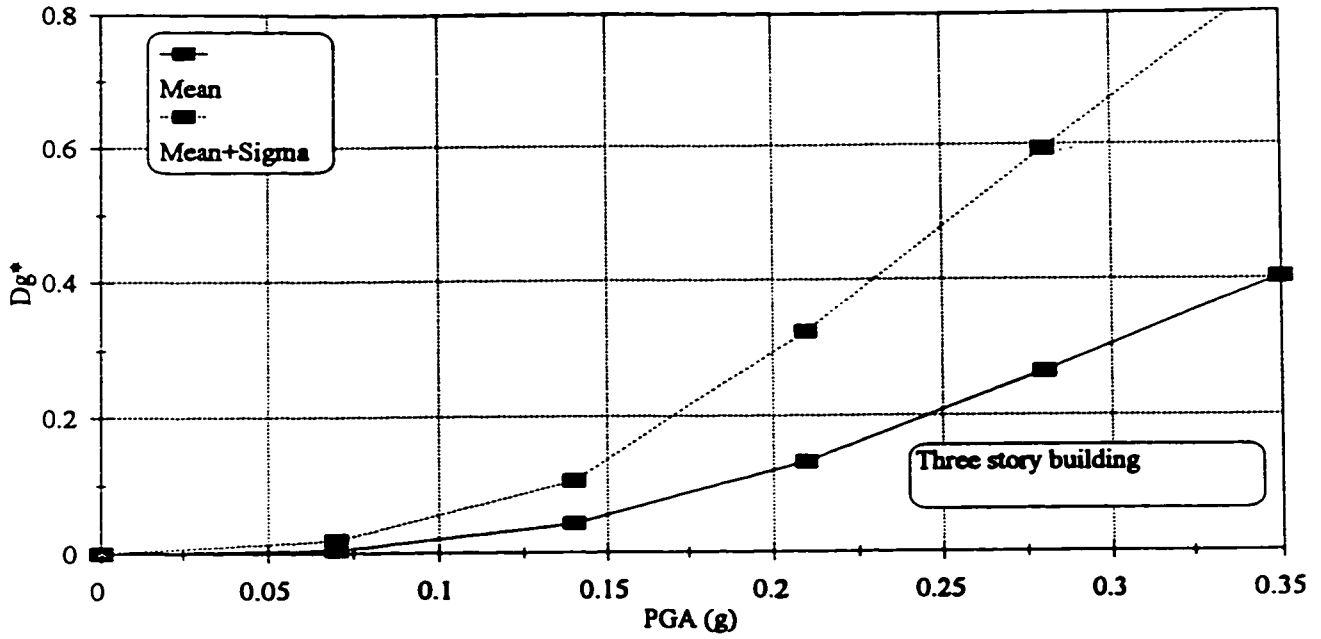
Figure 4.5 Relationship between the PGA and the strength based damage index D_g^*
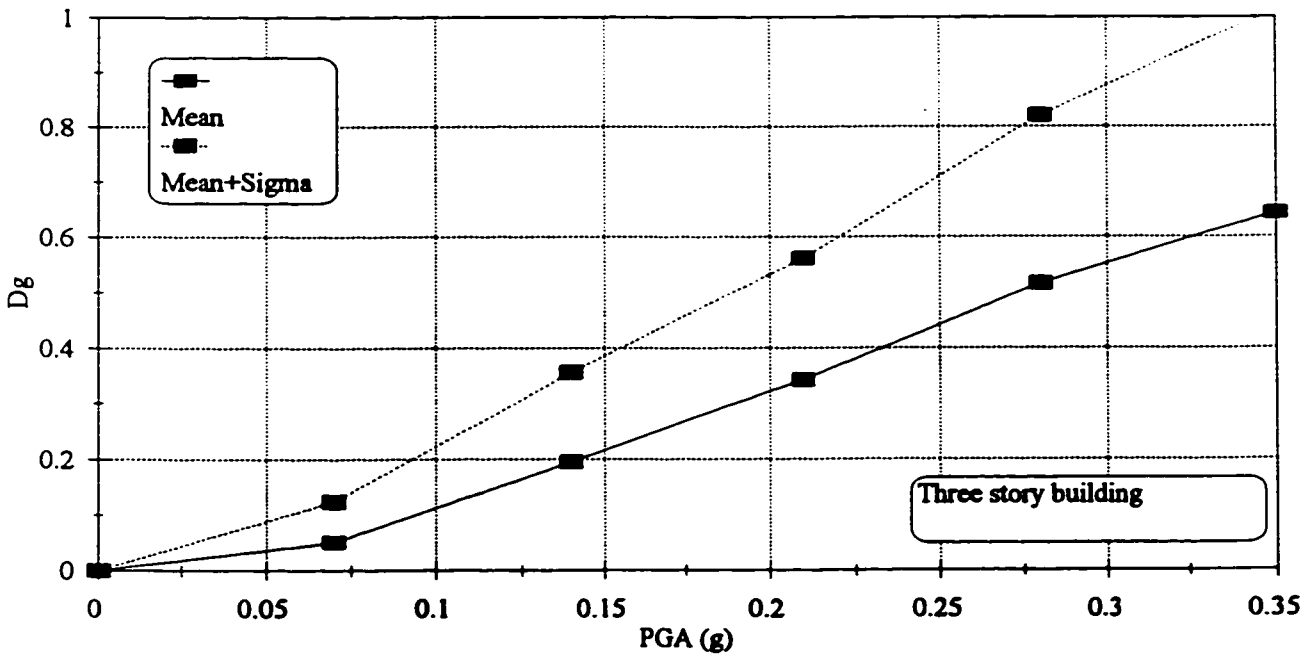
Figure 4.6 Relationship between the PGA and the stiffness based damage index D_g
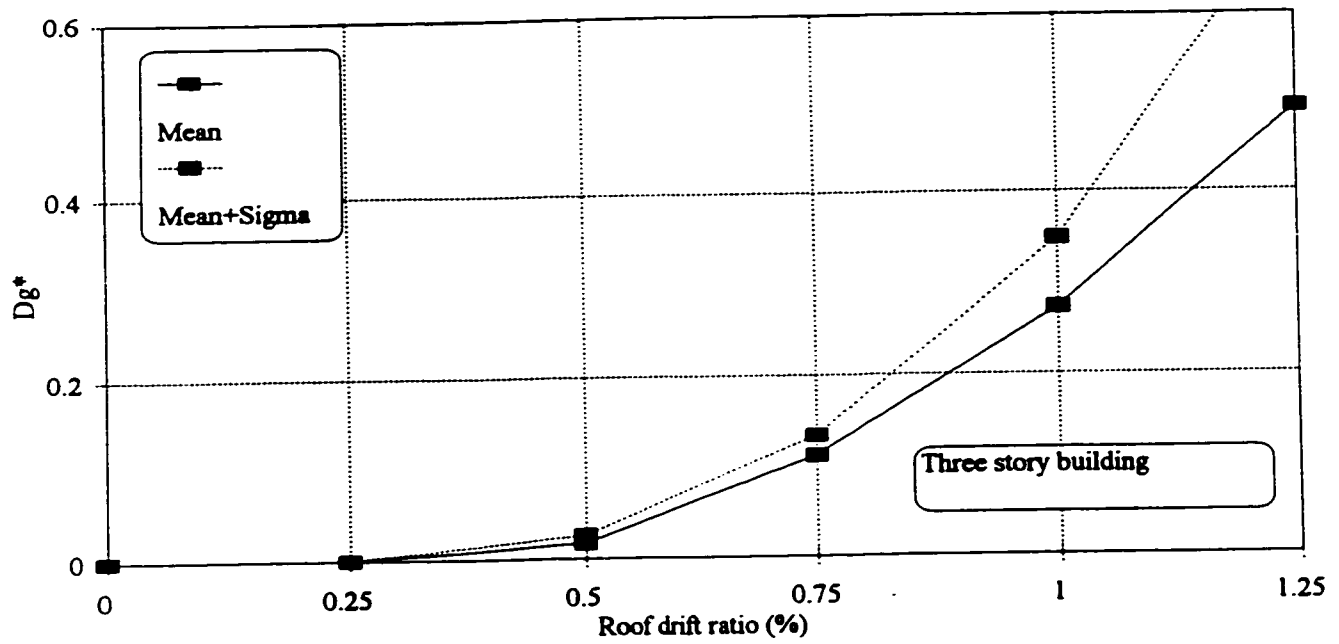
Figure 4.7 Relationship between the roof drift ratio and the mean of the damage index D_g^*
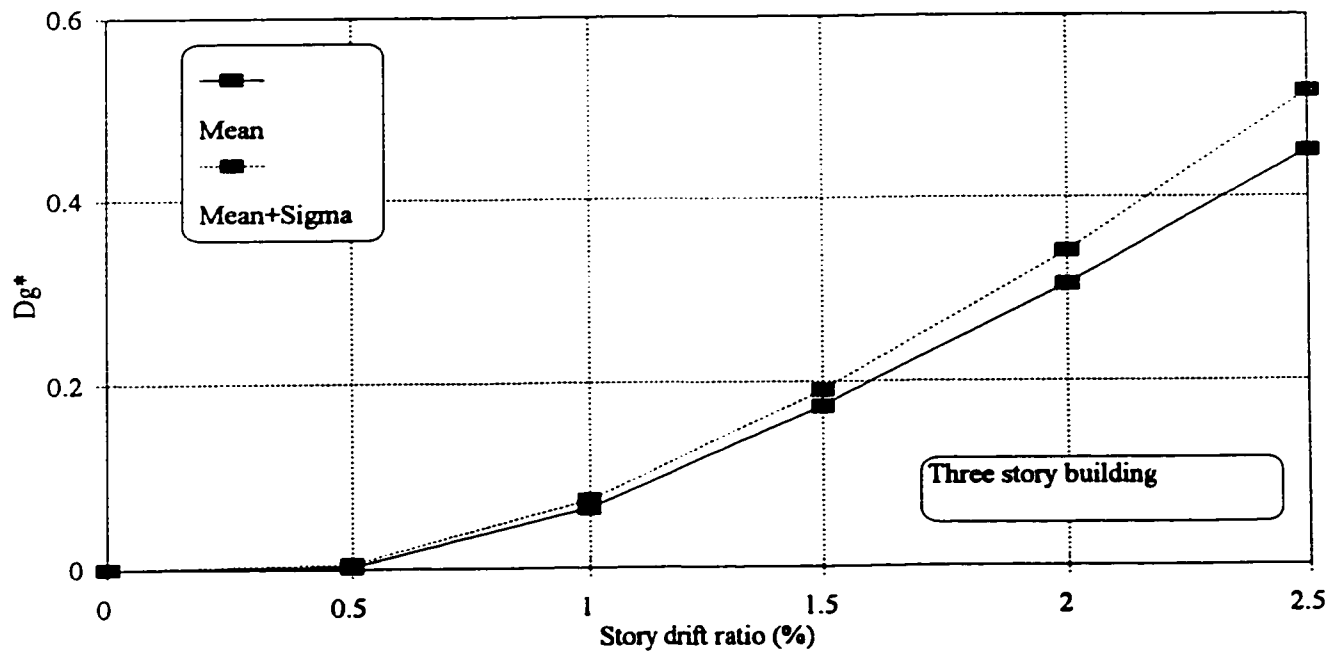
Figure 4.8 Relationship between the story drift ratio and the mean of damage index D_g^*
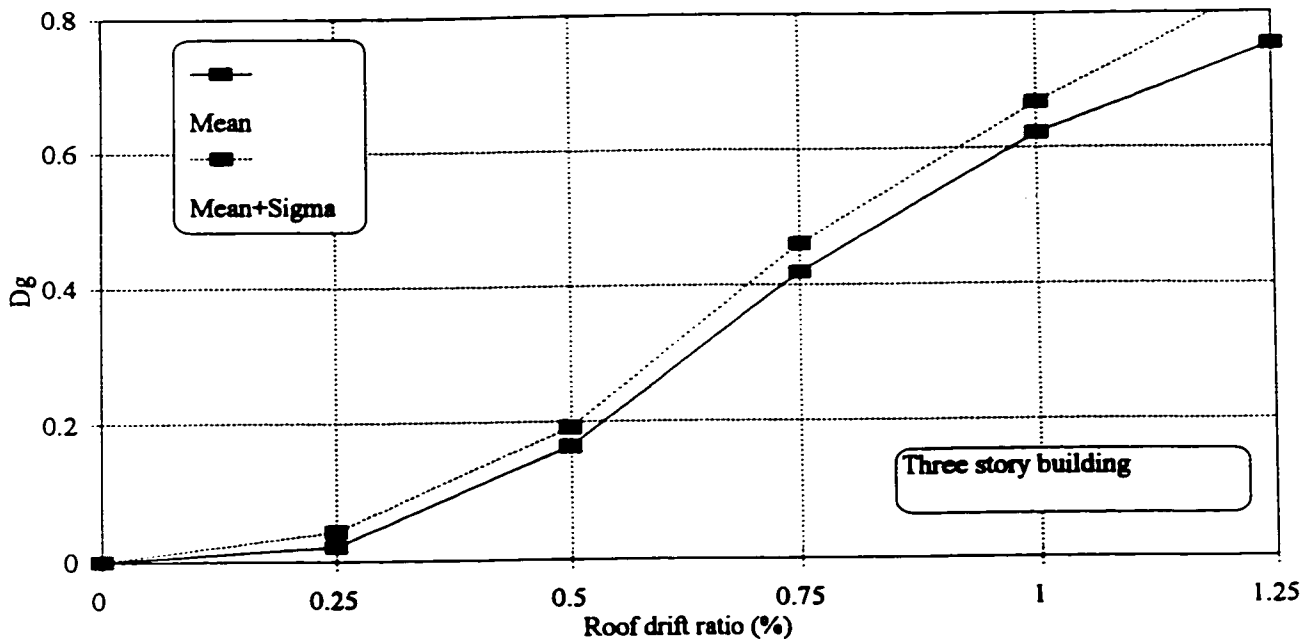
Figure 4.9 Relationship between the roof drift ratio and the mean of the damage index D_g
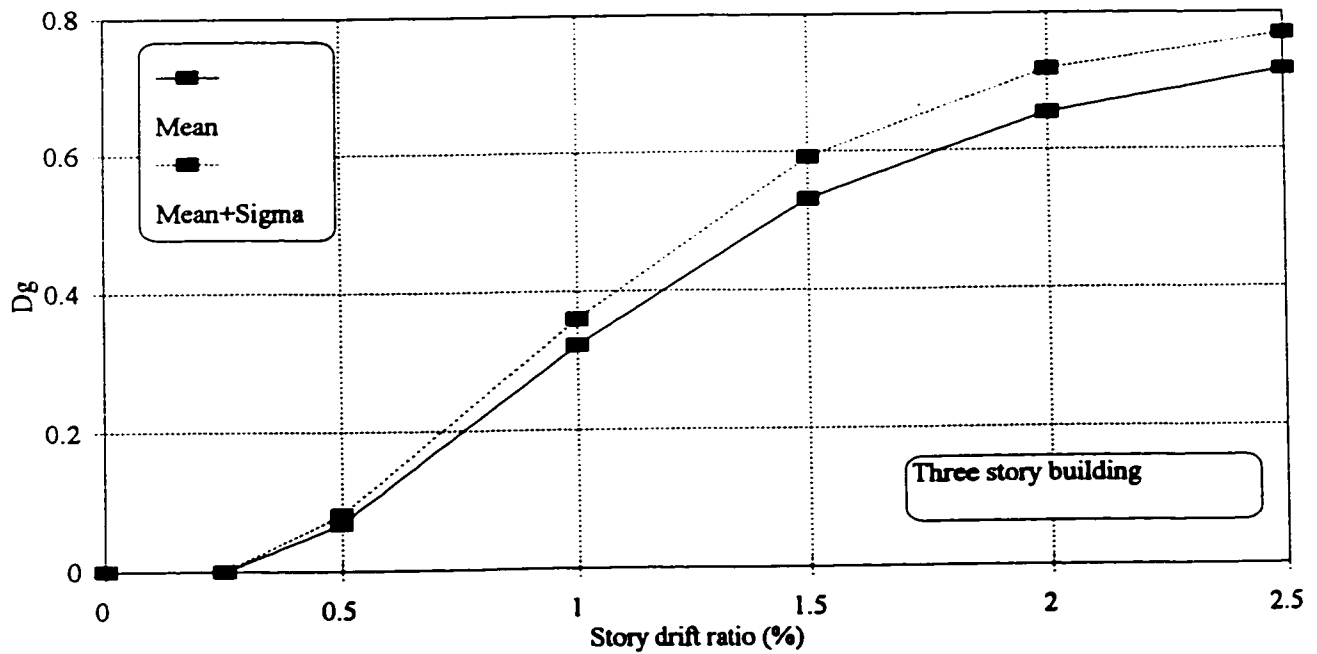
Figure 4.10 Relationship between the story drift ratio and the mean of the damage index D_g
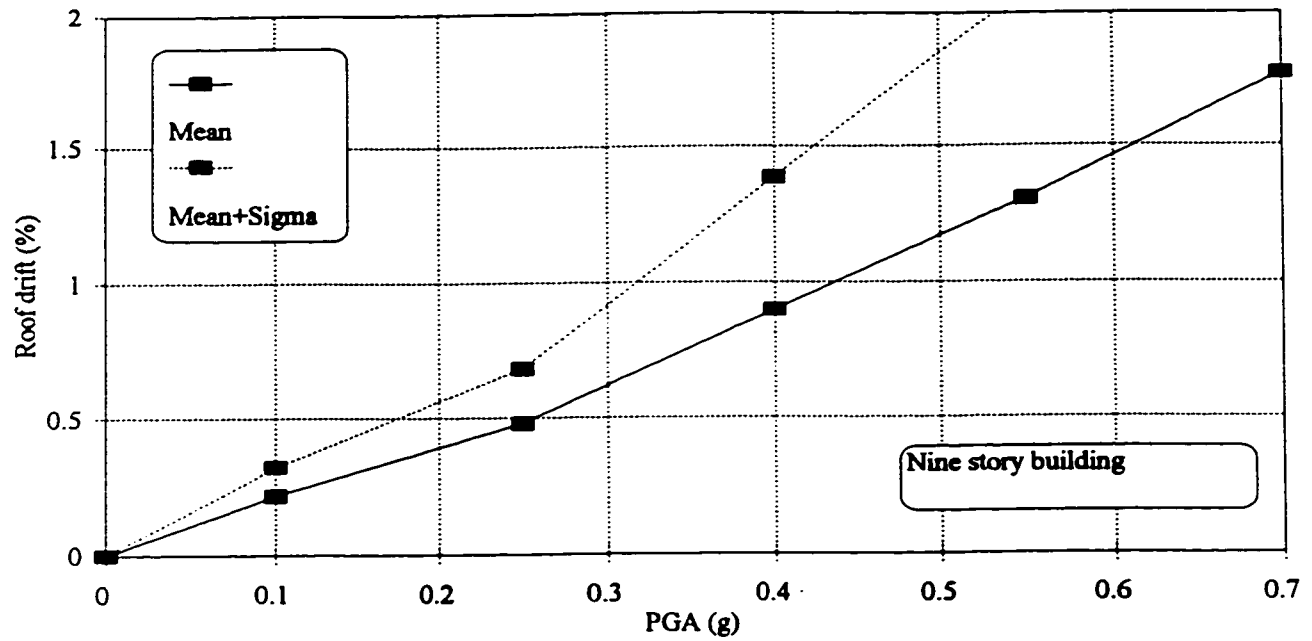
Figure 4.11 Roof drift ratio variation with the PGA
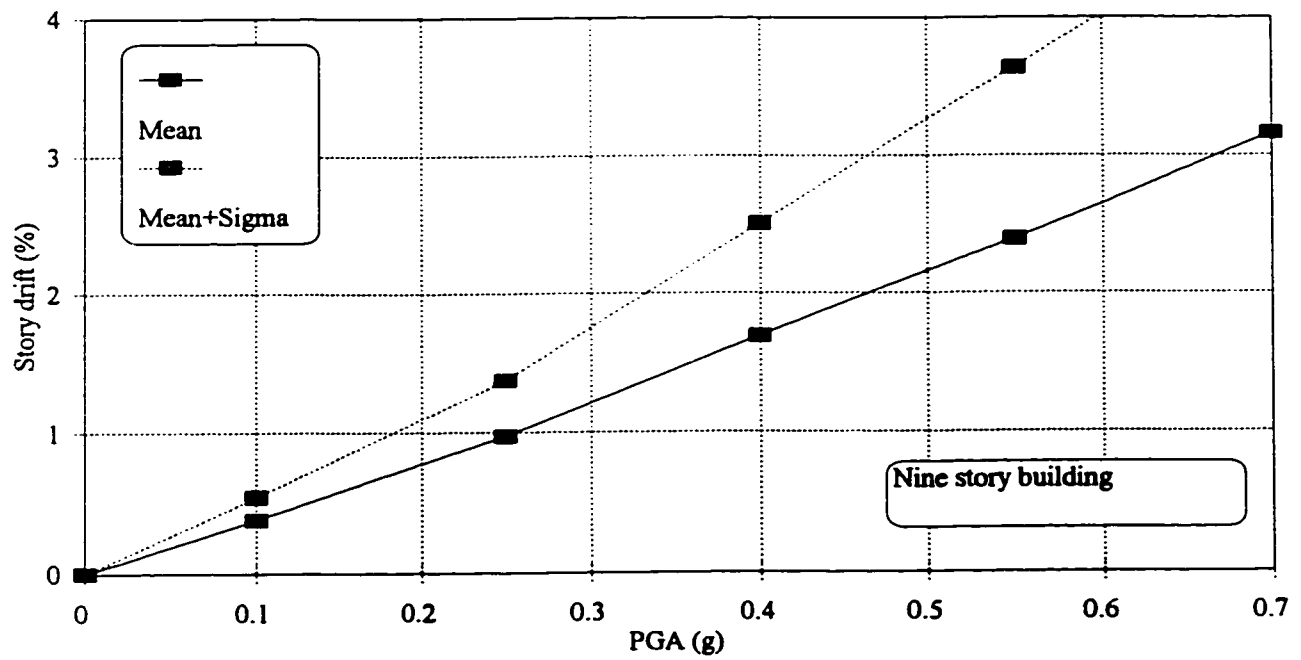
Figure 4.12 Story drift ratio variation with the PGA
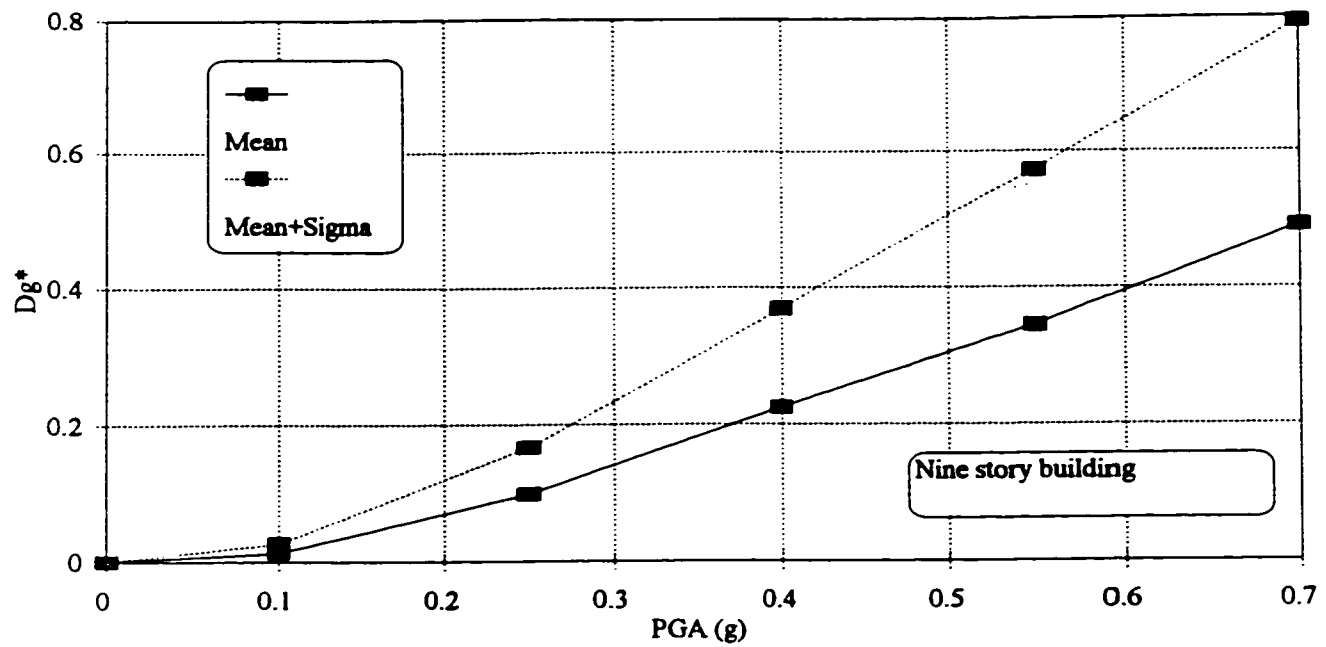
Figure 4.13 Damage index D_g^* variation with the PGA
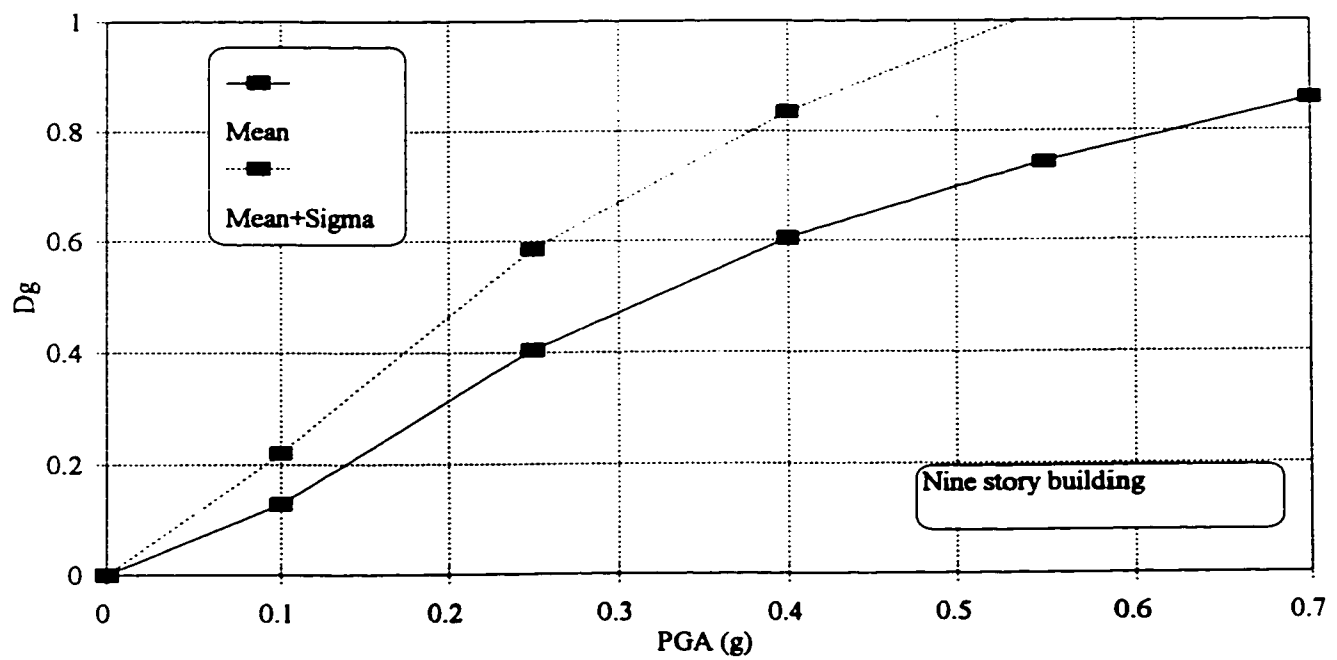
Figure 4.14 Damage index D_g variation with the PGA
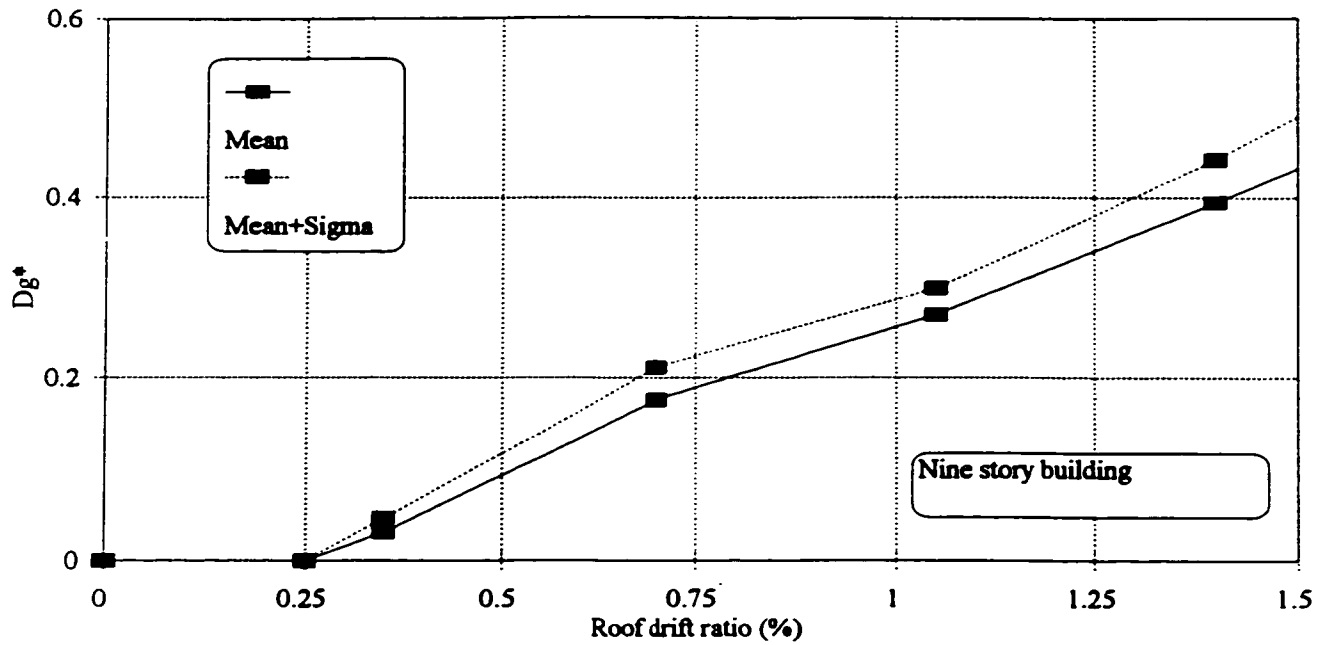
Figure 4.15 Variation of the damage index D_g^* with the roof drift ratio
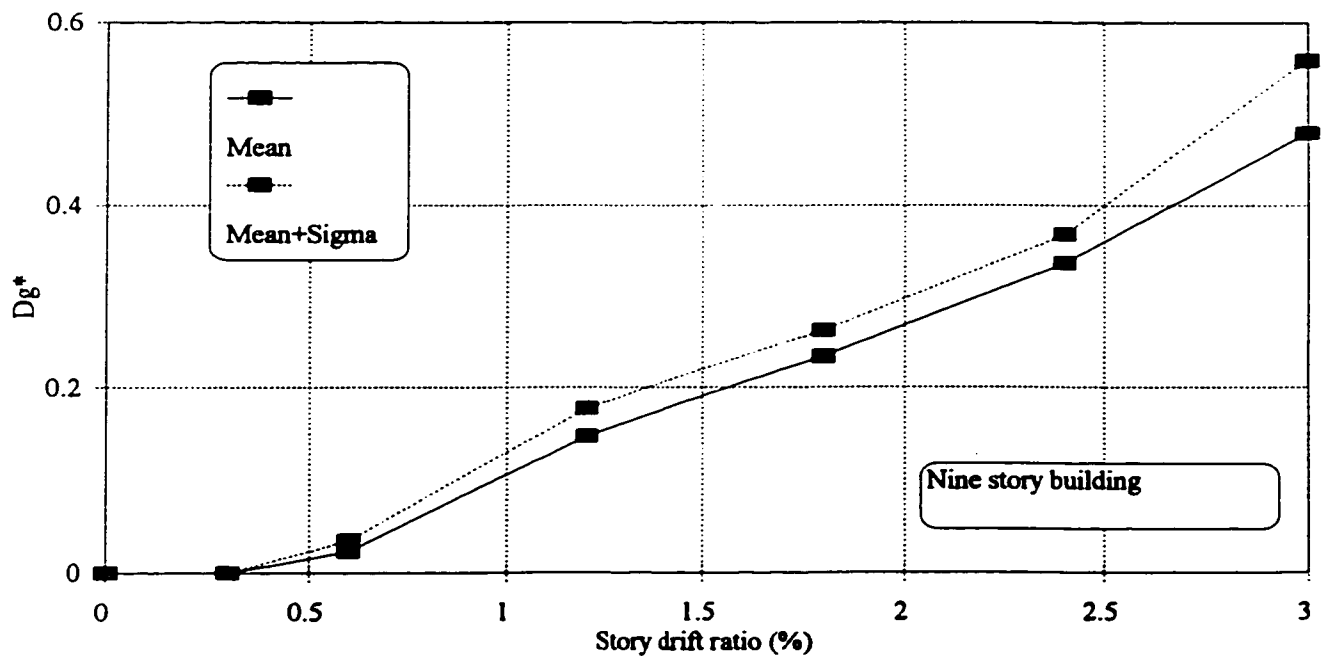
Figure 4.16 Variation of the damage index D_g^* with the story drift ratio
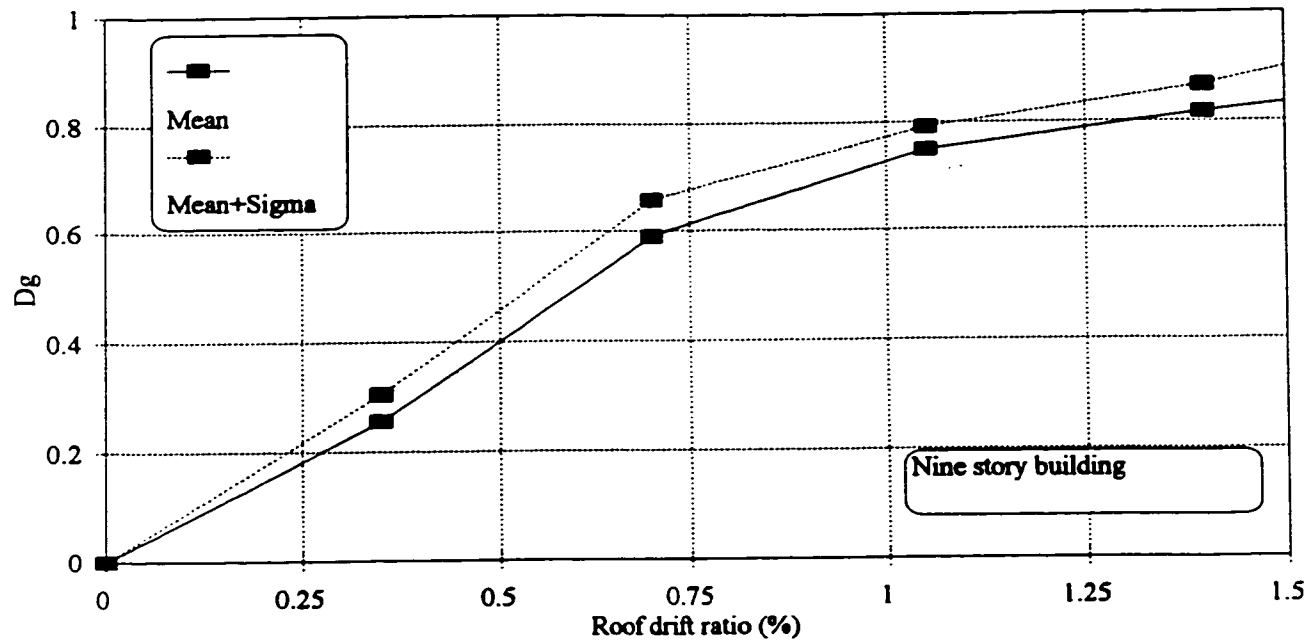
Figure 4.17 Variation of the damage index D_g with the roof drift ratio
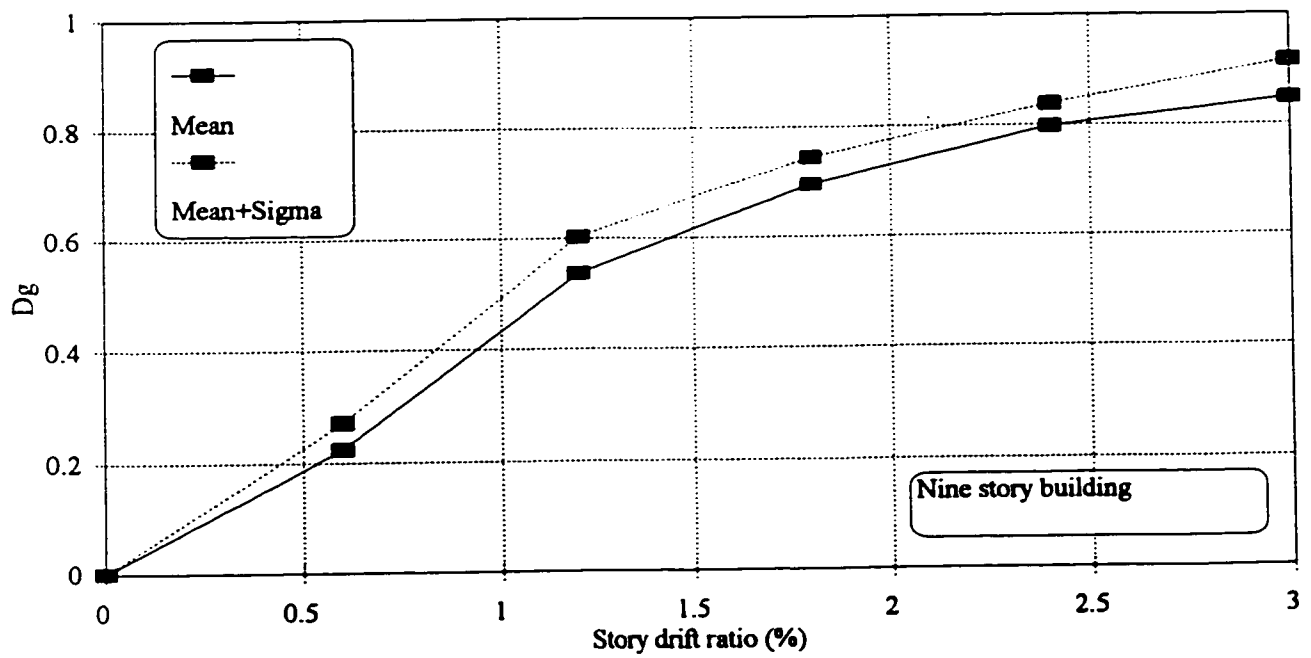
Figure 4.18 Variation of the damage index D_g with the story drift ratio
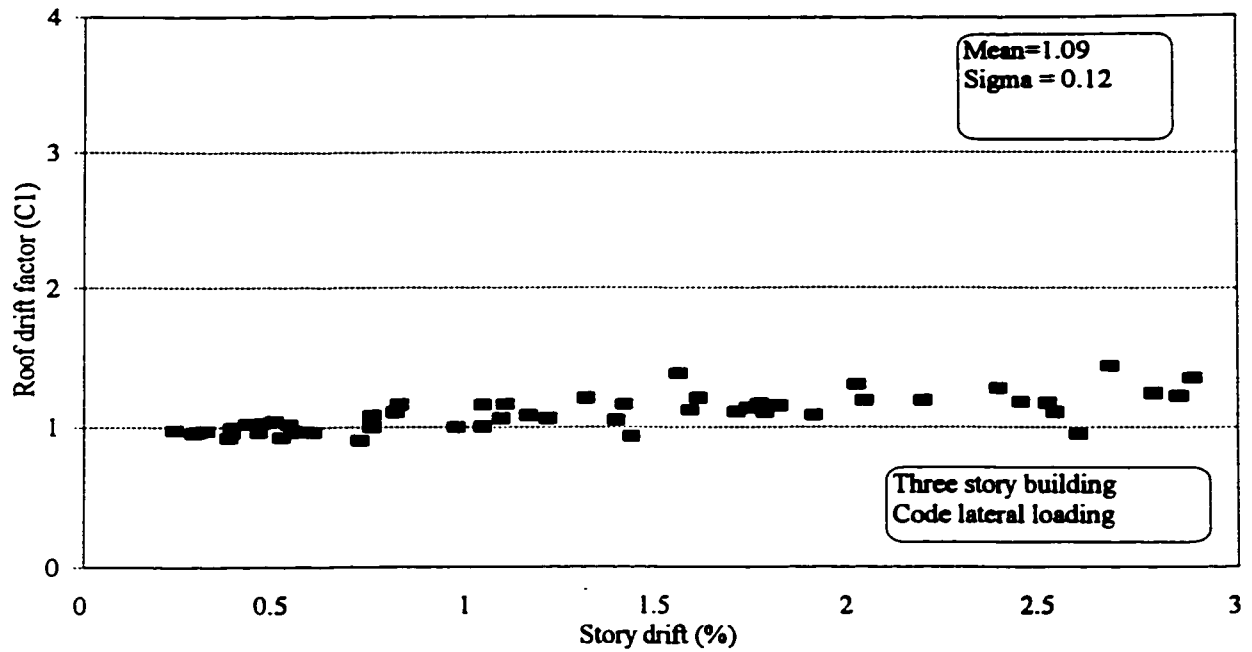
Figure 4.19 Relationship between the story drift ratio and the response factor C_1
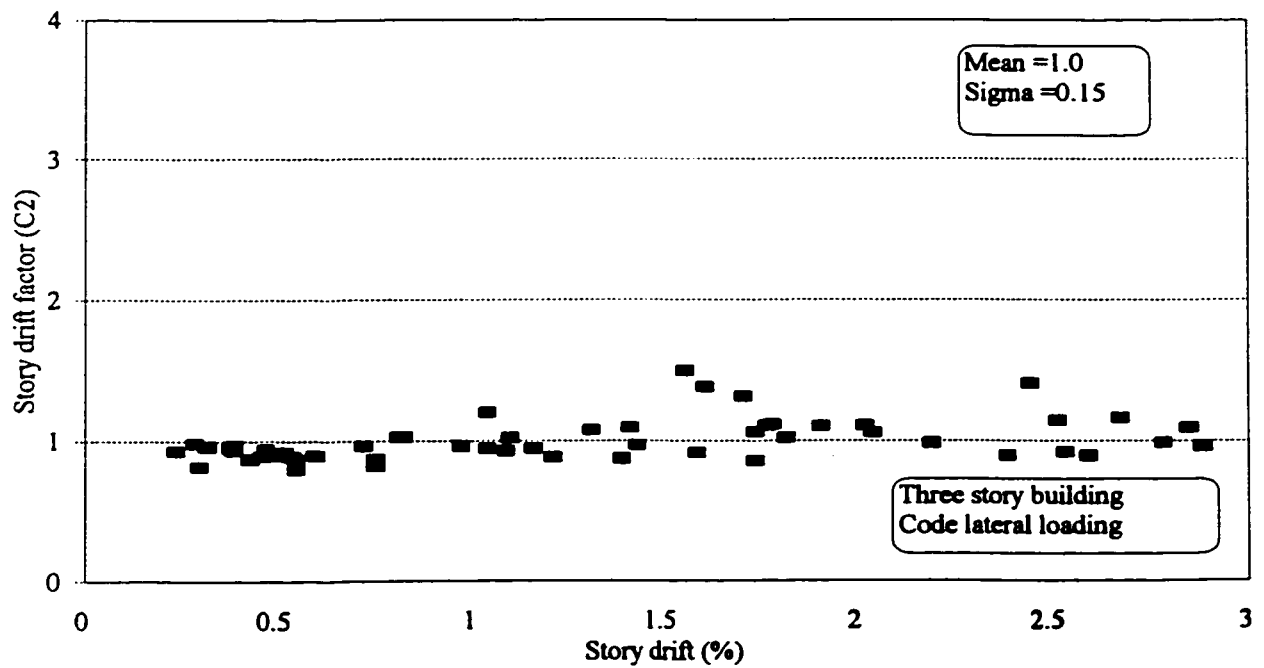
Figure 4.20 Relationship between the story drift ratio and the response factor C_2
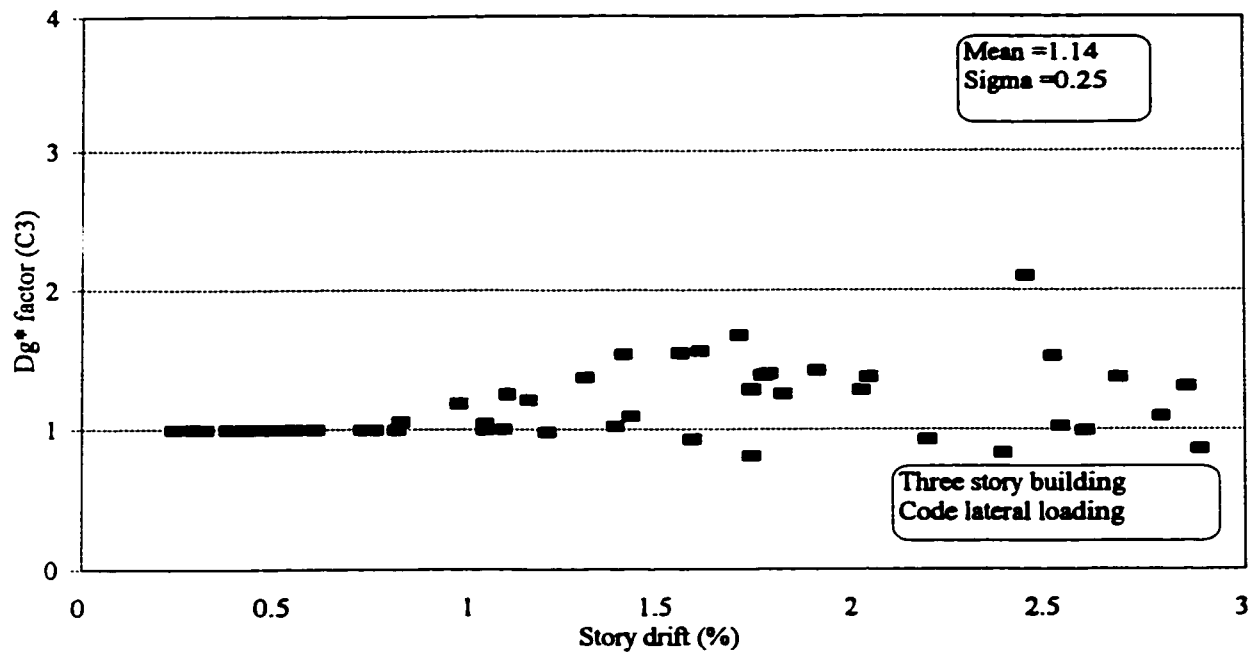
Figure 4.21 Relationship between the story drift ratio and the response factor C_3
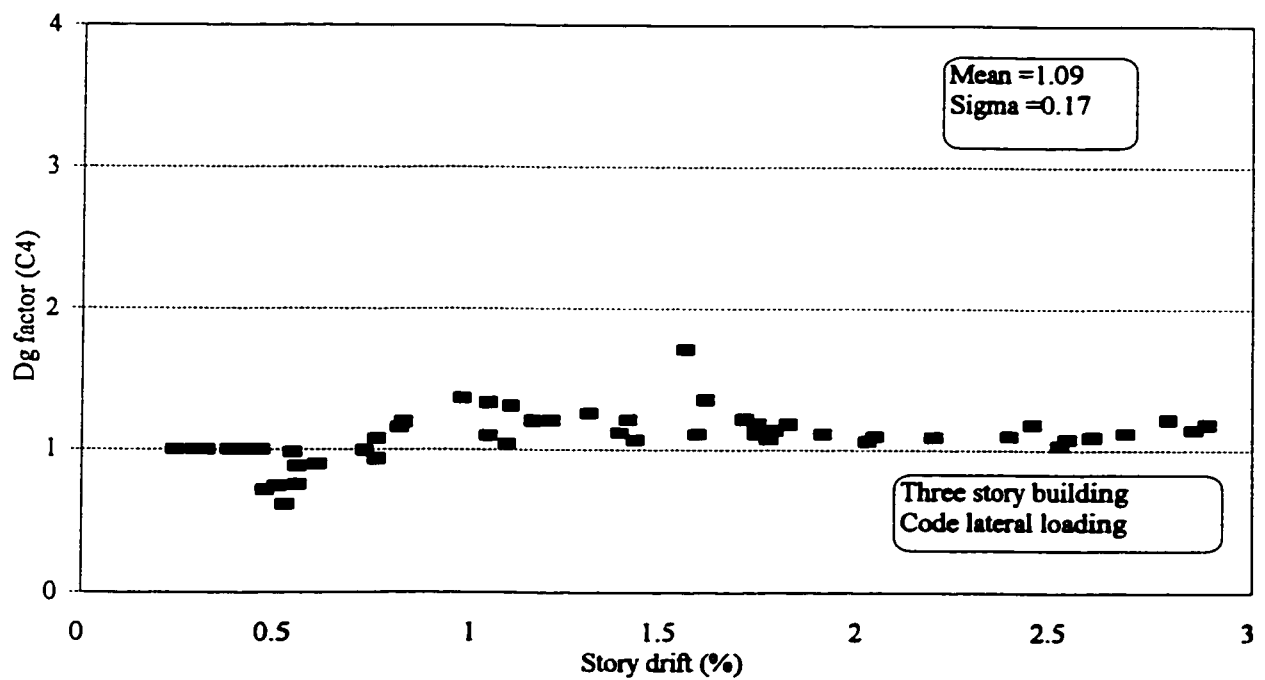
Figure 4.22 Relationship between the story drift ratio and the response factor C_4
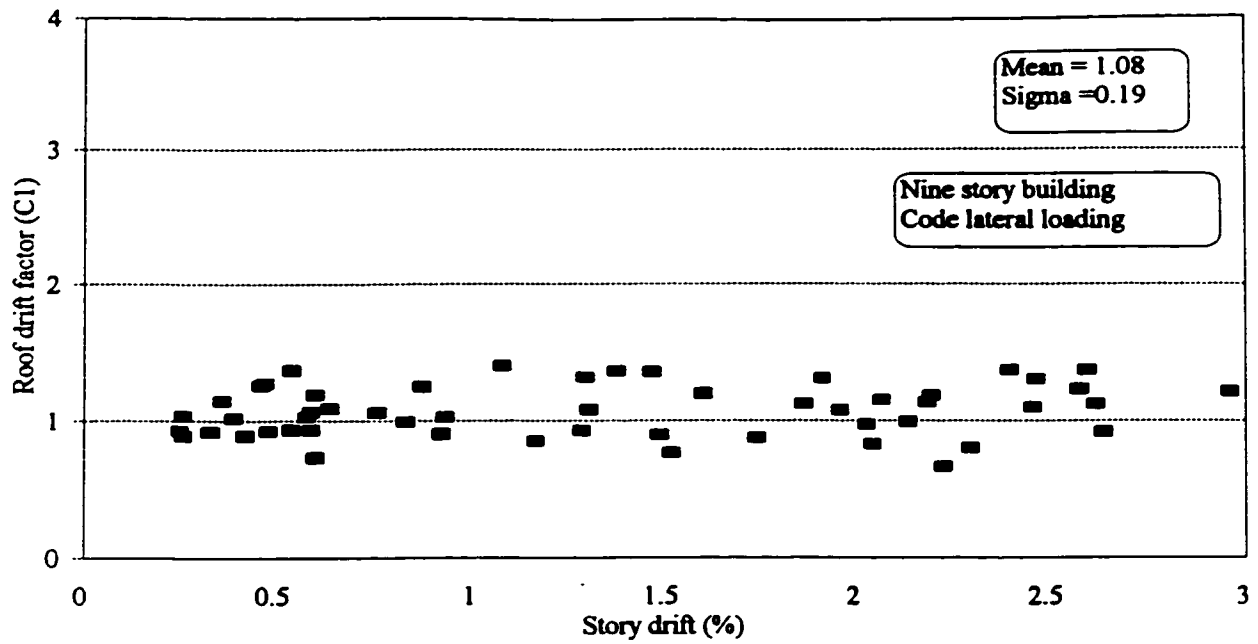
Figure 4.23 Relationship between the story drift ratio and the response factor C_1
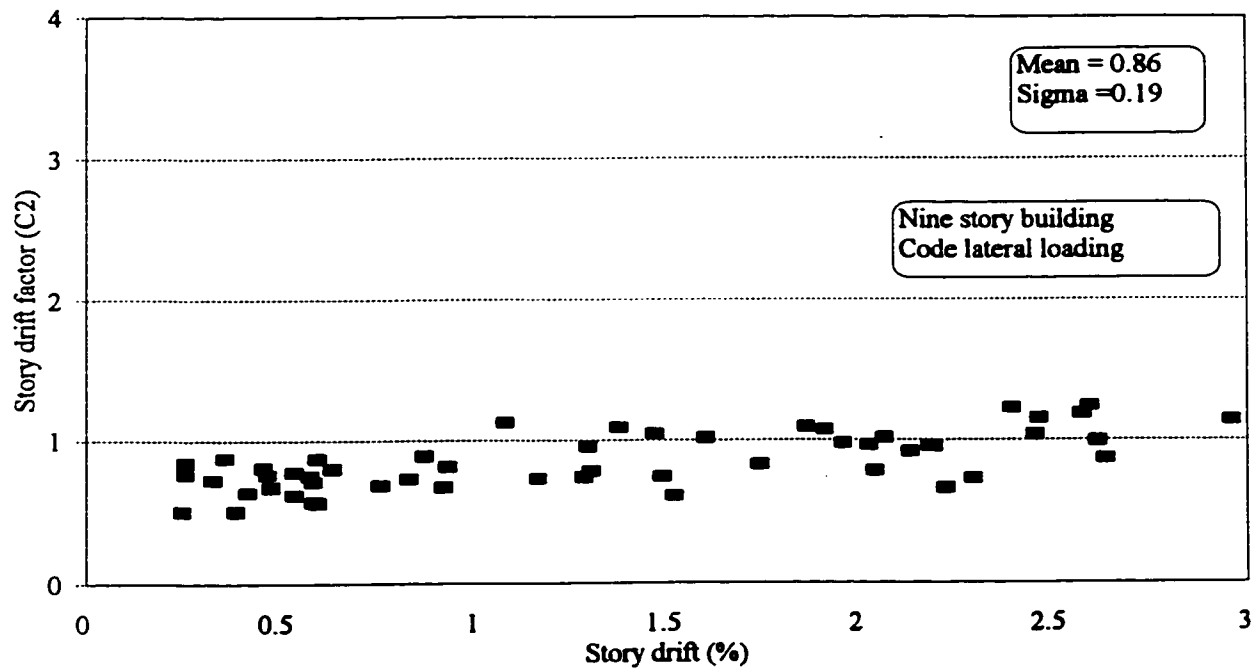
Figure 4.24 Relationship between the story drift ratio and the response factor C_2
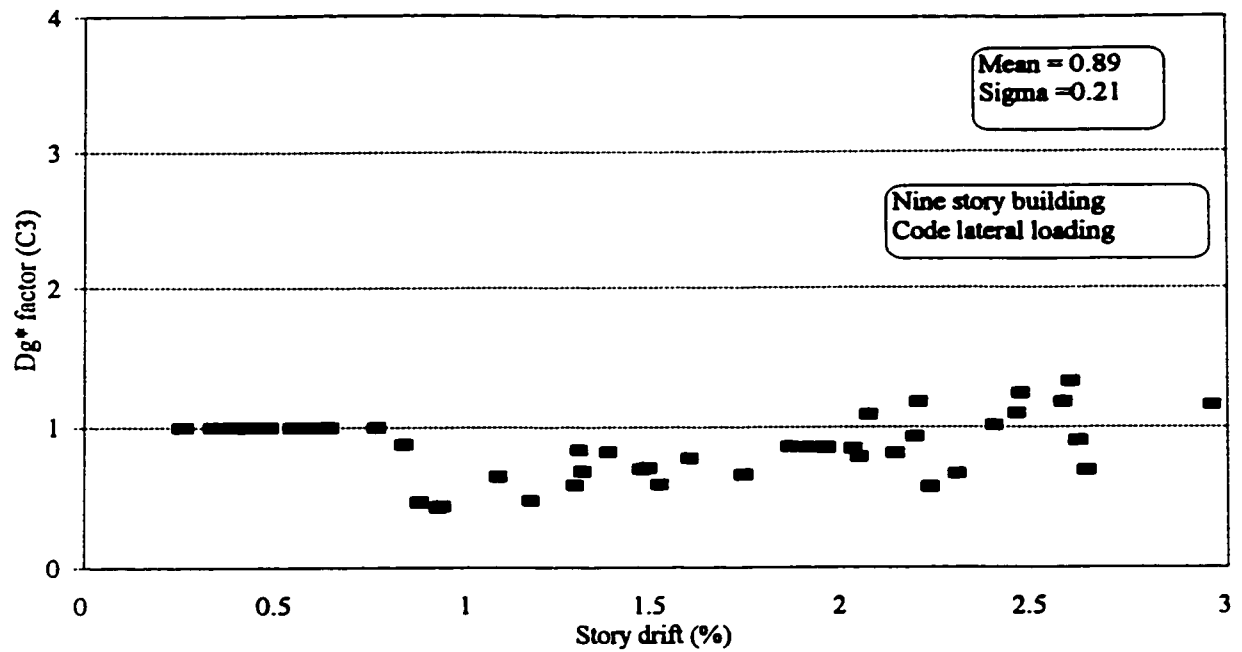
Figure 4.25 Relationship between the story drift ratio and the response factor C_3
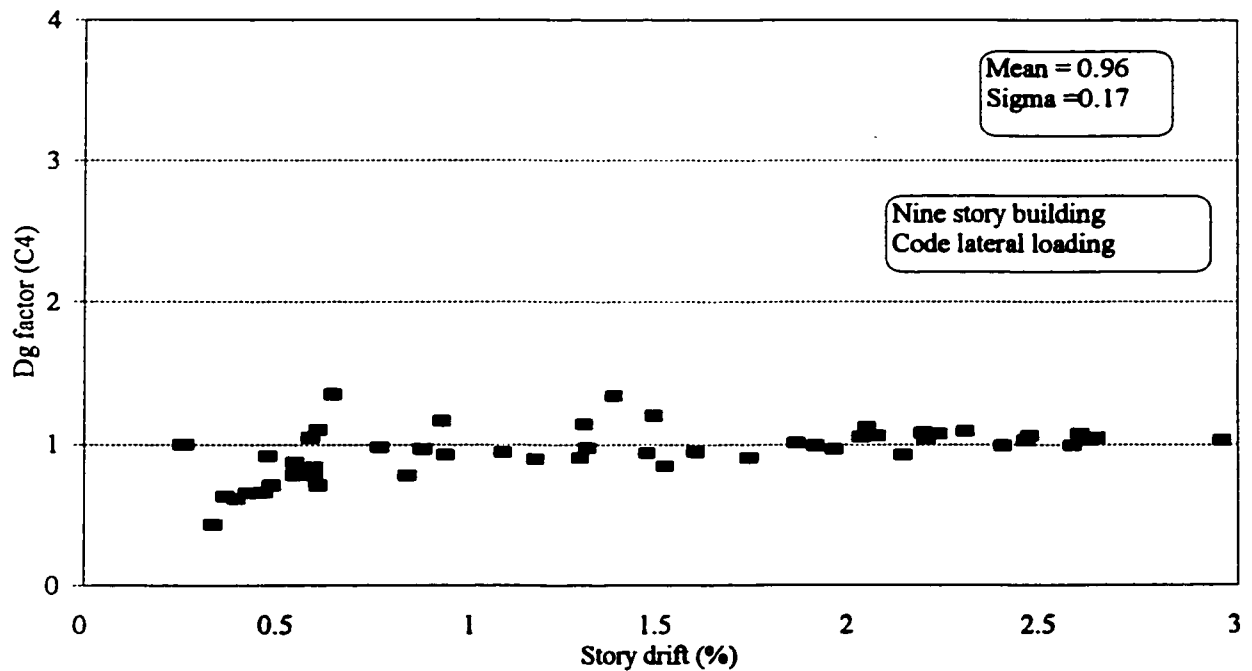
Figure 4.26 Relationship between the story drift ratio and the response factor C_4

CHAPTER 5

REHABILITATION OF RC BUILDINGS USING CONCENTRIC

STEEL BRACING

5.1 INTRODUCTION

To enhance the seismic performance of existing nonductile reinforced concrete buildings, steel braces may be inserted in the frame openings to increase the building stiffness and load carrying capacity. Examples of concentric steel bracing patterns that can be used include X-bracing, V-bracing and inverted V-bracing.

The seismic performance of the nonductile three-story reinforced concrete building described in Chapter 4 was studied when the building is rehabilitated using concentric X-bracing. For accessibility and ease of installation, the steel bracing is installed in the exterior frames of the building. Steel bracing members were modelled using a phenomenological model that accounts for steel yielding in tension and buckling in compression. The brace model was implemented into the DRAIN-2DX computer program.

The building was modelled as a series of planar frames connected at each floor level by rigid diaphragms. The effect of the arrangement of the steel bracing on the seismic behaviour of the rehabilitated building was evaluated. Steel bracing distributions along the frame height and along the frame bays were investigated. The dynamic analysis was conducted using the twelve ground motion records presented in Chapter 4. The effect of the geometric nonlinearity (P-Δ) was included in the analysis. The impact of steel bracing on the

144

levels of axial and shear forces developed in the rehabilitated building columns is evaluated. The effect of the amount of bracing and brace distribution along the frame height on the damage-deformation relationship of the rehabilitated buildings is studied.

5.2 DETAILS OF BRACE CONNECTIONS

The detail of the connection between the concentric X-bracing and the RC frame members is shown in figure 5.1. The force in the bracing member is transferred to the RC frame by means of steel plates attached to the ends of the RC columns and beams. The steel plates surrounding the beams are anchored through the concrete section while the steel plates of the column are welded together. The load of the bracing member is distributed to the beam and the column plates through a gusset plate. The steel plates attached to the ends of the RC columns may provide some confinement to the concrete. However this confinement will be limited to small number of the building columns and is expected to have minor effect on the overall building performance.

5.3 STEEL BRACE MODEL

Several models have been developed to represent the inelastic buckling behaviour of steel brace members. These models can be divided into two main types; finite element models (Fujimoto et al., 1973), and phenomenological models (Roder and Popov, 1977; Jain and Goel, 1978; Ikeda et al., 1984; Remennikov and Walpole, 1995). In the current study, the Jain and Goel model (1978) shown in figure 5.2, was chosen to represent the inelastic buckling behaviour of steel braces. In the figure, the load level "P_y" represents the load

capacity of the bracing member in tension, "P_c" corresponds to the buckling load capacity under monotonic loading and it can be reached once during the entire loading history. After the member buckles at the load level "P_c" the member will have a load-displacement relationship with negative slope (segment 1-2) as shown in the figure. Point "2" is defined by the residual buckling capacity "P_r" and a compression displacement equals five times the yield displacement in tension "Δ_y". Upon reversal of the loading direction at point "3" and reloading in tension, the member follows segments 3-4, 4-5 and 5-6. The location of point "4" controls the pinching that follows post buckling behaviour of the bracing members. The model was implemented into the DRAIN-2DX computer program. The model is able to mimic the behaviour of bracing members with effective slenderness ratio varying from 40 to 120. The behaviour of bracing members with effective slenderness ratio of 40 is closer to the plastic action range (yielding axially in compression), while the behaviour of bracing members with effective slenderness ratio of 120 is closer to the elastic buckling range. Although there are more complex models, the Jain and Goel model strikes a good balance between numerical simplicity and complex observed experimental behaviour (Badoux, 1987).

In the programming of the Jain and Goel brace element into the DRAIN-2DX code, two new features are introduced. The first feature provides an "event to event" tracing of the axial load-axial displacement loops as shown in figure 5.3. The exact deformation value at which the element enters new zones is detected and the new stiffness is computed, thus nullifying the unbalanced force induced by the change in the stiffness between different branches of the element hysteretic loops. Figure 5.3 represents a portion of the load-displacement relationship of the bracing element. Point "a" represents the current element

response and point "b" represents a control point similar to points 1, 2, 3, 4, 5 and 6 in figure 5.2. The load increment demand on the element calculated from the equilibrium of the entire structure using the element stiffness at point "a" is ΔP. Applying ΔP directly may lead to the development of unbalanced force due to the change in the stiffness before and after point "b". In the "event to event" solution strategy an event factor is computed for each element to determine the allowable level of load increment. The smallest event factor of all the structure elements is considered in determining the load increment to be applied to the structure.

A second feature is added to the element to prevent loading of the steel bracing members during the application of the gravity loads. This is needed since steel bracing members are added to the nonductile building after its construction. An additional branch with zero stiffness was added to the hysteretic loops presented in figure 5.2. This additional branch can be accessed from any point on the hysteretic loops of the bracing element. The activation of this branch is controlled by a parameter defined in the input file before gravity loads are applied to the structure. The element can also be returned to the original loops by changing the value of the parameter after the application of the gravity loads.

The main parameters that govern the hysteretic rules of the bracing model shown in figure 5.2 are the yield load "P_y", the initial buckling load "P_c", the residual buckling load "P_r" and the effective length of the bracing member "KL". The initial buckling load "P_c" can be calculated using the provisions of the CSA-S16.1-94. The residual buckling load "P_r" is specified as a fraction of the initial buckling load "P_c". It varies from 20% to 60% of "P_c" depending on the effective slenderness ratio of the bracing member (Jain and Goel, 1978). The following equation was proposed by (Lee and Goel, 1987) for calculating the residual

buckling load of tubular sections:

$$P_r = [0.4 - 0.0025\frac{KL}{r}]P_c \quad \text{for} \quad \frac{KL}{r} < 120 \tag{5.1}$$

where K is the effective length factor, L is the length of the bracing member and r is the radius of gyration of the cross section. Ikeda et al. (1984) provide guidance for calculating the residual buckling load of sections other than the tubular ones. The effective length factors for concentric X-bracing are influenced by the rigidity of the end connections and the connection at the intersection of the two brace members. In the current study, the bracing members are assumed to be connected at the intersection points. The effective length factors were taken as 0.5 for in-plane buckling and 0.67 for out- of-plane buckling as suggested by Pincheira (1992). The effective length factors apply to the full brace length.

5.4 THE STEEL BRACING PARAMETERS

Two parameters were introduced to define the resulting increase in the lateral load carrying capacity of the rehabilitated building and the distribution of the steel bracing along the building height. The first parameter "b" defines the increase in the overall lateral load carrying capacity of the nonductile building due to the addition of steel bracing. This parameter is defined as the ratio of the lateral load carrying capacity of the rehabilitated building to the lateral load carrying capacity of the existing building. The lateral load carrying capacity of the building is determined by conducting a static pushover analysis using the code lateral load distribution.

A second parameter "b_i" is used to describe the distribution of the steel bracing along

the building height. The parameter is defined for each story as the ratio between the algebraic sum of the lateral load carrying capacities of the steel bracing in the story to the algebraic sum of the lateral load carrying capacities of the steel bracing in all the building stories. The lateral load carrying capacity in this case is calculated as (P_m cos θ), where "P_m" is the load capacity of the steel brace member in the selected loading direction and is equal to P_y or P_c. The inclination angle of the brace member with the horizontal axis is "θ". In the case of X-bracing with all the brace members having a constant angle "θ" and the same material properties, the parameter "b_i" can be considered as the ratio between the algebraic sum of the areas of the steel braces in the ith story to the algebraic sum of the areas of the steel braces in all the building stories.

5.5 BRACE DISTRIBUTION ALONG THE FRAME HEIGHT

The steel bracing may be installed in one or several stories along the height of the building. The behaviour of four rehabilitation cases R_1, R_2, R_3 and R_4 were evaluated to study the effect of the brace distribution along the height on the seismic response of the rehabilitated building. The four rehabilitation cases are shown in figure 5.4. In the bracing case R_1, the brace members are selected as round hollow sections (HSS 114 x 8) and are distributed uniformly along the frame height. The clear width-to-thickness ratio is less than 14.0 for ductile behaviour as recommended by Lee and Goel (1987). The brace properties are as follows:

E=200,000 (MPa) f_y = 350 (MPa)   (P_y/ P_c) = 0.415

(P_r/ P_c) = 0.33   r = 37.7 (mm)   (KL / r) =113

where E is Young's modulus and f_y is the steel yield stress. The parameter "b" for the first rehabilitation case is approximately equal to 2.0. This represents the case where the lateral load carrying capacity of the rehabilitated building is twice that of the original structure. For the other three rehabilitation cases, the brace properties E, f_y, (P_y / P_e), (P_r / P_e), r, (KL / r) as well as the total area of the bracing members are kept constant. The brace distribution parameter b_i is the only variable as shown in figure 5.4 and summarized in table 5.1 for the four rehabilitation cases. The rehabilitation case R_2 has a linear distribution of the total bracing area along the building height instead of the uniform distribution in the first case R_1. In the rehabilitation case R_3, the total brace area is distributed in the first two stories of the building, while in the fourth case of rehabilitation R_4 the total brace area is distributed only in the first story. The performance of the four rehabilitation cases is investigated when using both static cyclic loading and earthquake loading.

5.5.1 Response Under the Effect of Static Cyclic Loading

The static cyclic analysis is a simple approach to study the complex problem of predicting force and deformation demands imposed on structures and their elements by severe earthquakes. All the rehabilitation cases shown in figure 5.4 were subjected to the roof displacement history shown in figure 5.5. The intensity of the cyclic loading was controlled by the parameter Z. The value of Z was changed between 0.1 to 0.5. The product of Z and u_y represents the roof displacement increment in the loading routine, where u_y is the yield roof displacement. Damage to the rehabilitation cases due to the application of the static loading was evaluated in terms of the story drift and the strength based damage index D_s^* as shown

in figures 5.6 and 5.7, respectively. From these figures, it is clear that the bracing distribution along the frame height has a significant effect on the inelastic response of the rehabilitated building. Figure 5.6 indicates that the rehabilitation case R_2 experienced lower level of story drift at a specific level of Z by comparison to the other rehabilitation cases. At high levels of the parameter Z, the damage index D_g^* for the rehabilitation case R_2 was significantly lower than for the other rehabilitation cases. The rehabilitation case R_2 is superior in its plastic mechanism by comparison to the other rehabilitation cases as it has uniform distribution of story drifts and story damage indices D_i among all the building stories as shown in table 5.2. In the rehabilitation case R_1, the concentration of deformation mainly in the first story led to a high level of deterioration in the building lateral load carrying capacity at relatively low levels of the parameter Z. In the bracing cases R_3 and R_4 with steel bracing provided only to the first one or two stories of the building, most of the building deformation was concentrated in the unbraced stories. The bracing cases R_3 and R_4 experienced high level of story drift and damage by comparison to the bracing case R_2.

The characteristics of the plastic mechanisms of the rehabilitation cases can be evaluated using the plastic mechanism parameter v presented in Chapter 4. The parameter v measures the variation in the story drift ratios corresponding to a roof drift ratio of 1.0% obtained from a static pushover analysis. Low values of v reflect uniform distribution of plastic behaviour along the height of the structure. A high value represents concentration of the deformation in one floor. The lower the value of v, the more desirable is the developed plastic mechanism of the building under the effect of lateral loading. The story drift ratios corresponding to 1.0% roof drift ratio of the four rehabilitation cases are shown in table 5.3.

The value of the parameter v for the second rehabilitation case, R_2, was the lowest among the values of the four rehabilitation cases. This indicates a more uniform distribution of story drift along the building height.

5.5.2 Free Vibration Characteristics

The free vibration characteristics of the four rehabilitation cases are listed in table 5.4. The change in the free vibration characteristics between the first and the second brace distribution cases is very small. However, there are significant changes in the fundamental periods and modal contributions of the third and fourth cases by comparison to those of the first and the second cases. The change in the free vibration characteristics suggests that the seismic demands may differ among the four rehabilitation cases. Table 5.5 summarizes the elastic spectral forces corresponding to the fundamental periods of the four rehabilitation cases due to the application of the various ground motion records when scaled to PGA level of 1.0 g. The elastic spectral forces are considered as an approximate relative measure of the intensity of the seismic demands for each of the rehabilitation cases. In general, an increase in the seismic demands is expected to occur as a result of the steel bracing rehabilitation. The only exception to this trend is in the case of San Fernando earthquake (record number 10). A significant reduction in the elastic spectral force of the ground motion has occurred as a result of rehabilitation. This is because the dominant period of the ground motion was approximately equal to the fundamental period of the existing structure. It is recognized that for each of the rehabilitation cases the seismic demands will depend on the characteristics of the particular ground motion used.

5.5.3 Response Under the Effect of Earthquake Loading

The seismic performance of the four rehabilitation cases was studied when subjected to scaled versions of the Monte Negro earthquake. The dynamic analysis was performed using a time step increment of 0.005 second and Rayleigh viscous-damping which was defined to achieve 2.0% damping in the first two natural modes of vibration of the building. Figures 5.8 to 5.10 represent the variation of the roof drift ratio, the story drift ratio and the damage index D_g^* with the PGA, respectively. Table 5.6 summarizes the story drift and the damage index distribution of the various stories in the four rehabilitation cases. The results in the table show that there is a good correlation between the maximum story drift ratio resulting from the earthquake loading and the level of the parameter v (listed in table 5.3 for the four rehabilitation cases). The second rehabilitation case with the lowest value of v exhibited the lowest drift ratio among all the rehabilitation cases, while the fourth rehabilitation case with the largest value of v exhibited poor performance despite the relatively low seismic demands as indicated from table 5.5.

Figure 5.11 shows examples of the distribution of damage due to the inelastic response of the existing building and the rehabilitation cases R_1, R_2, R_3 and R_4. The damage distribution of figure 5.11 was due to the application of the Monte Negro ground motion. The numbers in the figures show the formation sequence of some selected plastic hinges. Numbers in italic font are for the column hinges while numbers in regular font are for the beam hinges. For the case of the existing building (PGA=0.45 g), hinging started in the beams of the first floor due to pullout of the bottom reinforcement and yielding of the top reinforcement. With the increase in the intensity of the earthquake, damage spread to the

columns of the first and second stories because of the splice failure at the bottom ends and yielding of the reinforcement at the top ends. Beam hinging was also observed in the second floor because of pullout of the bottom reinforcement. Damage to the third story was minimal by comparison to the first and second stories.

For the rehabilitation cases R_1, R_2, R_3 and R_4, the inelastic response was characterized by severe column damage because of splice failure at the bottom ends and yielding of the reinforcement at the top ends. In the rehabilitation case R_1 (PGA=0.7 g), hinging starts in the first and second story columns adjacent to the steel bracing members. No damage was observed in the columns and beams of the third story. Buckling of the steel bracing members was observed in all the building stories.

In the rehabilitation case R_2 (PGA=0.7 g), hinging starts in the first and third story columns and in the beams of the second floor. At the final stage of response, all the building columns experienced splice failure at the bottom ends and yielding of the reinforcement at the top ends. The number of plastic hinges in this rehabilitation case was large by comparison to the case of the existing building and to the other rehabilitation cases. No damage was observed in the beams of the third floor. Buckling was observed in all the steel bracing members.

In the rehabilitation case R_3 (PGA=0.425 g), hinging starts in the third story columns. All the third story columns experienced splice failure at the bottom ends and yielding of the reinforcement at the top ends. Damage to the first and second stories was minor by comparison to the third story. Damage to the beams of the building floors was very limited. Brace buckling was observed in all the steel bracing members of the first story and in two of

the second story brace members.

In the rehabilitation case R_4 (PGA=0.415 g), hinging starts in the third story columns. All the second and third story columns experienced splice failure at the bottom ends and yielding of the reinforcement at the top ends. Damage also was observed in the beams of the second floor due to pullout of the bottom reinforcement. No damage was observed in the columns of the first story and in the beams of the first and third floors. Brace buckling was observed in some of the steel bracing members of the first story.

The seismic response of the two rehabilitation cases R_1 and R_2 was determined using the twelve ground motion records presented in Chapter 4. The seismic performance parameters of the two rehabilitation cases were related to the PGA level as shown in figures 5.12 to 5.15. The figures represent the relationships of the PGA level versus the mean of the roof drift ratio, the story drift ratio and the damage indices D_s^* and D_s, respectively. The results shown in the figures indicate that at a specific PGA level, the second rehabilitation case R_2 experienced lower levels of deformation and damage by comparison with the first rehabilitation case R_1. This confirms the results obtained when using only the Monte Negro ground motion record.

From the previous analysis and discussion, it can be concluded that adding steel bracing uniformly along the height of an existing nonductile building may not represent the optimum solution. It is possible to improve the plastic mechanism of the rehabilitated building by special arrangement of the lateral strength distribution along the frame height to force most of the building stories to contribute to the building overall deformation. This will lead to significant reduction in the damage level to the rehabilitated building under the effect of

seismic loading.

The parameter v is useful in evaluating the designed bracing systems and in selecting the best design. By excluding the effects of the seismic demand differences which result from the changes that may occur in the free vibration characteristics of the rehabilitation cases, it can be concluded that the lower the parameter, v, the lower is the story drift ratio that will develop under the effect of an earthquake loading. In the case of the three story building considered in this chapter, the linear distribution of steel bracing shown in case R_2 (figure 5.4 b) provided the best bracing scheme.

5.5.4 Effect of Brace Distribution on the Damage-Deformation Relationship

The relationship between the story drift and the damage index D_s^* for the two rehabilitation cases R_1 and R_2 due to the application of scaled versions of the Monte Negro earthquake is shown in Figure 5.16. The two rehabilitation cases include the same amount of steel bracing but with different distributions along the frame height. As shown in the figure, at a specific story drift ratio, the second rehabilitation case R_2 experienced lower level of damage than the first case R_1. The reason for this difference in the level of damage is because the maximum story drift shifted from the first story in the first rehabilitation case to the second story in the second rehabilitation case as shown in figure 5.17. The building members in the second story are subjected to lower axial forces by comparison to the building members in the first story. The results indicate that using story drift ratio as a sole measure of seismic damage is not an appropriate approach for the case of nonductile RC buildings rehabilitated using steel bracing. Steel bracing arrangement may cause a significant variations

in the story drift capacity of the rehabilitated buildings.

5.6 BRACE DISTRIBUTION ALONG THE FRAME BAYS

When distributing the steel bracing members along the frame bays the question may be raised as to whether to concentrate the steel bracing in one bay or to distribute it among the frame bays. To evaluate these options, two rehabilitation cases R_1 and R_5 were considered. The first rehabilitation case, R_1, is the uniform brace distribution case with b =2.0 (figure 5.4a). In the second rehabilitation case, R_5, all the steel bracing members were added uniformly along the height in only one bay of the frame as shown in figure 5.4 e. The same brace cross section of case R_1 was used in case R_5 in order to eliminate any variations that may occur in the brace behaviour due to the change of the brace cross section properties. The two rehabilitation cases were subjected to the static cyclic loading shown in figure 5.5. The performance of the two cases was compared in terms of story drift, damage indices as shown in table 5.7. The changes in the story drift ratio between the two rehabilitation cases are small, however, there is an increase in the level of damage in the second rehabilitation case. The damage index D_g^* was increased by about 13.0 % at Z=0.4. The increase in the damage level resulted from the increase in the axial compression forces in the building columns connected to the brace members. The deformation capacity of the RC column at peak strength decreases when it is subjected to an increasing compressive axial force. In the current study, the effect of the axial force on the deformation capacity at peak strength of the RC members is taken into account using an interaction diagram between the axial force and the curvature at peak strength. Column CO_3 shown in figure 5.4 exhibited an increase in the

compression axial force of about 66% (from 1401 to 2331 kN).

The two rehabilitation cases were subjected to scaled versions of the Monte Negro earthquake. The performance of the two cases was compared in terms of story drift and damage indices in table 5.8. The second rehabilitation case R_5 experienced higher levels of damage than the first case R_1, following the same trend as in the static analysis. Figure 5.18 shows the distribution of damage to the rehabilitation case R_5 due to the application of the Monte Negro ground motion (PGA=0.55 g). Damage distribution of the rehabilitation case R_1 was presented before in figure 5.11. The inelastic response of the two rehabilitation cases was characterized by severe column hinging in the first and second stories due to splice failure at the bottom ends and yielding of the reinforcement at the top ends. No damage was observed in the columns and beams of the third story.

Based on the previous static and dynamic analyses, it can be concluded that distributing the steel bracing members over more than one bay will provide better performance by comparison to the case of concentrating the steel brace in a single bay.

5.7 EFFECT OF THE AMOUNT OF BRACING ON RESPONSE

The seismic response of three different steel bracing rehabilitation cases R_1, R_6 and R_7 was evaluated using the twelve ground motion records presented in Chapter 4. The rehabilitation case R_1 is shown in figure 5.4 a, while the rehabilitation cases R_6 and R_7 are shown in figure 5.4 f and 5.4 g, respectively. The steel bracing in the rehabilitation cases R_1, R_6 and R_7 is uniformly distributed along the height with "b" equals approximately to 2.0, 1.5 and 2.5, respectively.

The three rehabilitation cases were intended to provide the existing building with different strength levels. The effects of the changes in the load carrying capacity and stiffness of the rehabilitation cases as well as the differences in ground motion characteristics on the seismic performance of the rehabilitated nonductile building were evaluated. The correlation between the seismic performance parameters of the rehabilitation cases and the PGA level of the ground motions was investigated.

5.7.1 Free Vibration Characteristics

The free vibration characteristics of the three rehabilitation cases are summarized in table 5.4. The steel bracing rehabilitation has a significant impact on the fundamental period of the building. A reduction of approximately 53% in the fundamental period has occurred in the third rehabilitation case R_7 by comparison to the fundamental period of the existing building. Such reduction may cause a significant increase in the seismic demands as simply represented by the elastic spectral force of the ground motion. Table 5.5 summarizes the elastic spectral forces of all the earthquake records when scaled to PGA=1.0 g. On average, an increase in the seismic demands is expected to occur with increasing the amount of steel bracing.

5.7.2 Effect of the Ground Motion Characteristics

It is recognized from the results presented in table 5.5 that for each of the rehabilitation cases the seismic demands will depend on the characteristics of the particular ground motion used. As example of the response, figures 5.19 to 5.22 represent the

relationships of the PGA level versus the roof drift, the story drift, the strength based damage index D_{ϵ}^{*} and the stiffness based damage index D_{k}, respectively, of the rehabilitation cases R_1, R_6 and R_7 when subjected to the Long Beach ground motion. A significant improvement in the seismic performance of the rehabilitated building was achieved with increasing the amount of steel bracing. This improvement can be attributed to the increase in the building strength when increasing the amount of steel bracing along with the small changes that has occurred in the seismic demands as a result of the associated stiffness increase. The seismic demands were compared using the elastic spectral forces of the rehabilitation cases shown in table 5.5. Figures 5.23 to 5.26 represent the relationships of the PGA level versus the roof drift, the story drift, the strength based damage index D_{ϵ}^{*} and the stiffness based damage index D_{g}, respectively, of the rehabilitation cases due to the application of the Near E. Coast of Honshu ground motion. A very small change in the seismic performance of the rehabilitated building was achieved when increasing the amount of steel bracing. This may be attributed to the significant increase in the spectral elastic forces (shown in table 5.5) when increasing the amount of steel bracing as a result of the associated stiffness increase. The seismic demand increases when the first natural period of the structure becomes close to the dominant period of the ground motion.

5.7.3 Mean of the Building Performance Parameters

The mean base shear coefficients of the three rehabilitation cases R_1, R_6 and R_7 due to the application of the twelve ground motion records reached 0.31, 0.23 and 0.39, respectively. The seismic performance parameters of the three rehabilitation cases were

related to the PGA level as shown in figures 5.27 to 5.30. The figures represent the relationships of the PGA level versus the mean of the roof drift ratio, the story drift ratio, the damage index D_g^* and the damage index D_g, respectively. The results shown in the figures indicate that on average, there was a significant improvement in the building seismic performance with increasing the amount of steel bracing regardless of the increase in the seismic demands due to the associated changes in the building stiffness. The coefficients of variation of the performance parameters reached in the three rehabilitation cases at PGA=0.4 g are summarized in table 5.9. The high levels of the coefficient of variation as shown in the table indicate the poor correlation between the PGA level and the building seismic performance parameters.

5.7.4 Damage Distribution

Figure 5.31 shows examples of the distribution of damage due to the inelastic response of the rehabilitation cases R_6 and R_7. The damage distribution of figure 5.31 was due to the application of the Monte Negro ground motion. Damage distribution of the rehabilitation case R_1 due to the application of the Monte Negro ground motion was presented before in figure 5.11. In the rehabilitation case R_6 (PGA=0.55 g), hinging starts in the first and second story columns. At the final stage of response, all the first story columns and most of the second story columns experienced splice failure at the bottom ends and yielding of the reinforcement at the top ends. Damage also was observed in the beams of the first and second floors mainly due to the pullout of the bottom steel. Damage to the third story was very limited by comparison to the first and second stories. Buckling was observed

in all the steel bracing members.

In the rehabilitation case R_7 (PGA=0.585 g), hinging starts in the first story columns by splice failure at the bottom ends and yielding of the reinforcement at the top ends. At the final stage of response, damage was concentrated in the first story columns and in the first floor beams. Damage to the second and third story was minimal by comparison to the first story. Brace buckling was observed in all the steel bracing members.

Damage to the three rehabilitation cases R_1, R_6 and R_7 due to the application of the Monte Negro ground motion was characterized by severe column hinging in the first story. Beam hinging was mainly due to the pullout of the bottom steel. Damage to the third story was minimal by comparison to the first and second stories. It was observed that with increasing the amount of steel bracing, damage tended to concentrate in the bottom columns and floors of the building. In the rehabilitation case R_6 with b=1.5, damage was distributed in the first and second stories of the building while in the rehabilitation case R_7 with b=2.5, damage was concentrated in the building first story. Damage distribution to the rehabilitation case R_1 with b=2.0, represented an intermidate case between the two rehabilitation cases R_6 and R_7.

5.7.5 Effect of the Amount of Bracing on the Damage-deformation Relationship

The impact of the amount of steel bracing on the relationship between the story drift and the strength based damage index D_s^* is evaluated. The two rehabilitation cases R_6 and R_7 were subjected to the static cyclic loading shown in figure 5.5 as well as scaled versions of the Monte Negro earthquake. The first case represents a uniform brace distribution with

b =1.5 while the second case represents a uniform brace distribution with b=2.5. Figure 5.32 represents the relationship between the damage index D_s^* and the story drift ratio due to the application of the static cyclic loading while figure 5.33 represents the same relationship but due to the application of the dynamic loading. The results shown in the figures indicate that increasing the amount of steel bracing will cause a corresponding increase in the level of damage at a specific story drift ratio. The increase in the damage index D_s^* at 2.5 % story drift reached approximately 19.0% and 16.0% for the dynamic and the static loadings, respectively. The increase in damage can be attributed to the fact that increasing the amount of steel bracing increases the level of axial forces acting on the building columns. Higher levels of axial compression forces may reduce the ductility of the rehabilitated building columns.

Although increasing the amount of steel bracing increases the level of damage at a specific story drift ratio, it will also cause a corresponding increase in the load carrying capacity of the rehabilitated building. This results in a significant reduction in the deformation and damage experienced by the rehabilitated building at a specific PGA level as indicated from the analysis results presented in section 5.7.3.

5.8 EFFECT OF THE GEOMETRIC NONLINEARITY (P-Δ)

In the case of reinforced concrete buildings rehabilitated using steel bracing, high levels of axial forces are expected to develop in the building columns adjacent to the steel bracing elements. High axial forces will result in more significant P-Δ effect. Neglecting the P-Δ effect (e.g., Pincheira, 1992) may be either because of software limitation or to simplify

the analysis.

The rehabilitation case R_7 shown in figure 5.4 g was used to evaluate the effect of the P-Δ. This rehabilitation case includes a heavy bracing system that is uniformly distributed along the height with b=2.5. The rehabilitated building was subjected to scaled versions of the Monte Negro earthquake. The analysis was conducted with and without considering the P-Δ effect. The results of the dynamic analysis are shown in figures 5.34 and 5.35. Figure 5.34 represents the relationship between the PGA level and the maximum story drift while figure 5.35 represents the relationship between the PGA level and the damage index D_s^*. From figure 5.34, at PGA=0.6 g, an increase of about 20% in the story drift is due to the P-Δ effects. The corresponding increase in the damage index D_s^* reached approximately 50 %.

These results indicate that the P-Δ can significantly affect the response of the rehabilitated nonductile buildings. It can increase the story drifts and the damage indices of the rehabilitated building when subjected to an earthquake loading. Neglecting the P-Δ effect in the inelastic analysis of braced reinforced concrete buildings can be a crude approximation.

5.9 EFFECT OF BRACING ON THE COLUMN AXIAL AND SHEAR FORCES

The effect of the steel bracing on the levels of axial and shear forces developed in the building columns is investigated. The X-bracing system resists the lateral loads by truss action. The truss consists of the bracing members and the building beams and columns. The truss behaviour will lead to the development of significant axial forces in the building columns. In addition, compression axial forces acting on the columns increase the column flexural strength thus increasing the shear force demands on the columns. In this section, the

levels of axial and shear forces acting on the column of the nonductile frame were investigated

for the rehabilitation case R_7 shown in figure 5.4 g which includes a heavy bracing system that

is uniformly distributed along the height with b=2.5.

Table 5.10 summarizes the maximum axial forces in the building columns adjacent to

the steel bracing members before and after rehabilitation due to the application of the Monte

Negro earthquake. The PGA of the earthquake was selected to produce significant inelastic

response of the structure. For the existing building the PGA was equal to 0.4g and for the

rehabilitated building it was taken as 0.585 g. In the table, the level of the axial force is

presented as the ratio between maximum force developed in the member and the axial

capacity of the member in compression or tension. The column axial capacity in compression

was calculated considering both the steel and the concrete contributions $(A_c \, f_c'+A_s \, f_y)$ while

in tension it was calculated considering only the steel contribution and neglecting the concrete

tensile strength $(A_s \, f_y)$, where f_c' is the concrete compressive strength, f_y is the steel yield

strength, A_c is the area of concrete and A_s is the area of steel. The results summarized in the

table indicate that the steel bracing caused a significant increase in the axial load levels acting

on the building columns. Axial tension forces were developed in the columns of the lower

stories which are connected to the steel brace members. The levels of axial forces are below

the column axial capacity as shown in the table. In addition, all the column axial forces are

below the axial load at the balanced condition of the column cross section. The ratio between

the balanced axial load and the column axial capacity in compression is equal to 0.41. The

axial forces developed in the building beams were small as compared to the axial force levels

developed in the building columns. The beam axial forces were significantly lower than the

beam axial load capacity levels.

The maximum shear forces developed in the building columns due to the application of the Monte Negro ground motion are presented in table 5.11. The table shows the maximum shear developed in the columns when the columns are subjected to compression and tensile axial forces. The shear capacity of the RC frame members were calculated using a shear strength equation proposed by Priestley et al. (1994). The predicted shear strength is the sum of three independent components as follows:

$$V = V_c + V_p + V_s \tag{5.2a}$$

where V_c is the concrete component, V_p is the axial load component and V_s is the transverse reinforcement component. The concrete component, V_c, reduces with increasing ductility. It is calculated as:

$$V_c = k \sqrt{f_c'} \ A_e \tag{5.2b}$$

where A_e is the effective shear area ($A_e=0.8 \ A_{gross}$). The parameter k depends on the member displacement ductility level. In the elastic range of response, k is equal to 0.29 while k is equal to 0.1 when the member undergoes severe inelastic deformation. The axial load component V_p depends on the member aspect ratio and is calculated as:

$$V_p = \frac{D - c}{2a} P \tag{5.2c}$$

where D is the section depth, c is the depth of the compression zone, a is half the length of the member which is assumed to bend in double curvature and P is the compressive axial load

acting on the RC member. The contribution of the transverse reinforcement is based on a truss mechanism and is estimated as:

$$V_s = \frac{A_v \, f_y \, D'cot30°}{S}$$

(5.2d)

where D' = the distance between centres of the peripheral hoop, A_v is the area of transverse reinforcement at spacing S along the member longitudinal axis and f_y is the steel yield strength. The stresses in equations 5.2 are in MPa, forces are in Newtons and dimensions are in mm.

The calculated shear capacity of the frame columns is equal to 143.0 kN, assuming the columns undergo severe inelastic deformation ($k=0.1$). The contribution of the compressive axial loads was neglected in the calculations leading to more conservative estimates to the shear strength. Compressive axial loads are expected to significantly increase the shear strength of the frame members as shown in equation 5.2c. The calculated column shear strength indicates that the shear capacity of the concrete columns exceeded the shear demands imposed by the ground motion record. For RC columns subjected to tensile axial forces, the contribution of the transverse reinforcement alone exceeded the shear demands imposed by the ground motion.

Local shear forces may be also developed in the building beam and column ends at the locations of the brace connections. Testes conducted by Goel and Masri (1994) and Maheri and Sahebi (1995) indicated the possibility of transferring the brace loading to the corner of the RC frames without producing local damage in the concrete members. Investigating the

force transfer mechanism at the brace connections will require microscopic analysis using the finite element method. In this type of analysis, the connection has to be subdivided into large number of small elements. Investigating the force transfer mechanism at the brace connections is out of scope of the current study.

5.10 APPLICATION OF THE SIMPLIFIED APPROACH

The simplified seismic performance evaluation approach presented in Chapter 4 was used to evaluate the seismic response of the rehabilitation case R_7, which includes a heavy steel bracing system. The analysis results of the approximate SDOF model and the MDOF braced building using the twelve ground motion records were compared and the accuracy of the simplified evaluation approach in predicting the seismic performance of braced nonductile RC buildings was evaluated.

5.10.1 Single Degree of Freedom Model

The properties of the SDOF model for the rehabilitation case, R_7, were calculated using the approach described in Chapter 4. Two different SDOF systems were used in the simplified analysis. The first SDOF system represents the elastic behaviour of the structure and is applicable up to 0.5% roof drift ratio. The second SDOF system represents the inelastic behaviour of the structure and is applicable when the roof drift ratio is greater than 0.5%. The damping ratio used in the equivalent SDOF system models was 2.0%. The properties of the elastic SDOF model was calculated as follows:

$$\{\Psi\}=\{0.38,\ 0.75,\ 1.0\}$$

{S}={1/6, 1/3, 1/2}

$M^* = 0.57$ x (building mass)= 969,912 kg

$L^* = 0.71$ x (building mass)=1,208,136 kg

$V^* = 0.81V$ (5.3)

The properties of the inelastic SDOF model was calculated as follows:

{Ψ}={0.82, 0.94, 1.0}

{S}={1/6, 1/3, 1/2}

$M^* = 0.85$ x (building mass)=1,446,360 kg

$L^* = 0.92$ x (building mass)=1,565,472 kg

$V^* = 0.95V$ (5.4)

The hysteretic force-displacement relationship of the SDOF model was represented using the model shown in figure 5.36. The model includes two steel brace elements (one in tension and one in compression) and one concrete spring element. The two brace elements provide an approximate representation of the contribution of the steel bracing members to the overall force-displacement relationship of the rehabilitated building. The concrete spring element provides the contribution of existing RC frames. The characteristics of the hysteretic force-displacement relationship of the steel bracing elements can be obtained by performing a static cyclic analysis on the braced building with all the frame joints considered as hinges. In this case, the braced bays of the frame works as a truss structure. The contribution of the existing RC frames can be considered as the difference between the total response of the braced building and the response of the steel bracing elements. The properties of the elements forming the system given in figure 5.36 can be selected to produce the same cyclic responses

as that of the steel bracing elements and the existing RC frames. A comparison between the cyclic responses of the MDOF and the SDOF systems was presented in figure 5.37. The good agreement shown in figure 5.37 indicates that the cyclic response of the MDOF system can be represented using the proposed SDOF model.

5.10.2 Seismic Analysis Results of the Simplified Approach

A comparison between the simplified dynamic analysis predictions and the actual response of the rehabilitation case, R_7, are presented in figures 5.38 to 5.41. The figures represent the relationships between the maximum story drift ratio on one side and the four response factors C_1, C_2, C_3 and C_4 on the other side. Definitions of the four response factors C_1, C_2, C_3 and C_4 are presented in Chapter 4. Figures 5.38 and 5.39 compare the predictions of the roof drift and the story drift, while figures 5.40 and 5.41 compare the predictions of the damage indices D_g^* and D_g, respectively.

The accuracy of the SDOF predictions for the story drift and the damage index D_g^* was studied as shown in figures 5.42 and 5.43. The figures show the number of ground motion records as a percentage of the total number that produced various levels of deviations of the SDOF predictions from the those of the MDOF model. The number of ground motion records that produced deviations in the story drift ratio more than 20.0% from the exact predictions was about 13 %. This indicates the applicability of the simplified approach for predicting the seismic response of braced nonductile RC buildings.

5.11 SUMMARY

The effect of brace distribution along the height on the characteristics of the plastic mechanism of the rehabilitated building was investigated by studying the responses of four rehabilitation cases. It was found that adding steel bracing uniformly distributed along the height of the existing nonductile building may not represent the optimum solution. The linear distribution of steel bracing along the height of the frame provided the best bracing scheme with lower damage level under the effect of seismic loading.

It was found that the degree of improvement in the seismic performance of the rehabilitated building is significantly dependent on the level of increase in the load carrying capacity as well as the changes in the seismic demand that result from the associated stiffness increase. On average, there was an improvement in the seismic performance of all the rehabilitation cases regardless of the increase in the seismic demands due to the associated changes in the building stiffness.

Steel bracing systems with different amounts of bracing or different distributions along the building height may cause different levels of damage at a specific story drift ratio. Thus, using story drift as a sole measure of damage is inappropriate in the case of existing buildings rehabilitated using steel bracing. The effect of the bracing distribution along the frame bays was studied. A good distribution should avoid concentrating the bracing members in one bay.

A simplified model was developed that includes two steel bracing elements and one SDOF concrete spring element. Good representation of the cyclic response of the rehabilitated building was obtained using the proposed model. The seismic analysis results of the simplified model and the MDOF braced building were found to be in close agreement.

Table 5.1 Brace distribution along the height of the rehabilitation cases

Case	Parameter b_i			Description
	b_1	b_2	b_3	
R_1	1/3	1/3	1/3	Uniform with height
R_2	1/2	1/3	1/6	Linear with height
R_3	1/2	1/2	0	Uniform bracing of the 1st and 2nd stories
R_4	1.0	0	0	First story only braced
R_5	1/3	1/3	1/3	Uniform with height
R_6	1/3	1/3	1/3	Uniform with height
R_7	1/3	1/3	1/3	Uniform with height

Table 5.2 Story drifts and damage indices from the static analysis.

Case	Z	Story drift			Stiffness based damage index			
		1ˢᵗ story	2ⁿᵈ story	3ʳᵈ story	D_s	D_1	D_2	D_3
R_1	0.1	1.04	0.54	0.23	0.38	0.55	0.21	0.02
	0.2	1.44	0.57	0.24	0.51	0.69	0.26	0.03
	0.3	1.85	0.57	0.24	0.60	0.77	0.29	0.04
	0.4	2.29	0.59	0.24	0.69	0.84	0.31	0.04
	0.5	2.73	0.60	0.24	0.75	0.87	0.33	0.05
R_2	0.1	0.66	0.73	0.43	0.26	0.32	0.28	0.07
	0.2	0.83	0.93	0.46	0.38	0.44	0.42	0.11
	0.3	1.01	1.15	0.48	0.46	0.51	0.51	0.14
	0.4	1.24	1.33	0.50	0.54	0.61	0.56	0.16
	0.5	1.47	1.50	0.50	0.61	0.69	0.62	0.18
R_3	0.1	0.35	0.32	1.15	0.23	0.04	0.01	0.56
	0.2	0.36	0.34	1.56	0.31	0.04	0.01	0.66
	0.3	0.37	0.34	2.01	0.40	0.04	0.01	0.75
	0.4	0.36	0.34	2.50	0.66	0.03	0.01	0.90
	0.5	0.36	0.34	2.99	0.84	0.03	0.02	0.96
R_4	0.1	0.09	1.27	0.46	0.37	0.00	0.60	0.17
	0.2	0.09	1.70	0.46	0.48	0.00	0.70	0.21
	0.3	0.09	2.13	0.47	0.64	0.00	0.82	0.24
	0.4	0.09	2.61	0.48	0.83	0.00	0.93	0.30

Table 5.3 Story drift ratio distribution corresponding to 1.0% roof drift ratio.

Bracing Case	Story drift ratio (%)			Parameter v
	First story	Second story	Third story	
R_1	2.2	0.58	0.22	0.60
R_2	1.18	1.32	0.5	0.25
R_3	0.34	0.31	2.35	0.68
R_4	0.07	2.48	0.45	0.74

Table 5.4 Free vibration characteristics of the rehabilitation cases

Case	First mode shape**					Second mode shape				
	T_1 sec	Modal mass*	1ˢᵗ floor displ.	2ⁿᵈ floor displ.	3ʳᵈ floor displ.	T_2 sec	Modal mass*	1ˢᵗ floor displ.	2ⁿᵈ floor displ.	3ʳᵈ floor displ.
Existing	0.99	0.90	0.42	0.79	1.00	0.32	0.08	1.00	0.50	-0.81
R_1	0.52	0.90	0.41	0.78	1.00	0.18	0.09	1.00	0.49	-0.79
R_2	0.50	0.84	0.30	0.67	1.00	0.19	0.13	1.00	0.95	-0.93
R_3	0.53	0.74	0.22	0.44	1.00	0.23	0.23	0.77	1.00	-0.61
R_4	0.72	0.69	0.08	0.61	1.00	0.23	0.09	0.26	1.00	-0.63
R_5	0.53	0.89	0.39	0.76	1.00	0.18	0.09	1.00	0.51	-0.78
R_6	0.65	0.90	0.41	0.78	1.00	0.22	0.09	1.00	0.50	-0.80
R_7	0.45	0.90	0.40	0.77	1.00	0.15	0.09	1.00	0.50	-0.78

** Mode shapes are normalized such that the maximum story displacement is equal to 1.0
* As a fraction of the total mass

Table 5.5 Elastic spectral acceleration of the rehabilitation cases

Rec. No.	Earthquake, (PGA=1.0 g)	Elastic spectral acceleration (g)							
		Existing	Case R_1	Case R_2	Case R_3	Case R_4	Case R_5	Case R_6	Case R_7
1	Parkfield, California	0.54	1.04	1.51	0.91	0.72	0.91	0.58	2.36
2	Nahanni, Canada	0.43	0.67	0.87	0.63	0.55	0.63	0.70	0.74
3	Imperial Valley, California	1.85	2.93	2.74	3.14	1.98	3.14	2.29	2.96
4	Kern County, California	1.09	2.24	2.06	2.17	1.53	2.17	2.04	4.32
5	San Fernando, California	1.33	1.72	1.65	1.79	1.01	1.79	1.43	1.74
6	San Fernando, California	1.04	1.99	1.91	2.25	1.27	2.25	1.22	2.43
7	Monte Negro, Yugoslavia	1.30	4.98	4.46	4.84	1.36	4.84	2.30	4.10
8	Long Beach, California	2.14	2.45	2.28	2.65	1.88	2.65	2.70	2.12
9	Lower California	1.41	2.25	2.22	2.38	1.77	2.38	2.58	2.42
10	San Fernando, California	3.61	2.92	1.94	3.01	2.11	3.01	1.83	1.90
11	Near E. Coast of Honshu, Japan	1.20	3.81	4.17	3.16	1.77	3.16	2.17	3.52
12	Mexico	2.31	3.54	3.61	3.96	2.60	3.96	3.45	2.84

Table 5.6 Story drifts and damage indices due to the Monte Negro earthquake.

Case	PGA (g)	Story drift			Stiffness based damage index		
		1st story	2nd story	3rd story	D_1	D_2	D_3
R_1	0.20	0.60	0.41	0.19	0.21	0.06	0.01
	0.30	0.92	0.58	0.22	0.45	0.18	0.02
	0.40	1.22	0.70	0.23	0.61	0.28	0.03
	0.50	2.00	0.79	0.25	0.75	0.40	0.04
	0.58	4.16	0.68	0.26	0.95	0.28	0.03
R_2	0.20	0.43	0.61	0.43	0.09	0.08	0.11
	0.30	0.53	0.78	0.53	0.17	0.16	0.21
	0.40	0.70	1.04	0.78	0.32	0.27	0.37
	0.50	0.81	1.34	1.01	0.43	0.34	0.50
	0.58	0.92	1.64	0.96	0.50	0.40	0.60
R_3	0.20	0.20	0.22	0.83	0.00	0.01	0.50
	0.30	0.33	0.34	1.36	0.00	0.01	0.71
	0.43	0.56	0.34	2.94	0.19	0.01	0.86
R_4	0.20	0.10	0.67	0.42	0.00	0.16	0.05
	0.30	0.11	0.90	0.61	0.00	0.41	0.23
	0.42	0.18	2.56	0.70	0.01	0.81	0.42

Table 5.7 The performance of distributed versus concentrated steel bracing
(Cyclic analysis)

Z	Distributed brace (Case R_1)		Concentrated brace in a single bay (Case R_5)	
	Story drift	$D_t^{\bullet}$	Story drift	$D_t^{\bullet}$
0.10	1.04	0.09	1.04	0.09
0.20	1.44	0.15	1.44	0.19
0.30	1.85	0.25	1.86	0.28
0.40	2.29	0.44	2.29	0.45
0.50	2.73	0.59	2.76	0.67

Table 5.8 The performance of distributed and concentrated steel bracing
(Dynamic analysis using the Monte Negro earthquake)

PGA (g)	Distributed brace (Case R_1)		Concentrated brace in a single bay (Case R_5)	
	Maximum story drift	$D_g^{\bullet}$	Maximum story drift	$D_g^{\bullet}$
0.20	0.60	0.03	0.57	0.04
0.30	0.92	0.06	0.89	0.07
0.40	1.22	0.14	1.21	0.16
0.50	2.04	0.34	2.07	0.39
0.55	3.14	0.74	3.52	0.85

Table 5.9 Coefficient of variations of the performance parameters
of the rehabilitation cases

Case	Coefficient of variation			
	Roof drift ratio	Story drift ratio	$D_g^{\bullet}$	D_g
R_1	0.60	0.82	1.17	0.78
R_6	0.54	0.72	1.11	0.73
R_7	0.52	0.70	1.03	0.74

Table 5.10 Maximum axial forces developed in the columns adjacent to the steel bracing of the three-story building due to the application of the Monte Negro earthquake

Story	Existing building		Braced building	
	Compression	Tension	Compression	Tension
1	0.11*	-	0.37	0.65
2	0.07	-	0.23	0.20
3	0.04	-	0.08	-

* As a ratio from the axial capacity of the columns

Table 5.11 Maximum shear forces (kN) developed in the columns adjacent to the bracing members of the existing building due to the application of the Monte Negro earthquake

Story	Maximum shear with compression axial force		Maximum shear with tensile axial force	
	Shear force	Axial force	Shear force	Axial force
1	133.10	1078.0	54.47	75.53
2	61.10	7.78	52.20	61.59
3	31.46	116.20	-	-
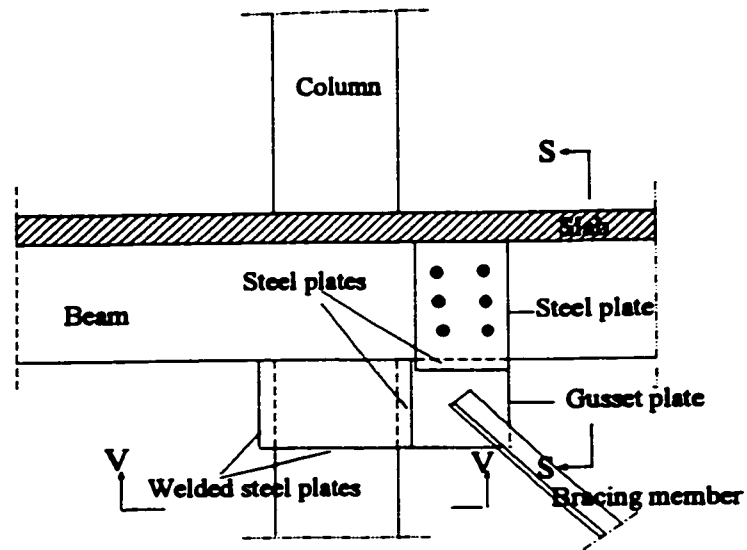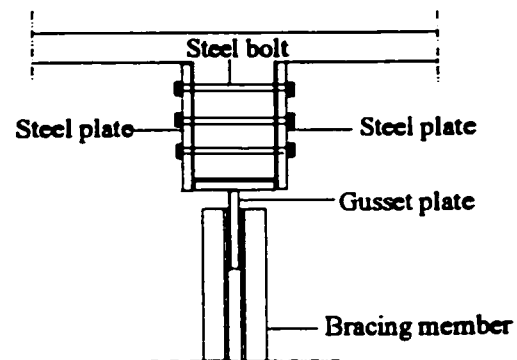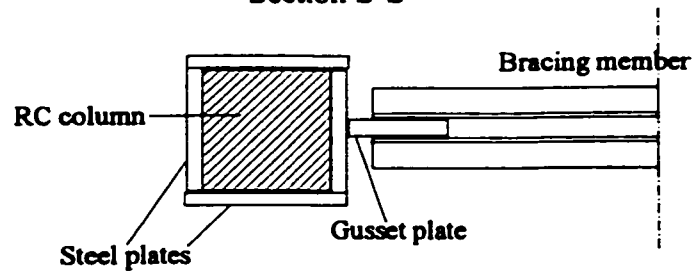
Figure 5.1 Details of a connection between brace member and RC frame
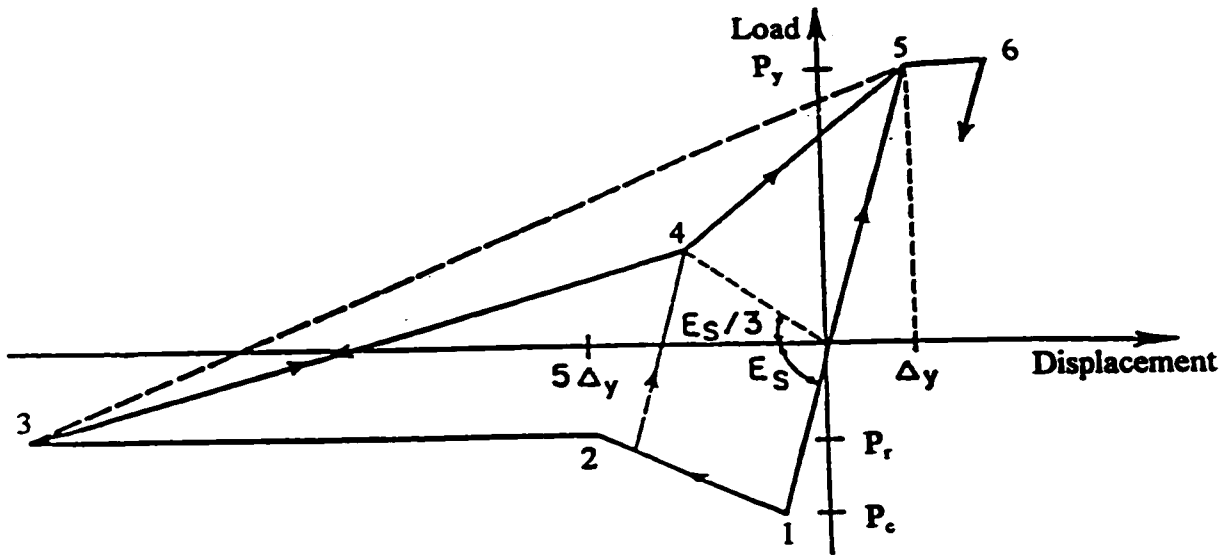
Figure 5.2 Hysteretic model of the steel bracing members (Jain and Goel, 1978)
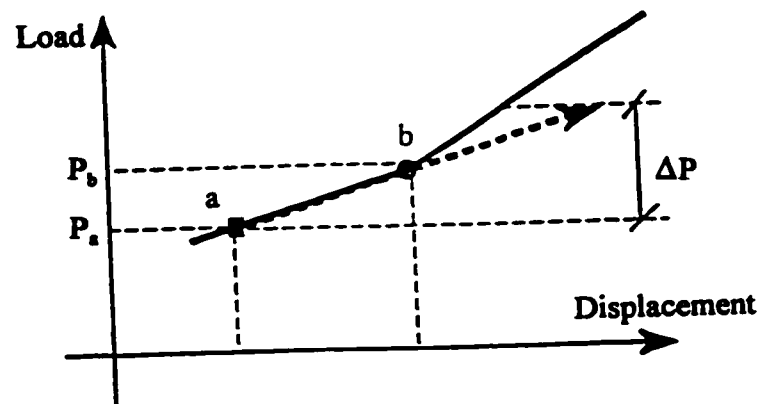
"b"   Control point between two branches

ΔP Load increment

Event factor $= (P_b - P_a)/\Delta P$

Figure 5.3 Event to event solution strategy
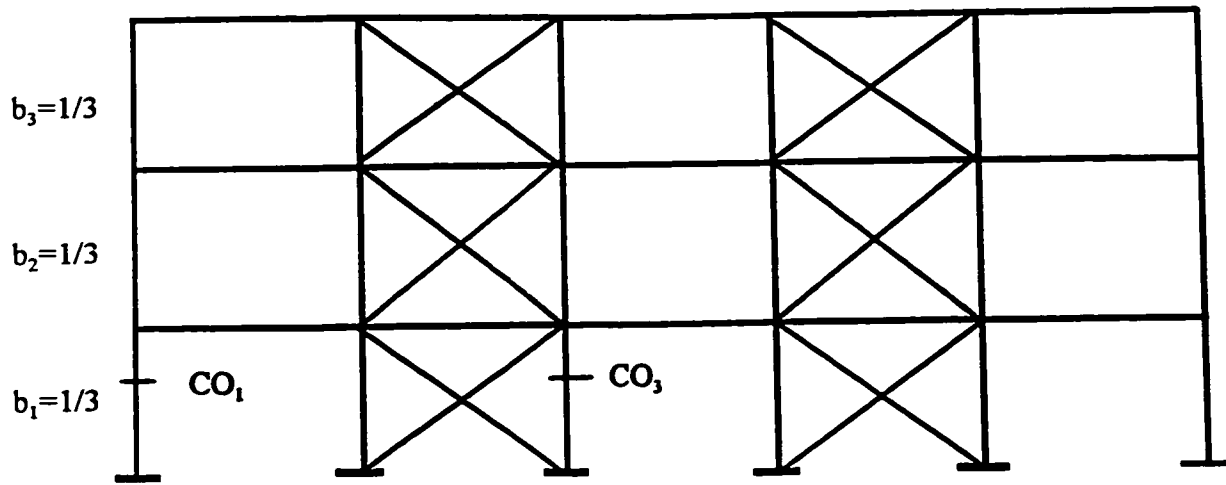
(a) Case R_1 Brace members are round hollow sections (HSS 114 x 8)
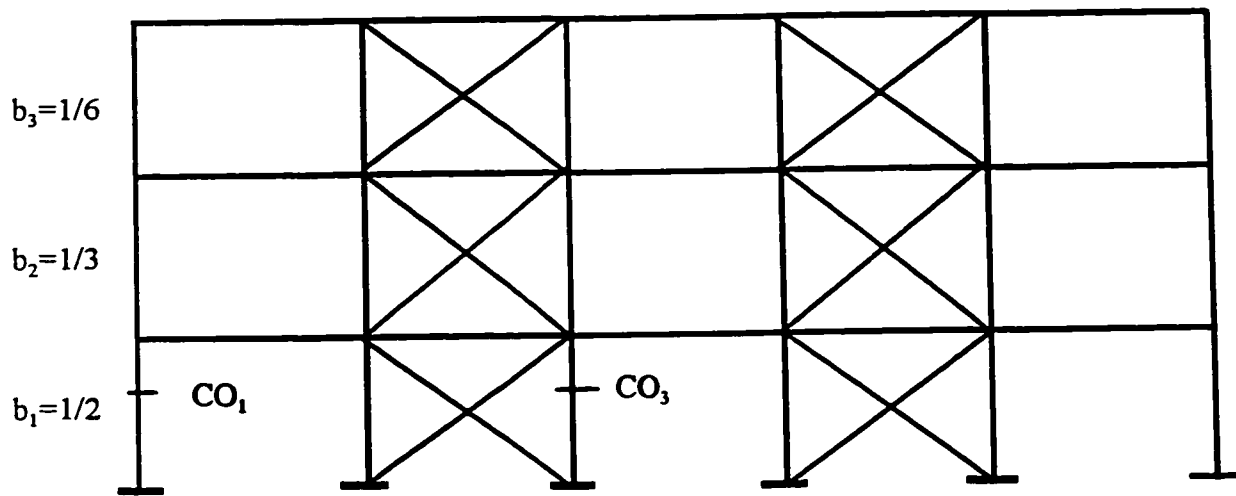
(b) Case R_2

Brace area of the 1st story = (1/2) x total brace area of case R_1
Brace area of the 2nd story = (1/3) x total brace area of case R_1
Brace area of the 3rd story = (1/6) x total brace area of case R_1

Figure 5.4 Rehabilitation cases for the nonductile three-story building

$b_3=1/2$

$b_2=1/2$

Brace area of the 1ˢᵗ story = (1/2) x total brace area of case R_1
Brace area of the 2ⁿᵈ story = (1/2) x total brace area of case R_1

(c) Case R_3

$b_1=1$

Brace area of the 1ˢᵗ story = total brace area of case R_1

(d) Case R_4
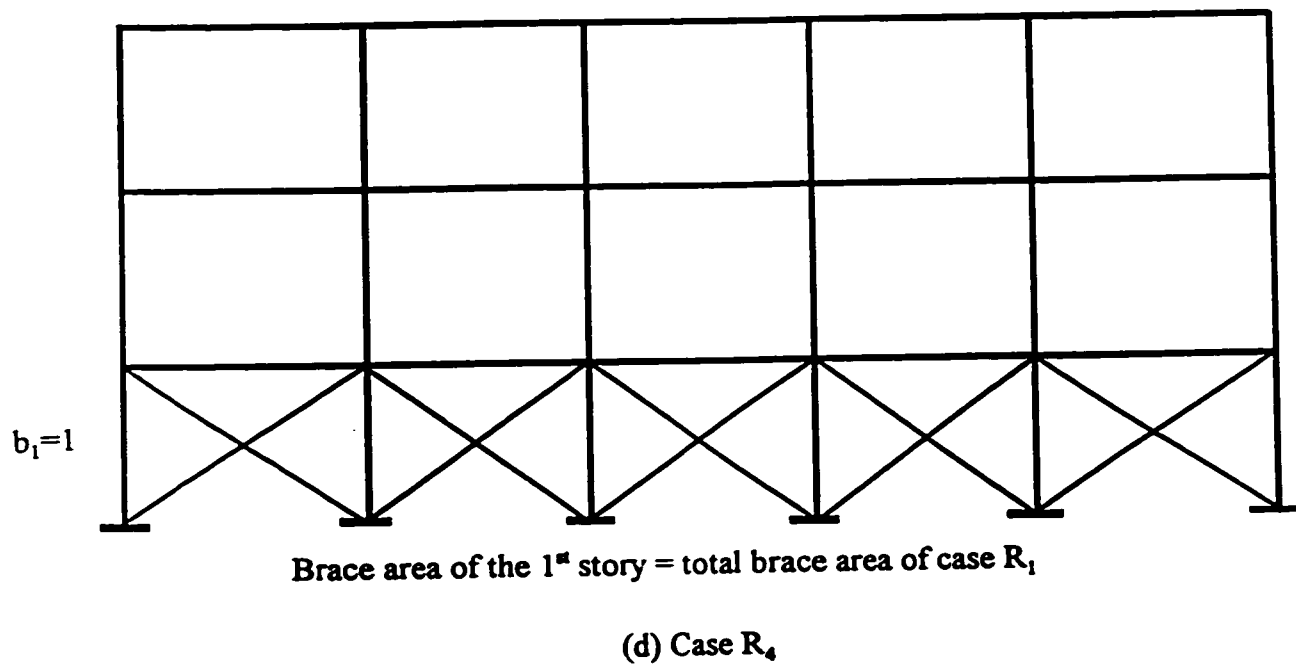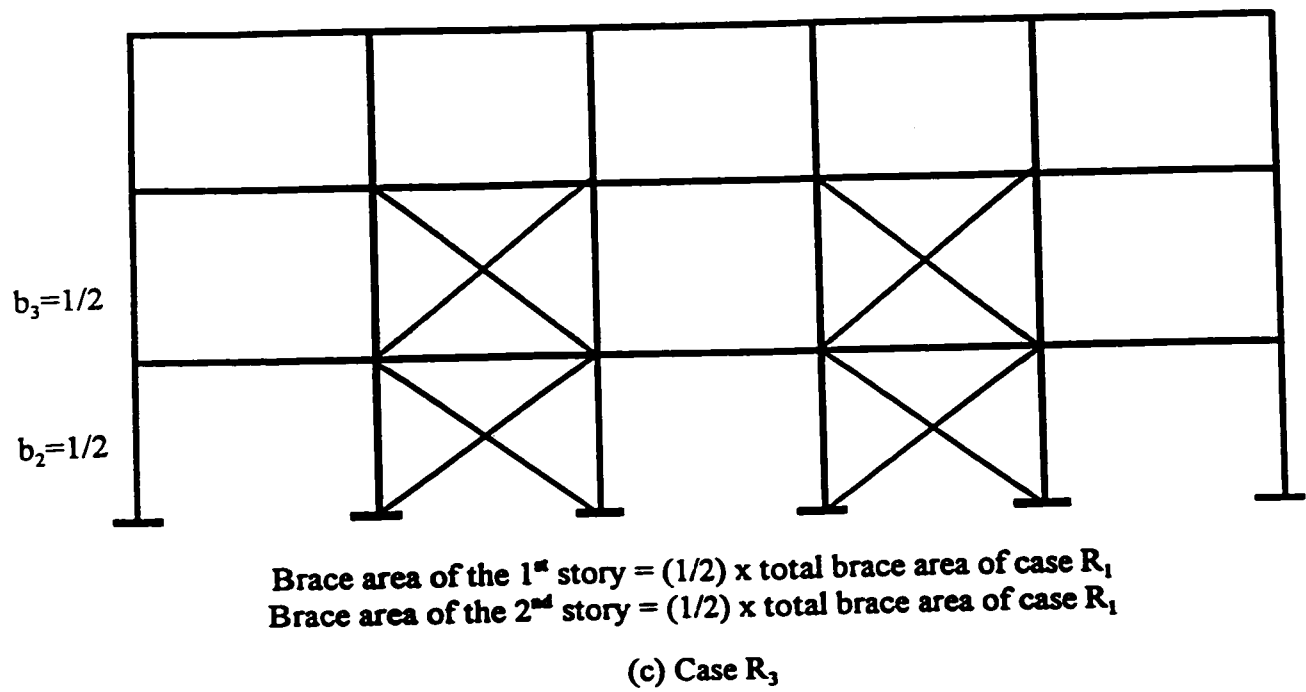
Figure 5.4 Rehabilitation cases for the nonductile three-story building (cont.)
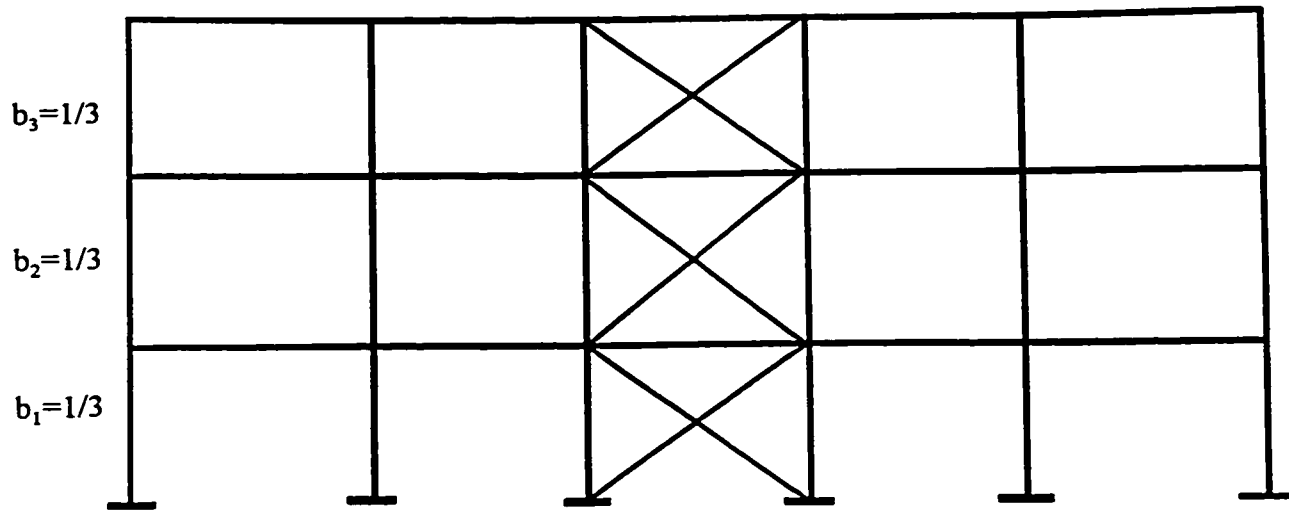
Brace member = 2(HSS 114 x 8)

(e) Case R₅
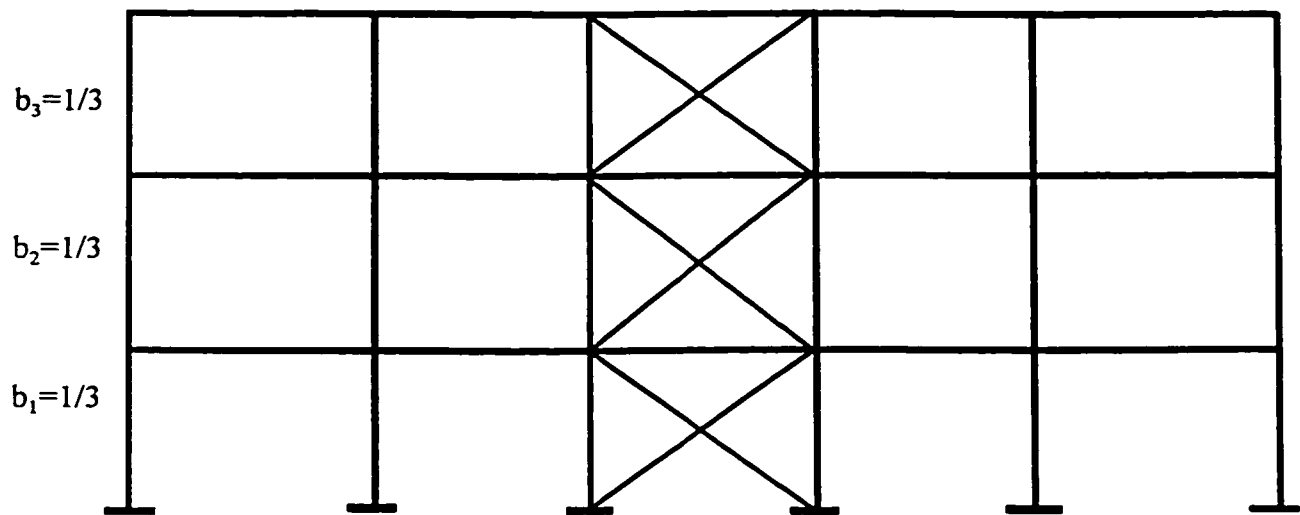
Brace members are round hollow sections (HSS 114 x 8)

(f) Case R₆

Figure 5.4 Rehabilitation cases for the nonductile three-story building (cont.)

$b_3=1/3$

$b_2=1/3$

$b_1=1/3$

Brace members (HSS 114.3x114.3x7.95)
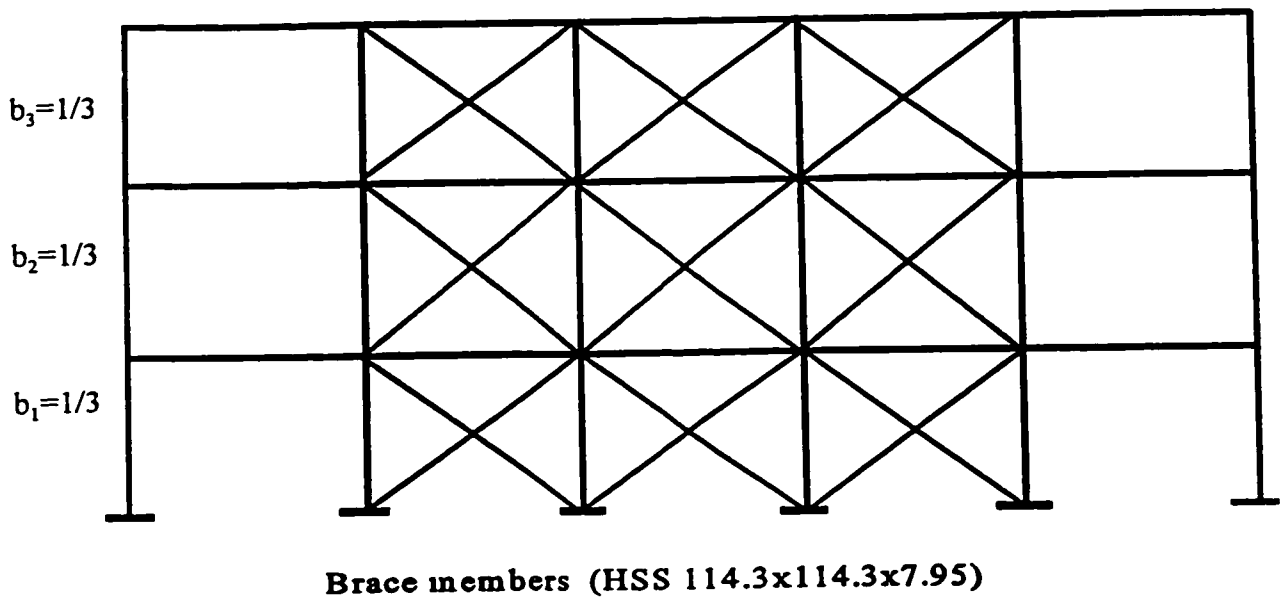
(g) Case R$_7$

Figure 5.4 Rehabilitation cases for the nonductile three-story building (cont.)
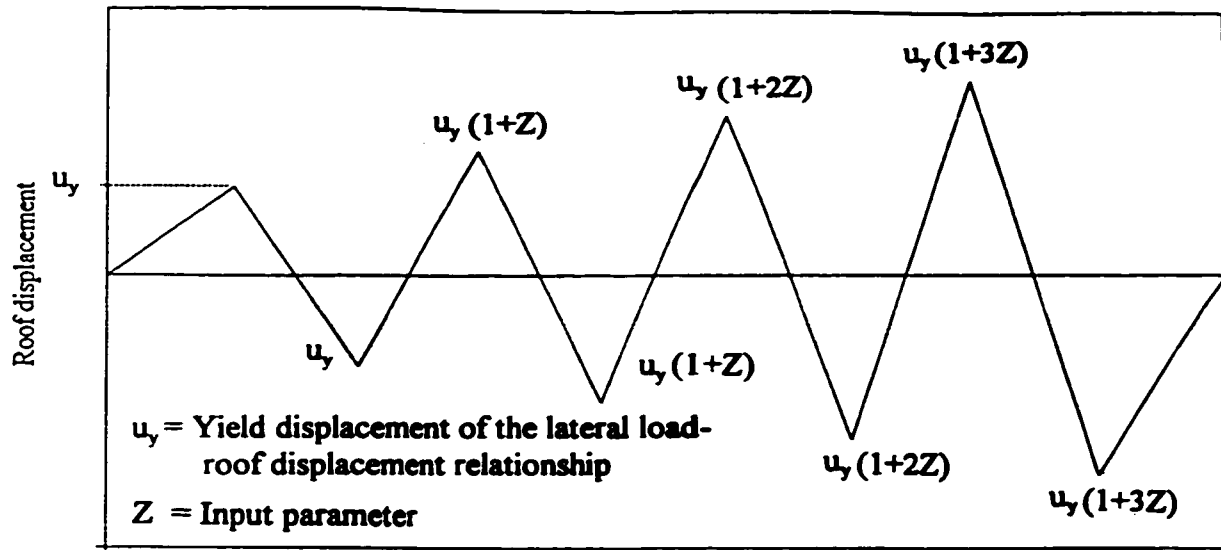
Figure 5.5 Roof displacement history of the static loading
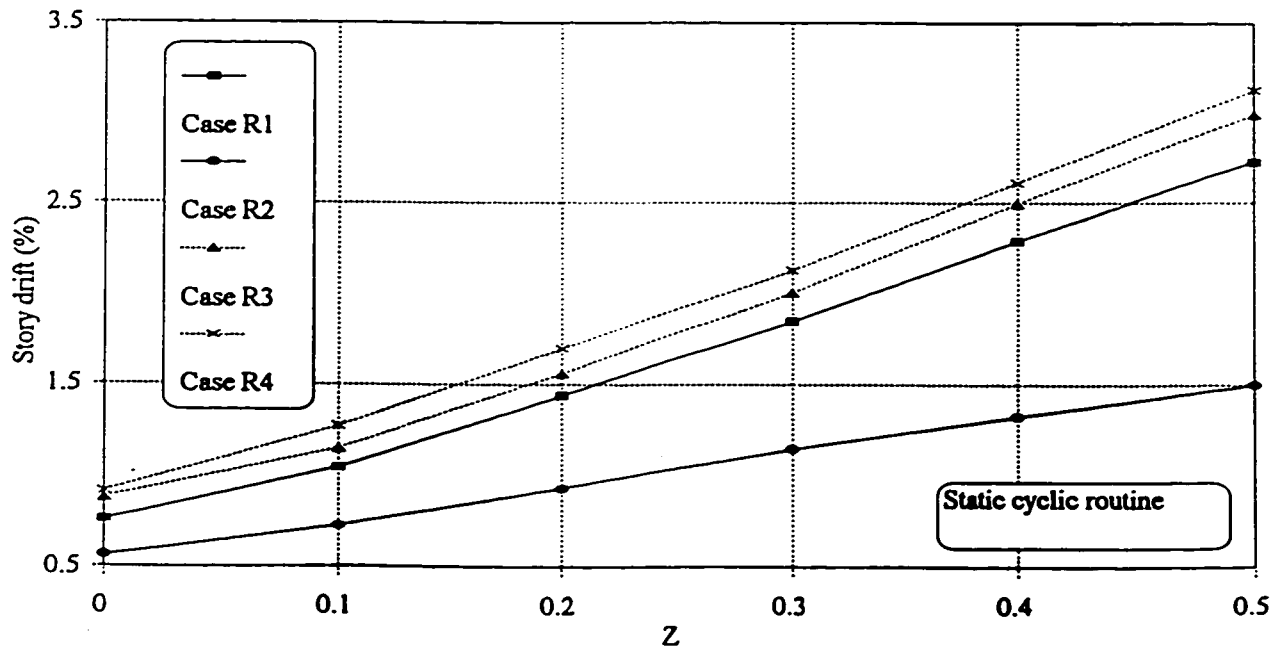
Figure 5.6 Relationships between the parameter Z and the story drift ratios of four rehabilitation cases (Static loading)
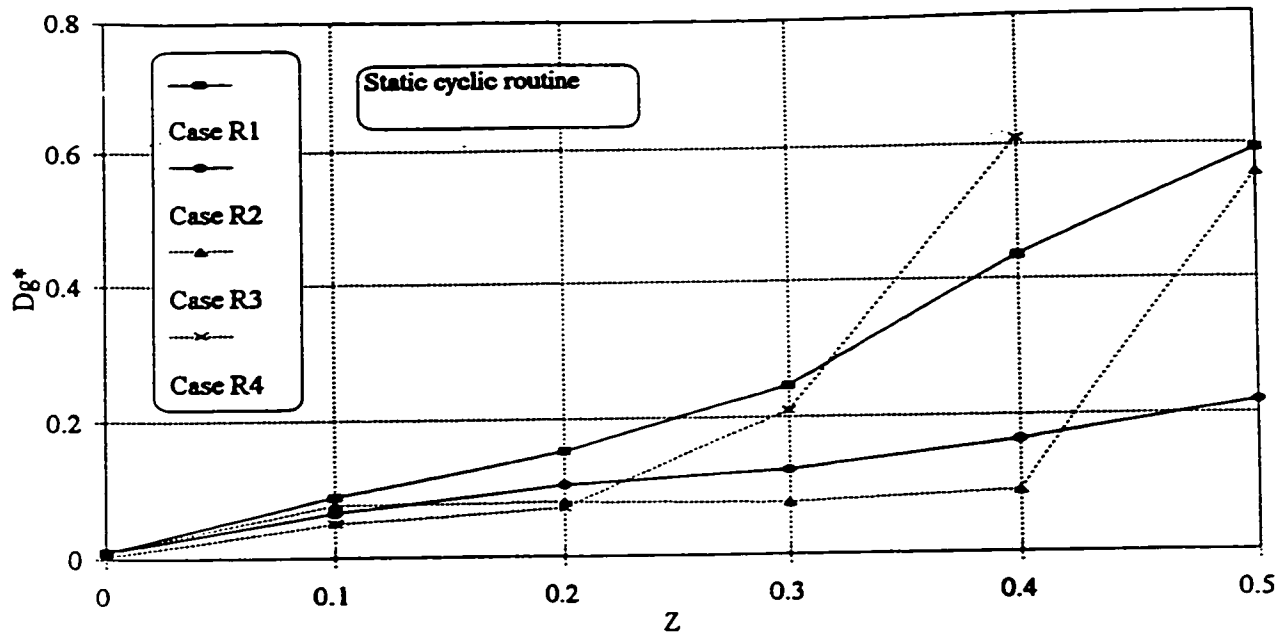
Figure 5.7 Relationships between the parameter Z and the strength based damage index D_g^* of four rehabilitation cases (Static loading)
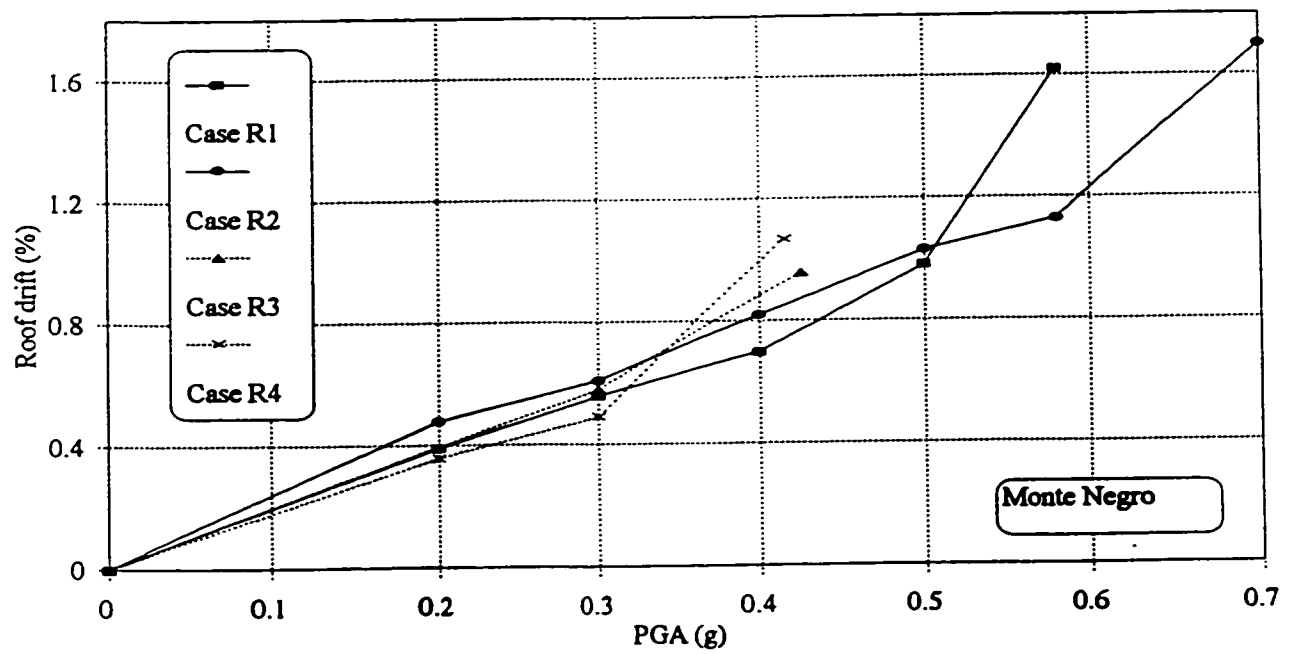
Figure 5.8 Relationships between the PGA level and the roof drift ratios of four rehabilitation cases (Dynamic loading)
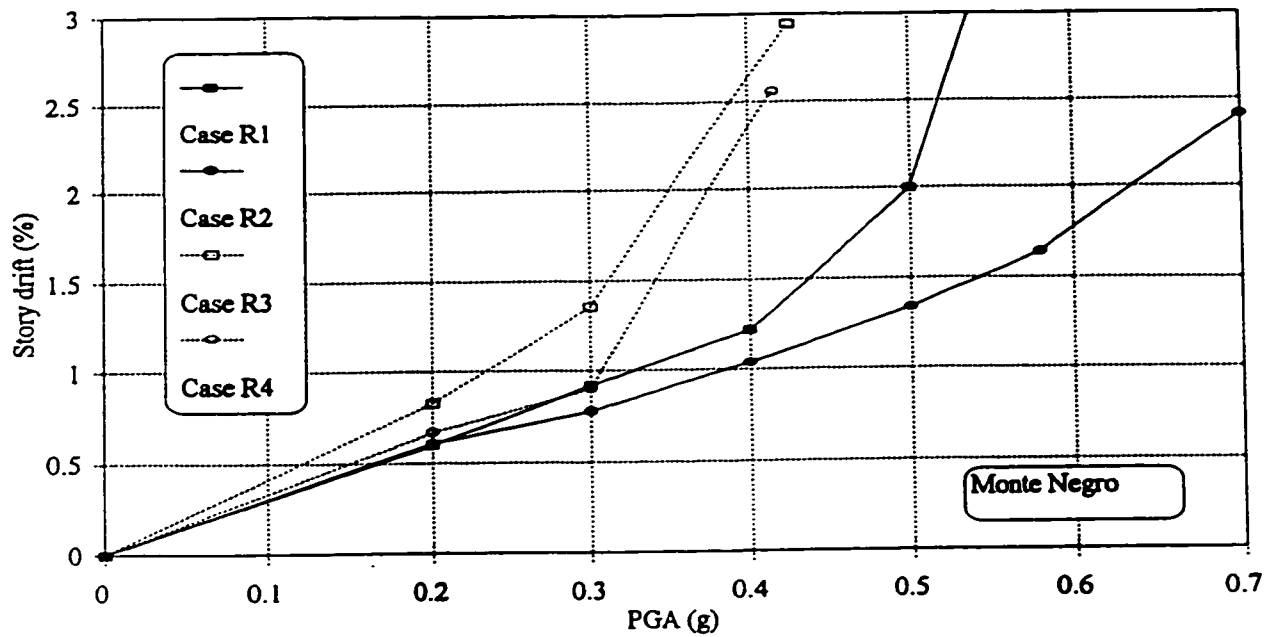
Figure 5.9 Relationships between the PGA level and the story drift ratios of four rehabilitation cases (Dynamic loading)
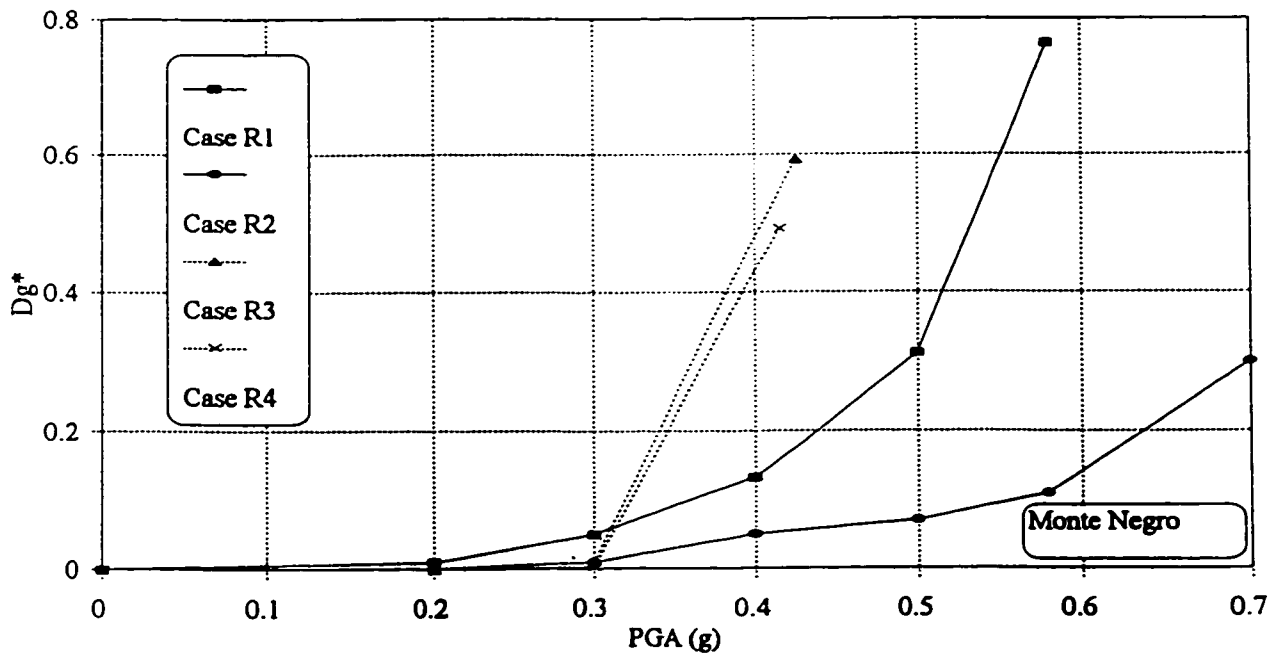
Figure 5.10 Relationships between the PGA level and the strength based damage index D_g^* of four rehabilitation cases (Dynamic loading)

○   Pullout of bottom beam reinforcement   ◐   Yielding of top beam reinforcement
■   Column splice failure   ▬   Column reinforcement yielding
▲   Brace buckling
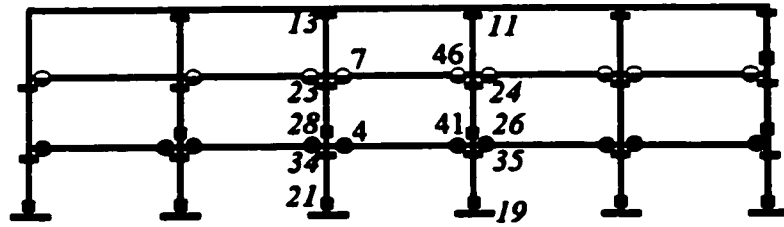
(a) Existing building, PGA= 0.45 g
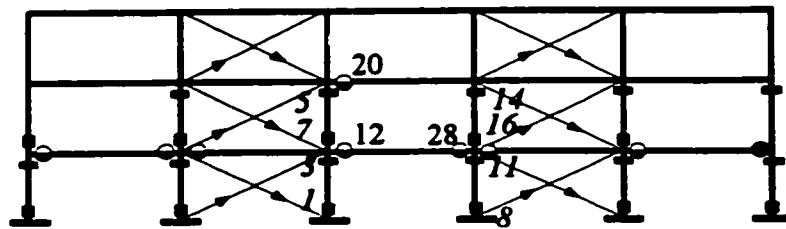
(b) Rehabilitation case R_1, PGA= 0.70 g

Figure 5.11 Hinge type and location of the existing building and the rehabilitated cases R_1, R_2, R_3 and R_4 due to the application of the Monte Negro earthquake
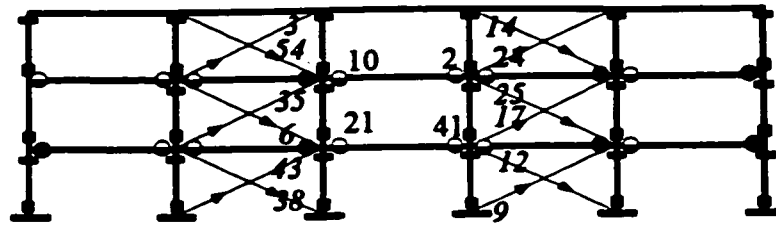
(c) Rehabilitation case R₂, PGA= 0.70 g
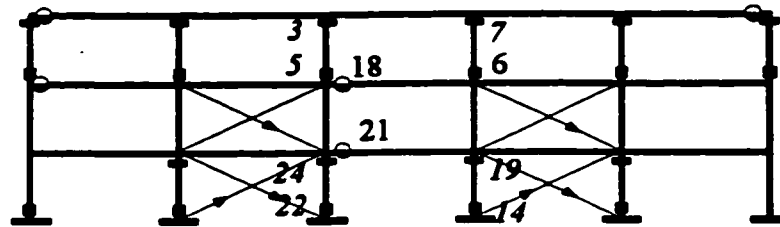
(d) Rehabilitation case R₃, PGA= 0.425 g
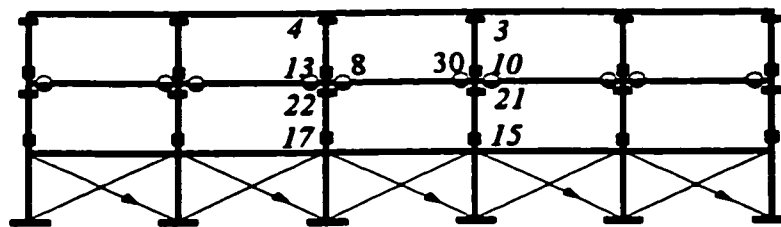
(e) Rehabilitation case R₄, PGA= 0.415 g

Figure 5.11 Hinge type and location of the existing building and the rehabilitated cases R₁, R₂, R₃ and R₄ due to the application of the Monte Negro earthquake (Cont.)
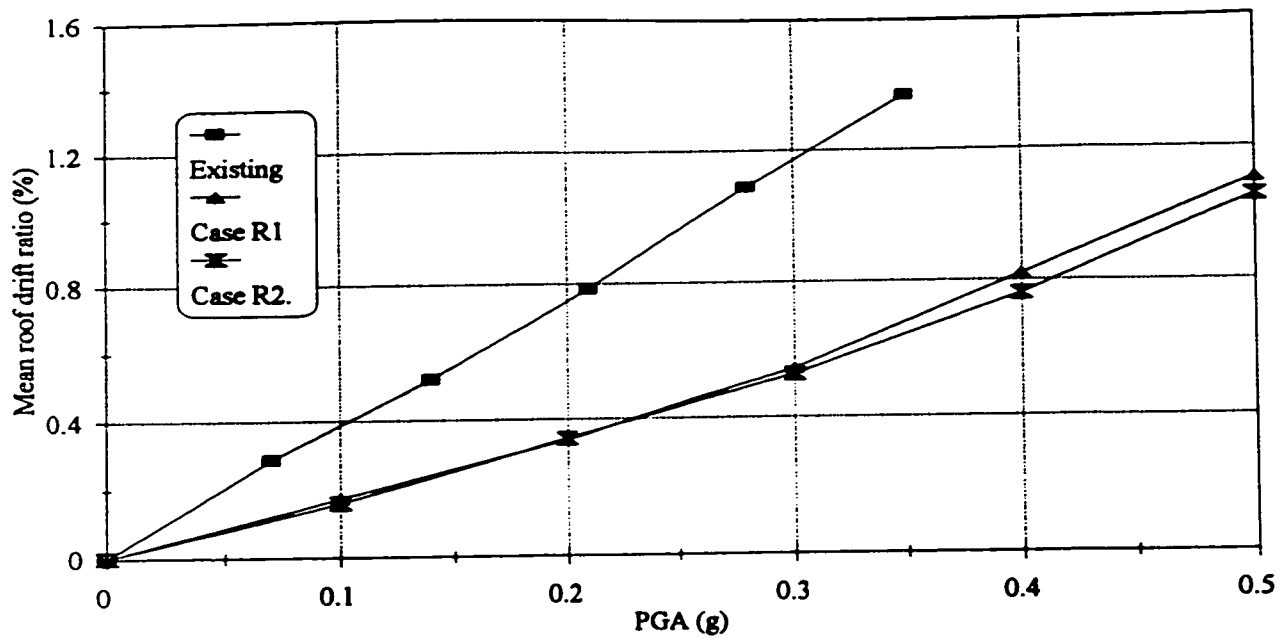
Figure 5.12 Relationships between the PGA level and the mean of the roof drift of the existing building and the rehabilitation cases R_1 and R_2
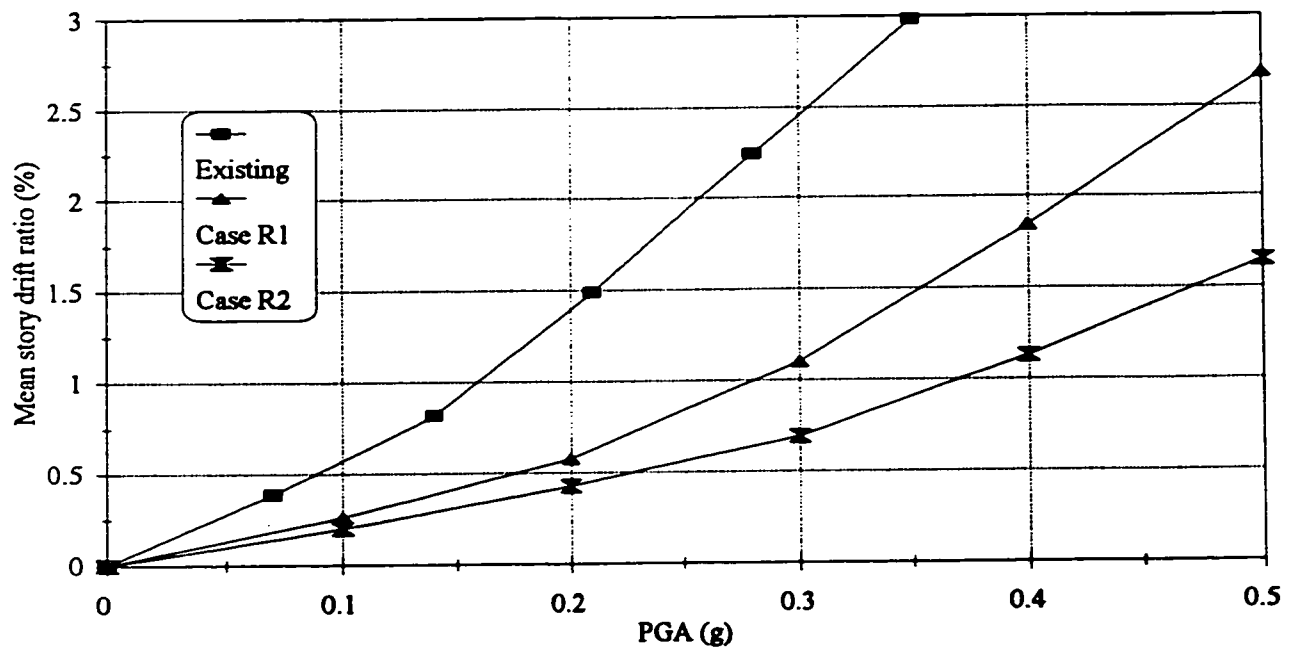
Figure 5.13 Relationships between the PGA level and the mean of the story drift of the existing building and the rehabilitation cases R_1 and R_2
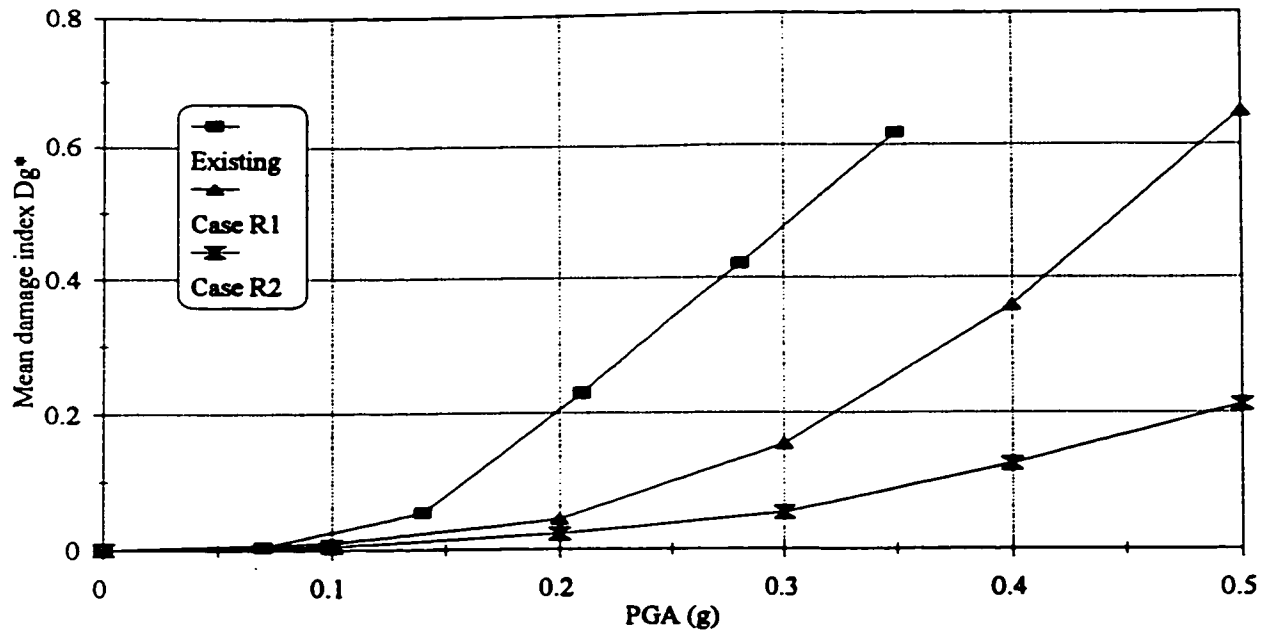
Figure 5.14 Relationships between the PGA level and the mean of the strength based damage index D_g^* of the existing building and the rehabilitation cases R_1 and R_2
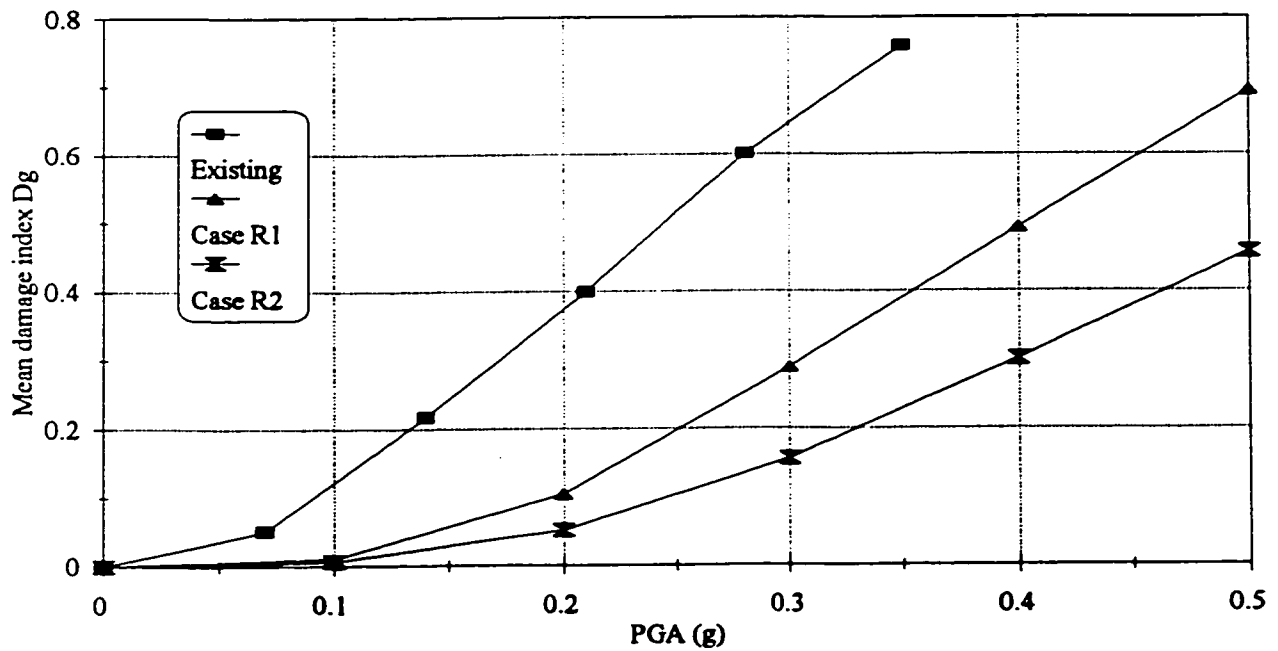
Figure 5.15 Relationships between the PGA level and the mean of the stiffness based damage index D_g of the existing building and the rehabilitation cases R_1 and R_2
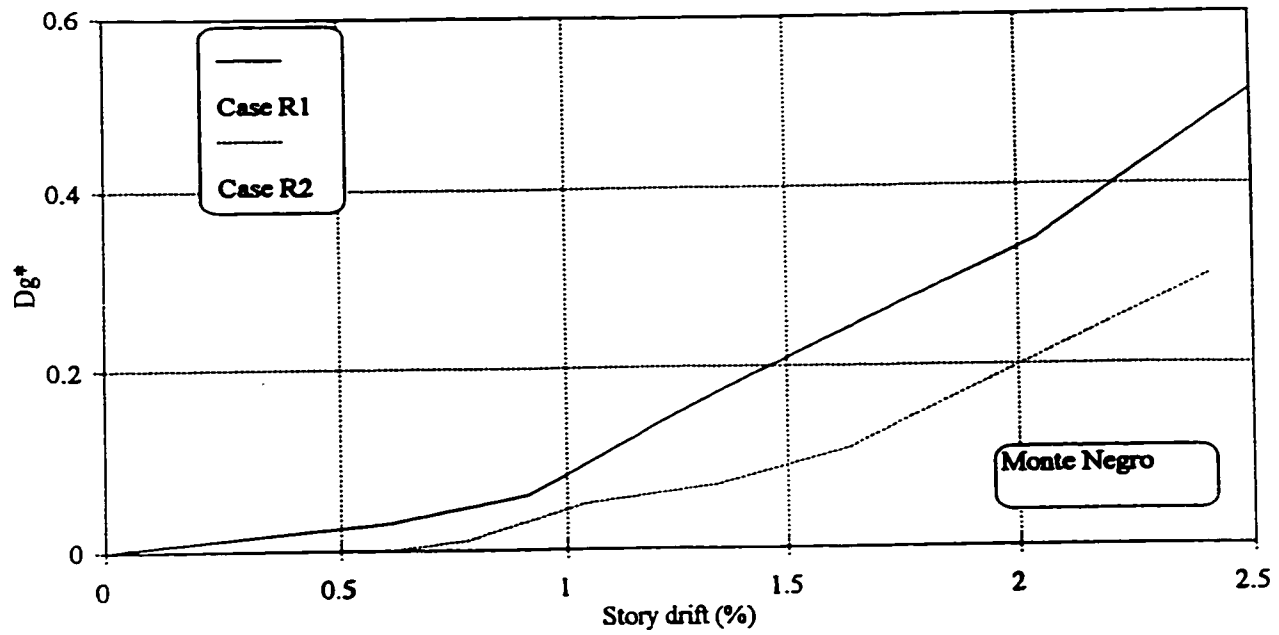
Figure 5.16 Effect of brace arrangement on the relationship between the story drift and the strength based damage index D_g^* (Dynamic loading)
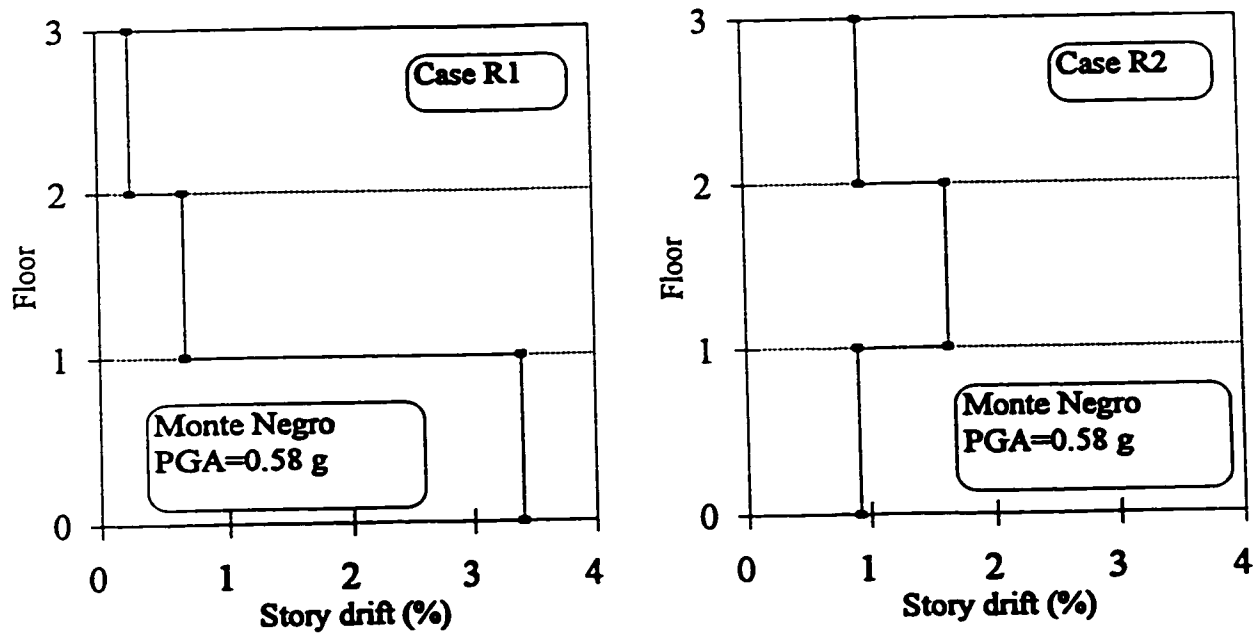
Figure 5.17 Story drift distributions (Dynamic loading)

o　Pullout of bottom beam reinforcement　　⊖　Yielding of top beam reinforcement
∎　Column splice failure　　　　　　　　　　▬　Column reinforcement yielding
▲　Brace buckling

Figure 5.18 Hinge type and location of the rehabilitation case R₃ due to the application of the
Monte Negro earthquake (PGA= 0.55 g)
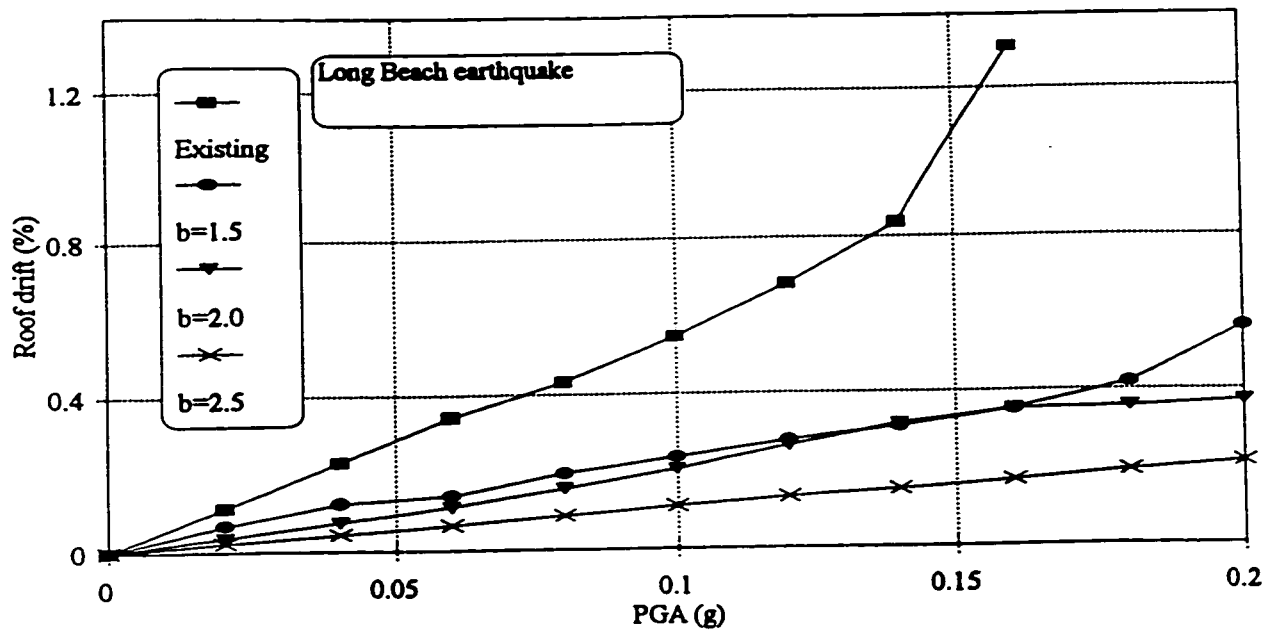
Figure 5.19 Relationships between the PGA level and the roof drift of the existing and rehabilitated three-story building
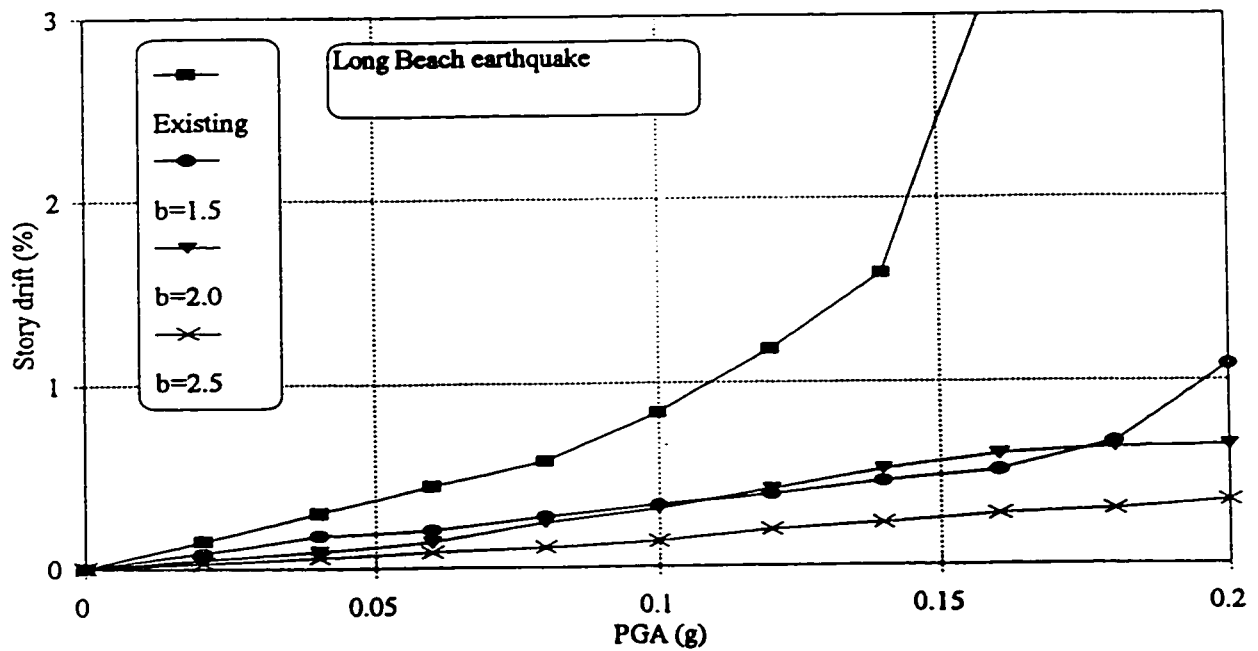
Figure 5.20 Relationships between the PGA level and the story drift of the existing and rehabilitated three-story building
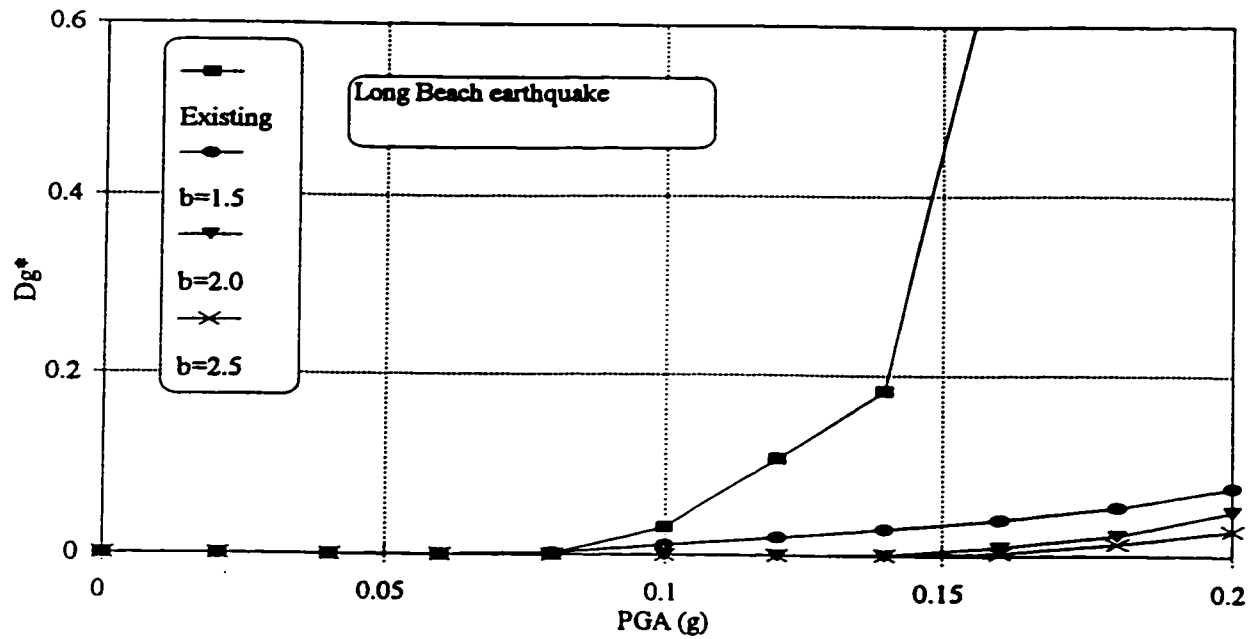
Figure 5.21 Relationships between the PGA level and the strength based damage index D_g^* of the existing and rehabilitated three-story building
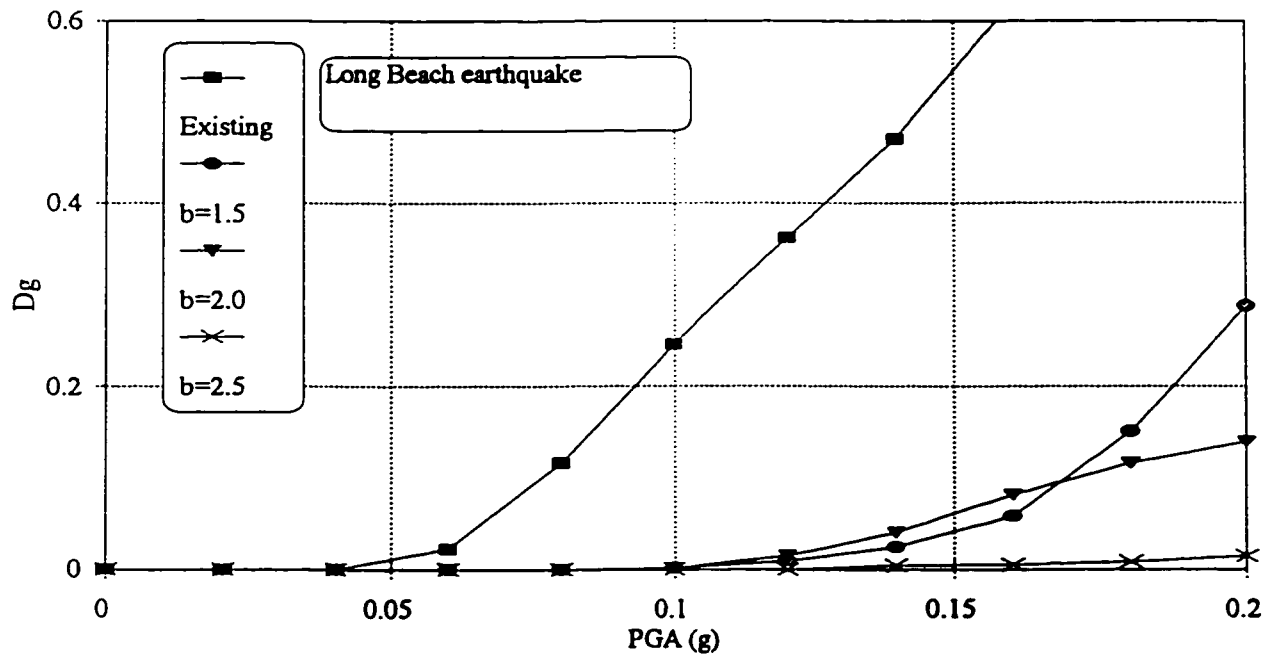
Figure 5.22 Relationships between the PGA level and the stiffness based damage index D_g of the existing and rehabilitated three-story building
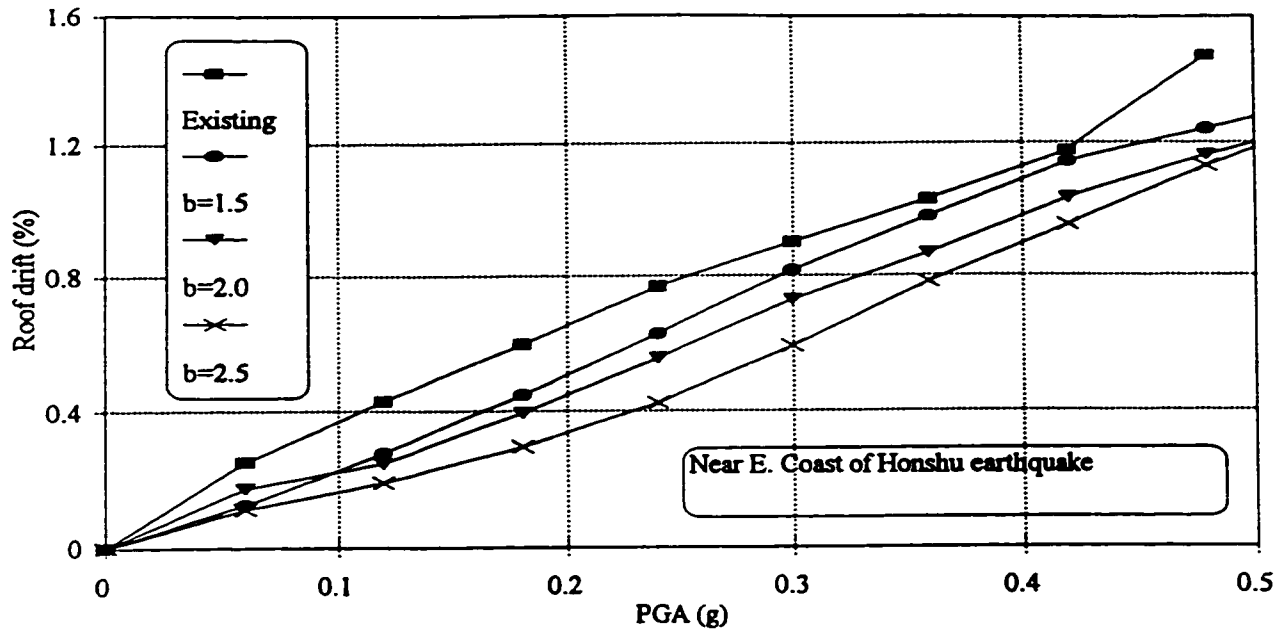
Figure 5.23 Relationships between the PGA level and the roof drift of the existing and rehabilitated three-story building
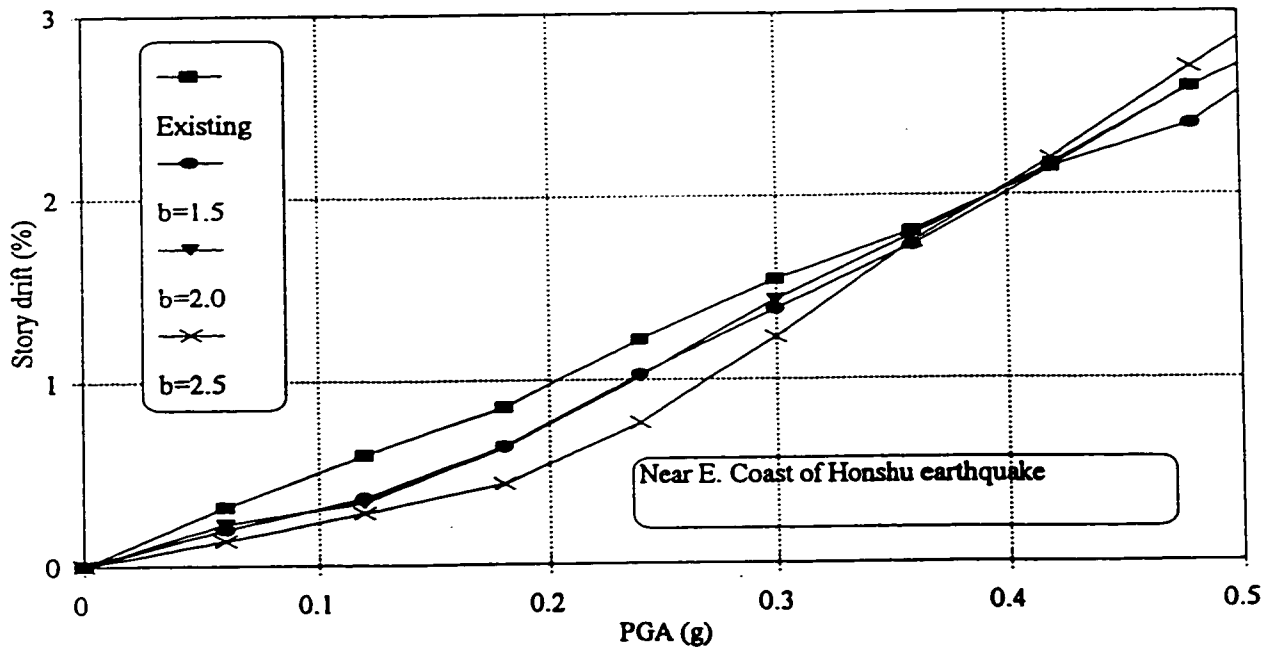
Figure 5.24 Relationships between the PGA level and the story drift of the existing and rehabilitated three-story building
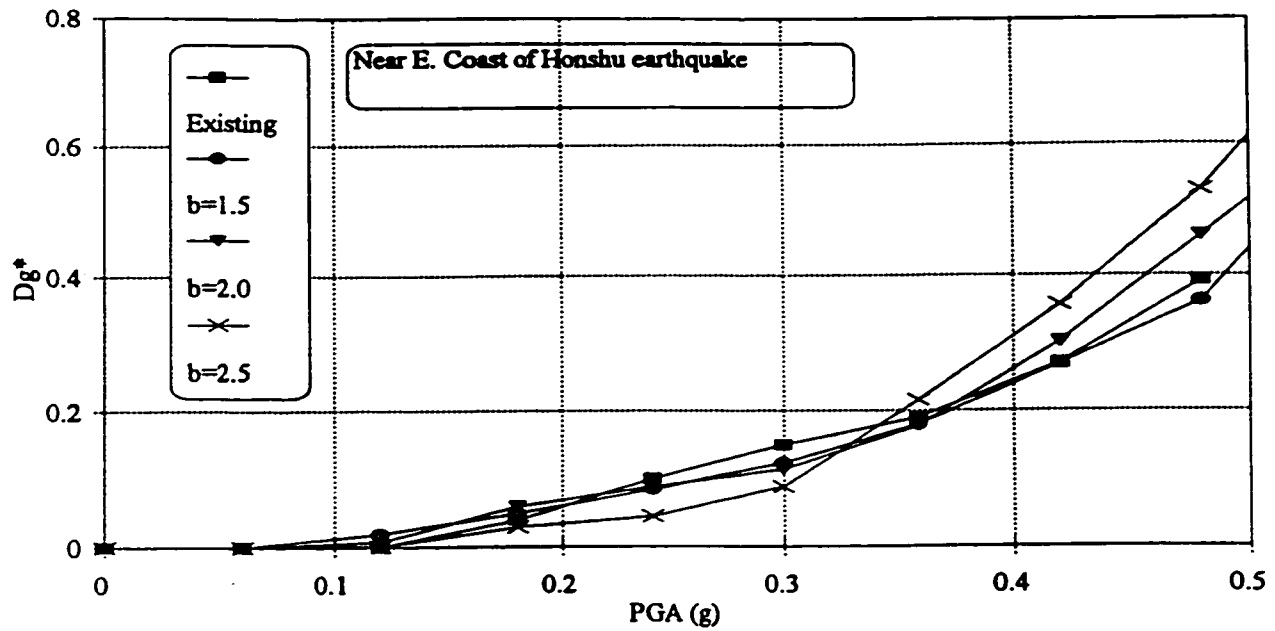
Figure 5.25 Relationships between the PGA level and the strength based damage index D_g^* of the existing and rehabilitated three-story building
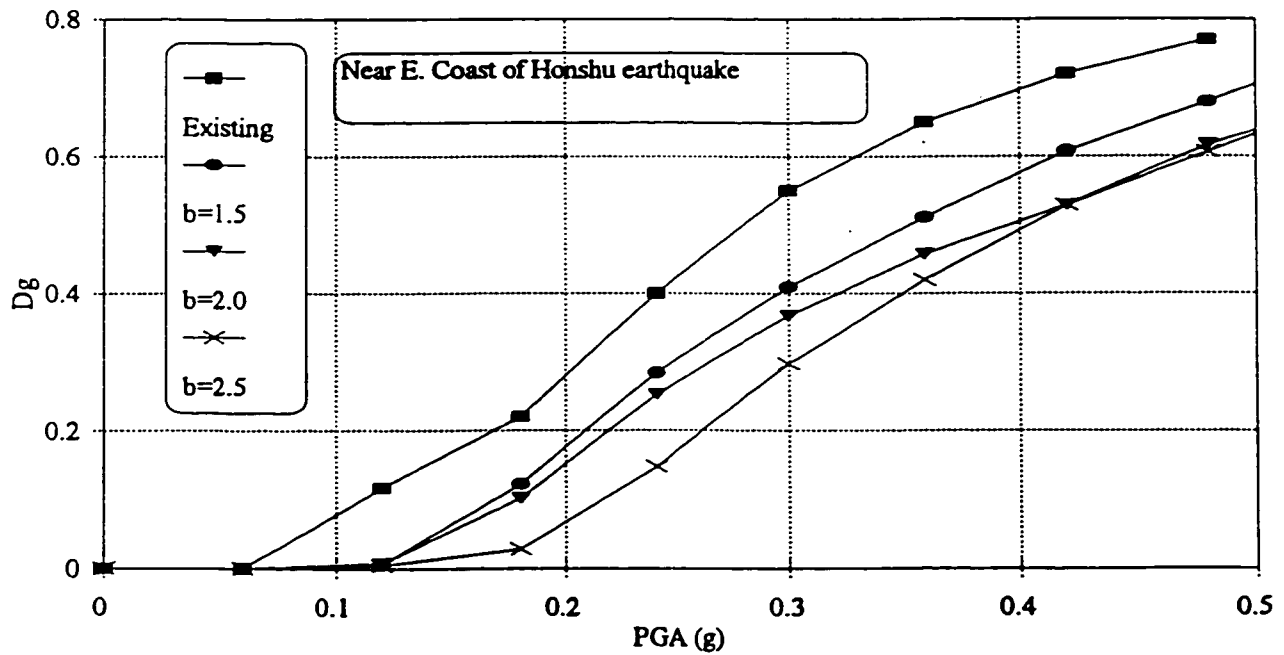
Figure 5.26 Relationships between the PGA level and the stiffness based damage index D_g of the existing and rehabilitated three-story building
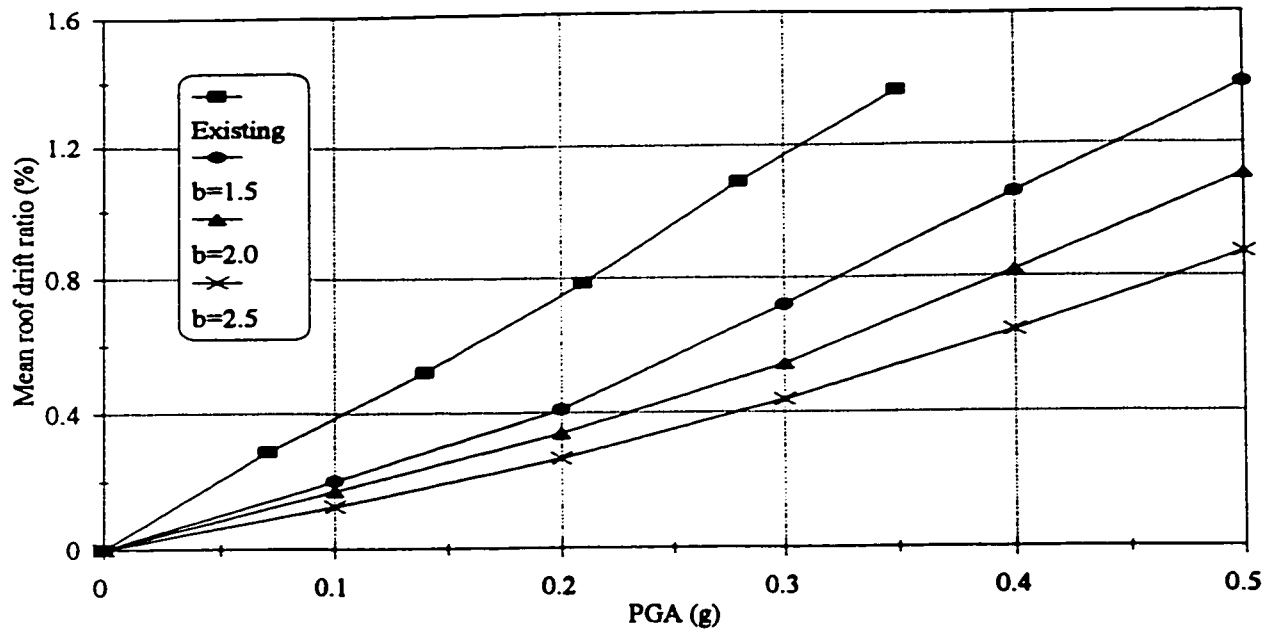
Figure 5.27 Relationships between the PGA level and the mean of the roof drift of the existing and rehabilitated three-story building
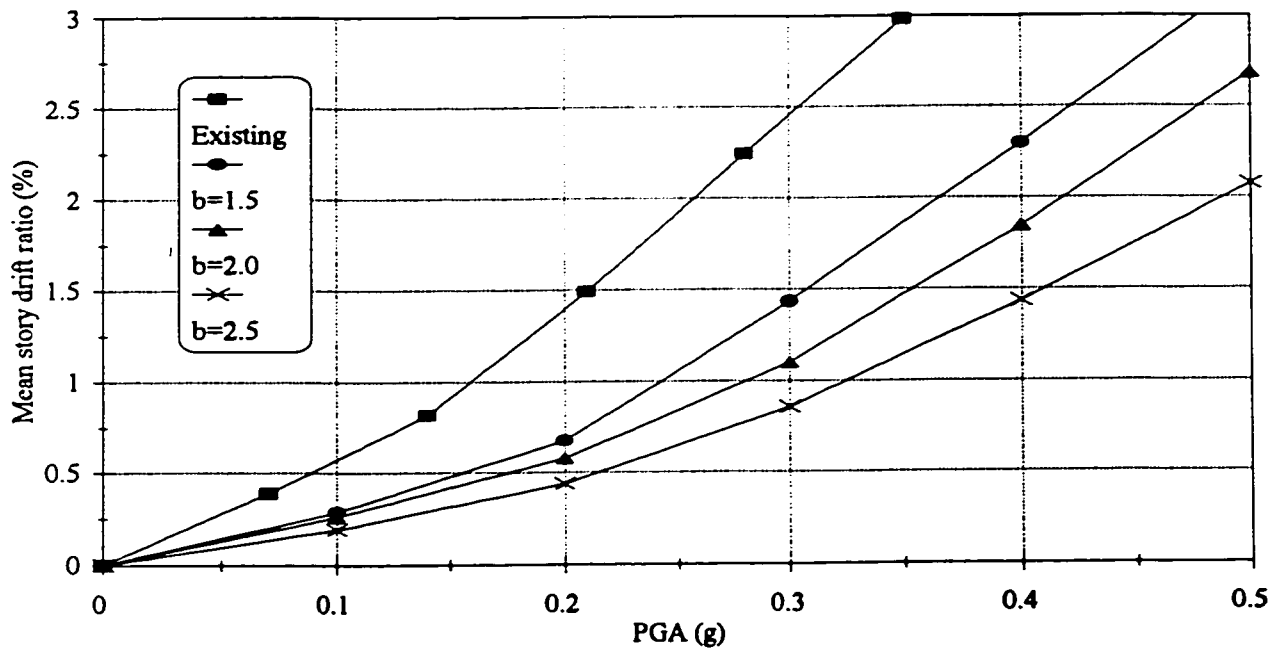
Figure 5.28 Relationships between the PGA level and the mean of the story drift of the existing and rehabilitated three-story building
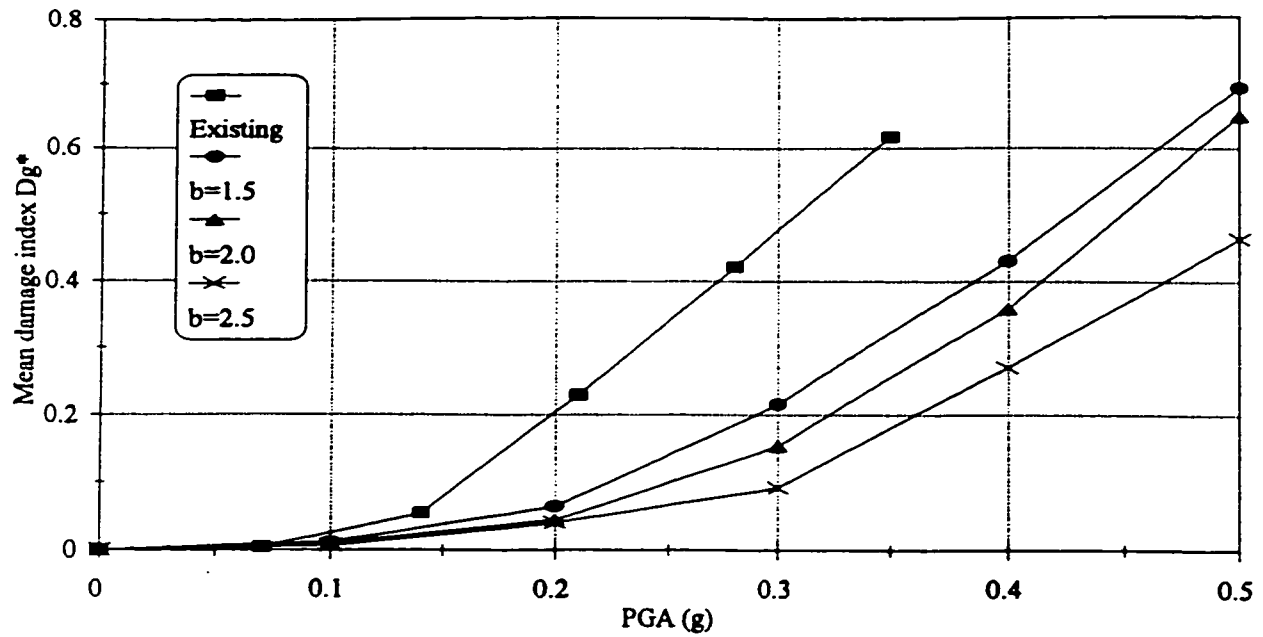
Figure 5.29 Relationships between the PGA level and the mean of the strength based damage index D_g^* of the existing and rehabilitated three-story building
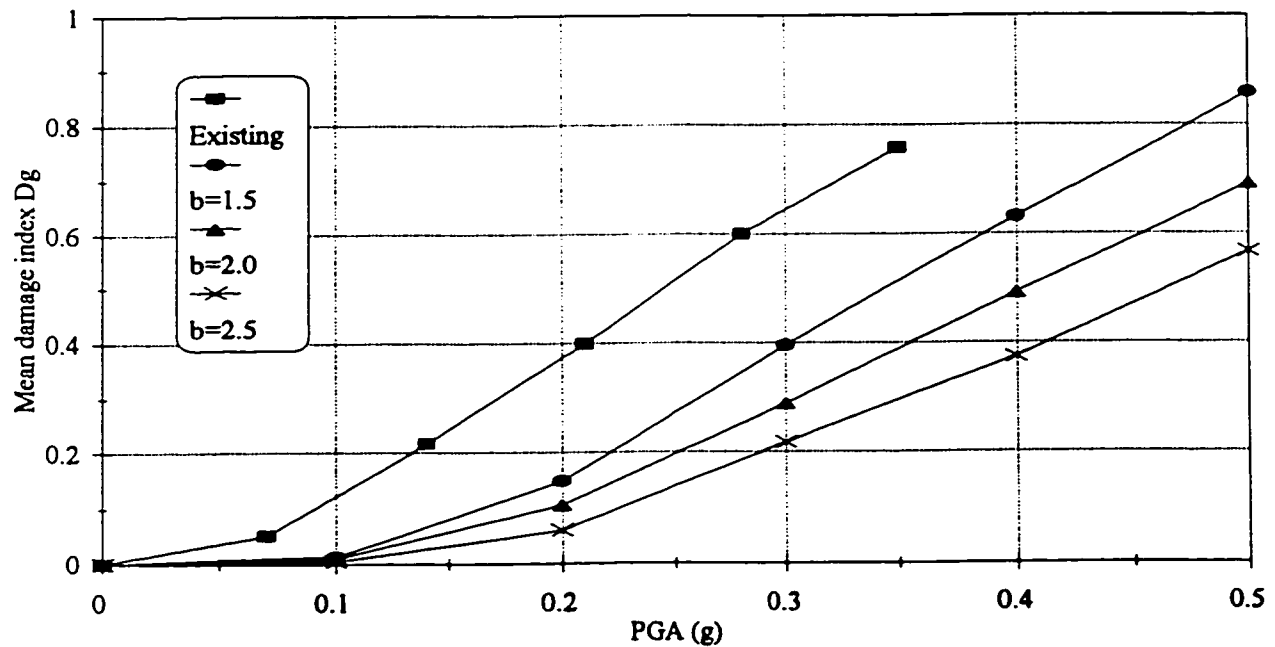
Figure 5.30 Relationships between the PGA level and the mean of the stiffness based damage index D_g of the existing and rehabilitated three-story building

○ Pullout of bottom beam reinforcement ⊖ Yielding of top beam reinforcement
■ Column splice failure ▬ Column reinforcement yielding
▲ Brace buckling
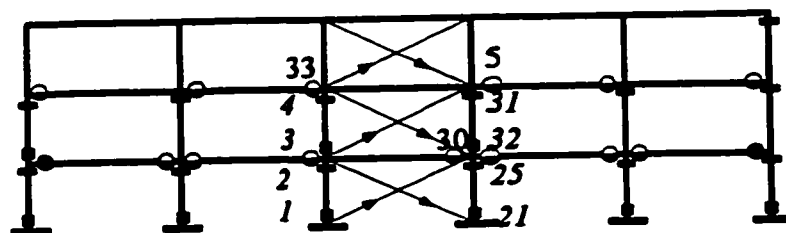
(a) Rehabilitation case R_6, PGA= 0.55 g
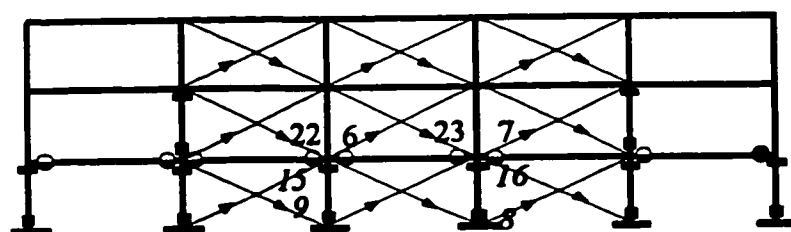
(b) Rehabilitation case R_7, PGA= 0.585 g

Figure 5.31 Hinge type and location of the rehabilitation cases R_6 and R_7 due to the application of the Monte Negro earthquake
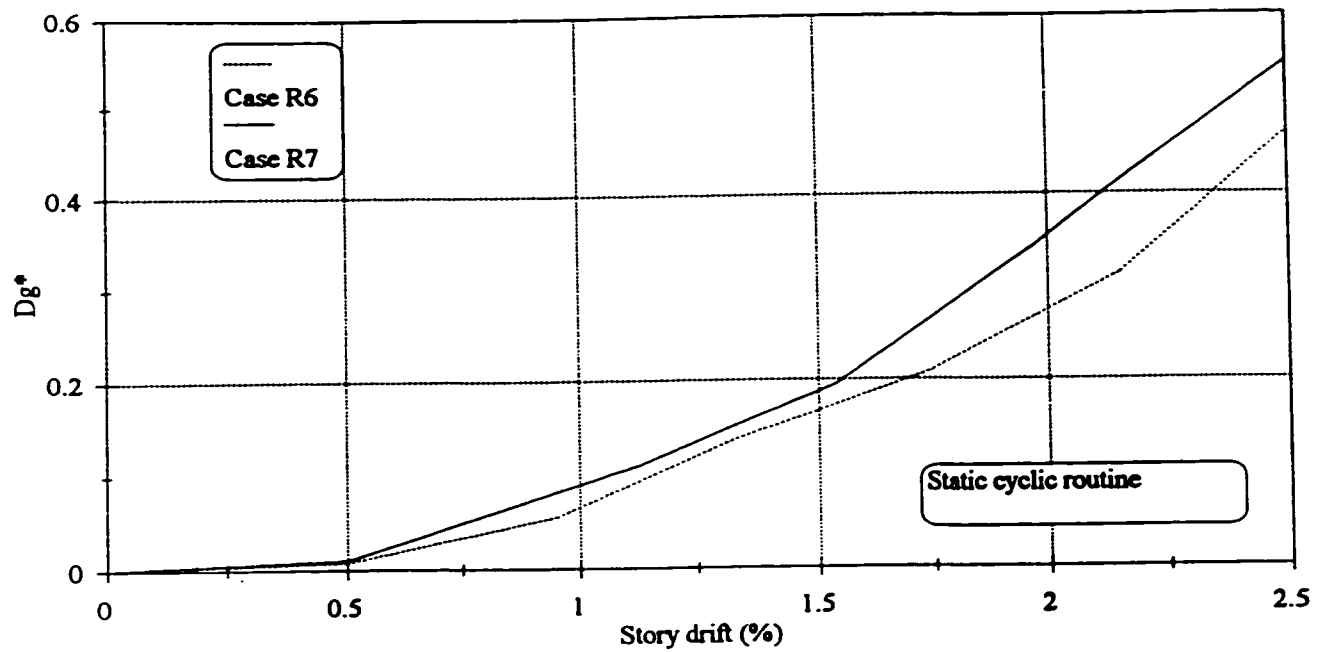
Figure 5.32 Effect of the amount of bracing on the relationship between the story drift and the damage index D_g^* (Static loading)
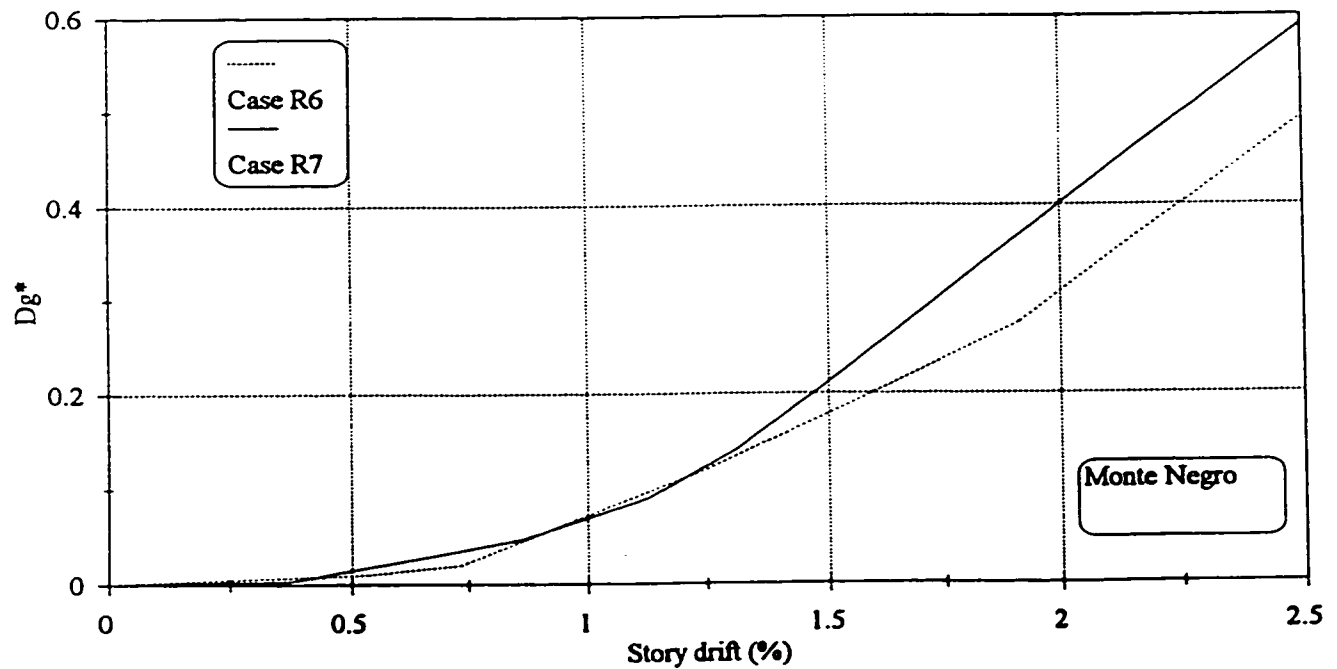
Figure 5.33 Effect of the amount of bracing on the relationship between the story drift and the damage index D_g^* (Dynamic loading)
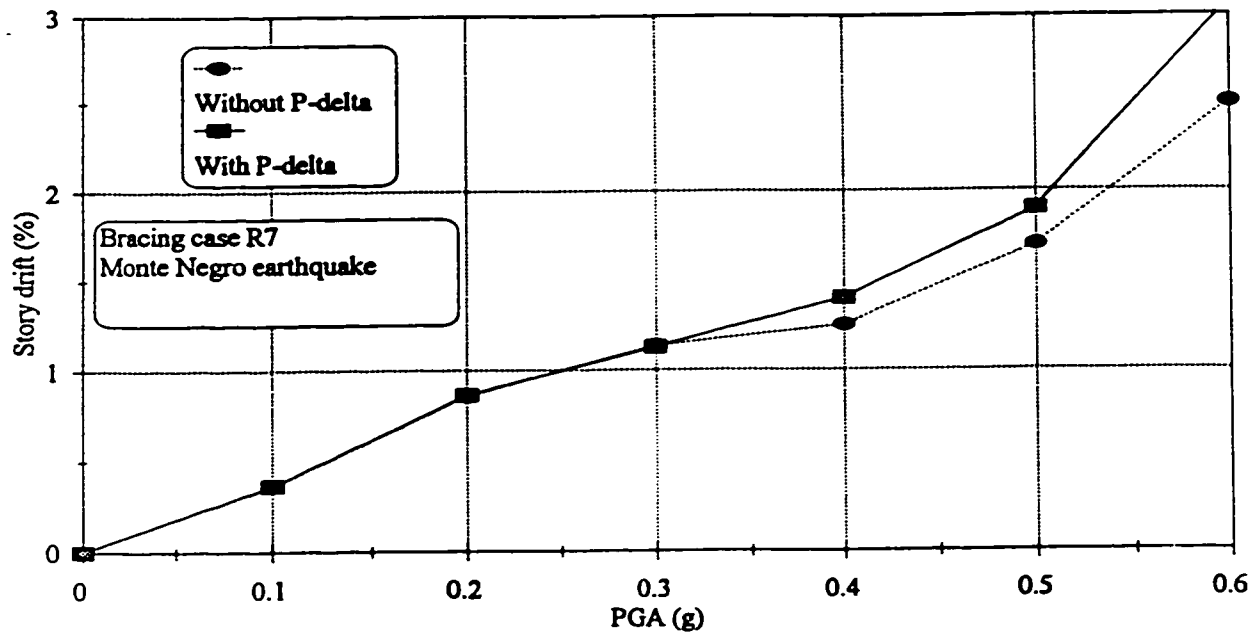
Figure 5.34 P-Δ effect on the relationship between the PGA and the story drift
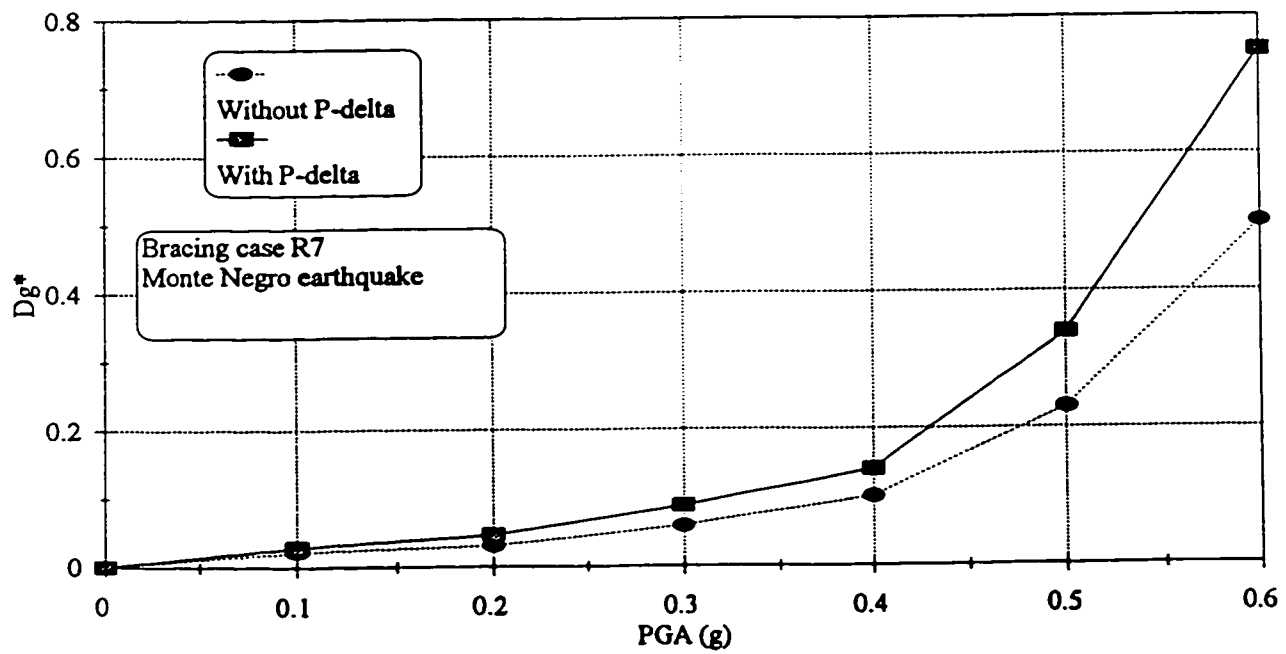
Figure 5.35 P-Δ effect on the relationship between the PGA and the damage index D_g^*

Concrete spring

Steel brace member

Steel brace member

Equivalent
mass

Ground motion
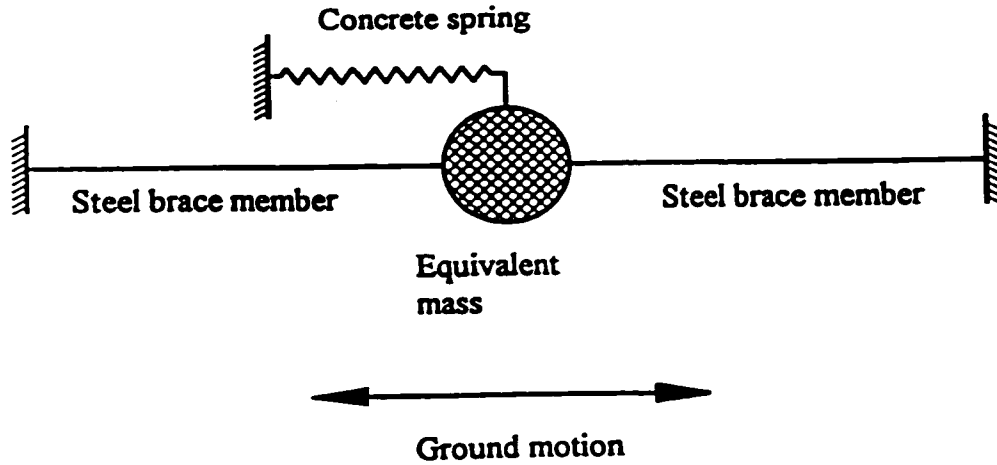
Figure 5.36 Simplified SDOF model for the braced RC building
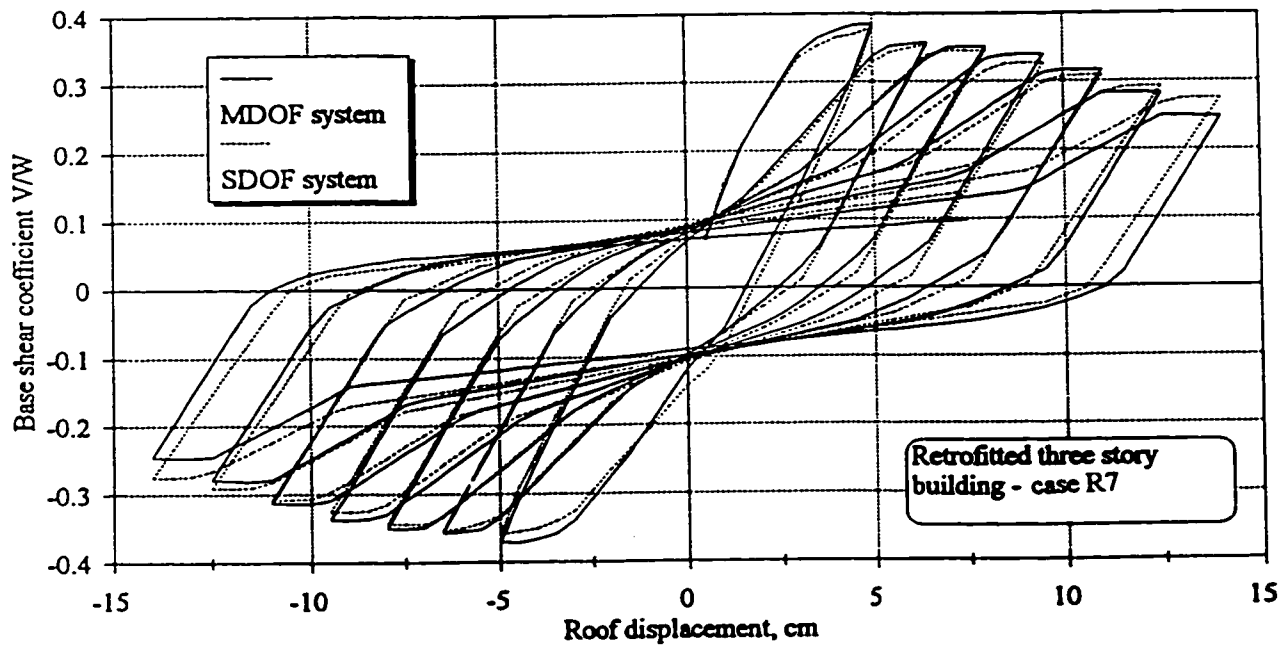
Figure 5.37 Comparison between the static cyclic behaviour of the MDOF model and the
SDOF system of the bracing case R$_7$
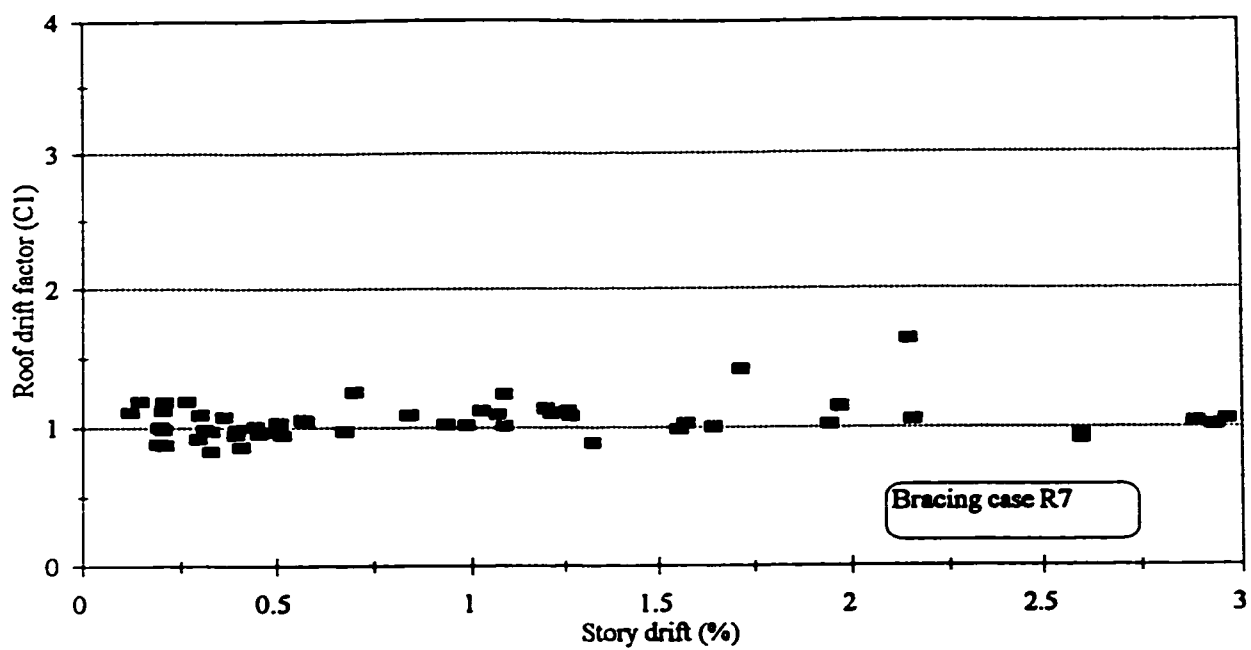
Figure 5.38 The relationship between the story drift and the response factor C_1
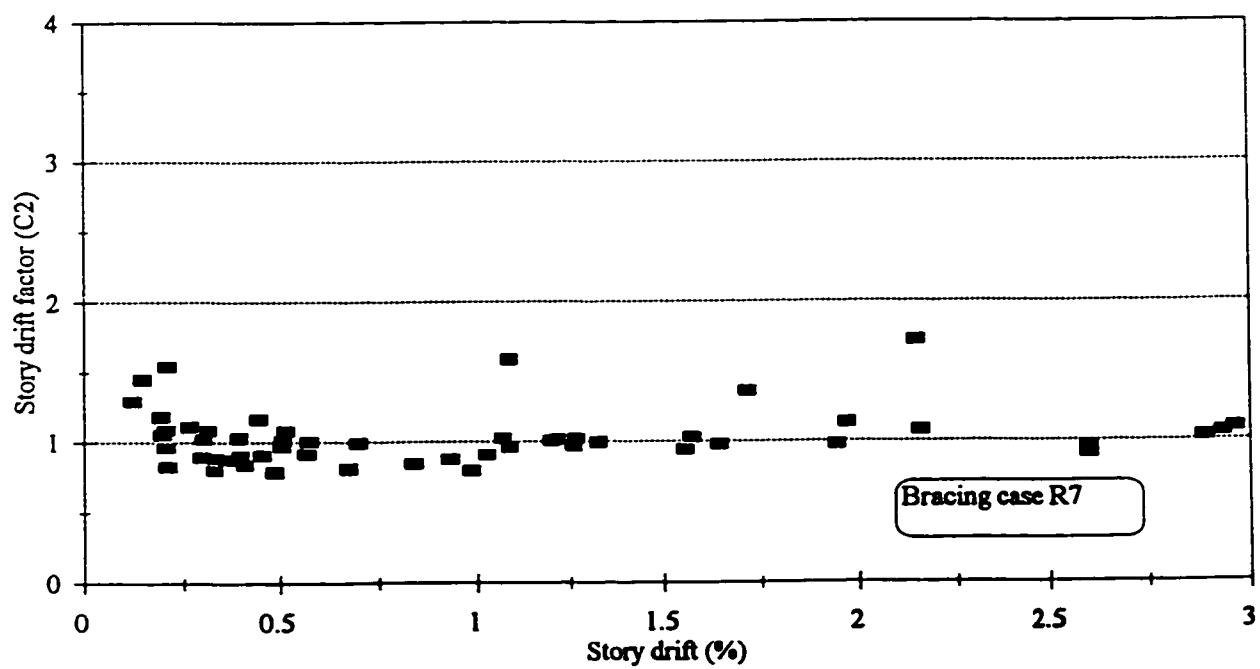
Figure 5.39 The relationship between the story drift and the response factor C_2
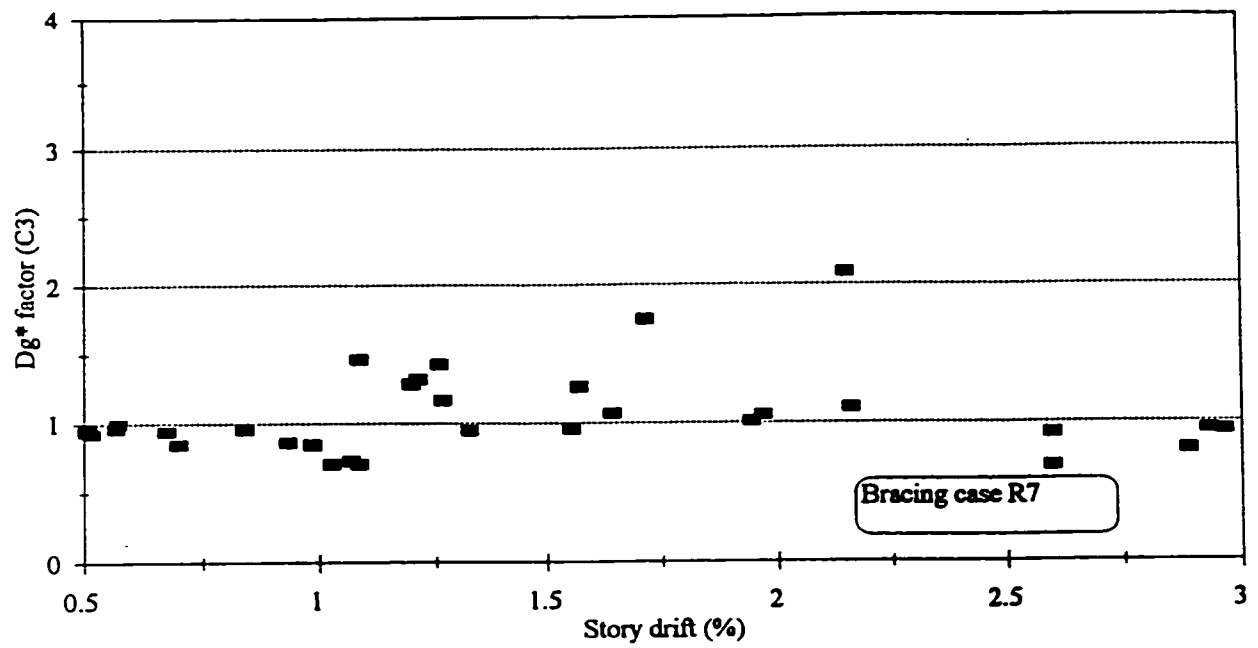
Figure 5.40 The relationship between the story drift and the response factor C_3
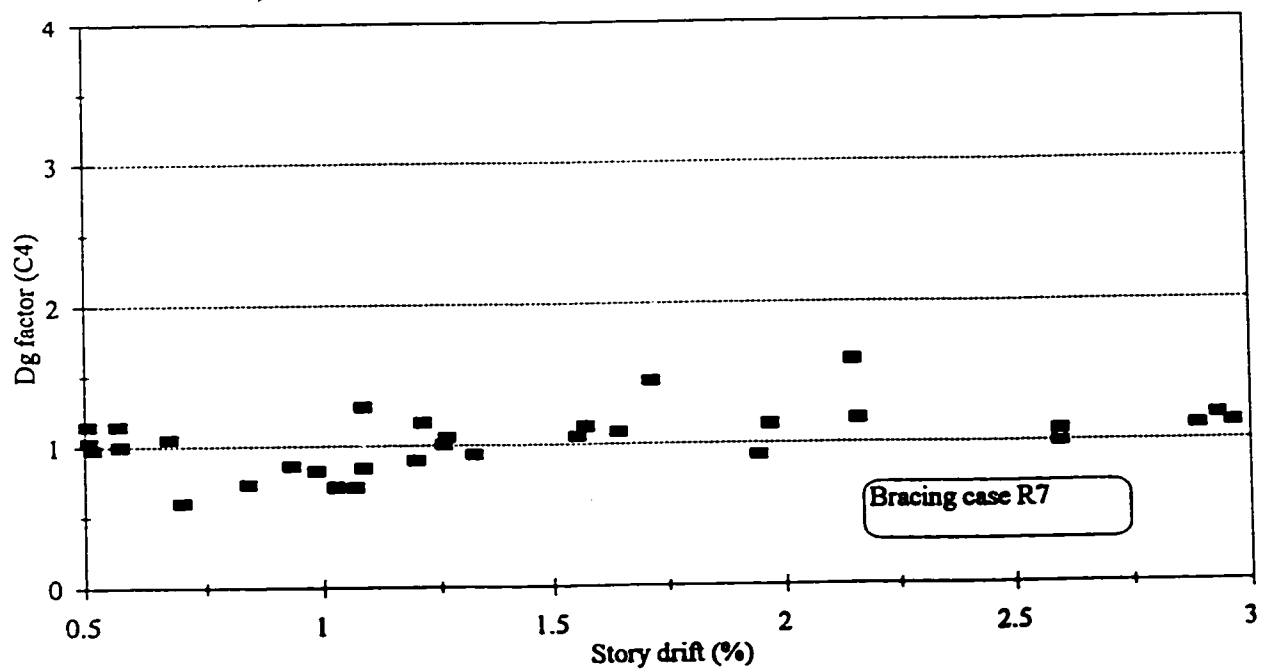
Figure 5.41 The relationship between the story drift and the response factor C_4
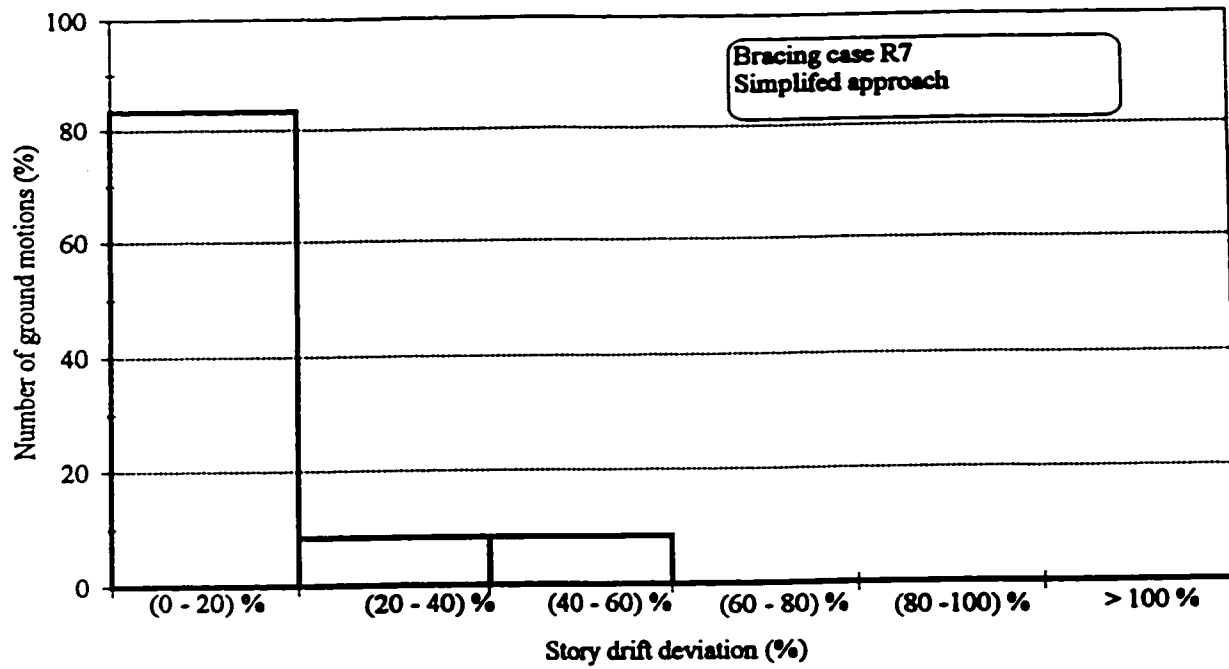
Figure 5.42 Deviations in the predicted story drift of the SDOF system
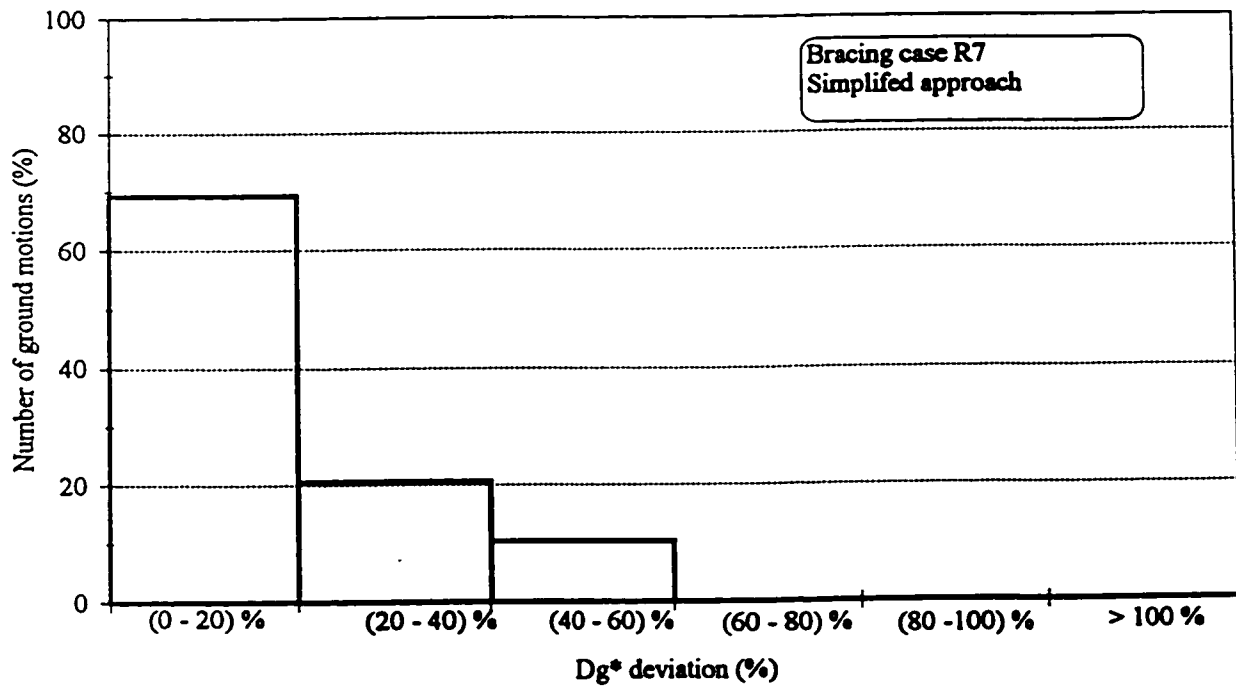
Figure 5.43 Deviations in the predicted strength based damage index D_s^* of the SDOF system

CHAPTER 6

ECCENTRIC STEEL BRACING REHABILITATION SYSTEM

6.1 INTRODUCTION

In eccentrically braced frames (EBFs), forces are transferred to the brace members through bending and shear forces developed in ductile steel links. The link is designed to act as a fuse by yielding and dissipating energy while preventing buckling of the brace members. Well-designed links provide a stable source of energy dissipation.

Different brace patterns are used in eccentrically braced steel frames. Examples of these patterns include V-bracing, K-bracing, X-bracing and Y-bracing (figure 6.1). Most of these patterns utilize short beam segments as active links. In reinforced concrete frames, the beams are incapable of performing as a ductile link for the steel bracing system that is inserted in the frame openings. A vertical steel shear link may be introduced by the Y-bracing pattern of figure 6.1 (Fehling et al., 1992). In this case, the vertical shear links can be attached to the RC frame beams. Special consideration should be given to the connection between the vertical shear link and the RC beam, this connection should have sufficient capacity to ensure its effectiveness in transmitting the forces when subjected to cyclic loading.

A shear link model presented by Ramadan and Ghobarah (1995) was modified and implemented in the DRAIN-2DX computer program. The shear link model is capable of representing both shear and flexural behaviours of the steel links under the effect of a cyclic loading. The model parameters were established based on experimental data.

207

The use of eccentric bracing in the rehabilitation of nonductile RC buildings will be investigated. Different rehabilitation cases are designed for the nonductile three-story building using concentric inverted-V and eccentric bracing systems. The hysteretic characteristics of the eccentric brace rehabilitation cases are studied under the effect of static cyclic load. The seismic performance of the rehabilitated frames using eccentric bracing is investigated under the effect of ground motion records with different characteristics. The effect of steel link strength distribution along the building height on the seismic behaviour of the rehabilitated building is evaluated.

6.2 DESIGN OF THE SHEAR LINKS AND THE BRACE MEMBERS

The selection of the link length and detailing are important aspects of the link design. Short shear links yield primarily in shear with plastic zone along the web length. On the other hand, long moment links yield primarily in flexure and develop plastic hinges at the link ends. Based on experimental investigation conducted by Hjelmstad and Popov (1983), it was found that shear links are more effective in energy dissipation and achieving greater ductility than moment links under the effect of cyclic loading. The link length should be selected to ensure that the link yields primarily in shear.

Vertical shear links shown in figure 6.1 are assumed to act as cantilevers. The brace members are assumed to be pin-connected to the vertical link while the link itself is considered fixed to the RC beam. The brace members will provide little constraint to the bottom ends of the vertical links against rotation. The critical length of a vertical shear link is calculated as:

$$e_{crit} = \frac{M_u}{V_u}$$ (6.1)

where e_{crit} is the maximum shear link length. M_u and V_u are the ultimate end moment and shear force for the shear link with a well stiffened web. Based on experimental data, the values of M_u and V_u are approximated as:

$$M_u = 1.2M_p , \qquad V_u = 1.5V_p$$ (6.2)

Substituting into equation 6.1 yields:

$$e_{crit} = 0.8\frac{M_p}{V_p}$$ (6.3)

Based on experimental data, Popov and Malley (1983) proposed the following formula for calculating the link length to ensure that the link yields primarily in shear:

$$e_{crit} = \frac{4b_f t_f}{t_w}$$ (6.4)

where b_f and t_f are the width and thickness of the flange and t_w is the web thickness. Equation 6.4 was developed for steel links having fixed ends with reverse curvature and equal end moments. Vertical shear links that have fixed connections with the RC beam and simple connections with the brace members are assumed to act as cantilevers and therefore the link length calculated from equation 6.4 is divided by two.

The maximum link deformation angle γ_{max} that can be achieved by the shear link is dependent on the link detailing. The link deformation angle is defined as the link lateral displacement over the link length for both the single and double curvature cases. Shear links with closely spaced web stiffeners exhibit relatively large ultimate deformation angles under the effect of cyclic loading. Kasai and Popov (1986) reported that the ultimate deformation angles for the same link section and stiffener configuration are not sensitive to the loading routine. They developed a formula for calculating the stiffener spacing that corresponds to a specific ultimate deformation level. The ultimate link deformation angle is defined as the maximum deformation angle developed by the link before the occurrence of considerable strength deterioration due to severe flange and web buckling of the link. It was found that the ultimate link deformation angle for well stiffened shear links may approach 0.1 rad (Michael and Popov, 1989).

Steel brace members in EBFs should be designed to ensure that they will behave elastically when subjected to an earthquake loading. Roeder and Popov (1977) recommended that a brace member should be designed as a compression member with its axial load capacity depending on the plastic strength of the steel link. An additional factor of safety of at least 1.5 should be applied to this axial load capacity to ensure that the brace does not buckle due to the link strain hardening.

6.3 ECCENTRIC BRACING CONNECTION DETAILS

Figures 6.2 and 6.3 show proposed details of the connections of an eccentric bracing system inserted in the openings of RC frame. Figure 6.2 shows the shear link connection

constructed at the beam mid-span The shear link is connected to steel plates which are anchored to the RC beam. The load of the bracing members is transformed to the shear link using an end plate. The connection between the brace members and the RC frame is shown in figure 6.3. The force in the brace member is transformed to the RC frame by bearing action on the RC members. This was accomplished using steel plates attached to the ends of the RC columns and beams. The steel plates surrounding the column are welded together while the steel plate of the beam is anchored to the concrete slab. The load of the bracing member will be distributed to the slab and the column plates through a gusset plate.

6.4 DEFORMATION CAPACITY OF EBFs

An important aspect in the design of eccentrically braced frames is the consideration of the deformation demands in the steel links. Figure 6.4 shows a plastic mechanism of an eccentrically braced steel frame, while figure 6.5 shows an assumed plastic mechanism of a reinforced concrete frame provided with a vertical steel link. In figures 6.4 and 6.5, small black circles indicate plastic flexural hinges and the cross-hatched line indicates a plastic shear hinge. In figures 6.4 and 6.5, Δ is the story displacement, H is the frame height, L is the frame span, e is the link length, θ is the story drift angle ($\theta=\Delta/$ H) and γ is the link deformation angle. For the RC frame shown in figure 6.5, the deformation angle of the link can be estimated approximately as $\gamma=\theta$ (H/e).

In eccentrically braced frames, e is usually much smaller than L and H, and therefore severe deformation demands are placed on the link. The link length plays an important role in determining the link deformation demand required to produce a specific story drift angle.

The longer the length of the shear link, the lower is the link deformation demand needed to produce a certain story drift angle. However, it should be taken into consideration that short shear links are capable of supplying large deformation angles before failure by comparison to long moment links. Based on experimental data, Michael and Popov (1989) reported that $\gamma=0.025$ radians provides a reasonable estimate of the plastic rotation capacity of long links, while for well stiffened short links, plastic rotations up to $\gamma=0.1$ radians are possible. These rotation levels were obtained by testing steel links having fixed ends with reverse curvature and equal end moments. These links can be considered as two cantilevers attached at the free ends and therefore the same rotation levels can be applied for the cantilever links. For the case of the reinforced concrete frame shown in figure 6.5, the maximum allowable story drift angle, θ_{max}, is calculated as:

$$\theta_{max} = \frac{e_{crit}\ \gamma_{all}}{H} \tag{6.5}$$

where γ_{all} is the allowable link deformation angle and e_{crit} is the maximum shear link length calculated using equation 6.3 or 6.4. For example, if $\gamma_{all}=0.1$ radians, H=4.0 m and e=0.50 m, then the maximum allowable story drift angle is equal to 0.0125 radians. Figure 6.5 (b) indicates that both the steel bracing system and the existing RC frame have to deform laterally to the same story displacement level. The deformation of the steel bracing system results mainly from the link yielding while the deformation of the RC frame is developed mainly by the formation of the plastic hinges in the frame members. The failure mechanism shown in figure 6.5 (b) represents one possible failure mechanism. Several other failure mechanisms

can be developed in the RC frame.

6.5 MODELLING OF THE LINK

Steel links are subjected to high levels of shear forces and bending moments in the active link regions. In the analysis of the performance of links, elastic and inelastic deformations of both the shear and flexural behaviours have to be taken into consideration. Several researchers attempted to develop link models for the dynamic inelastic analysis of EBFs (Roeder and Popov, 1977; Ricles and Popov, 1987; Ramadan and Ghobarah, 1995). A review of the available models of a link element can be found in Ramadan and Ghobarah (1995). Ramadan and Ghobarah (1995) modeled the link as a linear beam element with six nonlinear rotational and translational springs at each end as shown in figure 6.6. Three rotational bilinear springs were used to represent the flexural inelastic behaviour of the plastic hinge at the link end represented by the multilinear function shown in figure 6.7. Three translational bilinear springs were used to represent the inelastic shear behaviour of the link web represented by the multilinear function shown in figure 6.8. The values of M_y and V_y were considered equal to M_p and $0.9V_p$, respectively. The moment-rotation and the shear force-lateral displacement relationships of the steel link shown in figures 6.7 and 6.8 were defined based on the recommendations of Ricles and Popov (1987) and Ramadan and Ghobarah (1995). The moments and shear forces shown in the figures were given as:

$$V_{y1} = V_y \qquad\qquad M_{y1} = M_y$$

$$V_{y2} = 1.06\ V_y \qquad\qquad M_{y2} = 1.03\ M_y \qquad\qquad (6.6)$$

$$V_{y3} = 1.12\ V_y \qquad\qquad M_{y3} = 1.06\ M_y$$

The values of the stiffnesses shown in figures 6.7 and 6.8 were given as:

$$K_{2v} = 0.03 \ K_{1v} \qquad\qquad K_{2M} = 0.03 \ K_{1M}$$

$$K_{3v} = 0.015 \ K_{1v} \qquad\qquad K_{3M} = 0.015 \ K_{1M} \qquad\qquad (6.7)$$

$$K_{4v} = 0.002 \ K_{1v} \qquad\qquad K_{4M} = 0.002 \ K_{1M}$$

The moments, shear forces and stiffnesses described in equations 6.6 and 6.7 were developed for the two ends of a steel link having fixed ends with reverse curvature and equal end moments. These relationships are applicable also for cantilever type shear links. A steel link having fixed ends with reverse curvature and equal end moments can be considered as two cantilever type shear links. The values of K_{1M} and K_{1v} can be calculated as:

$$K_{1M} = 3EI \ /e \qquad\qquad K_{1v} = GA_{web}/e \qquad\qquad (6.8)$$

where, E is Young's modulus of steel, I is the moment of inertia of the link cross section, G is the modulus of rigidity of steel, e is the link length and A_{web} is the area of the web of the link section. Ricles and Popov (1987) concluded that, under the effect of cyclic loading, moment yielding obeys the kinematic hardening rule while shear yielding follows a combination of both isotropic and kinematic hardening.

In the current study, the vertical steel link was represented by linear cantilever element with only two inelastic rotational and translational springs at the fixed link end. Each of the springs was designed to produce directly the same relationships shown in figures 6.7 and 6.8 instead of using three bilinear springs as suggested by Ramadan and Ghobarah (1995). One of the developed springs represents the moment-rotation relationship while the other represents the shear force-shear displacement relationship. The developed springs were implemented in the DRAIN-2DX computer program. The force-deformation relationships

of the springs were determined using the forces and stiffness levels presented in equations 6.6

and 6.7. Under the effect of cyclic loading, the hardening rule of the moment spring is a

kinematic type, while for the shear spring, a special function was used to account for the

upper bound of the shear capacity (Ramadan and Ghobarah, 1995). The function determines

the maximum attainable shear force capacity after certain amount of plastic action. This

function has the shape:

$$\mathbf{V}_{yx} = V_y \, [1 + 0.8(1 - e^{-10ACC})] \tag{6.9}$$

where, V_y is the initial shear yield strength and ACC is the accumulated strain in the shear

spring.

6.6 REHABILITATION CASES

Three rehabilitation cases were designed for the existing nonductile three-story

building. In the first rehabilitation case (V_1), concentric inverted-V-brace was provided to

only three bays of the exterior frames of the building as shown in figure 6.9 a. All the steel

brace members have the same length, cross section and material properties. The brace

members were selected as round hollow sections (HSS 114 x 8). The effective length factors

for concentric inverted-V-bracing were considered as 1.0 for in-plane and out-of-plane

buckling. The Young's modulus is E=200,000 (MPa) and the steel yield stress is $f_y = 350$

(MPa). The brace buckling and residual capacities were calculated using the approach

described in Chapter 5. The calculated brace properties are; r = 37.7 (mm), (KL / r) =109,

$(P_y / P_c) = 0.44$, $(P_r / P_c) = 0.33$. In this rehabilitation case, the parameter "b" which defines

the increase in the load carrying capacity of the rehabilitated building was calculated as 1.7. This indicate that the lateral load capacity of the rehabilitated building is 1.7 times the load carrying capacity of the existing three-story building.

In the second rehabilitation case, E_1, vertical steel links were provided to the inverted-V-bracing systems as shown in figure 6.9 b. The properties and plastic capacities of the vertical steel links are summarized in table 6.1. The stiffness and the plastic capacities of the steel links in shear and flexure were calculated using Young's modulus, $E=200,000$ (MPa) and steel yield stress, $f_y = 300$ (MPa). The section and length of the vertical steel links (W200x46 and 0.60 m) were selected to satisfy equation 6.4 ($e_{cri}=4\ b_f\ t_f\ /t_w$) and to obtain a link shear strength lower than 2/3 the force level that causes brace buckling. The links are assumed to be properly stiffened to produce maximum levels of ultimate rotations. The value of the parameter "b" was calculated as 1.7 for the eccentric bracing rehabilitation case.

An eccentric brace rehabilitation case E_2 was designed in order to investigate the effect of the distribution of the steel link strengths along the rehabilitated building height. In Chapter 5, it was found that adding steel X-bracing uniformly with height to existing nonductile building structures may not represent the optimum solution. It was concluded that the steel X-brace distribution along the building height will have a strong effect on the characteristics of the developed plastic mechanism of the rehabilitated building under the effect of lateral loading and that the best distribution is that which provide the lowest value of the parameter v. The rehabilitation case E_2 has an eccentric brace distribution along the building height close to a linear distribution as shown in figure 6.9 c. The brace members and shear link properties are exactly the same as those used before in the rehabilitation case E_1.

The values of the parameter b_i which measure the distribution of the eccentric brace strength along the height are provided in the figure.

The effect of the eccentric bracing on the free vibration characteristics of the rehabilitated buildings was investigated. Table 6.2 summarizes the free vibration characteristics of the three rehabilitation cases V_1, E_1 and E_2. The rehabilitation cases with eccentric bracing have relatively lower stiffness and therefore longer fundamental period than the rehabilitation case with concentric bracing. The rehabilitation case E_2 has slightly shorter fundamental period than the rehabilitation case E_1. Table 6.3 summarizes the elastic spectral forces developed in the three rehabilitation cases due to the application of the twelve ground motion records described before in Chapter 4. The dynamic analysis was performed using 2.0% viscous damping. Significant scatter in the elastic spectral force levels of the three rehabilitation cases is observed for the ground motion records. The average elastic spectral force levels acting on the three rehabilitation cases V_1, E_1 and E_2 reached 2.49, 2.30 and 2.49, respectively.

6.7 PUSHOVER RESPONSE OF THE REHABILITATION CASES

A pushover analysis was conducted to evaluate the stiffness and strength characteristics of the three rehabilitation cases. The pushover was carried out using the code lateral load distribution. Figure 6.10 shows the lateral load-roof drift of the existing and the rehabilitated buildings. The ratios between the initial stiffness of the rehabilitated cases V_1, E_1 and E_2 to that of the existing building are 2.5, 2.2 and 2.4, respectively. Eccentric bracing rehabilitation caused lower increase in the building stiffness by comparison to the concentric

bracing. The parameter b was calculated as 1.7, 1.6 and 1.9 for the rehabilitation cases V_1, E_1 and E_2 respectively. The rehabilitation case E_2 caused higher increase in the load carrying capacity of the rehabilitated building than the bracing case E1 due to the change in the eccentric brace distribution along the height of the building. In figure 6.10, the lateral load-roof drift relationship of the rehabilitation case V_1 exhibited a drop in strength at about 0.35% roof drift ratio. This was because of buckling of some of the brace members at this stage of deformation. Buckling of a brace member will lead to a corresponding drop in the brace load capacity in compression.

The plastic mechanism parameter "v" presented in Chapter 3 was calculated for the three rehabilitation cases. It was pointed out in chapter 3 that the lower the value of v the more desirable is the developed plastic mechanism of the building under the effect of lateral loading. The value of v reached 0.43, 0.45, 0.50 and 0.20 for the existing building and the rehabilitation cases V_1, E_1 and E_2 respectively. These results indicate the improvement in the plastic mechanism of the rehabilitation case E_2 by comparison to the other bracing cases.

6.8 HYSTERETIC CHARACTERISTICS

The hysteretic characteristics of the eccentric bracing rehabilitation was investigated using a static cyclic analysis. The response of the eccentric bracing case E_1 was obtained due to the application of a static cyclic loading and was compared with those of the existing building and the concentric bracing case V_1. Static cyclic analysis of nonductile RC buildings using the code lateral load distribution can provide important information on the hysteretic aspects of the building under the effect of lateral loading. One of the important aspects of the

building response under the effect of lateral loading is the energy dissipation capacity of the load-displacement loops. Static cyclic analysis is especially useful when comparing the responses of the existing structure and different rehabilitation options.

A displacement controlled analysis was performed on the existing three-story building and the two rehabilitation cases V_1 and E_1 using the code lateral load distribution. The roof displacement of the buildings was controlled using the roof displacement history shown in figure 6.11. The lateral loading used in the analysis was the code lateral load distribution. Figures 6.12 to 6.14 represent the relationships between the roof drift ratio and the base shear coefficient of the existing building and the two rehabilitation cases. In these figures, the eccentric bracing rehabilitation case E_1 exhibited significant improvement in its hysteretic characteristics as compared to those of the existing building and the concentric bracing rehabilitation case V_1. This improvement in the hysteretic characteristics is mainly because of the enhancement in the plastic mechanism of the rehabilitation steel system as a result of the stable inelastic behaviour of the steel links. The cumulative dissipated energies calculated as the areas under the lateral load-displacement loops of figures 6.12 to 6.14 were compared in figure 6.15. In figure 6.15, the normalized dissipated energy = the dissipated energy / (building weight x building height). The figure indicates that eccentric bracing rehabilitation case is superior in its energy dissipation capacity as compared to the concentric bracing rehabilitation case. The significant improvement in the hysteretic characteristics of the eccentric bracing represent a major advantage of the eccentric bracing rehabilitation.

An important parameter that may affect the behaviour of the eccentric brace rehabilitation case is the link deformation angle developed in the steel links under the effect

of the static cyclic loading. Figures 6.16 represents the relationships between the roof drift ratio and the link maximum deformation angle in the various stories for the rehabilitation case with eccentric bracing. Figure 6.17 represents the relationship between the story drift ratio and the link deformation angle of the first story for the same rehabilitation case. In order to limit the link deformation angles below 0.1 radians, the roof and story drift ratios of the rehabilitated building should not exceed 0.88% and 1.83%, respectively. This limitation on the rehabilitated building deformation represents a major disadvantage of using eccentric bracing for rehabilitation of existing RC buildings.

The effect of eccentric steel bracing on the levels of axial and shear forces developed in the building members is evaluated. Eccentric steel bracing system will resist the lateral loads by producing axial forces in the building beams and columns. Tables 6.4 and 6.5 summarize the maximum axial forces developed in the frame members of the existing building and the rehabilitation cases V_1 and E_1 due to the application of the gravity loads and the static cyclic loading. In the tables, the level of axial forces is presented as the ratio of the maximum force developed in the member and the axial capacity of the member in compression or tension. The results summarized in table 6.4 indicate that the eccentric bracing caused an increase in the compressive axial load levels acting on the columns. No tensile axial forces were developed in the columns. Axial compression and tension forces were developed in the beams of the nonductile frame as shown in table 6.5. All the column axial forces are below the axial load at the balanced condition of the column cross section (The ratio between the balanced axial load and the column axial capacity in compression is equal to 0.41). The maximum axial force levels developed in the frame members of the rehabilitation case E_1 were

slightly lower than those developed in the rehabilitation case V_1.

The maximum shear forces developed in the frame members due to the application of the static cyclic loading are presented in tables 6.6 and 6.7. The table shows the maximum shear forces and the corresponding axial loads developed in the frame members of the rehabilitation cases V_1 and E_1 when subjected to the static cyclic loading. The maximum shear forces were calculated in two separate cases. The first case is when the member is subjected to a compressive axial force and the second case is when the member is subjected to a tensile axial force.

The levels of shear forces developed in the frame members of the rehabilitation cases V_1 and E_1 were found to be higher than the shear levels developed in the columns and beams of the existing building. The maximum shear force levels developed in the frame members of the rehabilitation case E_1 are lower than those developed in the frame members of the rehabilitation case V_1. The shear capacity of the frame members were calculated using the shear strength equation proposed by Priestley et al. (1994) which was presented in details in Chapter 5. The calculated shear capacities of the columns and beams are equal to 143.0 kN and 193.75 kN, respectively. The contribution of the axial compressive loads was neglected in the calculations, leading to more conservative estimates of the shear strength. The parameter k is considered equal to 0.1 assuming that the members suffered form severe inelastic deformation. The shear capacities of the concrete columns and beams of the bracing cases V_1 and E_1 are higher than the shear demands imposed by the static cyclic loading. For members subjected to tensile axial forces, the contribution of the transverse reinforcement alone exceeded the shear demands imposed by the cyclic loading.

6.9 SEISMIC RESPONSE

The seismic behaviour of the two rehabilitation cases V_1 and E_1 were studied under the effect of earthquake loading. The purpose of the study is to evaluate the effect of the changes in the stiffness and in the energy dissipation capacity of the eccentric bracing rehabilitation case on its seismic performance. The two rehabilitation cases V_1 and E_1 were subjected to scaled versions of the twelve ground motion records presented in Chapter 4. The seismic performance of the two rehabilitation cases were compared in terms of deformations and damage indices. The dynamic analysis of the building was performed using a time step increment of 0.005 second and Rayleigh damping which was defined to achieve 2.0% viscous damping in the first two natural modes of the building.

Table 6.8 summarizes the maximum roof drift, story drift of the two rehabilitation cases due to the application of scaled versions of the twelve ground motion records. The table shows that in eight of the ground motion records (no. 1,2,3,4,5,8,10 and 11), the eccentric bracing rehabilitation case achieved significantly lower deformation levels than those of the concentric bracing rehabilitation case. In the remaining four ground motion records (no. 6,7,9 and 12), the eccentric bracing rehabilitation case experienced deformation levels that are slightly higher than those of the concentric bracing rehabilitation case. The performance of the eccentric bracing rehabilitation when subjected to records 6,7,9, and 12 may be because of the changes in the stiffness which may lead to an increase in the seismic demands of the ground motions as compared to those of the concentric bracing case. The change in the seismic demands in case of records 9 and 12 may be attributed to the changes in the building elastic stiffness. For these ground motions, the elastic spectral forces of the eccentric bracing

case E_1 are higher than those of the concentric bracing case V_1 as shown in table 6.3. In case

of records 6 and 7, the change in the seismic demands may be attributed to the changes in the

building inelastic stiffness which can not be evaluated from the elastic spectral forces

presented in table 6.3. Table 6.9 summarizes the strength and stiffness based damage indices

of the two rehabilitation cases due to the application of scaled versions of the twelve ground

motion records. The results summarized in the tables 6.8 and 6.9 indicate that for many of the

ground motion records, eccentric bracing rehabilitation showed an improvement in the seismic

performance by comparison to the concentric bracing rehabilitation. This improvement in

performance can be attributed to the enhanced energy dissipation capacity of the eccentric

bracing rehabilitation.

Table 6.10 summarizes the link deformation angles of the eccentric bracing case due

to the application of the ground motion records. The ratio between the link deformation

angle γ and the story drift angle θ is calculated and is presented in the table. This ratio was

found to be close to the ratio calculated from equation 6.5 (γ/θ =H/e= 6.0). This indicates

that this ratio can be approximately considered independent on the loading condition. The

difference between the γ/θ ratio calculated from equation 6.5 and the values obtained from

the dynamic analysis is because the axial deformations of the brace members and the RC

frame members were neglected in the derivation of equation 6.5.

The mean of the seismic performance parameters of the eccentric bracing case E_1 are

calculated at multiples of 0.1 g increments for all the earthquake records. The performance

parameters are compared with those of the existing three-story building and the rehabilitation

case V_1. The seismic performance parameters are related to the PGA level as shown in

figures 6.18 to 6.21. The figures represent the relationships of the PGA level versus the mean of the roof drift, the story drift and the damage indices D_e^* and D_p respectively. The results shown in the figures indicate that on average, the eccentric brace rehabilitation caused a significant improvement in the seismic performance by comparison with the response of the existing building. The mean levels of deformation and damage indices were significantly lower in the eccentric bracing case E_1 than in the concentric bracing case V_1. At PGA=0.5 g, the ratios between the performance parameters of case V_1 to those of case E_1 were, 1.18, 1.23, 1.53, 1.20 for the roof drift, the story drift, the damage index D_e^* and the damage index D_p respectively. The improved performance of the eccentric bracing case E1 can be attributed to the enhancement in the energy dissipation capacity of the eccentric bracing as a result of the stable inelastic behaviour of the steel links.

Figure 6.22 shows examples of the distribution of damage due to the inelastic response of the rehabilitation cases V_1 and E_1. The damage distribution of figure 6.22 was due to the application of the Monte Negro ground motion. The numbers in the figures show the formation sequence of some selected plastic hinges. Numbers in italic font are for the column hinges while numbers in regular font are for the beam hinges. Damage distribution of the existing three-story building due to the application of the Monte Negro ground motion was presented in Chapter 5. In the rehabilitation case V_1 (PGA=0.475 g), hinging starts in the beams of the first and second floors due to pullout of the bottom reinforcement and yielding of the top reinforcement. With the increase in the earthquake intensity, damage spreads to the columns of the first and second stories. At the final stage of response, all the first story columns experienced splice failure at the bottom ends and yielding of the reinforcement at the

top ends. No damage was observed in the columns and beams of the third story. Brace buckling was observed in all the steel bracing members of the first and second stories and in three brace members of the third story.

Damage to the RC members of the rehabilitation case E_1 due to the application of the Monte Negro ground motion (PGA=0.475 g) was similar to that of the rehabilitation case V_1. Hinging starts in the beams of the first and second floors and spread to the columns of the first and second stories with the increase in the earthquake intensity. The columns and beams of the third story remained undamaged. All the steel brace members of the rehabilitation case E_1 behaved elastically. Yielding of steel shear links occurred in all the building stories.

6.10 EFFECT OF THE STEEL LINK DISTRIBUTION ALONG THE HEIGHT

The effect of the steel link distribution along the height of the RC building was investigated by comparing the seismic responses of the two rehabilitation cases E_1 and E_2 with eccentric bracing. The two rehabilitation cases have different distribution of eccentric bracing along the RC building height. The seismic performance of the eccentric brace rehabilitation case E_2 was obtained using the selected twelve ground motion records. Table 6.11 summarizes the maximum roof drifts and story drifts experienced by the rehabilitation case when subjected to the ground motion records. The damage indices calculated for the same rehabilitation case are summarized in table 6.12 while the link deformation angles are given in table 6.13.

The mean of the seismic performance parameters of the eccentric bracing case E_2 are calculated at multiples of 0.1 g increments for all the earthquake records. The performance

parameters are compared with those of the existing building and the rehabilitation case E_1. The seismic performance parameters are related to the PGA level as shown in figures 6.23 to 6.26. The figures represent the relationships of the PGA level versus the mean of the roof drift, the story drift and the damage indices D_s^* and D_s, respectively. The results shown in the figures indicate that in general, the eccentric bracing case E_2 achieved significantly lower deformation and damage indices than those of the rehabilitation case E_1. The enhanced seismic performance of the bracing case E_2 is mainly because of the improvement in the plastic mechanism of the building as indicated from the values of the parameter v calculated for both the rehabilitation cases in section 6.7. The value of v reached 0.50 and 0.20 for the rehabilitation cases E_1 and E_2, respectively. The lower value of v for the rehabilitation case E_2 is because of the uniformity of the story displacement along the building height.

The levels of axial and shear forces developed in the building members of the rehabilitation case E_2 due to the application of the Monte Negro earthquake (PGA=0.6 g) are presented in tables 6.14 and 6.15, respectivelly. The level of axial force is presented as the ratio of the maximum force developed in the member and the axial capacity of the member in compression or tension. The results summarized in table 6.14 indicate that the maximum axial force levels developed in the rehabilitation case E_2 are close to the levels developed in the rehabilitation case E_1. No tensile axial forces were developed in the columns. Axial compression and tension forces were developed in the beams of the nonductile frame. All the column axial forces are below the axial load at the balanced condition of the column cross section. The maximum shear force levels developed in the frame members of the rehabilitation case E_2 (Table 6.15) are close to the levels developed in the columns and beams

of the rehabilitation case E_1. The variation in the maximum shear forces calculated for each of the building stories of the rehabilitation case E_2 was small due to the uniformity of the story displacement along the building height. The shear capacities of the concrete columns and beams (calculated before in section 6.8) are higher than the shear demands developed in the frame members of the rehabilitation case E_2 due to the application of the earthquake loading.

Damage distribution of the rehabilitation cases E_1 and E_2 due to the application of the Monte Negro ground motion is shown in figure 6.22. The damage distribution of the rehabilitation case E_1 was discussed in section 6.9. In the rehabilitation case E_2 (PGA=0.475 g), hinging starts in the beams of the second floor and in the columns of the third story. With the increase in the earthquake intensity, damage spread to the beams of the first floor and to the second story columns. At the final stage of response damage spread to the columns of the first story. All the first and third story columns experienced splice failure at the bottom ends and yielding of the reinforcement at the top ends. No damage was observed in the beams of the third floor. All the steel brace members of the rehabilitation case E_2 behaved elastically and all the steel shear links experienced shear yielding.

The number of plastic hinges in RC members of the rehabilitation case E_2 was larger than that of the rehabilitation case E_1. This can be attributed to the improvement in the plastic mechanism of the rehabilitation case E_2 which led to the participation of more RC elements in the building inelastic response. The improvement in the plastic mechanism of the rehabilitation case E_2 is also demonstrated in figure 6.27. The figure shows the damage distribution of the rehabilitation cases E_1 and E_2 due to the application of the El Centro ground motion. The number of of plastic hinges in RC members of the rehabilitation case

E_2 was significantly larger than that of the rehabilitation case E_1.

6.11 SUMMARY

An analytical model for vertical shear links was implemented in the DRAIN-2DX computer program. One concentric and two eccentric steel bracing rehabilitation cases were analyzed. Eccentric bracing cases exhibited better ability to dissipate energy under the effect of static cyclic load as compared to the behaviour of the concentric bracing case. The improvement in the hysteretic characteristics of the eccentric bracing cases was attributed to the stable inelastic behaviour of the vertical shear links.

The analysis performed on the eccentric brace rehabilitation case indicated that the link deformation angle is an important parameter. In order to limit the link deformation angle below the allowable level γ_a, the story drift angle (story displacement / story height) of the rehabilitated building should not exceed γ_a x (link length / story height). This limitation on the rehabilitated building deformation represents a major disadvantage of the use of eccentric bracing in seismic rehabilitation of existing concrete buildings.

The improvement in the seismic performance of the nonductile building when using well designed eccentric bracing rehabilitation is expected to be greater than that of the concentric bracing as long as the building deformation remains below the limits that cause the maximum allowable link deformation angle. The relationship between the deformation angle, γ, of the vertical links and the story drift angle, θ, can be approximated as $\theta = \gamma$ x (link length / story height). This relationship was found to be independent of the loading conditions.

The distribution of the vertical link strength along the building height was found to

have a significant effect on the characteristics of the developed plastic mechanism under the effect of lateral load. It is suggested that the distribution of vertical steel link strength along the height of the building should be selected to obtain a uniform distribution of story drift along the frame height. The uniformity of story displacement along the building height can be evaluated using the parameter v introduced in Chapter 3.

Table 6.1 Properties of the vertical links used in rehabilitating the three story building

Section	$M_y = M_p$ (kN.m)	$V_y = 0.9V_p$ (kN)	e (m)	K_{1M} (kN.m)	K_{1v} (kN/m)
W200x46	148.80	203	0.60	4.55×10^4	167100

Table 6.2 Free vibration characteristics of the rehabilitation cases

Case	First mode shape					Second mode shape				
	T_1 (sec)	Modal mass*	1st floor displ.	2nd floor displ.	3rd floor displ.	T_2 (sec)	Modal mass*	1st floor displ.	2nd floor displ.	3rd floor displ.
V_1	0.46	0.91	0.43	0.79	1.00	0.16	0.08	1.00	0.48	-0.81
E_1	0.59	0.91	0.44	0.80	1.00	0.20	0.08	1.00	0.47	-0.81
E_2	0.57	0.84	0.30	0.65	1.00	0.22	0.13	1.00	0.99	-0.94

* As a fraction of the total mass

Table 6.3 Elastic spectral forces (V/W) of the rehabilitation cases

Rec. No.	Earthquake	Elastic spectral force		
		Concentric brace case V_1	Eccentric brace case E_1	Eccentric brace case E_2
1	Parkfield, California	2.14	0.53	0.61
2	Nahanni, Canada	0.88	0.79	0.67
3	Imperial Valley, California	3.36	2.77	2.97
4	Kern County, California	3.49	2.19	2.20
5	San Fernando, California	1.73	1.90	1.86
6	San Fernando, California	2.15	1.83	2.28
7	Monte Negro, Yugoslavia	4.18	3.08	3.76
8	Long Beach, California	2.11	3.46	3.21
9	Lower California	2.42	2.69	2.88
10	San Fernando, California	1.75	2.56	2.96
11	Near E. Coast of Honshu, Japan	3.42	2.50	2.69
12	Mexico	2.27	3.29	3.86

Table 6.4 Maximum axial forces developed in the frame columns adjacent to steel members of the bracing cases V_1 and E_1 due to the application of the static cyclic loading

Story	Existing building		Bracing case V_1		Bracing case E_1	
	Compression	Tension	Compression	Tension	Compression	Tension
1	0.11*	-	0.22	-	0.20*	-
2	0.07	-	0.13	-	0.12	-
3	0.04	-	0.04	-	0.05	-

* As a ratio from the axial capacity

Table 6.5 Maximum axial forces developed in the frame beams of the bracing cases V_1 and E_1 due to the application of the static cyclic loading

Story	Existing building		Bracing case V_1		Bracing case E_1	
	Compression	Tension	Compression	Tension	Compression	Tension
1	0.001*	0.05*	0.025	0.30	0.021*	0.30*
2	0.005	0.02	0.027	0.33	0.024	0.24
3	0.003	0.01	0.027	0.31	0.020	0.23

* As a ratio from the axial capacity

Table 6.6 Maximum shear forces (kN) developed in the frame columns adjacent to steel members of the bracing cases V_1 and E_1 due to the application of the static cyclic loading

Story	Maximum shear with compressive axial force			
	Bracing case V_1		Bracing case E_1	
	Shear force	Axial force	Shear force	Axial force
1	105.2	864.0	100.4	796.7
2	72.2	524.4	74.3	270.9
3	21.3	135.6	50.4	137.7

Table 6.7 Maximum shear forces (kN) developed in the frame beams of the bracing cases V_1 and E_1 due to the application of the static cyclic loading

Story	Maximum shear with compressive axial force				Maximum shear with tensile axial force			
	Bracing case V_1		Bracing case E_1		Bracing case V_1		Bracing case E_1	
	Shear	Axial	Shear	Axial	Shear	Axial	Shear	Axial
1	159.3	117.9	140.6	167.2	120.6	131.5	84.6	133
2	138.1	96.65	129.1	143.5	118.2	124.2	81.1	160.4
3	53.3	150.2	97.79	142.4	55.7	58.5	50.8	150.4

Tabie 6.8 Displacement response of the rehabilitation cases V_1 and E_1

Earthquake No.*	PGA (g)	Drift of the concentric bracing case V_1 (%)				Drift of the eccentric bracing case E_1 (%)			
		Roof	1st story	2nd story	3rd story	Roof	1st story	2nd story	3rd story
1	1.80	1.68	3.18	1.48	0.61	0.94	1.71	1.19	0.50
2	1.75	1.16	2.31	1.08	0.35	0.97	1.80	0.93	0.39
3	0.48	1.00	2.26	0.62	0.13	0.87	1.87	0.66	0.23
4	0.50	1.00	2.13	0.80	0.13	0.85	1.55	0.81	0.23
5	0.50	1.04	2.33	0.69	0.20	0.84	1.76	0.66	0.28
6	0.65	0.88	1.56	0.84	0.27	0.79	1.65	0.62	0.37
7	0.48	0.97	1.84	0.89	0.27	0.91	1.92	0.69	0.23
8	0.28	collapse	collapse	collapse	collapse	0.77	1.71	0.59	0.24
9	0.40	0.83	1.75	0.63	0.20	0.87	1.85	0.73	0.19
10	0.32	1.31	3.27	0.72	0.12	0.88	1.85	0.64	0.21
11	0.50	1.21	2.26	1.19	0.29	1.01	1.96	0.92	0.24
12	0.28	0.83	1.69	0.76	0.12	0.84	1.84	0.62	0.25

* The earthquakes corresponding to these numbers are listed in table 6.3

Table 6.9 Damage indices of the rehabilitation cases V_1 and E_1

Earthquake No.*	PGA (g)	Damage indices of the bracing case V_1		Damage indices of the bracing case E_1	
		$D_t^{\bullet}$	D_g	$D_t^{\bullet}$	D_g
1	1.80	0.66	0.85	0.27	0.72
2	1.75	0.36	0.70	0.21	0.64
3	0.48	0.48	0.72	0.26	0.59
4	0.50	0.45	0.70	0.23	0.60
5	0.50	0.40	0.65	0.20	0.48
6	0.65	0.20	0.51	0.19	0.49
7	0.48	0.24	0.59	0.30	0.50
8	0.28	collapse	collapse	0.17	0.52
9	0.40	0.21	0.47	0.26	0.51
10	0.32	0.77	0.86	0.28	0.57
11	0.50	0.31	0.64	0.26	0.62
12	0.28	0.21	0.52	0.25	0.53

* The earthquakes corresponding to these numbers are listed in table 6.3

Table 6.10 Link deformation angel γ (radians) of the retrofitting case E_1

Earthquake No.*	PGA (g)	1st story	2nd story	3rd story	$\gamma_{max}/\theta_{max}$
1	1.80	0.094	0.066	0.025	5.53
2	1.75	0.101	0.051	0.018	5.63
3	0.48	0.107	0.035	0.009	5.73
4	0.50	0.088	0.044	0.009	5.70
5	0.50	0.100	0.034	0.012	5.71
6	0.65	0.094	0.032	0.017	5.69
7	0.48	0.110	0.036	0.009	5.74
8	0.28	0.098	0.030	0.010	5.71
9	0.40	0.106	0.033	0.008	5.72
10	0.32	0.106	0.039	0.007	5.75
11	0.50	0.113	0.050	0.009	5.74
12	0.28	0.105	0.032	0.010	5.72

* The earthquakes corresponding to these numbers are listed in table 6.3

Table 6.11 Displacement response of the rehabilitation case E_2

Earthquake No.*	PGA (g)	Drift of the eccentric brace case E_2 (%)			
		Roof	1st story	2nd story	3rd story
1	1.80	1.01	1.68	0.88	1.43
2	2.20	1.43	1.36	1.66	1.67
3	0.72	1.02	1.05	1.51	0.68
4	0.73	1.27	1.61	1.76	0.68
5	0.68	1.40	1.74	1.60	0.98
6	1.00	1.19	1.38	1.53	1.44
7	0.60	1.44	1.63	1.61	1.26
8	0.35	1.08	1.83	1.05	0.56
9	0.54	1.12	1.44	1.37	0.69
10	0.42	1.19	1.66	1.41	0.52
11	0.50	1.09	0.92	1.66	0.77
12	0.40	1.37	1.62	1.74	0.87

* The earthquakes corresponding to these numbers
are listed in table 6.3

Table 6.12 Damage indices of the rehabilitation case E_2

Earthquake No.*	PGA (g)	Damage indices of the brace case E_2	
		$D_s^{\bullet}$	D_s
1	1.80	0.20	0.64
2	2.20	0.22	0.67
3	0.72	0.15	0.61
4	0.73	0.25	0.74
5	0.68	0.21	0.66
6	1.00	0.22	0.66
7	0.60	0.22	0.61
8	0.35	0.17	0.52
9	0.54	0.21	0.59
10	0.42	0.33	0.50
11	0.50	0.15	0.49
12	0.40	0.33	0.56

* The earthquakes corresponding to these numbers are listed in table 6.3

Table 6.13 Link deformation angel γ (radians) of the rehabilitation case E_2

Earthquake No.*	PGA (g)	1st story	2nd story	3rd story	$\gamma_{max}/\theta_{max}$
1	1.80	0.094	0.048	0.080	5.61
2	2.20	0.076	0.093	0.094	5.65
3	0.72	0.058	0.085	0.035	5.67
4	0.73	0.092	0.100	0.035	5.67
5	0.68	0.099	0.091	0.053	5.71
6	1.00	0.078	0.086	0.080	5.67
7	0.60	0.093	0.091	0.070	5.71
8	0.35	0.105	0.058	0.028	5.74
9	0.54	0.082	0.077	0.036	5.69
10	0.42	0.094	0.079	0.026	5.69
11	0.50	0.051	0.094	0.040	5.69
12	0.40	0.092	0.099	0.047	5.70

* The earthquakes corresponding to these numbers are listed in table 6.3

Table 6.14 (a) Maximum axial forces developed in the frame columns adjacent to steel members of the bracing case E_2 due to the application of the Monte Negro earthquake (PGA=0.6 g)

Story	Existing building		Bracing case E_2	
	Compression	Tension	Compression	Tension
1	0.11*	-	0.15*	-
2	0.07	-	0.11	-
3	0.04	-	0.05	-

* As a ratio from the axial capacity

Table 6.14 (b) Maximum axial forces developed in the frame beams of the bracing case E_2 due to the application of the Monte Negro earthquake (PGA=0.6 g)

Story	Existing building		Bracing case E_2	
	Compression	Tension	Compression	Tension
1	0.003*	0.06*	0.022	0.30
2	0.005	0.04	0.028	0.33
3	0.005	0.03	0.018	0.23

* As a ratio from the axial capacity

Table 6.15 (a) Maximum shear forces (kN) developed in the columns adjacent to steel members of the bracing case E_2 due to the application of the Monte Negro earthquake (PGA=0.6 g)

Story	Maximum shear with compression axial force	
	Shear force	Axial force
1	93.9	532.6
2	93.0	454.5
3	81.6	152.6

Table 6.15 (b) Maximum shear forces (kN) developed in the frame beams of the bracing case E_2 due to the application of the Monte Negro earthquake (PGA=0.6 g)

Story	Maximum shear with compression axial force		Maximum shear with tensile axial force	
	Shear force	Axial force	Shear force	Axial force
1	141.0	112.2	88.6	145.9
2	141.4	125.9	92.2	52.1
3	109.5	135.5	81.1	136.9
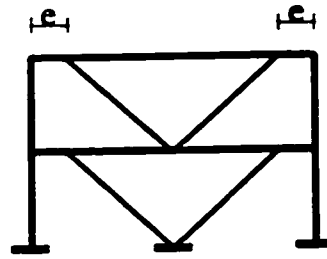
(a) V-bracing
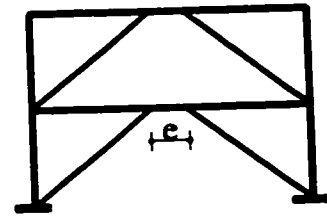
(b) K-bracing
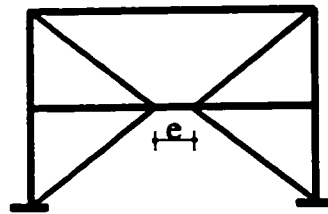
(c) X-bracing
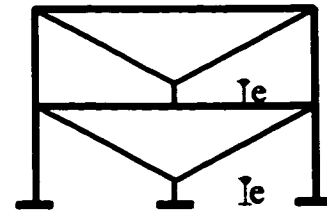
(d) Y-bracing

Figure 6.1 Various types of eccentrically braced steel frames
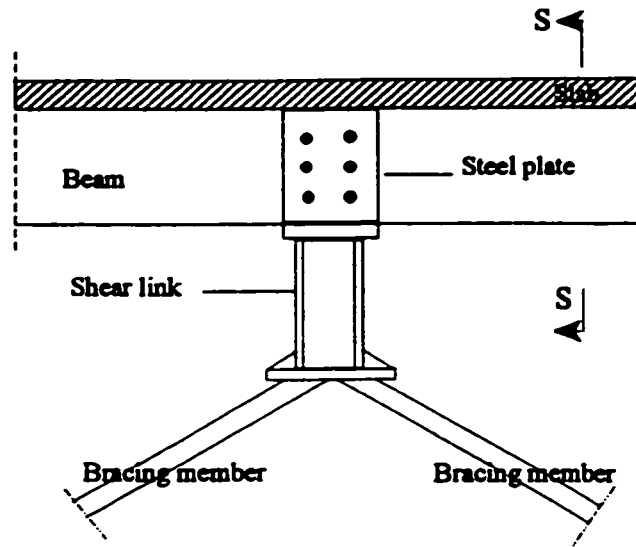
(a) Elevation
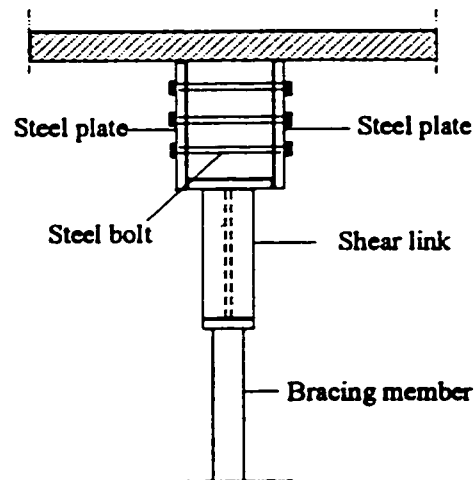
(b) Section S-S

Figure 6.2 Connection details of a vertical steel link
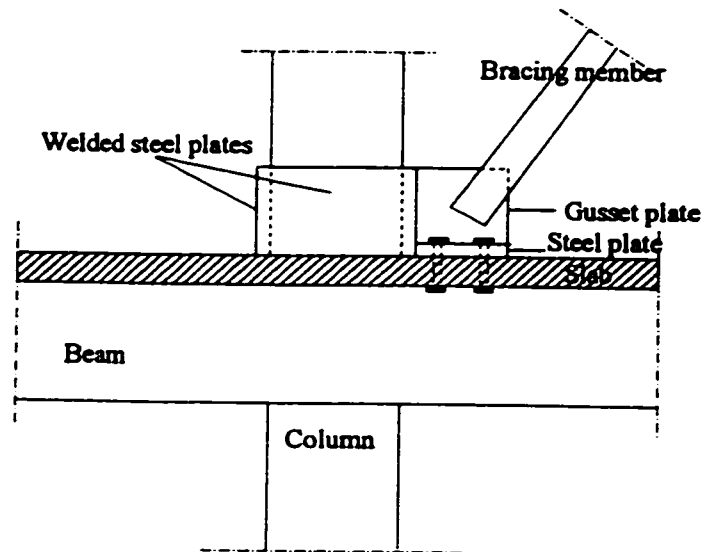
Figure 6.3 Details of a connection between steel brace member and RC frame

(a) Original frame

(b) Plastic mechanism
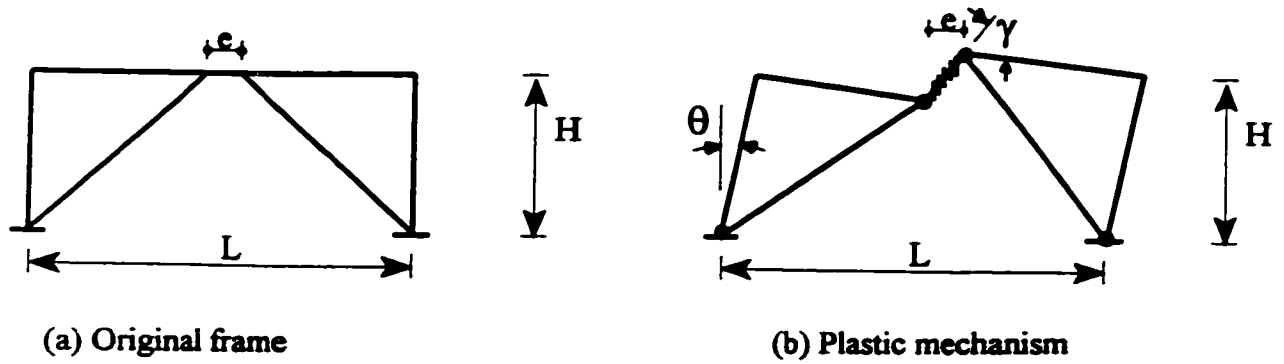
Figure 6.4 A plastic mechanism of an eccentrically braced steel frame

(a) Original frame

(b) Plastic mechanism
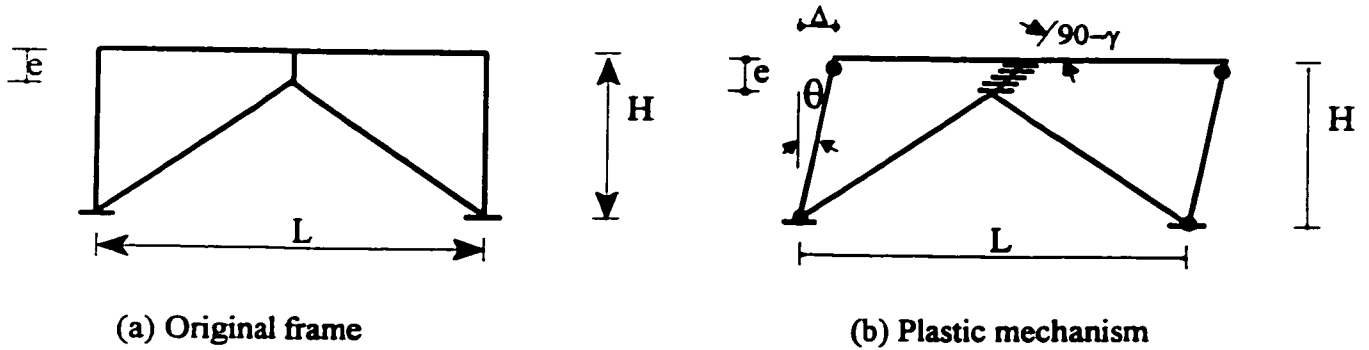
Figure 6.5 An assumed plastic mechanism of a reinforced concrete frame provided with a vertical steel link

Moment hinge springs   Moment hinge springs

Primary node i   Elastic Beam Element   Primary node J

Slaved node i'   Slaved node J'

Shear hinge springs   Shear hinge springs

Zero Length   Link length e   Zero Length
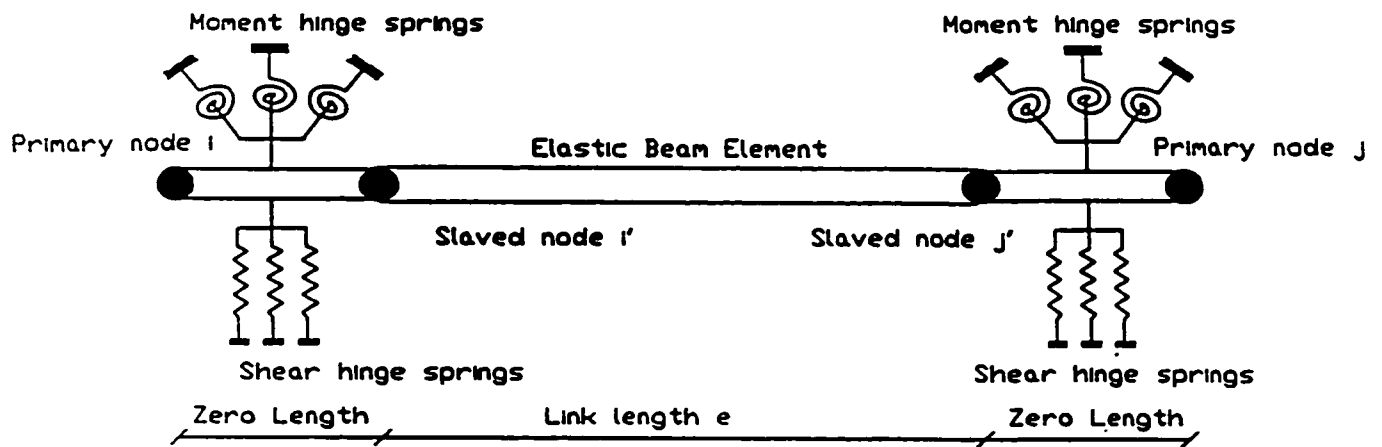
Figure 6.6 Link model (Ramadan and Ghobarah, 1995)
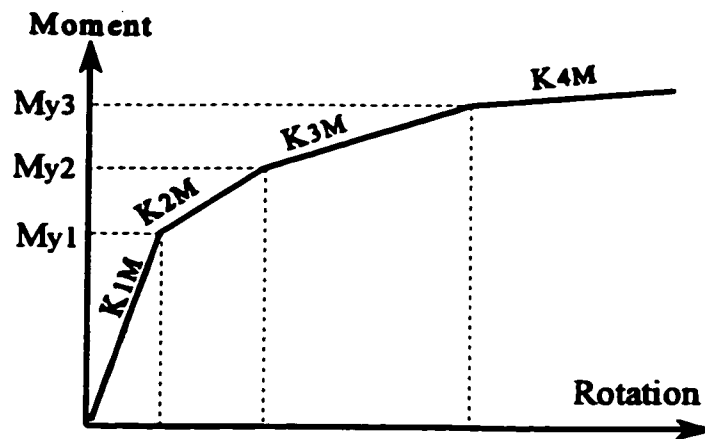
Figure 6.7 Moment-rotation relationship of a steel link
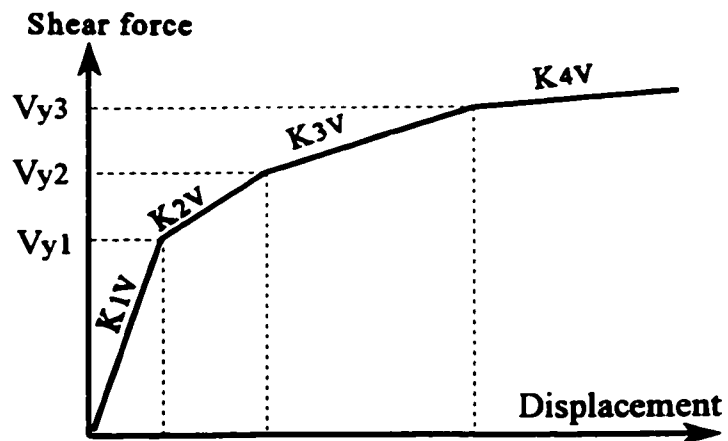
Figure 6.8 Shear force-shear deformation relationship of a steel link

(a) Case V_1
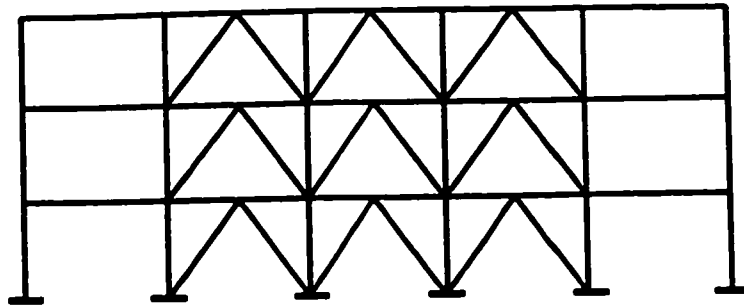
Brace members are (HSS 114.3 x 114.3 x 7.95)

(b) Case E_1
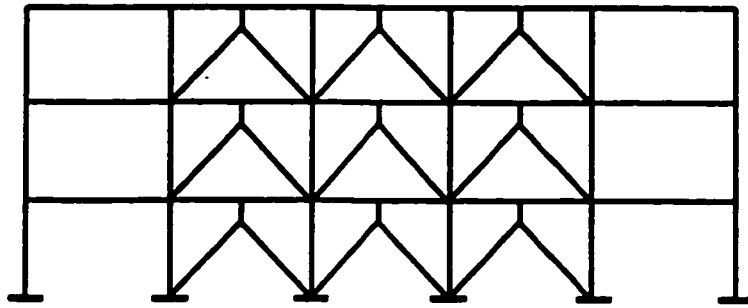
Brace members are (HSS 114.3 x 114.3 x 7.95)
Link elements are W200x46, e= 0.6 m

(c) Case E_2
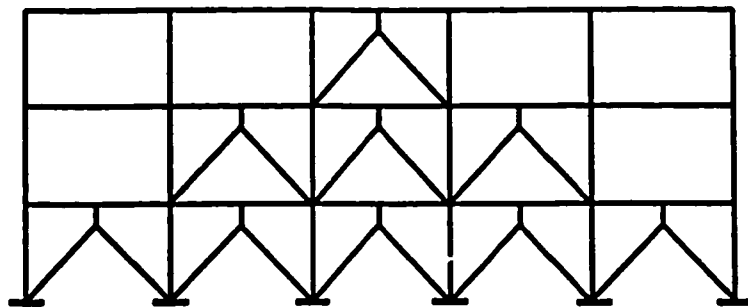
$b_3=1/9$

$b_2=1/3$

$b_1=5/9$

Brace members are (HSS 114.3 x 114.3 x 7.95)
Link elements are W200x46, e=0.6 m

Figure 6.9 Rehabilitation cases
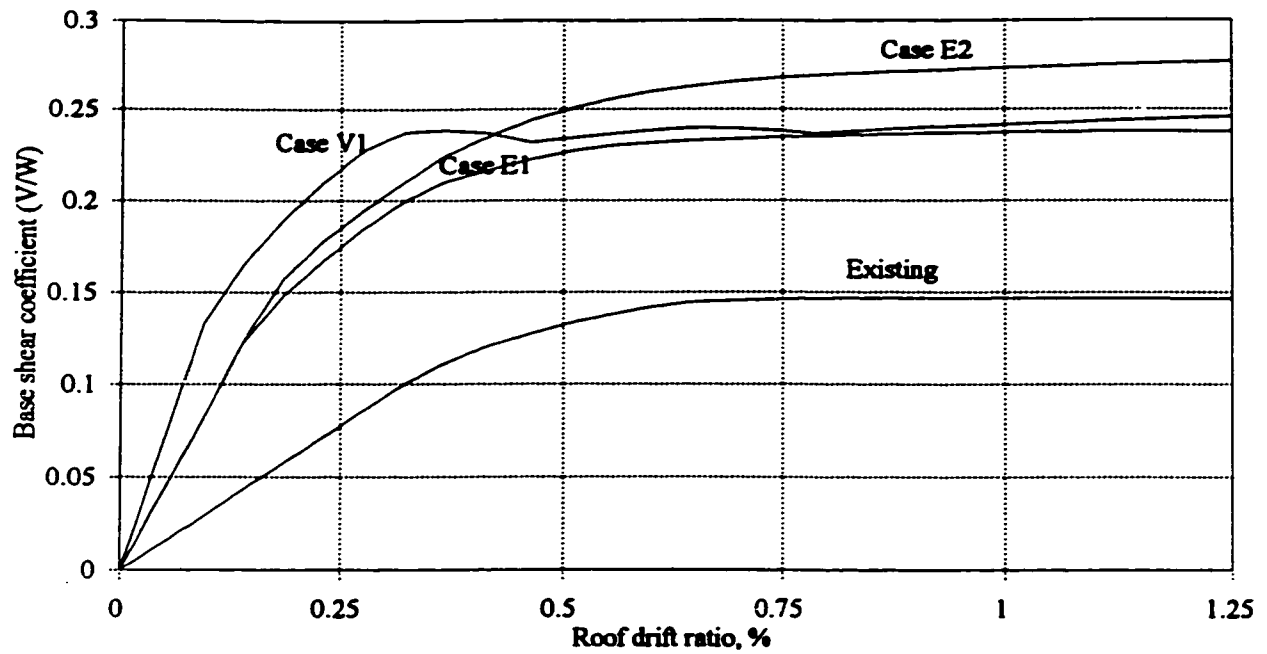
Figure 6.10 Pushover results of the existing building and the rehabilitation
cases V_1, E_1 and E_2
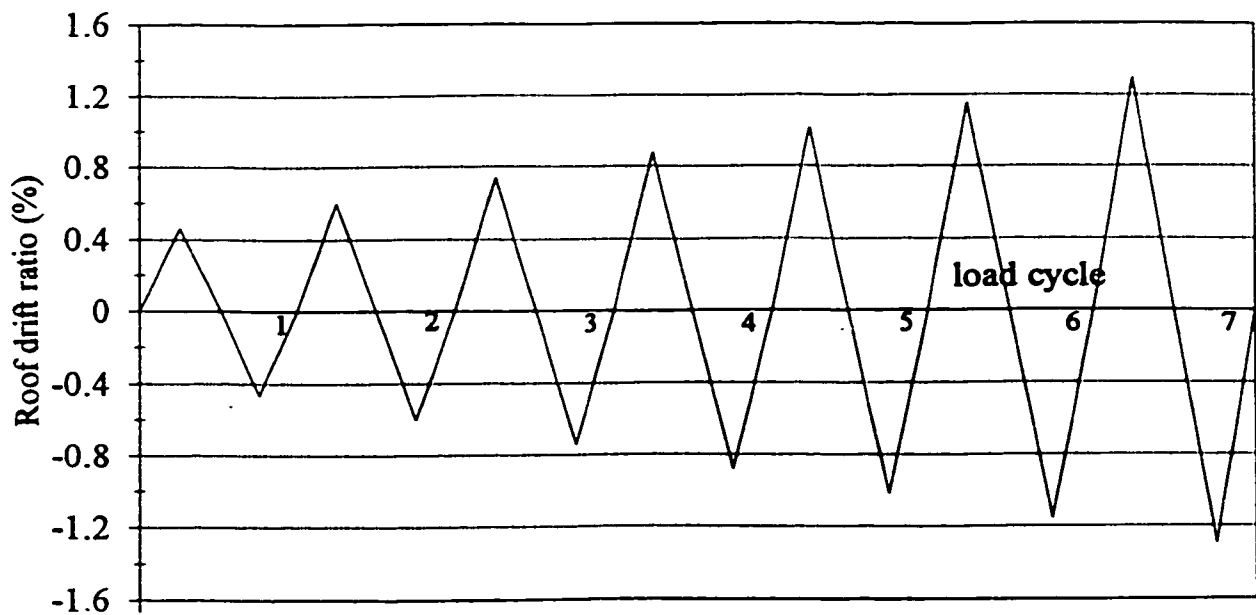
Figure 6.11 Roof displacement history for the static cyclic analysis
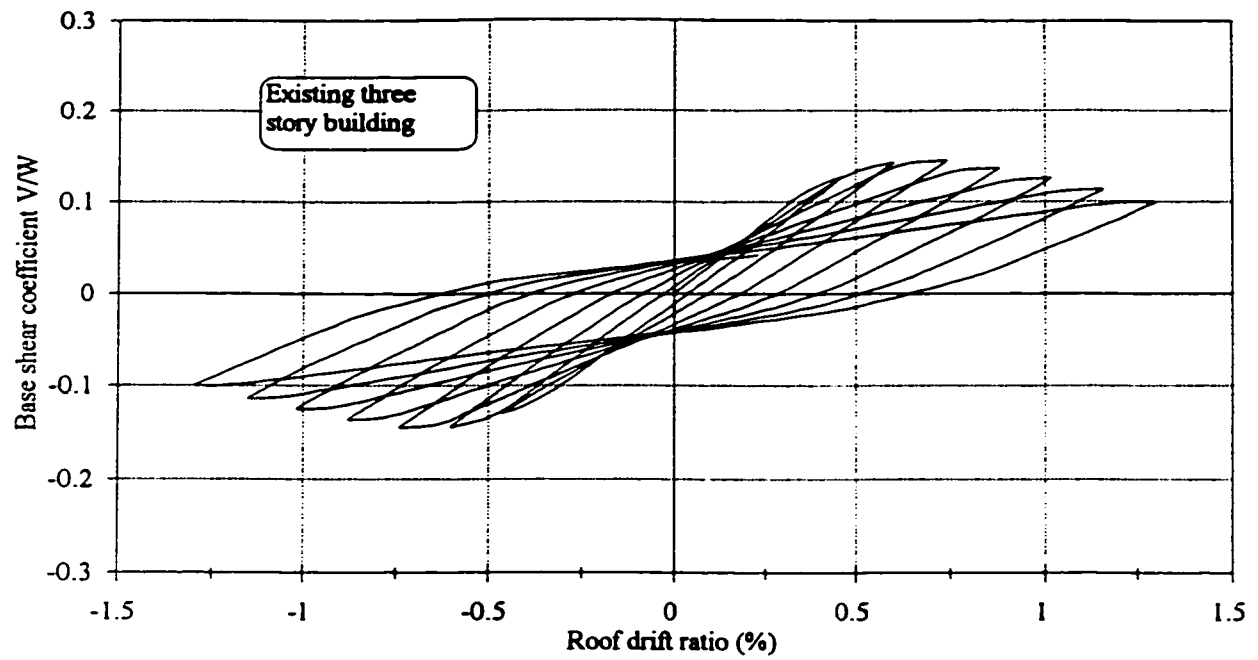
Figures 6.12 Relationship between the roof drift ratio and the base shear coefficient of the existing building
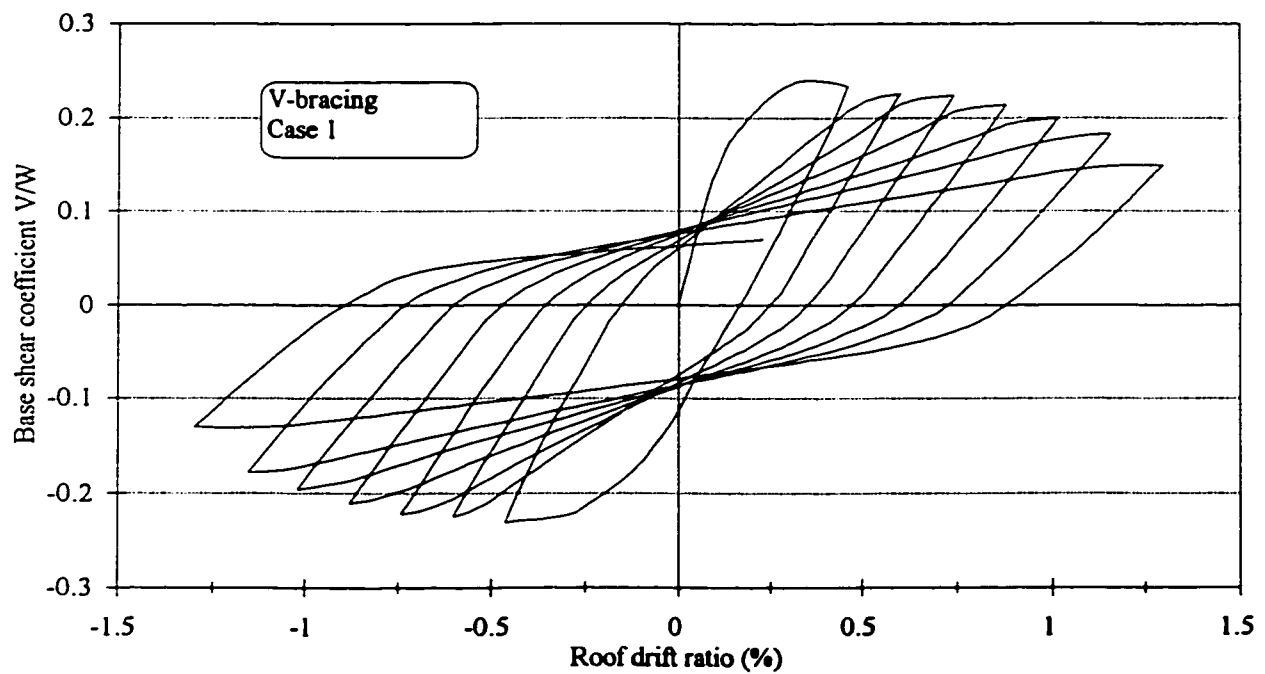
Figures 6.13 Relationship between the roof drift ratio and the base shear coefficient of the rehabilitation case V_1
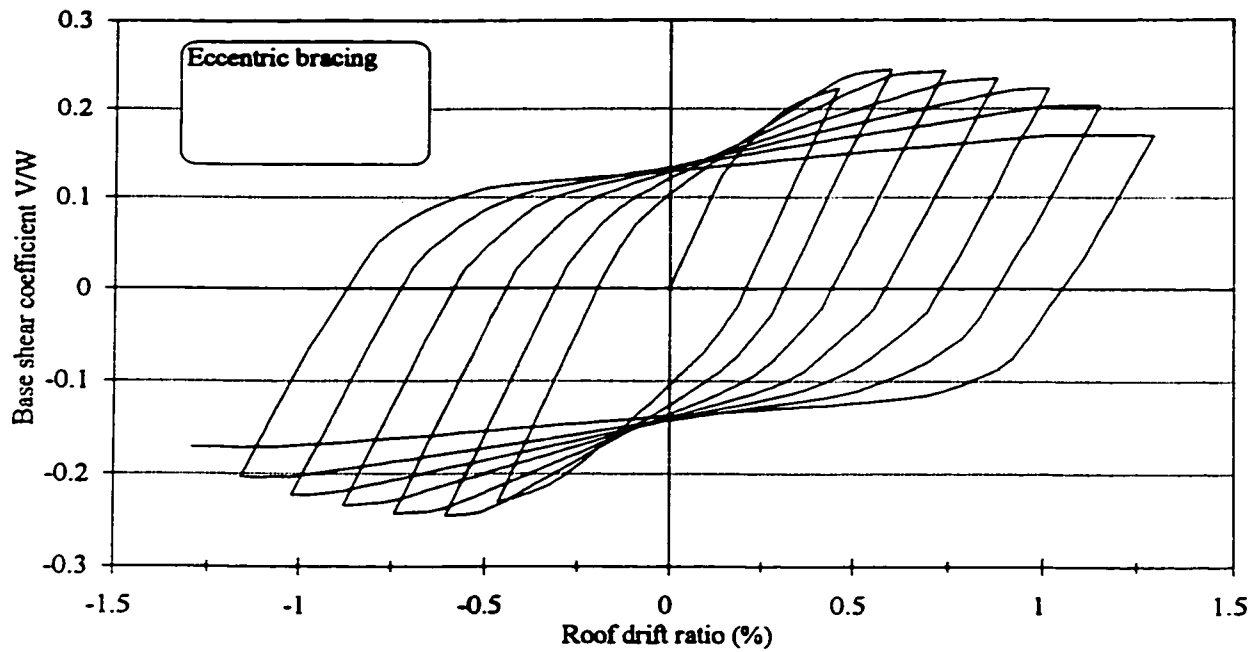
Figures 6.14 Relationship between the roof drift ratio and the base shear coefficient of the rehabilitation case E_1
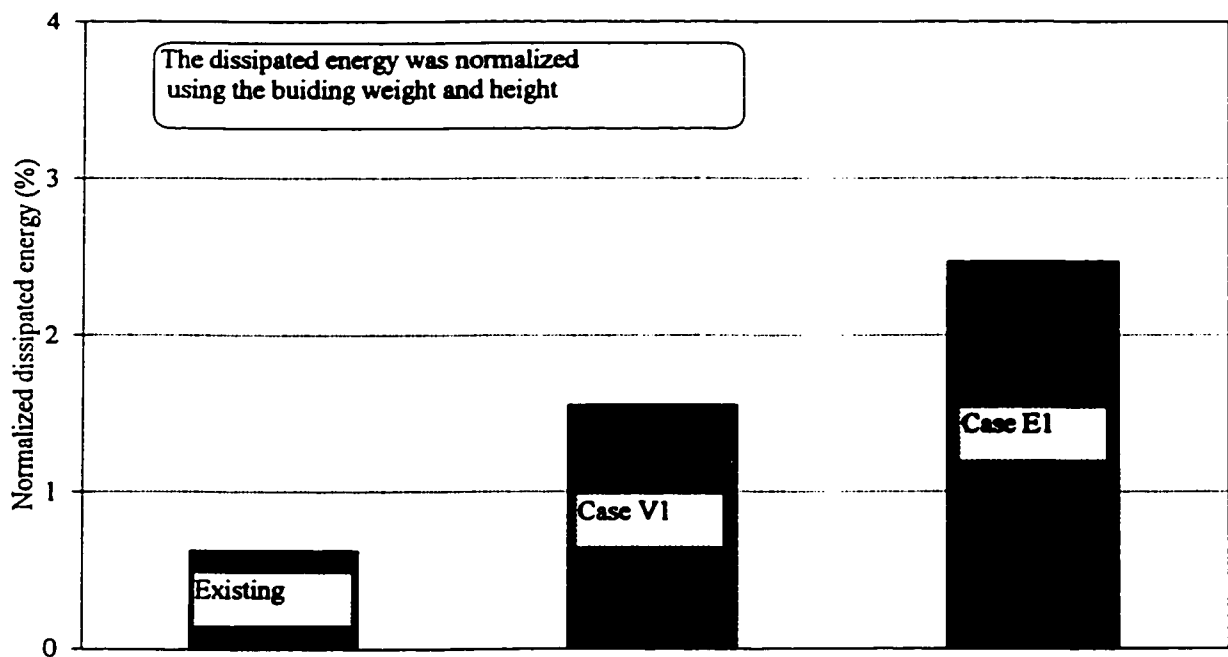
Figures 6.15 The dissipated energy of the existing building and the rehabilitated cases V_1 and E_1
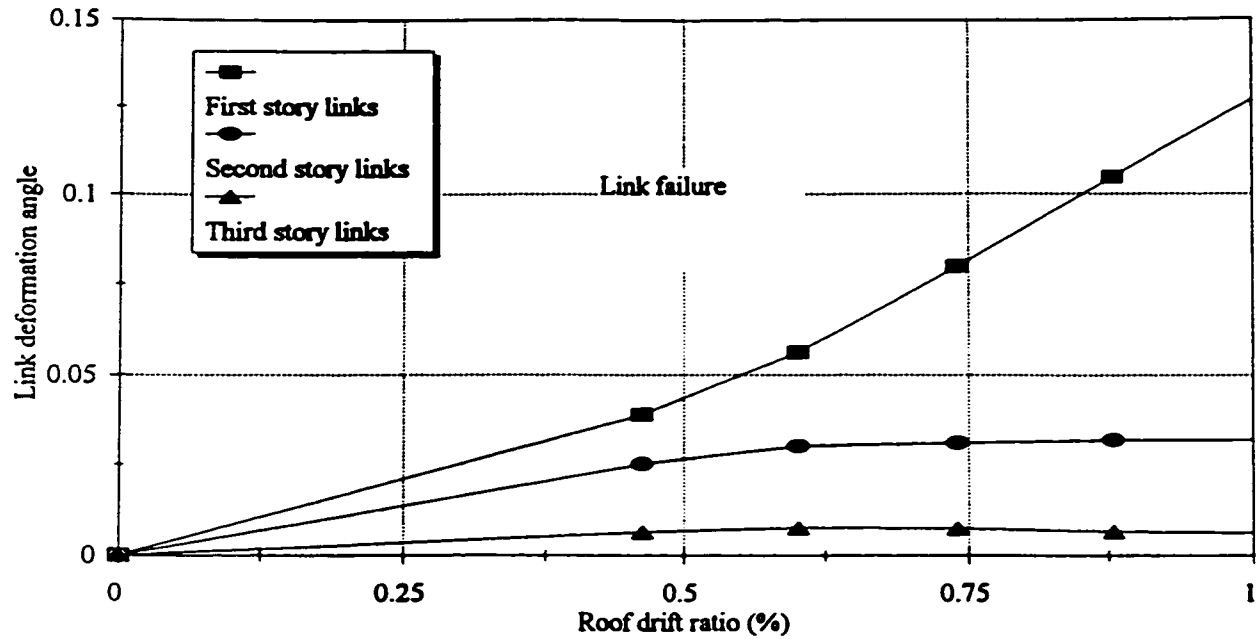
Figure 6.16 The relationships between the roof drift and the link maximum deformation angle in the various stories for the rehabilitation case E_1
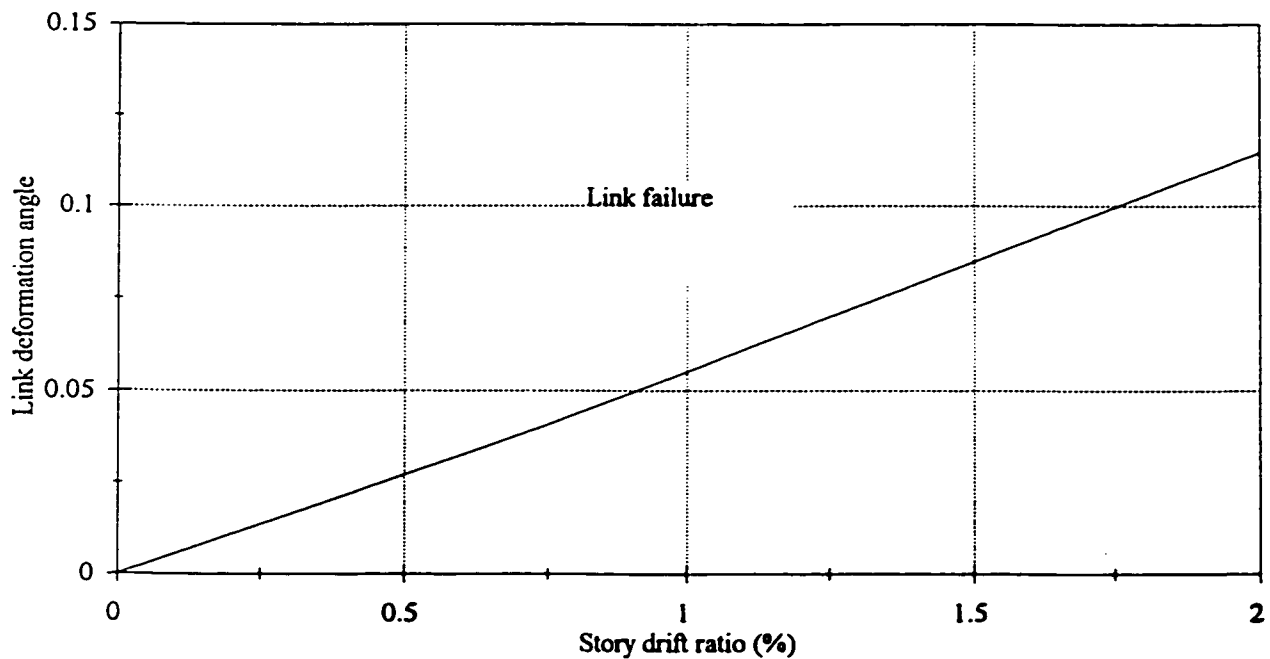
Figure 6.17 The relationship between the story drift and the link deformation angle of the first story for the rehabilitation case E_1
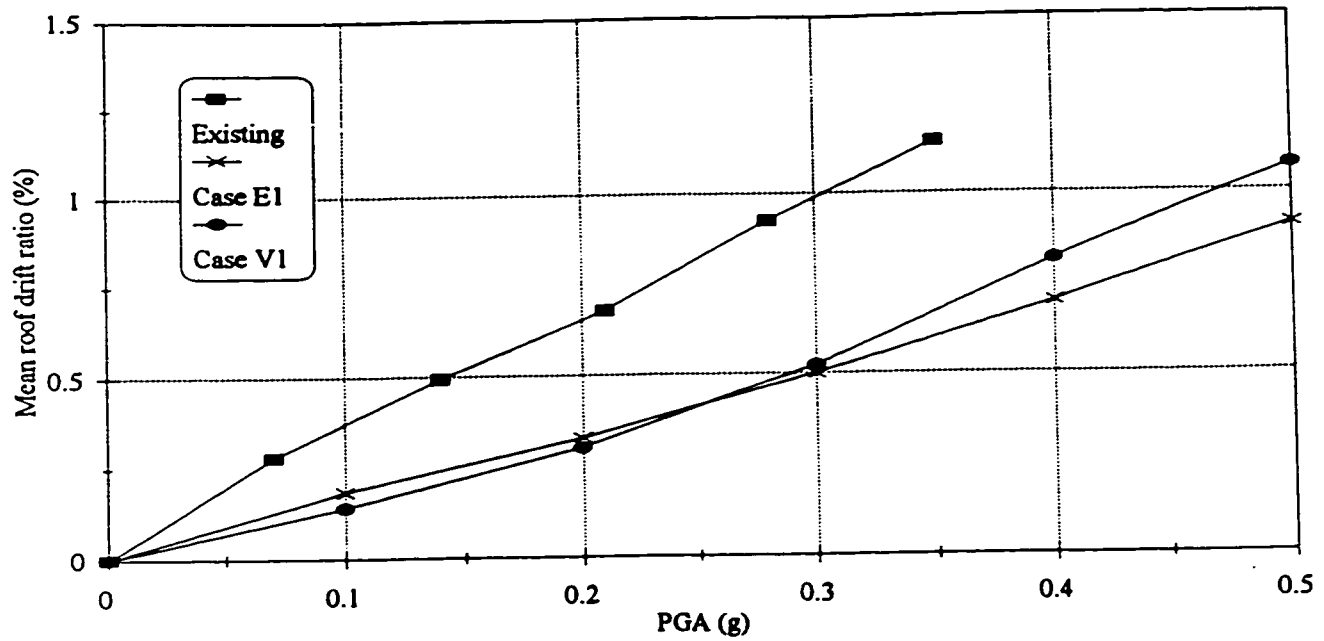
Figure 6.18 The relationship between the PGA and the mean of the roof drift
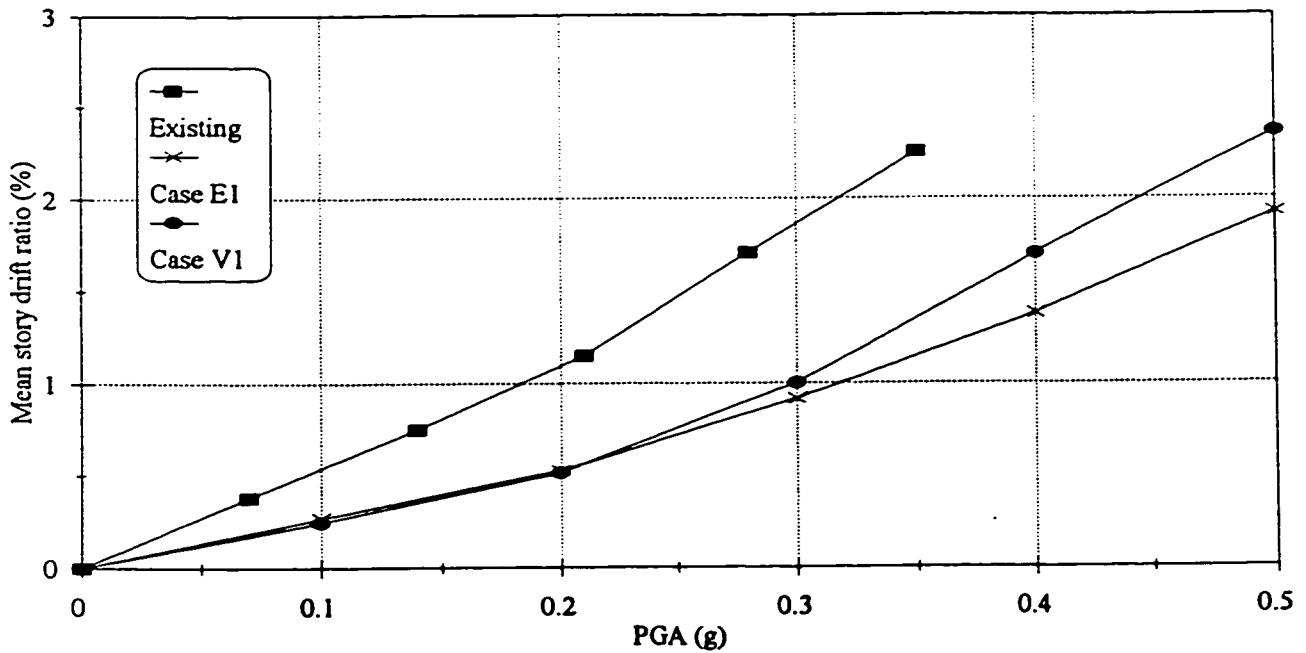
Figure 6.19 The relationship between the PGA and the mean of the story drift
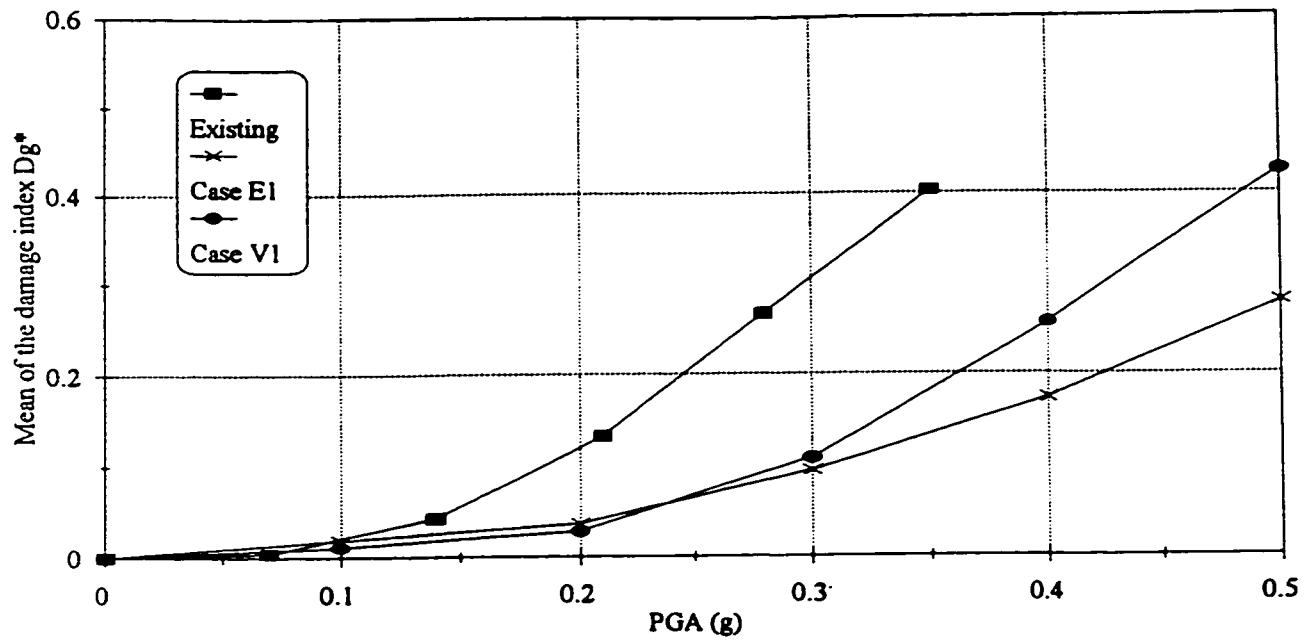
Figure 6.20 The relationship between the PGA and the mean of the damage index D_g^*
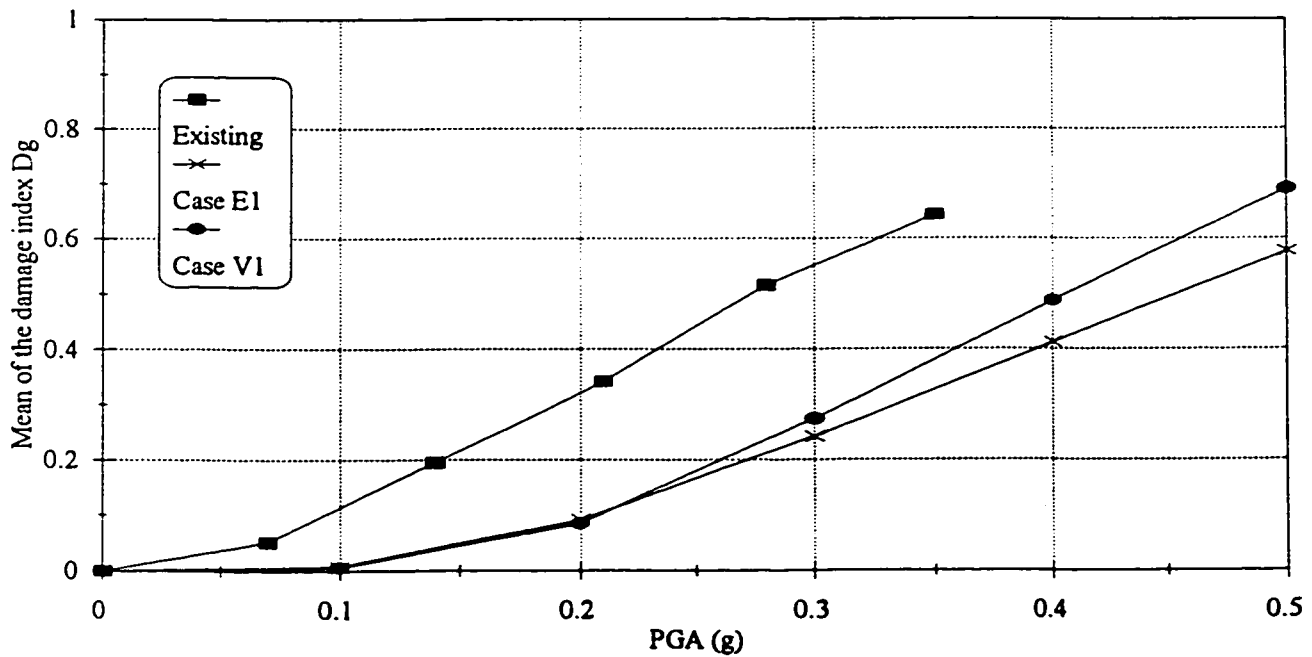
Figure 6.21 The relationship between the PGA and the mean of the damage index D_g

o Yielding of top beam reinforcement
- Column reinforcement yielding
☐ Shear link yielding
▲ Brace buckling

⊙ Pullout of beam bottom reinforcement
   (or beam yielding in positive moment)
▪ Column splice failure
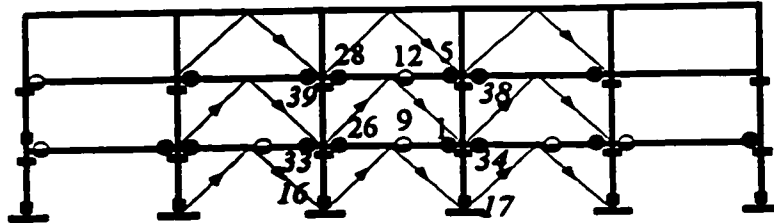
(a) Rehabilitation case V_1, PGA= 0.475g
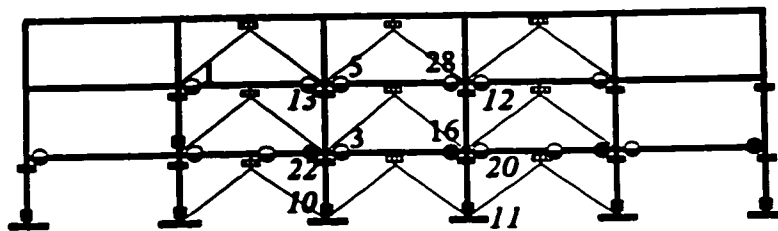
(b) Rehabilitation case E_1, PGA= 0.475 g
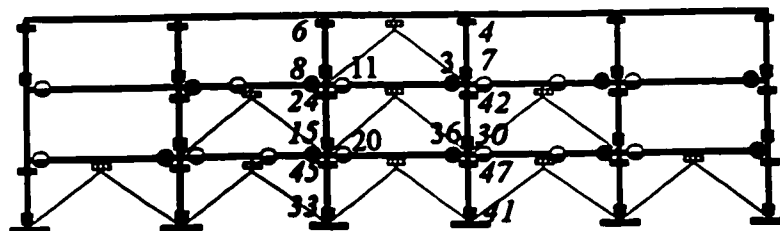
(c) Rehabilitation case E_2, PGA= 0.60 g

Figure 6. 22 Hinge type and location of the rehabilitation cases V_1, E_1 and E_2 due to the application of the Monte Negro earthquake
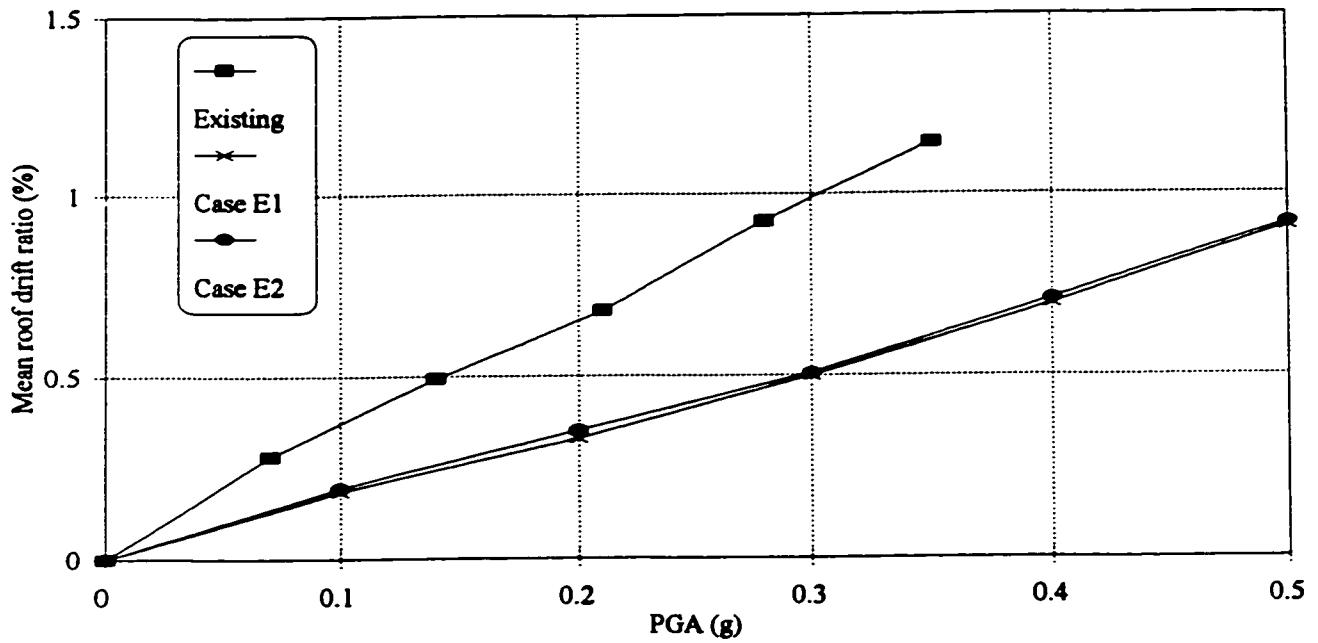
Figure 6.23 The relationship between the PGA and the mean of the roof drift
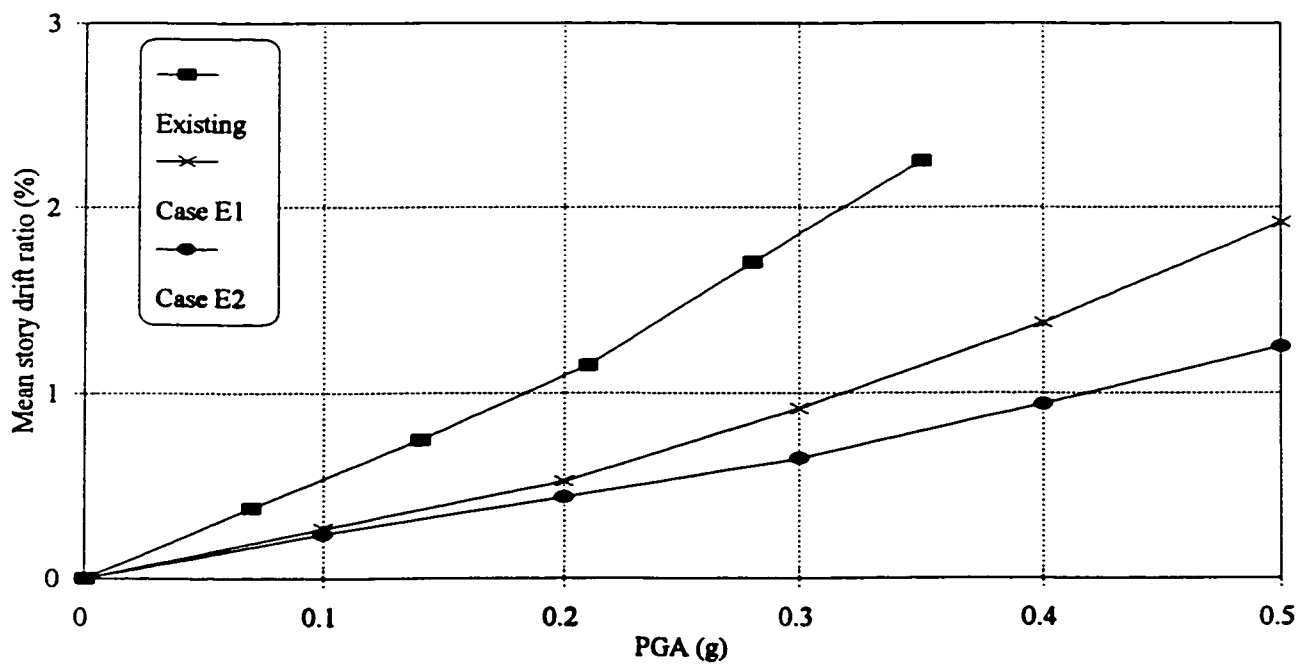
Figure 6.24 The relationship between the PGA and the mean of the story drift
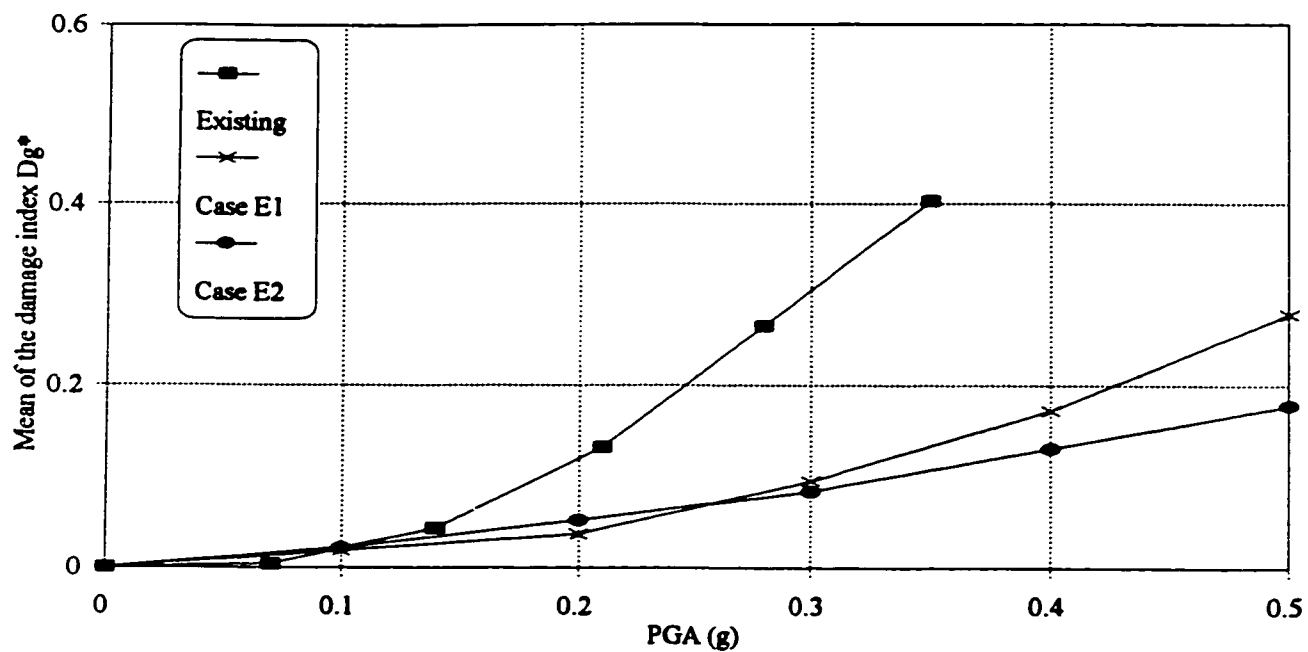
Figure 6.25 The relationship between the PGA and the mean of the damage index D_g^*
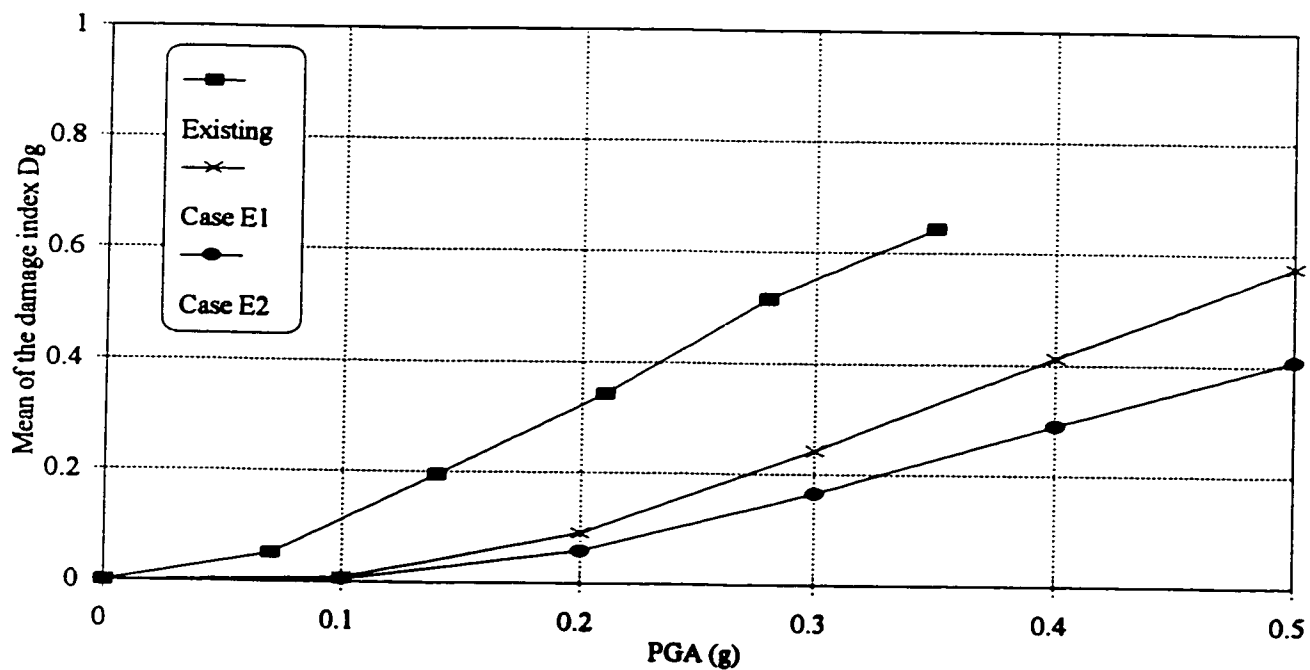
Figure 6.26 The relationship between the PGA and the mean of the damage index D_g

o   Yielding of top beam reinforcement   ⊖   Pullout of beam bottom reinforcement
–   Column reinforcement yielding   (or beam yielding in positive moment)
☐   Shear link yielding   ▪   Column splice failure
▲   Brace buckling

(a) Rehabilitation case E_1, PGA=0.475 g

(b) Rehabilitation case E_2, PGA=0.72 g

Figure 6.27 Hinge type and location of the rehabilitation cases E_1 and E_2 due to the application of El Centro earthquake

CHAPTER 7

SEISMIC PERFORMANCE OF THE REHABILITATED

NINE-STORY BUILDING

7.1 INTRODUCTION

The seismic performance of the nonductile nine-story building presented in Chapter 4 was determined when rehabilitated using concentric steel X-bracing inserted in the frame openings and steel frames attached to the building exterior frames. The steel beams and columns were represented using the steel beam-column element of the DRAIN-2DX computer program. Seismic damage to the rehabilitated nonductile nine-story building was evaluated in terms of roof drift, story drift and damage indices that measure the deterioration of the building stiffness and load carrying capacity.

The seismic performance of rehabilitated nine-story building was determined using the selected twelve ground motion records presented in Chapter 4. The effects of the characteristics of both the ground motions and the steel systems on the seismic performance of the rehabilitated building were evaluated. The rehabilitation cases considered for the nonductile nine-story building included, the addition of steel bracing into the RC frame openings and the attachment of a moment resisting steel frame and a braced steel frame to the RC building exterior frames. The impact of the steel systems on the levels of axial and shear forces developed in the rehabilitated building columns is evaluated. The simplified approach presented in Chapter 2 was applied for predicting the seismic response of the rehabilitated

building. The accuracy of the simplified approach in calculating the seismic performance parameters of the rehabilitated nine-story building was evaluated.

7.2 CONCENTRIC X-BRACE REHABILITATION

The performance of the concentric bracing rehabilitation was investigated in this section. The steel bracing was provided to one bay only of the building exterior frames. The brace members were selected as round hollow sections (HSS 114 x 8) and were distributed uniformly along the frame height. Two brace configurations were considered as shown in figure 7.1. The brace properties of configuration I are similar to the brace properties presented in section 5.5, while the brace properties of configuration II are similar to the brace properties presented in section 6.6.

The lateral load-roof drift relationships of the existing and the rehabilitated nine-story building were determined using a pushover analysis. The pushover analysis was performed using the lateral load distribution specified by the National Building Code of Canada (NBCC, 1995). The pushover results are shown in figure 7.2. Brace configuration I provided more strength and stiffness to the rehabilitated nine-story building than those provided by brace configuration II. However, brace configuration II is more economical in terms of the amount of steel required for rehabilitation.

In the rest of this chapter, the concentric bracing rehabilitation is represented only by brace configuration I. The parameter b for this rehabilitation case is approximately equal to 1.5. This indicates that the load carrying capacity of the rehabilitated building is 1.5 times the load carrying capacity of the existing building.

7.2.1 Free Vibration Characteristics of the Braced Nine-Story Building

The free vibration characteristics of the braced nine-story building is summarized in table 7.1. A reduction of about 26 % in the fundamental period of the nine-story building has occurred as a result of the steel brace rehabilitation. Table 7.2 summarizes the elastic spectral forces for all the earthquake records corresponding to the fundamental period of the existing and the rehabilitated nine-story building. The elastic spectral force can be considered as an approximate relative measure of the intensity of the seismic demands acting on the building. In most of the twelve ground motion records, the steel brace rehabilitation led to an increase in the seismic demand acting on the nonductile nine-story building.

7.2.2 Seismic Performance of the Braced Nine-Story Building

In this section, the seismic response of the braced nine-story building when subjected to the ground motions was determined. Table 7.3 presents the global seismic response parameters (deformations and damage indices) of the rehabilitated building for each of the ground motion records when scaled to different PGA levels. The relationships between the mean of the seismic performance parameters and the PGA level of the ground motion are shown in figures 7.3 to 7.6. The figures represent the variations of the mean roof drift ratio, story drift ratio and the damage indices D_g and D_g^* with the PGA level. The results indicate that the steel brace rehabilitation resulted in an improvement in the building seismic performance parameters. The reductions in the seismic performance parameters reached approximately 28.0%, 23.0%, 34.0% and 16.0% at PGA=0.4 g for the mean roof drift, story drift and the damage indices D_g and D_g^*, respectively.

Figures 7.7 and 7.8 show examples of the distribution of damage due to the inelastic response of the existing and the braced nine-story buildings, respectively. The damage distributions of figures 7.7 and 7.8 was due to the application of the Long Beach ground motion. The numbers in the figures shows the formation sequence of some selected plastic hinges. Numbers in italic font are for the column hinges while numbers in regular font are for the beam hinges. For the case of the existing building (PGA=0.24 g), the inelastic response was dominated by beam hinging either because of pullout of the bottom reinforcement or yielding of the top reinforcement. Beam hinging starts in the bottom stories and then spreads to the other stories with the increase in the intensity of the earthquake. At a late stage of response, some column plastic hinges start to develop at the column top ends. This was followed by hinging of the bottom ends of the first story columns.

For the case of the braced building (PGA=0.23 g), the inelastic response starts in the bottom three stories by beam hinging due to pullout of the bottom beam reinforcement and yielding of the top beam reinforcement. With the increase in the intensity of the earthquake, beam hinging starts to spread to the other stories and column hinging starts to develop in both the top and bottom ends of the columns adjacent to the steel bracing members. At a late stage of response, hinging starts in some of the columns that are not adjacent to the bracing members. Damage to the top three stories was relatively small by comparison to the bottom stories. Brace buckling in compression and yielding in tension were observed in most of the brace members up to the eighth story. The brace members of the ninth story remained in the elastic range. The post buckling behaviour of the steel brace members was taken into account in the brace model.

Table 7.4 shows the distribution of the maximum axial forces in the building columns connected to the steel bracing members before and after rehabilitation in case of the Long Beach earthquake. In the table, the level of the axial force is presented as the ratio between maximum force developed in the member and the axial capacity of the member in compression or tension. The column axial capacity in compression was calculated considering both the steel and the concrete contributions while in tension it was calculated considering only the steel contribution and neglecting the concrete tensile strength. Axial tensile forces were developed in the lower story columns connected to the steel bracing members. The axial forces developed in the other columns of the building are compression and are relatively smaller in magnitude than the axial forces acting on the columns adjacent to the steel bracing members.

The results summarized in table 7.4 indicate that the rehabilitation of the nine-story building using steel bracing inserted in the frame openings caused a significant increase in the axial load levels acting on the building columns. High levels of axial tensile forces were developed in the first story columns adjacent to the bracing members. These high levels of axial forces developed in the building columns represent an undesirable situation especially when these forces approach the axial capacity of the columns in compression or tension. A possible solution for the problem of axial force increase in the building columns is by providing steel members along the columns to increase their axial load resistance or by replacing the steel bracing scheme by an attached steel frames to the building exterior frames.

7.3 REHABILITATION USING ATTACHED STEEL FRAMES

Attached steel frames can be used as a rehabilitation technique for nonductile reinforced concrete buildings. The stiffness and strength characteristics of both the existing RC building and the attached steel frames play an important role in determining the overall performance of the rehabilitated building. The steel frames can be designed as moment resisting frames or braced steel frames. Moment resisting steel frames and braced steel frames have different hysteretic characteristics. Figure 7.9 shows suggested details of a connection between steel frame and an RC frame to transfer the loads between the two systems at the joint locations. In the figure, the steel frame members are welded to a steel plate at the joint location. The steel plate is anchored to the RC members using anchor bolts that bear on a steel plate attached to the other side of the RC member.

To investigate the seismic performance of the existing nine-story building when rehabilitated using flexible moment resisting steel frames versus that when using stiff concentrically braced steel frames, two steel frames were designed to rehabilitate the existing nine-story building. The steel frames are moment resisting frame and a concentrically braced steel frame. The steel frames are assumed to be attached to the building exterior frames. In the following sections, the seismic performance of the rehabilitated nine-story nonductile building was studied using scaled versions of the selected twelve ground motion records listed in table 4.1.

7.4 MOMENT RESISTING STEEL FRAMES

The steel moment resisting frame is advantageous architecturally as it provides

unobstructed space between the columns and it also has enhanced energy dissipation capacity. However, moment resisting frames have low stiffness as compared to braced steel frames. This will affect the distribution of the lateral forces between the original RC building and the steel frames especially in the linear elastic range of response. Two identical moment resisting steel frames were designed to be attached to the two sides of the nonductile nine-story building. The design details and the performance characteristics of these frames is presented in the following subsections.

7.4.1 Design of the steel frames

The moment resisting steel frames were assumed to have three bays and were designed to sustain only the earthquake loading. The frames were designed for nominal base shear coefficient (V/W) equal to 0.05, which is equivalent to 2503.9 kN. This base shear level represents approximately the load carrying capacity of the existing building and it was selected with the intention of doubling the load carrying capacity of the existing structure. The lateral load was distributed to each floor using the formula specified by the National Building Code of Canada (NBCC, 1995). Preliminary moments and axial forces in the beams and columns due to lateral loading were obtained by elastic analysis assuming constant inertia of all the frame members. Then, preliminary beam and column sizes were selected assuming the nominal yield stress of the structural steel is 300 MPa. The analysis was refined until final member sizes were selected. The ductility requirements concerning local stability of the frame members were satisfied in accordance with the CSA-S16.1-94. The final member sizes are shown in figure 7.10.

7.4.2 Characteristics of the Rehabilitated Building

A pushover analysis was conducted in order to compare the initial stiffness and the load carrying capacity of the rehabilitated building using moment resisting steel frames (Case MRF1) with those of the existing building. The lateral load-roof displacement relationships of the existing and the rehabilitated nine-story building are shown in figure 7.11. The results of the pushover analysis indicate that the ratio between the initial stiffness of the rehabilitated building and that of the existing building is equal approximately to 1.25. The ratio between the lateral load carrying capacity of the rehabilitated building and that of the existing building, b, is equal approximately to 2. The free vibration characteristics of the rehabilitated building are summarized in table 7.1. The attached moment resisting steel frames caused a reduction of approximately 12.0% in the fundamental period of the nonductile nine-story building. Table 7.2 summarizes the elastic spectral forces corresponding to the fundamental period of rehabilitated building for all the earthquake records when scaled to PGA=1.0 g. On average, it is observed that attaching the steel frames to the nonductile building caused an increase in the seismic demands, simply represented by the elastic spectral forces of the ground motions.

In the elastic range of response, the contribution of the steel frames in resisting the lateral forces is relatively small. The attached moment resisting frames are expected to resist only 20.0% from the applied lateral load. The small contribution of the moment resisting steel frames in resisting the lateral load in the elastic range of response is attributed to their low elastic stiffness. However, when the rehabilitated building enters the inelastic range of deformation, the contribution of the steel moment resisting frames in resisting the lateral loads is expected to increase.

7.4.3 Seismic performance

An inelastic dynamic analysis was carried out on the rehabilitated nine-story building using the selected twelve ground motion records. The effect of the geometric nonlinearity (P-Δ) was considered in the analysis. The seismic analysis results are presented in table 7.5. The table presents the global seismic response parameters (deformations and damage indices) for each of the ground motion records when scaled to different PGA levels. The PGA scale factors of each of the ground motion records were selected to produce various levels of the building response, including severe inelastic deformation.

Table 7.6 summarizes the maximum deformation demands in the steel frame members due to the application of the various earthquakes. The deformation demands were presented as the ratio between the maximum rotation and the yield rotation. The maximum deformation demands was 0.014 rad. (μ_a= 3.8) and occurred due to the effect of El Centro ground motion. For steel members, this rotation demands are not significant. The low level of inelastic deformation demands is due to the high flexibility of the moment resisting steel frame.

The relationships between the PGA level and the mean of the building seismic performance parameters due to the application of the twelve ground motion records are presented in figures 7.12 to 7.15. These figures show the relationships between the PGA level and the mean of the roof drift ratio, story drift ratio, strength based damage index D_s^* and the stiffness based damage index D_ρ respectively. The seismic analysis results of the rehabilitated nine-story building indicate that the attached moment resisting steel frames caused an improvement in the building seismic performance parameters. At PGA=0.4 g, the reductions in the seismic performance parameters reached approximately 18.0%, 23.0%,

21.0% and 14.0% for the mean roof drift ratio, story drift ratio and the damage indices D_g^* and D_p respectively.

Figures 7.16 and 7.17 show examples of the distribution of damage due to the inelastic response of the rehabilitation case MRF1. The damage distribution of figures 7.16 and 7.17 is due to the application of the Long Beach ground motion (PGA=0.24 g) and the Mexico ground motion (PGA=0.5 g), respectively. The damage distribution of the RC frame shown in figures 7.16a and 7.17a is nearly similar to the damage distribution of the existing frame which was discussed in section 7.2.2. The inelastic response was dominated by beam hinging either because of pullout of the bottom reinforcement or yielding of the top reinforcement. With the increase in the intensity of the earthquake, beam hinging was followed by the development of some column plastic hinges. Figures 7.16b and 7.17b show the distribution of damage in the moment resisting steel frame. Plastic hinges developed in both the columns and the beams of the frame. The top three stories experienced relatively small levels of damage by comparison to the bottom stories.

Table 7.7 summarizes the distributions of the story drifts along the building height due to the application of different ground motion records. The results in the table indicate that the third, fourth and fifth stories of the building experienced a higher level of deformation by comparison to the other building stories. This observation is true for most of the selected twelve ground motion records and agrees with the dynamic results of the existing nine-story building which were presented in Chapter 4. The deformation level of the top three stories was relatively small. There was no increase in the level of column axial forces of the rehabilitated building by comparison to the case of the existing building. The maximum

developed axial force in the concrete columns of the rehabilitation case MRF1 as a ratio of the column axial capacity in compression is 0.16. This represents a major advantage of the attached steel frame rehabilitation by comparison with the steel bracing system.

7.5 BRACED STEEL FRAMES

The lateral forces in concentrically braced steel frames are resisted by axial forces in the bracing members. The high elastic stiffness of the braced steel frame makes it an efficient system in resisting the lateral forces acting on the rehabilitated building in the elastic range of response. However, the inelastic cyclic performance of such systems has shown that repeated buckling of the brace members causes a reduction in the brace resistance, leading to a significant decrease in the capability of the concentrically braced frames to dissipate energy.

Two identical braced steel frames were designed to be attached to the two sides of the nonductile nine-story building. The design details and the performance characteristics of these frames are presented in the following subsections.

7.5.1 Design of the Braced Steel Frames

The braced steel frames were assumed to have two bays and were designed to resist only the seismic loading. The steel frames were designed for nominal base shear coefficient (V/W) of 0.05 which is equivalent to 2503.9 kN. The base shear was distributed to each floor using the formula specified by the National Building Code of Canada (NBCC, 1995). The beams were assumed to be pin-connected to the columns. The braced steel frame relies mainly on the axial load resistance of the brace members in resisting the applied lateral loads.

The beam and column member sizes were selected assuming the nominal yield stress of the structural steel is 300 MPa. The brace members were selected as hollow sections with nominal yield stress of 350 MPa. In selecting these members, the ductility requirements concerning local stability of the frame members were satisfied in accordance with the CSA-S16.1-94. The frame columns and beams were designed to remain elastic during response of the frame under the effect of lateral loading. The inelastic behaviour of the steel frame results from diagonal brace buckling in compression and yielding in tension. The final member sizes are shown in figure 7.18.

7.5.2 Characteristics of the Rehabilitated Building

Figure 7.19 shows the lateral load-roof displacement relationships of the existing and the rehabilitated nine-story building using attached braced steel frames (Case BF1). From the results of a pushover analysis, the ratio between the initial stiffness of the rehabilitated building BF1 and that of the existing RC building is equal approximately to 2.2. The ratio between the lateral load carrying capacity of the rehabilitated building and that of the existing building, b, is equal approximately to 2.0. The free vibration characteristics of the rehabilitated building are summarized in table 7.1. The braced steel frames caused a reduction of approximately 34.0% in the fundamental period of the original nine-story building. From table 7.2 which summarizes the elastic spectral forces corresponding to the fundamental period of rehabilitated building, it is observed that on average, using stiff braced frames in rehabilitating the nonductile building will cause a significant increase in the seismic demands, simply represented by the elastic spectral forces. In the elastic range of response, the

contribution of the attached braced steel frames in resisting the lateral forces is significant. The attached braced steel frames are expected to resist approximately 54.0% of the applied lateral load.

7.5.3 Seismic performance

An inelastic dynamic analysis was carried out on the rehabilitated nine-story building (BF1) using the selected twelve ground motion records. The rehabilitated building response to the ground motions is presented in table 7.8. The table shows the global seismic response parameters (deformations and damage indices) for each of the ground motion records when scaled to different PGA levels. The relationships between the PGA level and the mean of the building seismic performance parameters due to the application of the twelve ground motion records are shown in figures 7.20 to 7.23. These figures represent the relationships between the PGA level and the mean of the roof drift, story drift, strength based damage index D_s^* and the stiffness based damage index D_p respectively. The figures indicate that rehabilitation of the nine-story building using braced steel frames caused a significant improvement in the building seismic performance parameters. At PGA=0.4 g, the reductions in the seismic performance parameters reached approximately 34.0%, 32.0%, 52.0% and 29.0% for the mean roof drift ratio, story drift ratio and the damage indices D_s^* and D_p respectively.

Figures 7.24 and 7.25 show examples of the distribution of damage due to the inelastic response of the rehabilitation case BF1. The damage distribution of figures 7.24 and 7.25 is due to the application of the Long Beach ground motion (PGA=0.2g) and the Mexico ground motion (PGA=0.55 g), respectively. Figures 7.24a and 7.25a show the damage distribution

to the RC frame. Damage to the RC frame of the rehabilitation case BF1 was characterized by the development of large number of beam hinges caused by the pullout of the bottom beam reinforcement and yielding of the top beam reinforcement. This was accompanied by the development of small number of column plastic hinges. Damage to the top three stories was relatively small by comparison to the other building stories. Figures 7.24b and 7.25b show the distribution of damage in the steel frame. Brace buckling in compression and yielding in tension were observed in most of the brace members up to the eighth story. The brace members of the ninth story remained in the elastic range.

Table 7.9 summarizes the distributions of the story drifts along the rehabilitated building height due to the application of different ground motion records. The results in the table indicate that the second, third and fourth stories of the rehabilitated building experienced higher levels of deformation by comparison to the other building stories. This was observed for most of the selected twelve ground motion records. The deformation levels of the top three stories were relatively small. There was no increase in the levels of column axial forces of the rehabilitation case BF1 by comparison to those of the existing building. The maximum developed axial force in the concrete columns of the rehabilitation case BF1 as a ratio of the column axial capacity in compression is 0.16.

7.6 COMPARING OF THE REHABILITATION CASES

In the case of medium-rise buildings, the system of steel bracing inserted in the frame openings caused high levels of axial forces in the building columns. By comparison, a major advantage of the attached steel frame rehabilitation systems is in avoiding the significant

changes in the levels of column axial forces. The rehabilitation cases with attached steel frames have column axial force levels close to the levels of the existing building.

In all the rehabilitation cases of the nine-story building, the shear forces developed in the frame members were below the shear capacities of these members. The maximum shear forces developed in the frame members due to the application of Mexico earthquake are presented in tables 7.10. The shear capacities of the concrete columns and beams were calculated using the equations presented in Chapter 5 and were found much higher than the shear demands imposed by the earthquake loading. The shear demands developed in the RC members were calculated on the basis of assumed concentric connections between the steel elements and the RC frame members.

The calculations of the elastic spectral forces of the rehabilitated nine-story building shown in table 7.2 indicate that on average, the rehabilitation case BF1 attracted more seismic forces than the rehabilitation case MRF1. However, the inelastic dynamic results showed that the rehabilitation case BF1 exhibited better performance than the rehabilitation case MRF1. At PGA=0.4 g, the reduction in the roof drift, story drift and damage indices D_g^* and D_g reached approximately 18.0%, 23.0%, 21.0% and 14.0% for the case MRF1 and 34.0%, 32.0%, 52.0% and 29.0% for the case BF1, respectively. The two rehabilitation cases BF1 and MRF1 have approximately equal lateral load carrying capacities. This indicates that rehabilitation of medium rise nonductile buildings using stiff braced steel frames will lead to better performance than when using flexible moment resisting steel frames.

The analysis results presented in sections 7.2, 7.3 and 7.4 as well as those in Chapter 5 indicate that the steel systems are more efficient in rehabilitating low-rise nonductile

buildings than in medium-rise nonductile buildings. This conclusion was reached by comparing the maximum reduction in the response parameters results from the rehabilitation of the nine-story and the three-story buildings with inserted steel bracing in the frame openings. For the three-story building the rehabilitation case R_5 was considered as it has approximately the same value of the parameter b as the nine-story case. For example, the reduction in the story drift reached 37.0 % in case of the three-story building and only 11.0 % in case of the nine story building. Also, the maximum reduction in the response parameters results from the rehabilitation case BF1 of the nine-story building and the rehabilitation case R_1 of the three-story building was compared. The two rehabilitation cases have b equal approximately to 2.0. The reduction in the story drift reached 51.0 % in case of the three-story building and only 32.0 % in case of the nine story building. The differences in the degrees of improvements in the seismic performance parameters of the three- and nine-story buildings due to steel system rehabilitation may be attributed to the differences in the vibrational characteristics of both buildings. The analysis results indicate that bracing the nine-story building will significantly shorten the fundamental period and therefore cause a significant increase in the seismic demands acting on the building.

In case of the braced nine-story building, the level of increase in the column axial forces is much higher than in case of the braced three-story building. The levels of axial forces developed in the braced three-story building were below the allowable axial capacities of the concrete columns. The inserted steel bracing system was only efficient in rehabilitating low-rise nonductile buildings.

7.7 APPLICATION OF THE SIMPLIFIED APPROACH

The simplified seismic performance evaluation approach presented in Chapter 2 was applied for evaluating the seismic response of the rehabilitation case with attached moment resisting steel frame. The hysteretic characteristics of the force-displacement relationships of both the steel frames and the existing reinforced concrete building were considered in modelling the force-displacement relationship of the approximate single degree of freedom model. The analysis results of the approximate SDOF model and the MDOF braced building using the twelve ground motion records were compared and the accuracy of the simplified evaluation approach in predicting the seismic performance of braced nonductile RC buildings was evaluated.

7.7.1 Single Degree of Freedom Model

The properties of the SDOF model for the rehabilitated building were calculated using the approach described in Chapter 2. Two different SDOF systems were used in the simplified analysis. The first SDOF system is for representing the elastic behaviour of the structure and is applicable up to 0.5% roof drift ratio. The second SDOF system is for representing the inelastic behaviour of the structure and is applicable when the roof drift ratio is greater than 0.5%. The damping ratio used in the equivalent SDOF system models was 2.0%. The properties of the elastic SDOF model was calculated as follows:

$\{\Psi_o\}^T = \{ 0.08, 0.19, 0.31, 0.45, 0.57, 0.69, 0.82, 0.93, 1.0 \}$

$\{S\}^T = \{0.02, 0.04, 0.06, 0.08, 0.10, 0.12, 0.13, 0.15, 0.31\}$

$M^* = 3.68 \times (\text{story mass}) = 2,084,607 \text{ kg}$

$L^* = 5.04 \times (\text{story mass}) = 2,857,188 \text{ kg}$

$V^* = 0.76 \text{ V}$ (7.1)

The properties of the inelastic SDOF model was calculated as follows:

$\{\Psi_1\}^T = \{ 0.07, 0.19, 0.33, 0.49, 0.64, 0.77, 0.88, 0.96, 1.0\}$

$\{S\}^T = \{0.02, 0.04, 0.06, 0.08, 0.10, 0.12, 0.13, 0.15, 0.31\}$

$M^* = 4.08 \times (\text{story mass}) = 2,314,339 \text{ kg}$

$L^* = 5.33 \times (\text{story mass}) = 3,022,255 \text{ kg}$

$V^* = 0.79 \text{ V}$ (7.2)

The hysteretic force-displacement relationship of the SDOF model was represented using two spring elements in parallel, one for representing the behaviour of the existing nonductile building and the other representing the behaviour of the attached steel frames. The characteristics of the hysteretic force-displacement relationships of the two springs were selected to produce the same cyclic responses as those of the existing building and the attached steel frames. The applied lateral load distribution is that suggested by the National Building Code of Canada (NBCC, 1995).

7.7.2 Seismic Analysis Results of the Simplified Approach

A comparison between the simplified dynamic analysis predictions and the actual response of the rehabilitation case was presented in figures 7.26 to 7.29. The figures represent the relationships between the four response factors C_1, C_2, C_3 and C_4 and the story drift ratio. The definitions of the four response factors C_1, C_2, C_3 and C_4 are presented in Chapter 4. Figures 7.26 and 7.27 compare the predictions of the roof drift and the story drift,

while figures 7.28 and 7.29 compare the predictions of the damage indices D_s^* and D_t,

respectively. The mean and standard deviation of the four response factors C_1, C_2, C_3 and C_4

are shown on the figures. On average, the results indicate that the simplified approach

overestimated the roof drift ratio of the building and underestimated the story drift ratio and

the damage indices. This trend agrees with the results of the existing nine-story building

which were presented in Chapter 4. The standard deviations for the damage indices are much

higher than those of the roof drift and the story drift ratios. This trend was also observed in

the results of the existing building presented in Chapter 4.

7.8 SUMMARY

The seismic performance of the nonductile nine-story building was investigated when

rehabilitated using concentric steel X-bracing inserted in the frame openings and steel frames

attached to the building exterior frames. The attached steel frames were designed to double

the lateral load carrying capacity of the existing building. A major advantage of the attached

steel frame rehabilitation systems by comparison with steel bracing rehabilitation is in avoiding

the significant increase in the levels of axial forces in the building columns.

On average, the rehabilitated nine-story building experienced lower levels of

deformation and damage. There was no significant changes in the level of axial forces in the

building columns as a result of attaching the steel frames to the existing building. The

rehabilitation case with attached braced steel frames attracted more seismic forces than the

rehabilitation case with attached moment resisting steel frames. However, the inelastic

dynamic results indicated that rehabilitating medium-rise nonductile buildings using stiff

braced steel frames will lead to better performance than when using flexible moment resisting steel frames.

The analysis results indicated that the steel systems are more efficient in rehabilitating low-rise nonductile buildings than medium-rise nonductile buildings. The maximum reduction in the response parameters resulted from rehabilitating the three-story building is much higher than in the case of the nine-story building. The analysis results indicated the applicability of the simplified approach for predicting the seismic response of the rehabilitated medium-rise nonductile buildings.

Table 7.1 Free vibration characteristics of the existing and rehabilitated nine-story building

Case	First mode		Second mode	
	T_1 (sec)	Modal mass*	T_2 (sec)	Modal mass*
Existing building	2.26	0.79	0.79	0.11
Braced building	1.68	0.79	0.57	0.12
MRF1	2.00	0.78	0.72	0.11
BF1	1.50	0.77	0.50	0.14

* As a fraction from the total mass

MRF1 is the rehabilitation case with attached moment resisting steel frames

BF1 is the rehabilitation case with attached braced steel frames

Table 7.2 Elastic spectral forces corresponding to the fundamental periods of the existing and rehabilitated nine-story building

Rec. No.	Earthquake (PGA=1.0 g)	Elastic spectral force (V/W)			
		Existing building	Braced building	Using MRF1	Using BF1
1	Parkfield, California	0.21	0.29	0.24	0.33
2	Nahanni, Canada	0.10	0.23	0.10	0.35
3	Imperial Valley, California	0.62	0.67	0.59	0.59
4	Kern County, California	0.40	1.21	0.54	0.89
5	San Fernando, California	0.45	0.56	0.50	1.22
6	San Fernando, California	0.44	0.54	0.35	0.77
7	Monte Negro, Yugoslavia	0.60	0.73	0.65	0.82
8	Long Beach, California	2.31	2.26	2.63	1.76
9	Lower California	0.41	0.66	0.46	0.65
10	San Fernando, California	0.68	1.30	0.87	1.94
11	Near E. Coast of Honshu, Japan	0.27	0.57	0.31	0.62
12	Mexico	1.52	1.91	1.56	2.14

Table 7.3 Global seismic response parameters of the braced nine-story building

Record No.	Earthquake	PGA (g)	Roof drift ratio, %	Story drift ratio, %	D_s^*	D_s
1	Parkfield, California	0.40	0.31	0.64	0.06	0.27
		1.20	0.82	1.63	0.19	0.64
		2.00	1.25	2.41	0.33	0.82
2	Nahanni, Canada	0.60	0.26	0.44	0.00	0.11
		1.80	0.71	1.30	0.16	0.54
		3.00	1.23	2.56	0.42	0.80
3	Imperial Valley, California	0.15	0.23	0.40	0.00	0.10
		0.50	0.69	1.55	0.23	0.66
		0.75	1.45	3.18	0.58	0.77
4	Kern County, California	0.14	0.30	0.41	0.00	0.14
		0.42	0.59	1.17	0.14	0.47
		0.70	1.30	2.50	0.43	0.76
5	San Fernando, California	0.12	0.18	0.28	0.00	0.00
		0.36	0.62	1.02	0.13	0.54
		0.60	1.64	3.49	0.54	0.85
6	San Fernando, California	0.11	0.16	0.27	0.00	0.00
		0.33	0.40	0.69	0.04	0.31
		0.55	1.46	2.89	0.39	0.79
7	Monte Negro, Yugoslavia	0.15	0.31	0.48	0.00	0.17
		0.45	0.96	2.18	0.22	0.70
		0.75	1.50	3.05	0.64	0.77

Table 7.3 (continued) Global seismic response parameters of the braced nine-story building

Record No.	Earthquake	PGA (g)	Roof drift ratio, %	Story drift ratio, %	D_s^*	D_s
8	Long Beach, California	0.05	0.27	0.36	0.01	0.09
		0.14	1.17	2.52	0.27	0.69
		0.23	1.72	3.36	0.50	0.81
9	Lower California	0.20	0.27	0.60	0.03	0.23
		0.60	0.66	1.44	0.20	0.67
		1.00	1.25	2.56	0.51	0.79
10	San Fernando, California	0.10	0.34	0.62	0.05	0.21
		0.30	0.85	1.85	0.19	0.56
		0.50	1.55	2.97	0.43	0.82
11	Near E. Coast of Honshu, Japan	0.20	0.26	0.56	0.04	0.21
		0.60	0.62	1.32	0.17	0.64
		1.00	1.56	3.14	0.61	0.80
12	Mexico	0.10	0.37	0.66	0.05	0.30
		0.30	0.79	1.60	0.20	0.68
		0.50	1.54	3.16	0.57	0.78

Table 7.4 Maximum axial forces developed in the columns connected to the bracing members of the nine-story building due to the Long Beach earthquake (PGA=0.23)

Story	Existing building		Braced building	
	Compression	Tension	Compression	Tension
1	0.22*	-	0.46	1.03
2	0.20	-	0.40	0.83
3	0.17	-	0.34	0.64
4	0.20	-	0.28	0.44
5	0.17	-	0.22	0.33
6	0.13	-	0.16	0.24
7	0.15	-	0.16	0.10
8	0.10	-	0.09	-
9	0.05	-	0.03	-

* As a ratio of the axial capacity of the columns

Table 7.5 Global seismic response parameters of the rehabilitation case MRF1

Record No.	Earthquake	PGA (g)	Roof drift ratio, %	Story drift ratio, %	D_s^*	D_s
1	Parkfield, California	0.45	0.43	0.74	0.04	0.33
		1.35	1.03	1.78	0.25	0.73
		2.25	1.88	2.88	0.59	0.81
2	Nahanni, Canada	0.72	0.31	0.64	0.01	0.14
		2.16	1.28	2.01	0.26	0.73
		3.60	1.54	2.69	0.53	0.85
3	Imperial Valley, California	0.16	0.31	0.52	0.01	0.21
		0.48	0.99	2.00	0.25	0.78
		0.80	1.84	2.82	0.46	0.82
4	Kern County, California	0.16	0.30	0.50	0.01	0.20
		0.48	0.77	1.39	0.29	0.74
		0.80	1.59	2.69	0.59	0.88
5	San Fernando, California	0.13	0.25	0.34	0.01	0.03
		0.39	0.80	1.31	0.19	0.64
		0.65	2.08	3.44	0.51	0.88
6	San Fernando, California	0.13	0.18	0.32	0.00	0.00
		0.39	0.69	1.16	0.17	0.62
		0.65	2.11	3.41	0.54	0.87
7	Monte Negro, Yugoslavia	0.15	0.38	0.58	0.01	0.26
		0.45	1.14	2.06	0.24	0.78
		0.75	1.88	3.17	0.61	0.87

Table 7.5 (cont.) Global seismic response parameters of the rehabilitation case MRF1

Record No.	Earthquake	PGA (g)	Roof drift ratio, %	Story drift ratio, %	D_s^*	D_s
8	Long Beach, California	0.05	0.36	0.52	0.01	0.24
		0.14	1.14	1.99	0.24	0.74
		0.24	2.28	3.95	0.62	0.85
9	Lower California	0.28	0.39	0.72	0.07	0.38
		0.84	1.13	1.87	0.30	0.82
		1.40	2.06	3.37	0.73	0.90
10	San Fernando, California	0.10	0.38	0.59	0.01	0.19
		0.30	0.91	1.61	0.29	0.72
		0.50	1.42	4.41	0.42	0.82
11	Near E. Coast of Honshu, Japan	0.24	0.28	0.61	0.01	0.24
		0.72	0.80	1.85	0.26	0.77
		1.20	1.80	3.16	0.71	0.84
12	Mexico	0.10	0.48	0.69	0.04	0.32
		0.30	1.08	1.65	0.24	0.75
		0.50	1.47	2.81	0.53	0.84

Table 7.6 Performance of the steel members of the rehabilitation case MRF1

Rec. No.	Earthquake	PGA (g)	μ_a
1	Parkfield, California	2.25	2.74
2	Nahanni, Canada	3.60	3.61
3	Imperial Valley, California	0.80	3.81
4	Kern County, California	0.80	3.25
5	San Fernando, California	0.65	3.63
6	San Fernando, California	0.65	2.58
7	Monte Negro, Yugoslavia	0.75	3.28
8	Long Beach, California	0.24	3.56
9	Lower California	1.40	2.63
10	San Fernando, California	0.50	3.59
11	Near E. Coast of Honshu, Japan	1.20	3.31
12	Mexico	0.50	3.21

μ_a = (maximum rotation/yield rotation)

Table 7.7 Story drift distributions of the rehabilitation case MRF1

Record No.	Earthquake	PGA (g)	Story drift ratios								
			1st	2nd	3rd	4th	5th	6th	7th	8th	9th
1	Parkfield, California	0.45	0.45	0.67	0.65	0.73	0.74	0.54	0.50	0.47	0.53
		1.35	1.00	1.49	1.56	1.78	1.62	1.45	1.17	1.21	0.97
		2.25	2.14	2.82	2.88	2.68	2.09	1.78	1.94	1.80	1.23
2	Nahanni, Canada	0.72	0.28	0.39	0.35	0.38	0.37	0.43	0.64	0.56	0.40
		2.16	0.79	1.21	1.38	1.70	1.66	1.71	2.01	1.45	1.21
		3.60	2.07	2.60	2.63	2.69	2.46	2.35	2.15	2.07	1.49
3	Imperial Valley, California	0.16	0.34	0.52	0.48	0.47	0.40	0.35	0.44	0.43	0.29
		0.48	0.68	1.14	1.25	1.53	1.62	1.75	2.00	1.33	0.62
		0.80	1.32	2.11	2.49	2.82	2.82	2.31	2.74	1.90	1.02
4	Kern County, California	0.16	0.34	0.48	0.42	0.50	0.50	0.39	0.42	0.47	0.35
		0.48	0.63	1.06	1.25	1.39	1.22	1.05	1.03	1.07	0.63
		0.80	1.36	2.17	2.43	2.69	2.27	2.13	2.29	1.84	0.79
5	San Fernando, California	0.13	0.19	0.29	0.31	0.34	0.30	0.26	0.32	0.30	0.21
		0.39	0.64	1.09	1.22	1.31	1.17	1.23	1.23	0.93	0.43
		0.65	1.13	2.04	2.74	3.44	3.41	2.80	3.10	1.90	0.78
6	San Fernando, California	0.13	0.18	0.25	0.23	0.26	0.27	0.25	0.32	0.28	0.22
		0.39	0.61	1.03	1.10	1.16	0.98	0.75	0.75	0.60	0.49
		0.65	1.76	2.78	3.31	3.41	2.83	2.15	1.66	1.15	0.68
7	Monte Negro, Yugoslavia	0.15	0.35	0.54	0.52	0.58	0.52	0.42	0.46	0.40	0.27
		0.45	0.90	1.70	1.94	2.06	1.75	1.22	1.27	1.22	0.60
		0.75	1.96	2.89	3.15	3.17	2.87	2.08	1.95	1.71	1.08

Table 7.7 (cont.) Story drift distributions of the rehabilitation case MRF1

Record No.	Earthquake	PGA (g)	Story drift ratios								
			1st	2nd	3rd	4th	5th	6th	7th	8th	9th
8	Long Beach, California	0.05	0.31	0.48	0.49	0.52	0.44	0.36	0.38	0.29	0.17
		0.14	0.73	1.43	1.79	1.99	1.74	1.28	0.96	0.49	0.27
		0.24	1.23	2.45	3.25	3.92	3.95	3.27	2.38	0.72	0.36
9	Lower California	0.28	0.46	0.72	0.68	0.67	0.52	0.51	0.71	0.66	0.34
		0.84	0.74	1.35	1.63	1.85	1.87	1.71	1.74	1.33	0.69
		1.40	2.01	2.64	2.99	3.37	3.21	2.83	2.32	1.95	1.43
10	San Fernando, California	0.10	0.27	0.44	0.49	0.59	0.54	0.44	0.43	0.28	0.18
		0.30	0.50	0.92	1.18	1.59	1.61	1.35	1.17	0.79	0.41
		0.50	0.94	1.50	1.59	1.78	2.28	3.04	4.41	1.95	0.59
11	Near E. Coast of Honshu, Japan	0.24	0.37	0.49	0.44	0.56	0.54	0.53	0.61	0.58	0.37
		0.72	0.74	1.26	1.24	1.45	1.44	1.41	1.85	1.51	0.95
		1.20	2.35	3.01	3.16	2.86	2.27	2.08	2.49	2.17	1.92
12	Mexico	0.10	0.40	0.63	0.66	0.69	0.59	0.49	0.47	0.38	0.26
		0.30	0.75	1.33	1.44	1.65	1.56	1.40	1.34	0.85	0.47
		0.50	1.74	2.36	2.49	2.81	2.46	2.15	2.18	1.45	0.67

Table 7.8 Global seismic response parameters of the rehabilitation case BF1

Record No.	Earthquake	PGA (g)	Roof drift ratio, %	Story drift ratio, %	D_s^*	D_s
1	Parkfield, California	0.45	0.35	0.68	0.06	0.29
		1.35	0.79	1.63	0.17	0.68
		2.25	1.30	2.66	0.38	0.85
2	Nahanni, Canada	0.70	0.35	0.62	0.04	0.25
		2.10	0.72	1.23	0.16	0.54
		3.50	1.45	2.76	0.47	0.82
3	Imperial Valley, California	0.20	0.29	0.45	0.00	0.11
		0.60	0.92	1.65	0.18	0.69
		1.00	1.86	3.88	0.85	0.85
4	Kern County, California	0.18	0.31	0.49	0.00	0.19
		0.54	0.64	1.33	0.16	0.50
		0.90	1.49	2.97	0.60	0.83
5	San Fernando, California	0.13	0.26	0.39	0.00	0.08
		0.39	0.65	1.05	0.11	0.50
		0.65	1.44	2.95	0.34	0.80
6	San Fernando, California	0.17	0.26	0.41	0.00	0.05
		0.51	0.63	1.19	0.10	0.50
		0.85	2.15	4.38	0.78	0.89
7	Monte Negro, Yugoslavia	0.13	0.26	0.43	0.00	0.06
		0.39	0.79	1.69	0.12	0.63
		0.65	1.22	2.74	0.31	0.78

Table 7.8 (cont.) Global seismic response parameters of the rehabilitation case BF1

Record No.	Earthquake	PGA (g)	Roof drift ratio, %	Story drift ratio, %	D_s^*	D_s
8	Long Beach, California	0.04	0.16	0.20	0.00	0.00
		0.12	0.61	1.10	0.12	0.50
		0.20	1.73	3.51	0.46	0.78
9	Lower California	0.22	0.26	0.58	0.03	0.23
		0.66	0.77	1.59	0.20	0.69
		1.10	1.24	2.81	0.50	0.82
10	San Fernando, California	0.12	0.35	0.59	0.01	0.21
		0.36	0.98	2.06	0.17	0.64
		0.60	1.52	3.11	0.39	0.81
11	Near E. Coast of Honshu, Japan	0.24	0.27	0.67	0.05	0.23
		0.72	0.77	1.54	0.17	0.67
		1.20	1.75	3.54	0.70	0.86
12	Mexico	0.11	0.37	0.74	0.04	0.30
		0.33	0.96	2.01	0.21	0.71
		0.55	1.42	2.97	0.39	0.84

Table 7.9 Story drift distributions of the rehabilitation case BF1

Record No.	Earthquake	PGA (g)	Story drift ratios								
			1st	2nd	3rd	4th	5th	6th	7th	8th	9th
1	Parkfield, California	0.45	0.37	0.60	0.68	0.65	0.40	0.41	0.49	0.38	0.28
		1.35	0.96	1.51	1.62	1.63	0.98	0.78	0.59	0.55	0.34
		2.25	1.38	2.28	2.66	2.42	1.50	1.08	0.82	0.68	0.58
2	Nahanni, Canada	0.70	0.35	0.59	0.62	0.61	0.46	0.43	0.46	0.40	0.30
		2.10	0.64	1.10	1.23	1.06	0.99	1.00	0.95	0.86	0.52
		3.50	2.11	2.75	2.76	2.46	1.68	1.36	1.38	0.89	0.48
3	Imperial Valley, California	0.20	0.29	0.39	0.37	0.40	0.34	0.38	0.45	0.38	0.28
		0.60	0.70	1.28	1.48	1.53	1.65	1.44	1.08	0.61	0.39
		1.00	2.90	3.60	3.88	3.38	2.06	1.09	0.94	0.77	0.45
4	Kern County, California	0.18	0.31	0.49	0.47	0.45	0.39	0.35	0.38	0.34	0.26
		0.54	0.66	1.20	1.33	1.12	0.63	0.49	0.58	0.53	0.35
		0.90	1.92	2.62	2.97	2.82	1.56	0.90	0.89	0.69	0.41
5	San Fernando, California	0.13	0.25	0.35	0.35	0.39	0.35	0.29	0.30	0.25	0.19
		0.39	0.37	0.64	0.81	1.05	0.98	0.88	0.85	0.51	0.31
		0.65	1.20	2.37	2.95	2.72	2.41	1.84	1.27	0.59	0.37
6	San Fernando, California	0.17	0.26	0.35	0.30	0.28	0.33	0.34	0.41	0.32	0.23
		0.51	0.63	1.13	1.19	0.99	0.61	0.51	0.58	0.50	0.32
		0.85	2.62	3.81	4.38	4.14	2.66	1.01	0.77	0.57	0.34
7	Monte Negro, Yugoslavia	0.13	0.28	0.38	0.30	0.33	0.33	0.34	0.43	0.31	0.24
		0.39	0.86	1.59	1.69	1.41	0.93	0.52	0.56	0.43	0.28
		0.65	1.42	2.29	2.74	2.50	1.40	0.93	0.91	0.63	0.40

Table 7.9 (cont.) Story drift distributions of the rehabilitation case BF1

Record No.	Earthquake	PGA (g)	Story drift ratios								
			1st	2nd	3rd	4th	5th	6th	7th	8th	9th
8	Long Beach, California	0.04	0.14	0.20	0.19	0.20	0.18	0.16	0.16	0.13	0.10
		0.12	0.54	0.99	1.10	0.98	0.64	0.43	0.40	0.29	0.23
		0.20	1.78	2.93	3.51	3.48	2.47	0.95	0.53	0.41	0.28
9	Lower California	0.22	0.39	0.58	0.49	0.37	0.37	0.39	0.39	0.29	0.24
		0.66	0.69	1.22	1.46	1.59	1.36	0.77	0.60	0.48	0.32
		1.10	1.77	2.38	2.66	2.81	2.07	1.03	0.74	0.61	0.40
10	San Fernando, California	0.12	0.37	0.59	0.54	0.49	0.52	0.47	0.45	0.35	0.27
		0.36	0.71	1.58	2.06	2.06	1.41	0.66	0.60	0.41	0.28
		0.60	1.06	1.94	2.49	3.11	2.94	1.94	0.80	0.57	0.38
11	Near E. Coast of Honshu, Japan	0.24	0.41	0.67	0.57	0.42	0.42	0.41	0.53	0.46	0.31
		0.72	0.77	1.40	1.50	1.54	1.43	1.04	0.74	0.52	0.32
		1.20	2.45	3.24	3.54	3.10	2.17	1.60	1.19	0.75	0.39
12	Mexico	0.11	0.47	0.74	0.65	0.52	0.44	0.38	0.40	0.31	0.22
		0.33	0.78	1.64	2.01	1.86	1.36	0.85	0.58	0.38	0.26
		0.55	1.25	2.20	2.87	2.97	2.21	0.98	0.58	0.47	0.31

Table 7.10 Maximum shear forces developed in the RC members due to the application of Mexico earthquake

Case	Columns			Beams
	Bottom three stories	Middle three stories	Top three stories	
Existing building	165.60	123.80	94.03	102.20
Braced building	237.20	159.50	65.67	109.90
MRF1	170.40	149.70	92.58	101.90
BF1	177.20	140.00	65.31	110.50
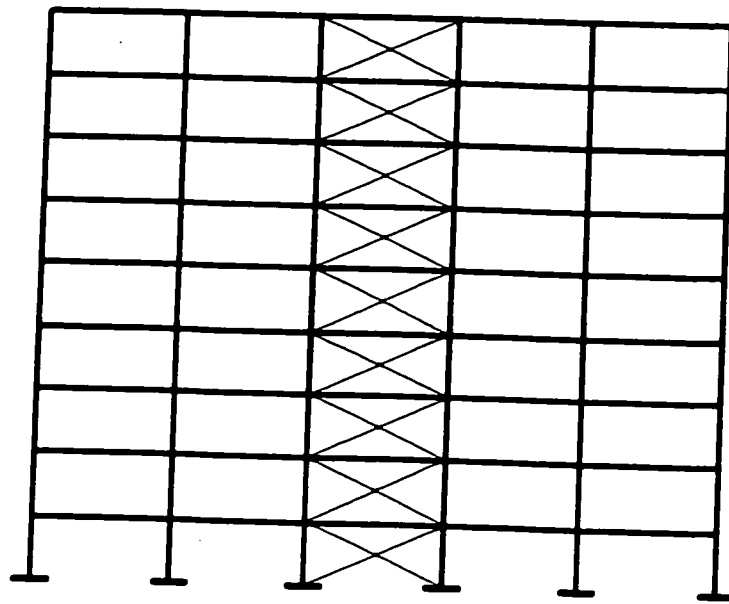
(a) Bracing case I
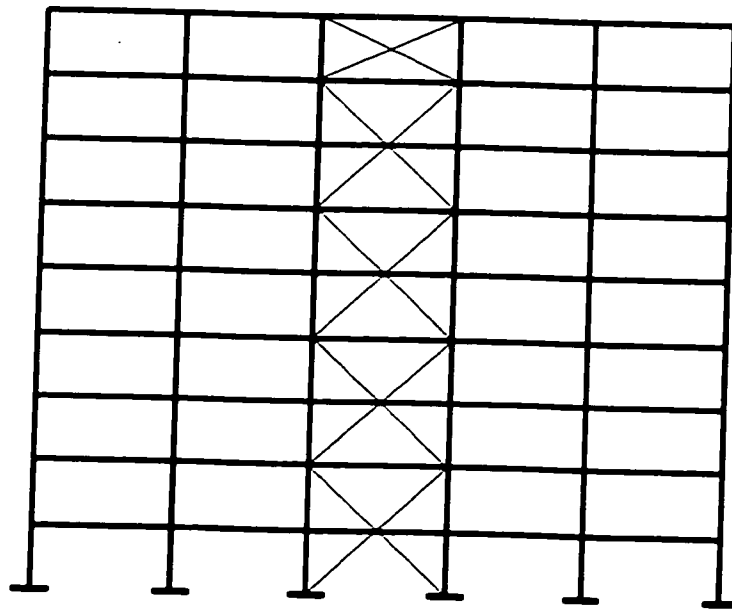
(b) Bracing case II

Figure 7.1 Rehabilitation of the nine-story building using concentric bracing
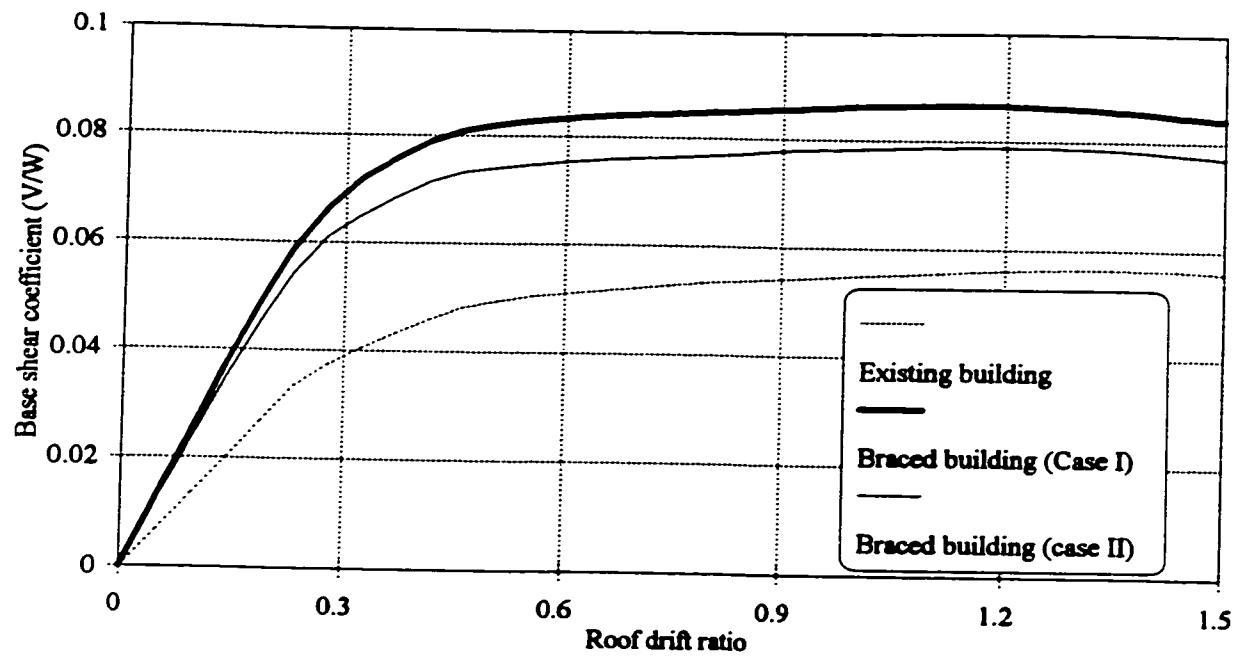
Figure 7.2 Pushover results of the existing and the braced nine-story building
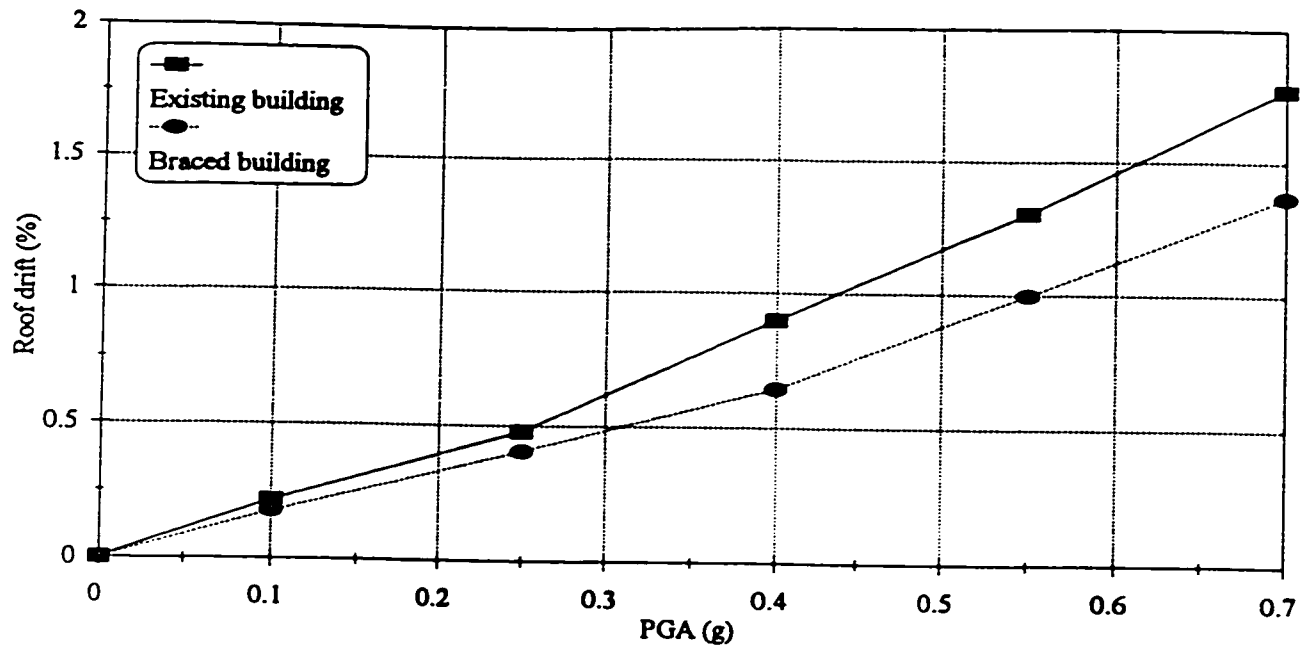
Figure 7.3 variation of the mean roof drift ratio with the PGA level
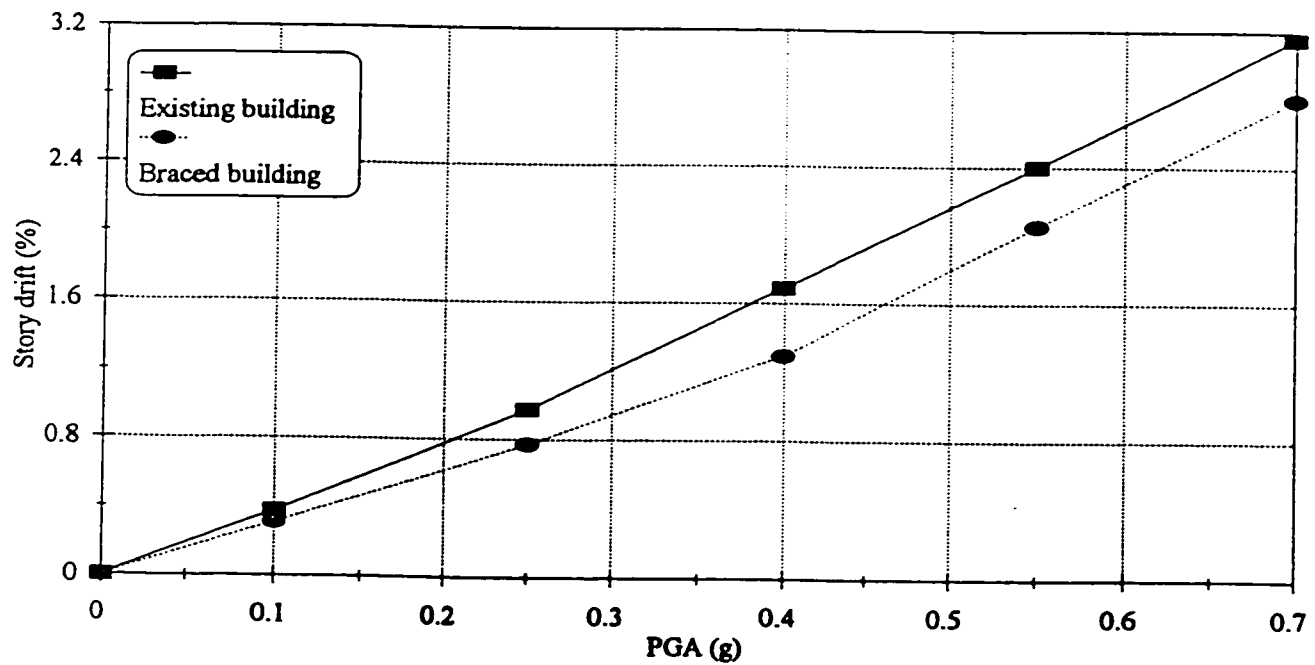
Figure 7.4 variation of the mean story drift ratio with the PGA level
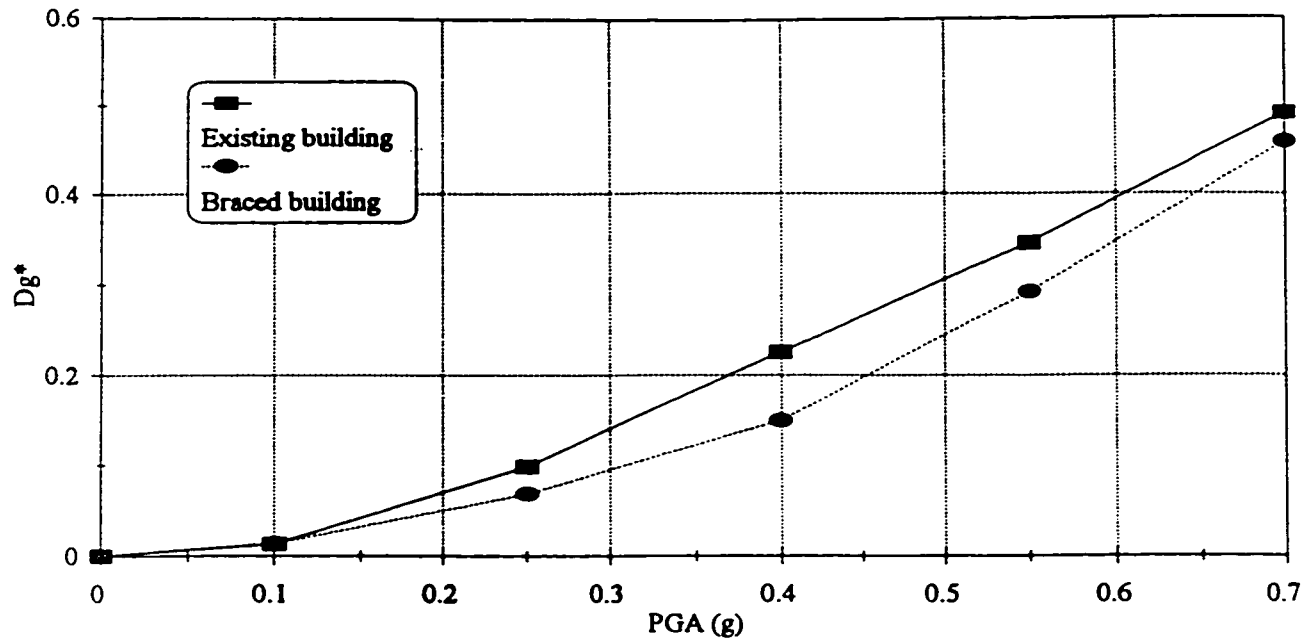
Figure 7.5 variation of the mean damage index D_g^* with the PGA level
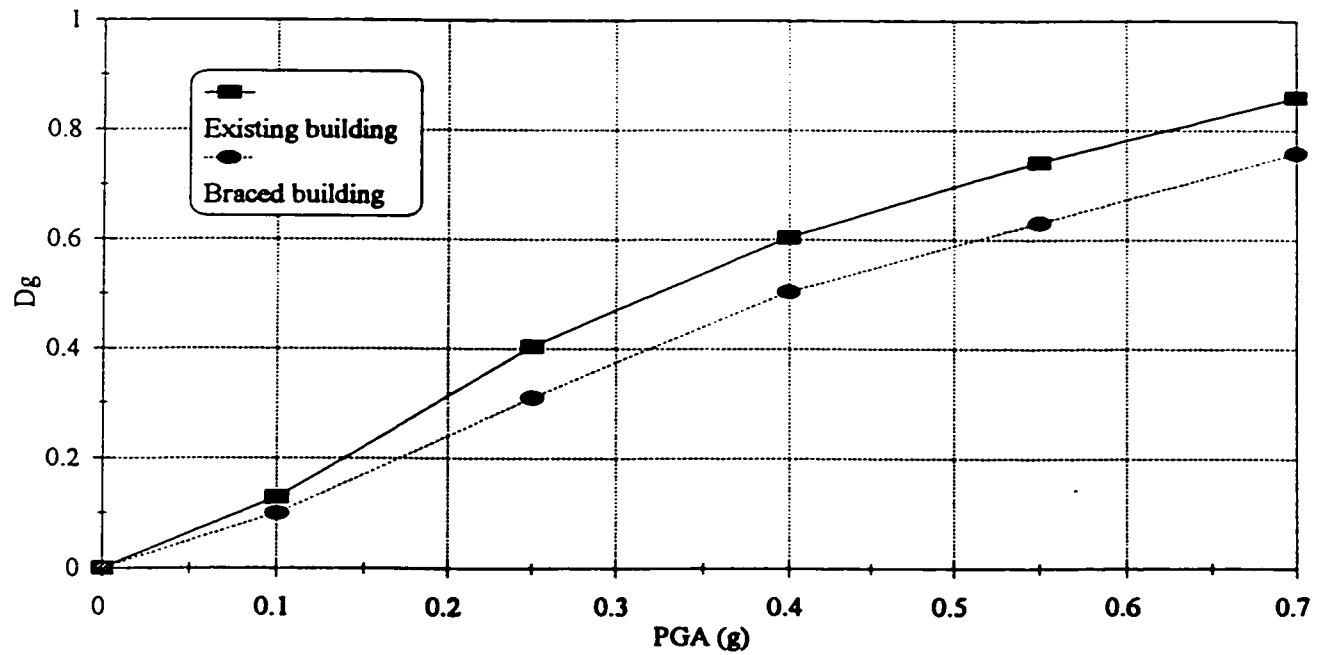
Figure 7.6 variation of the mean damage index D_g with the PGA level

o Pullout of bottom beam reinforcement   θ Yielding of top beam reinforcement

■ Column splice failure   — Column reinforcement yielding

▲ Brace buckling

Figure 7.8 Hinge type and location of the braced 9-story frame due to the Long Beach earthquake (PGA= 0.23g)

Figure 7.7 Hinge type and location of the existing 9-story frame due to the Long Beach earthquake (PGA= 0.24g)
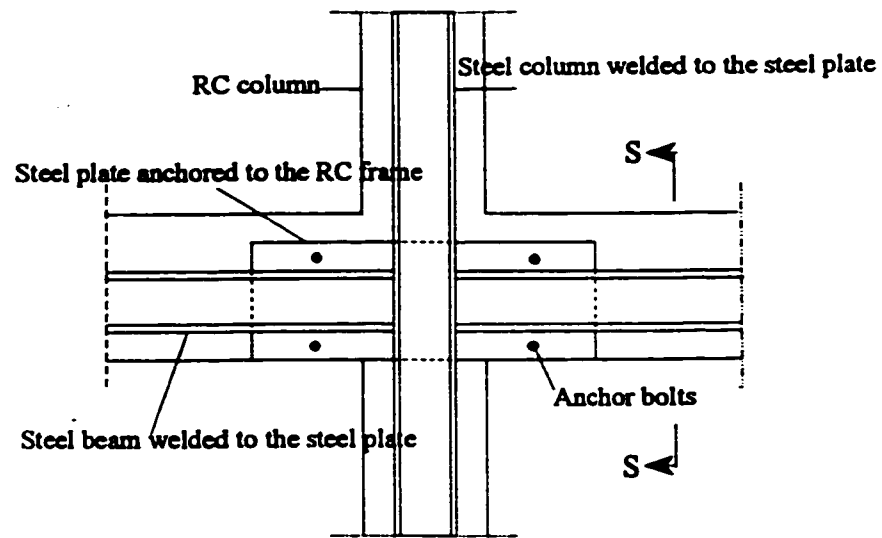
(a) Elevation
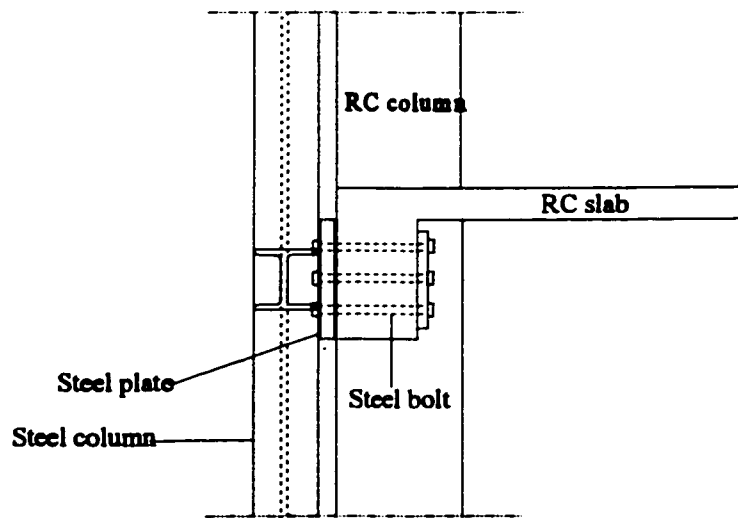
(b) Section S-S

Figure 7.9 Details of a connection between steel frame and RC Frame
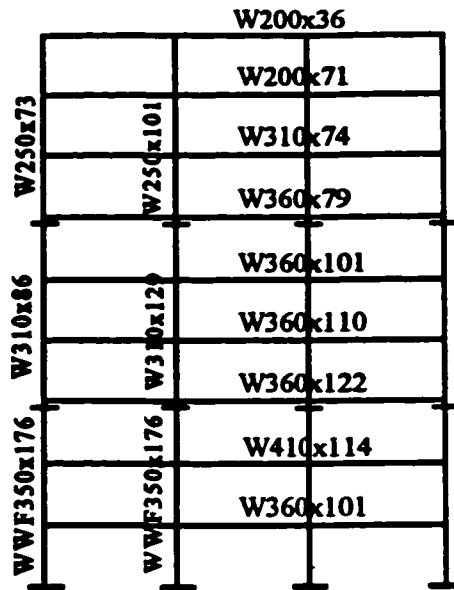
Figure 7.10 Details of the moment resisting steel frame
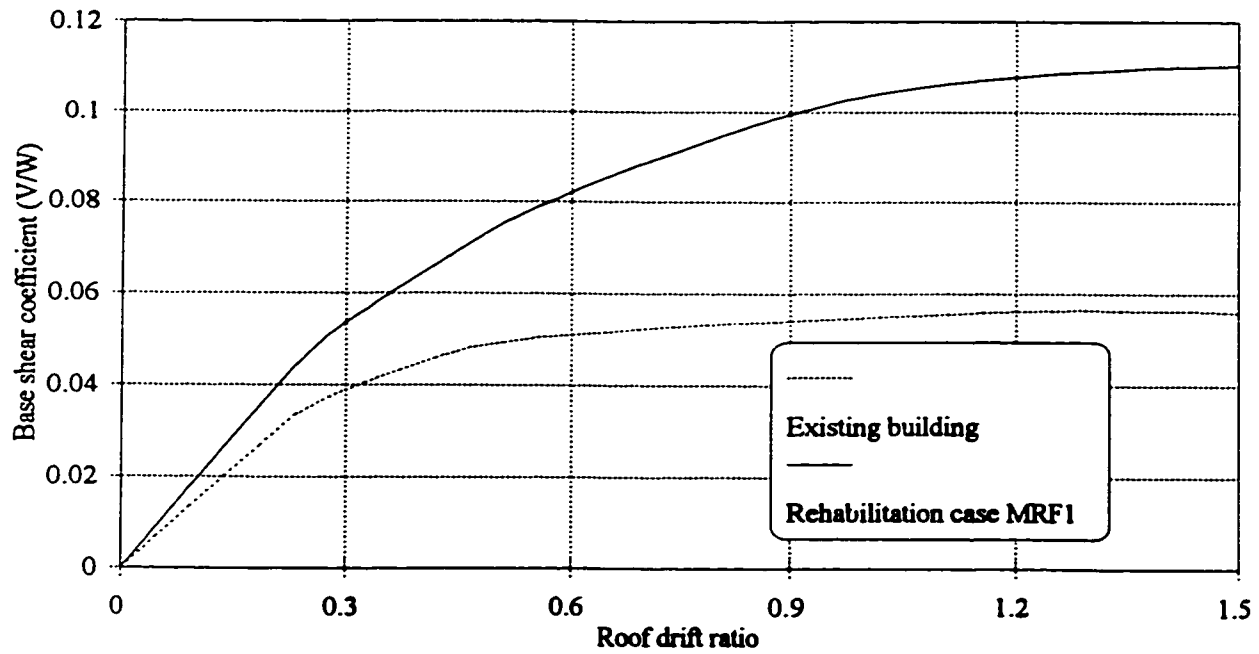
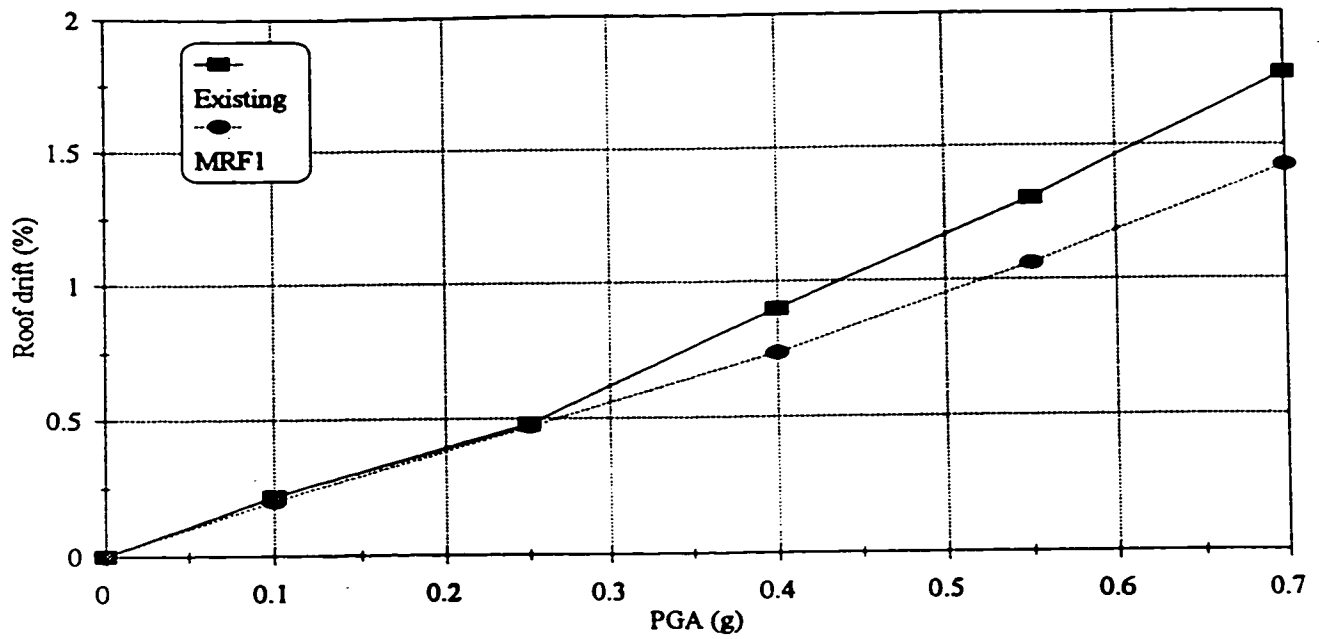Figure 7.11 Pushover results of the existing building and the rehabilitation case MRF1

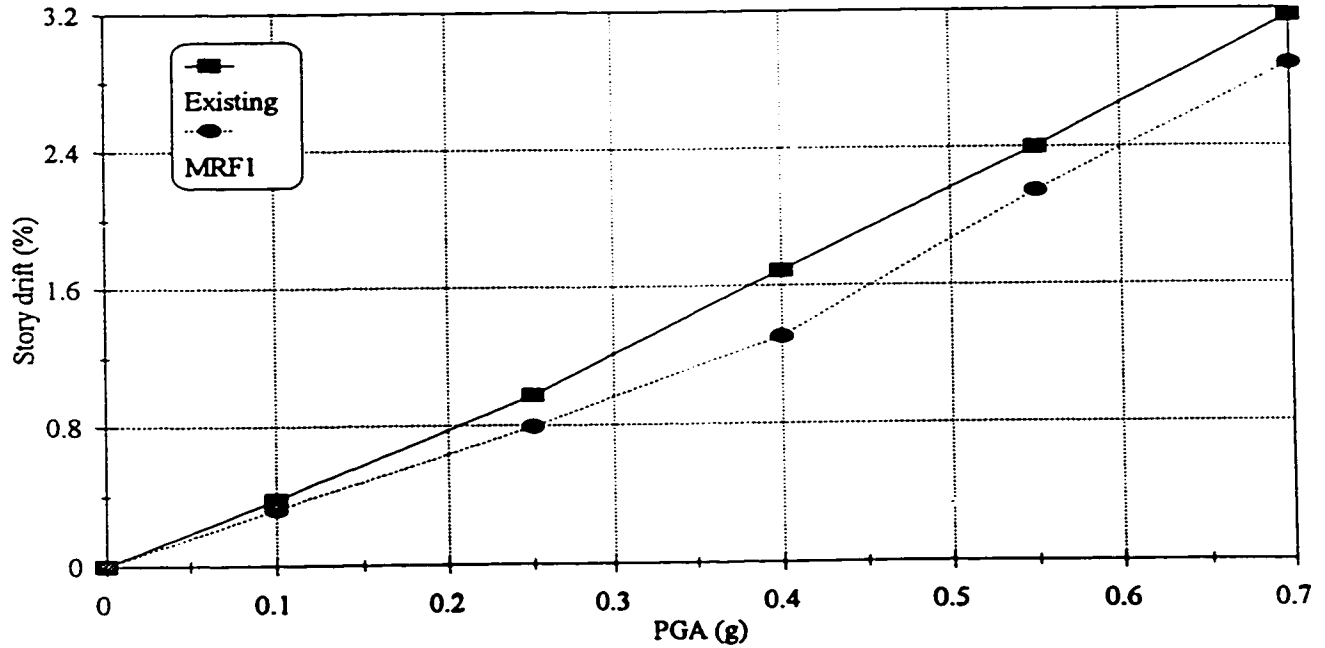Figure 7.12 **Relationship between the PGA level and the mean of the roof drift ratio**

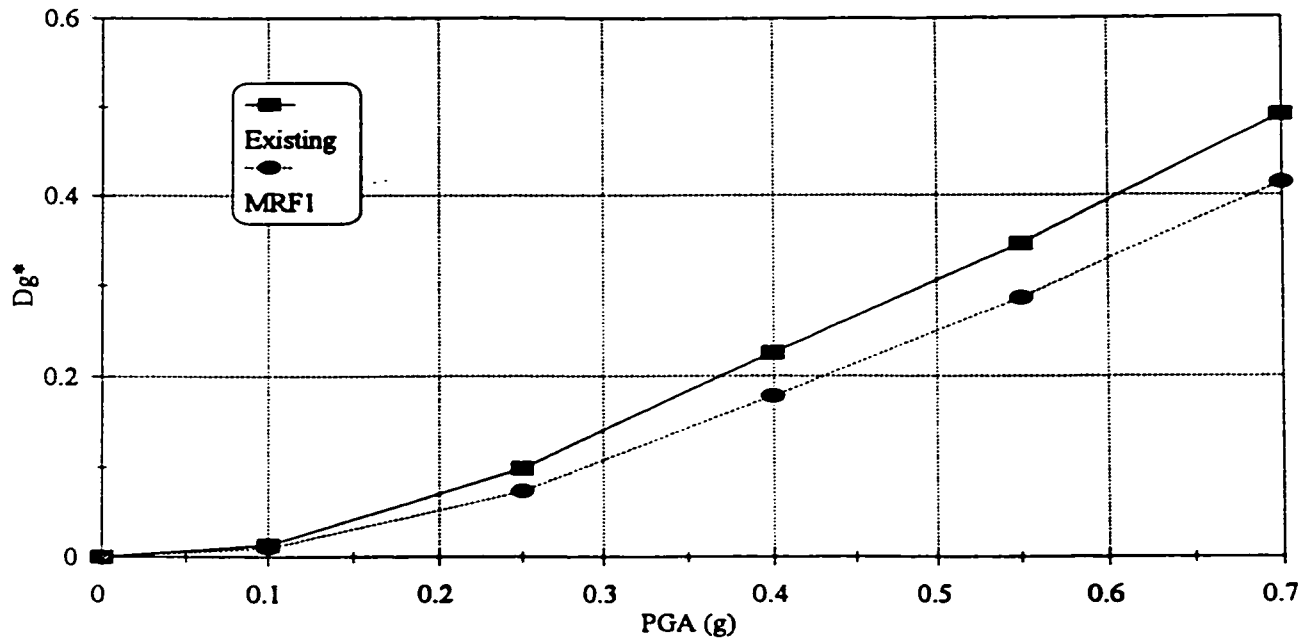Figure 7.13 **Relationship between the PGA level and the mean of the story drift ratio**

Figure 7.14 Relationship between the PGA level and the mean of the damage index D_g^*
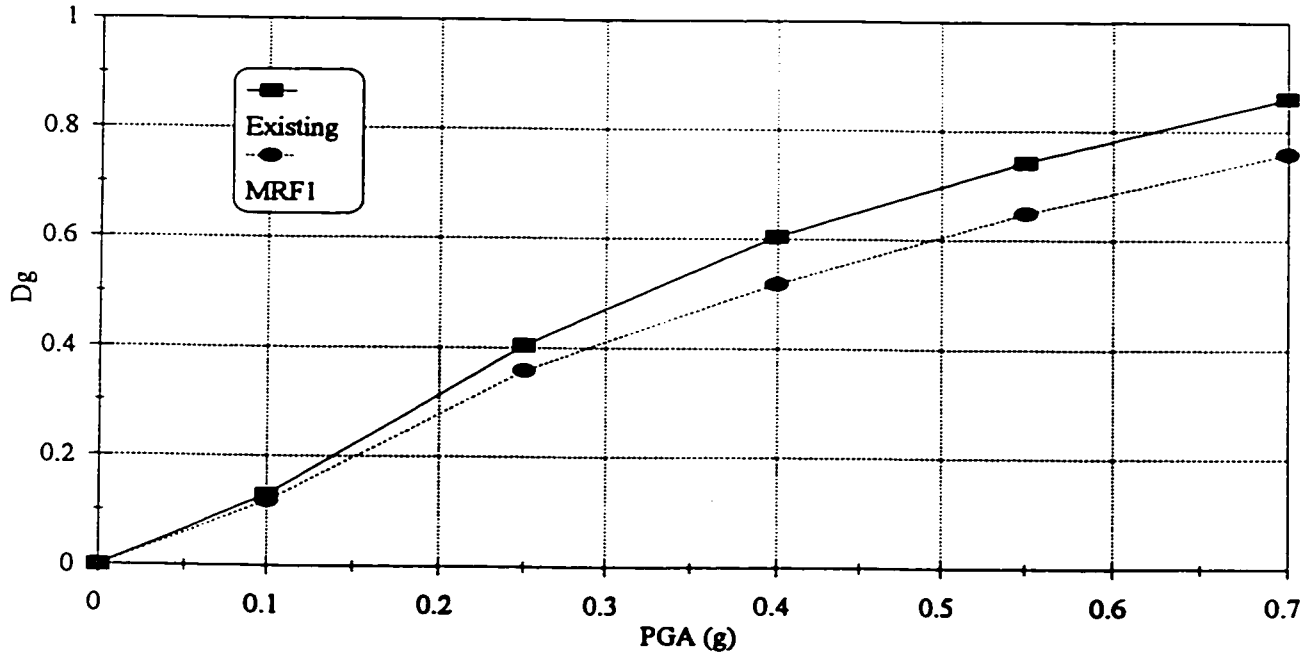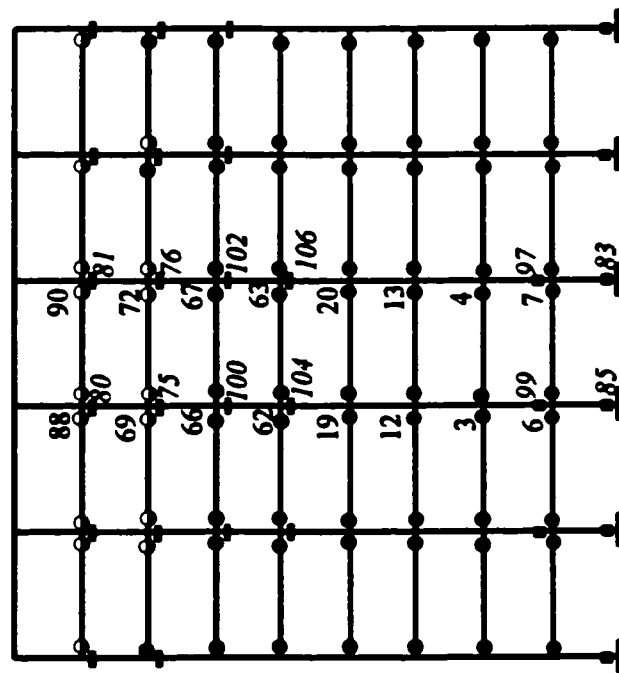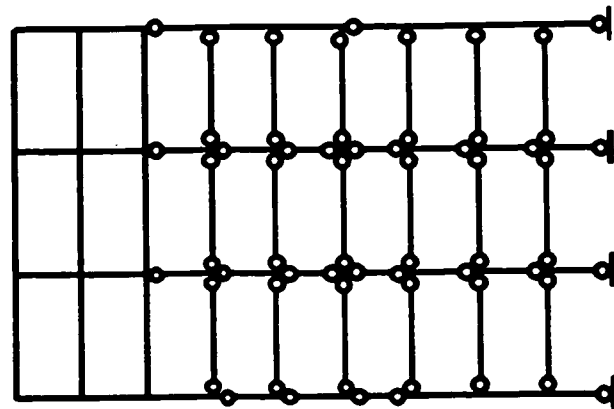

Figure 7.15 Relationship between the PGA level and the mean of the damage index D_g

Pullout of bottom beam reinforcement   •   Yielding of top beam reinforcement

■   Column splice failure   ▬   Column reinforcement yielding

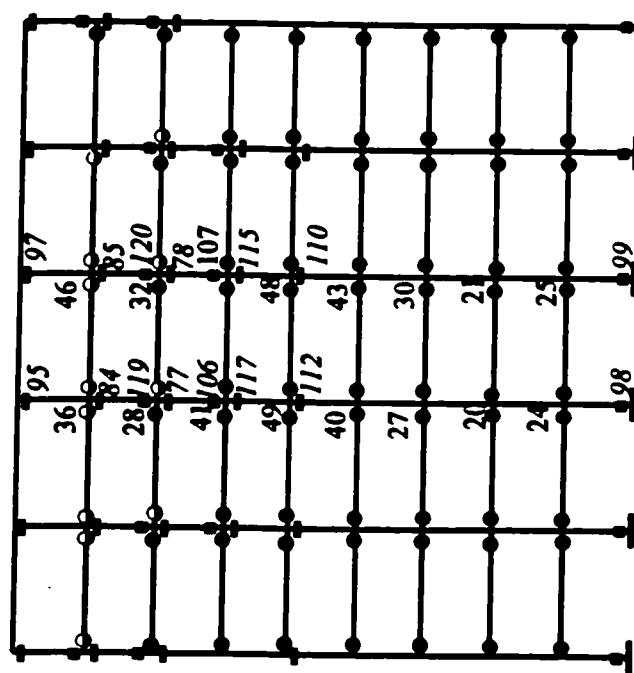▲   Brace buckling   ○   Plastic hinge in a steel member

(a) RC frame   (b) Steel frame

Figure 7.16 Hinge type and location of the rehabilitation case
MRF1 due to the Long Beach earthquake (PGA= 0.24g)

Pullout of bottom beam reinforcement   o

Column splice failure   ■

Brace buckling   ▲

Yielding of top beam reinforcement   o

Column reinforcement yielding   ▬

Plastic hinge in a steel member   o

(a) RC frame
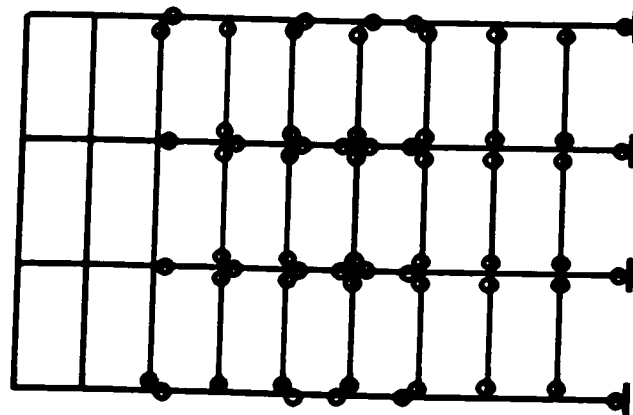
(b) Steel frame

Figure 7.17 Hinge type and location of the rehabilitation case MRF1 due to the Mexico earthquake (PGA= 0.50g)
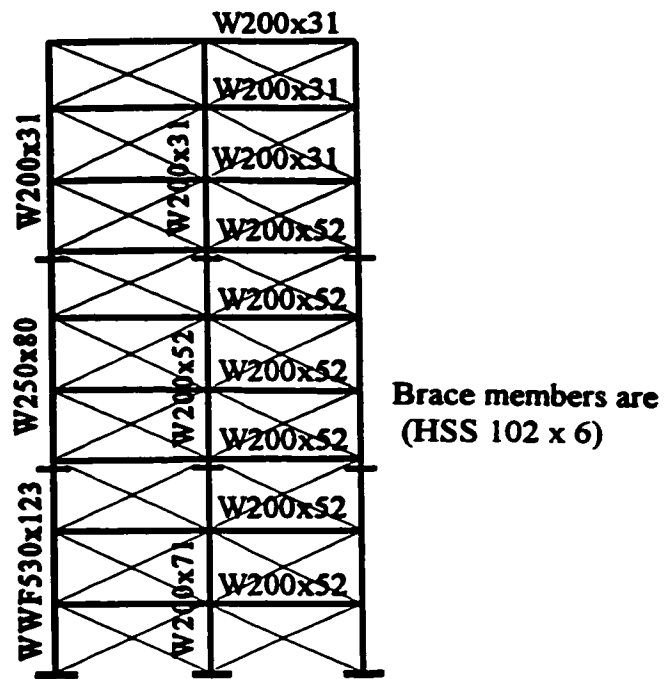
Figure 7.18 Details of the braced steel frame
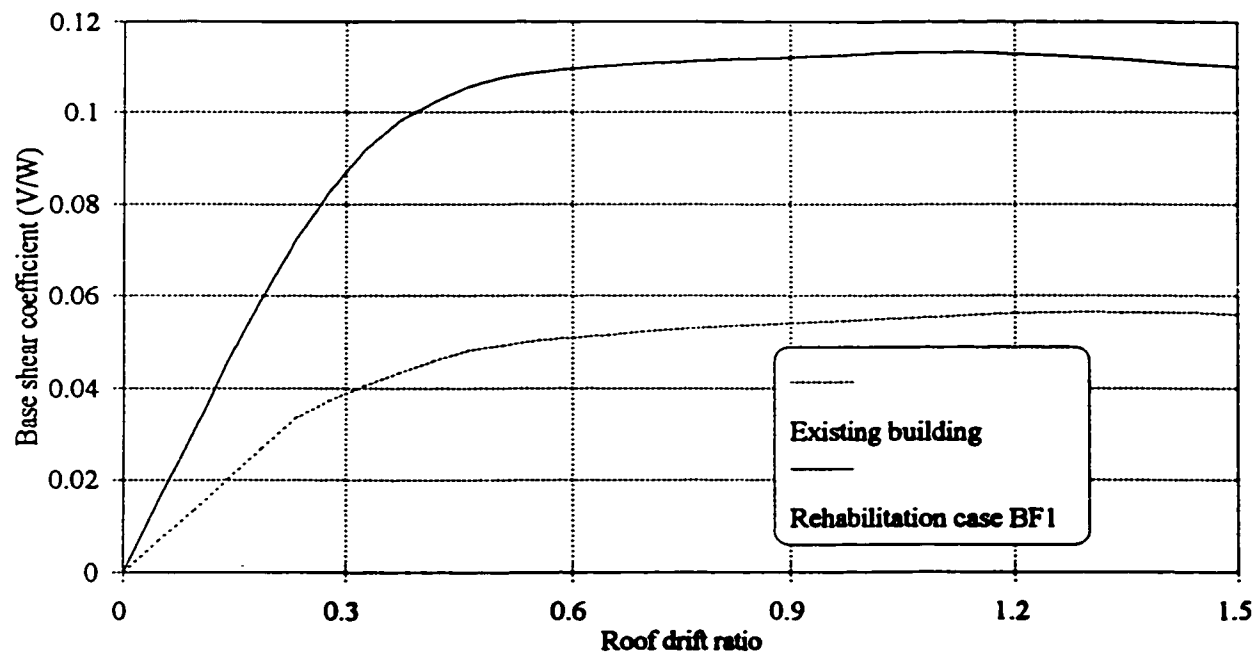
Figure 7.19 Pushover results of the existing building and the rehabilitation case BF1
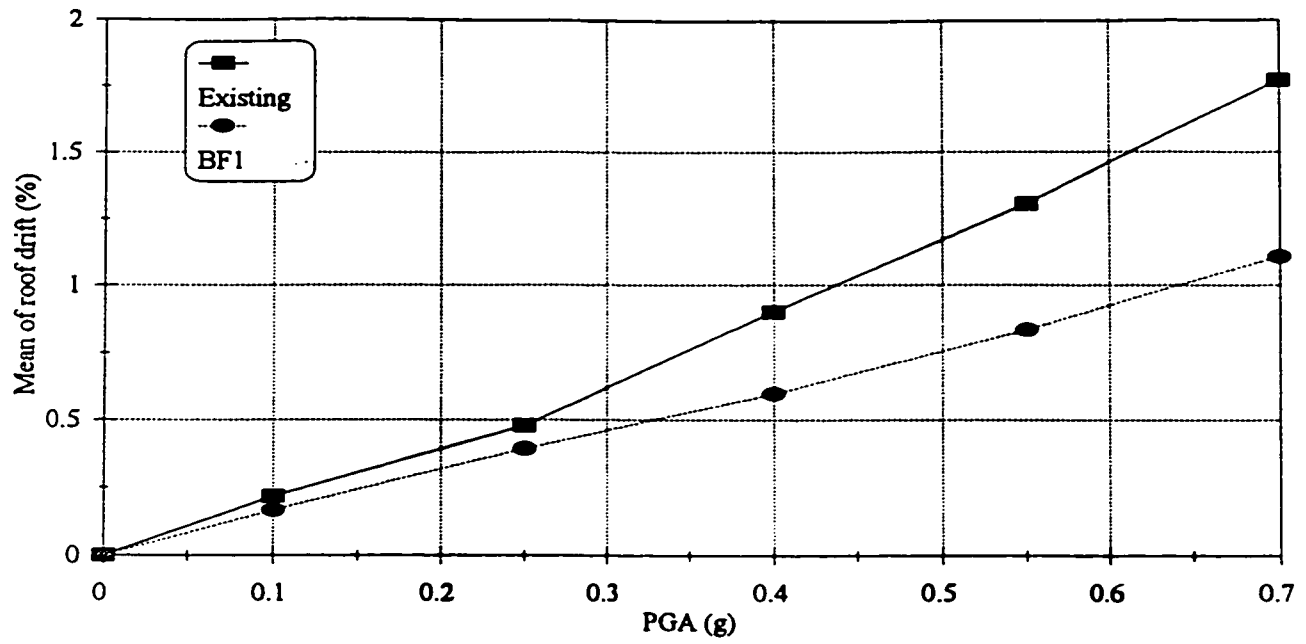
Figure 7.20 **Relationship between the PGA level and the mean of the roof drift ratio**
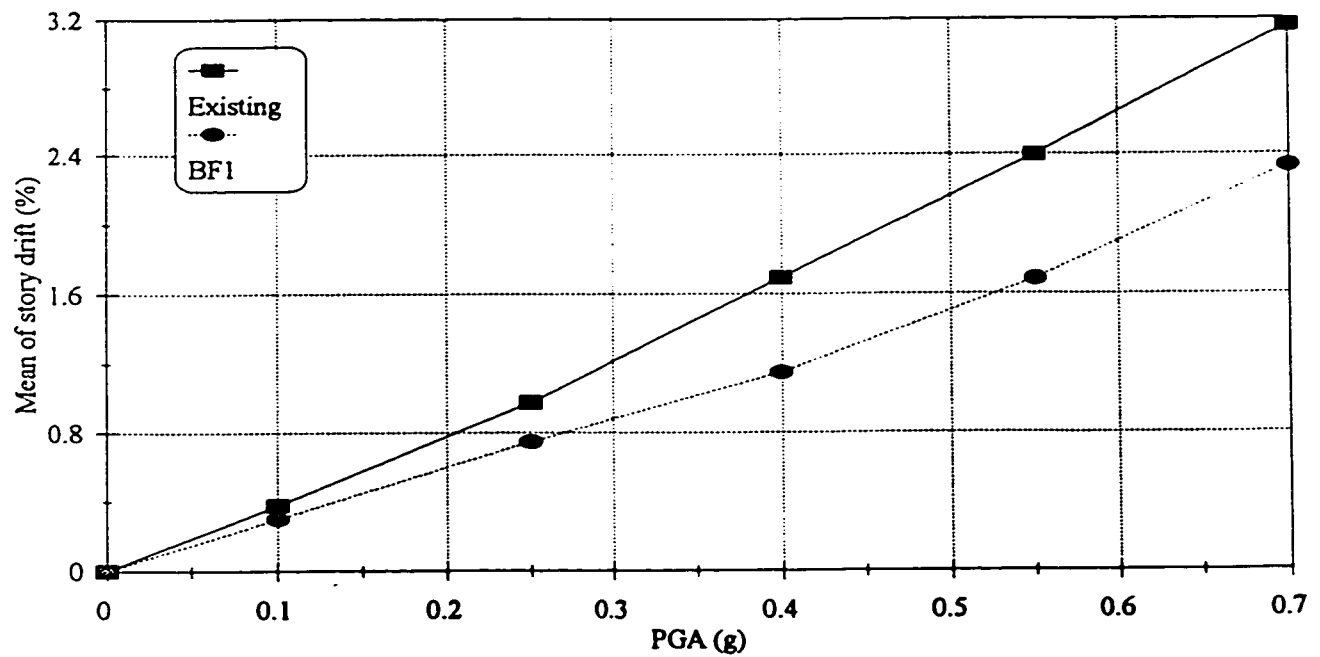
Figure 7.21 **Relationship between the PGA level and the mean of the story drift ratio**
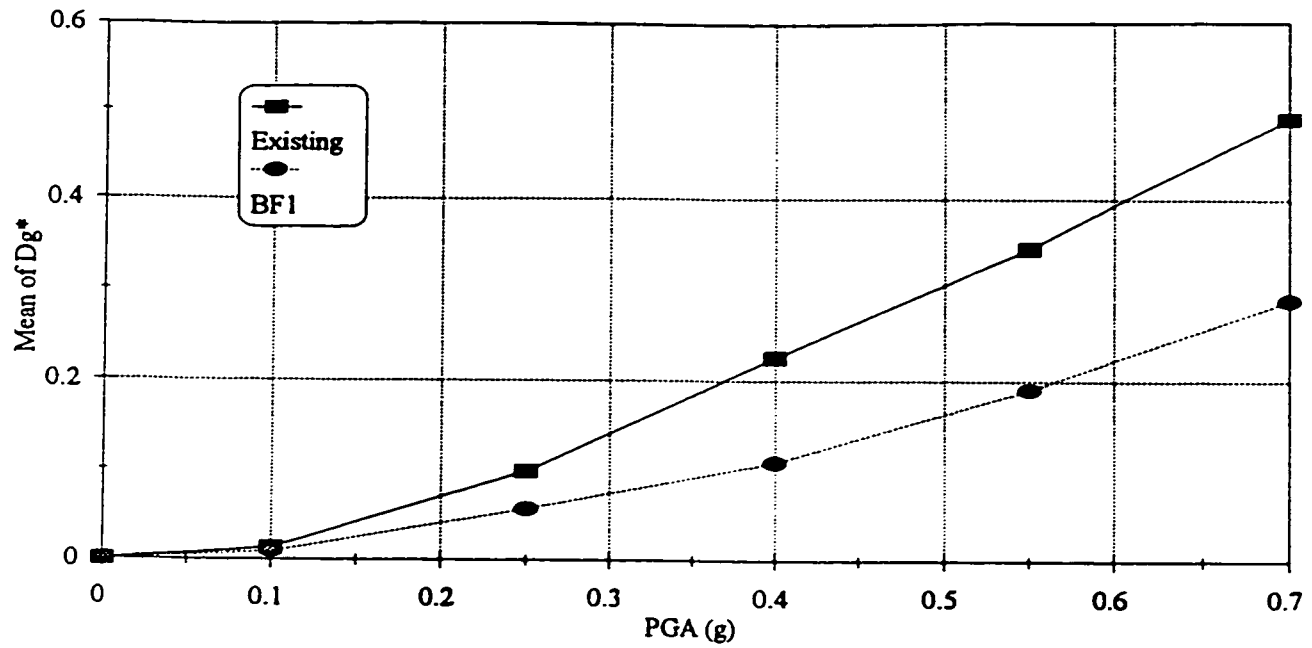
Figure 7.22 Relationship between the PGA level and the mean of the damage index D_g^*
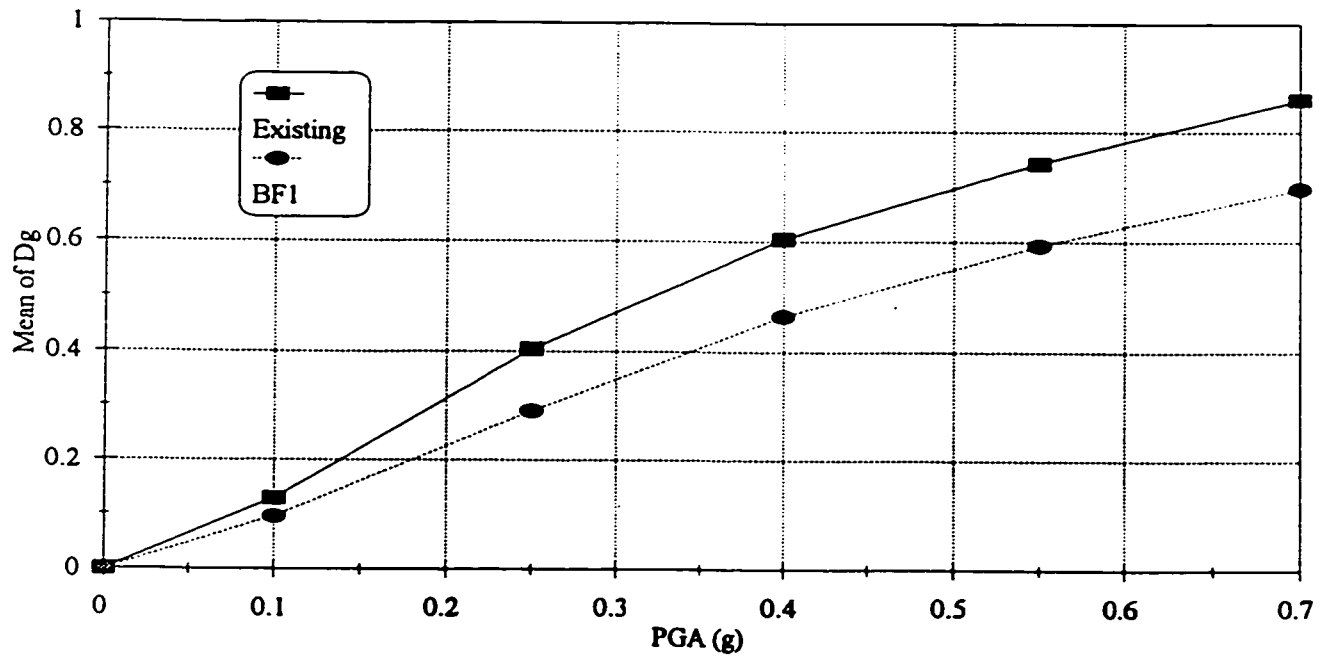
Figure 7.23 Relationship between the PGA level and the mean of the damage index D_g

Pullout of bottom beam reinforcement   o   Yielding of top beam reinforcement
Column splice failure   •   Column reinforcement yielding
Brace buckling

(a) RC frame

(b) Steel frame

Figure 7.24 Hinge type and location of the rehabilitation case
BF1 due to the Long Beach earthquake (PGA= 0.2g)

Figure 7.25 Hinge type and location of the rehabilitation case
BF1 due to the Mexico earthquake (PGA= 0.55g)
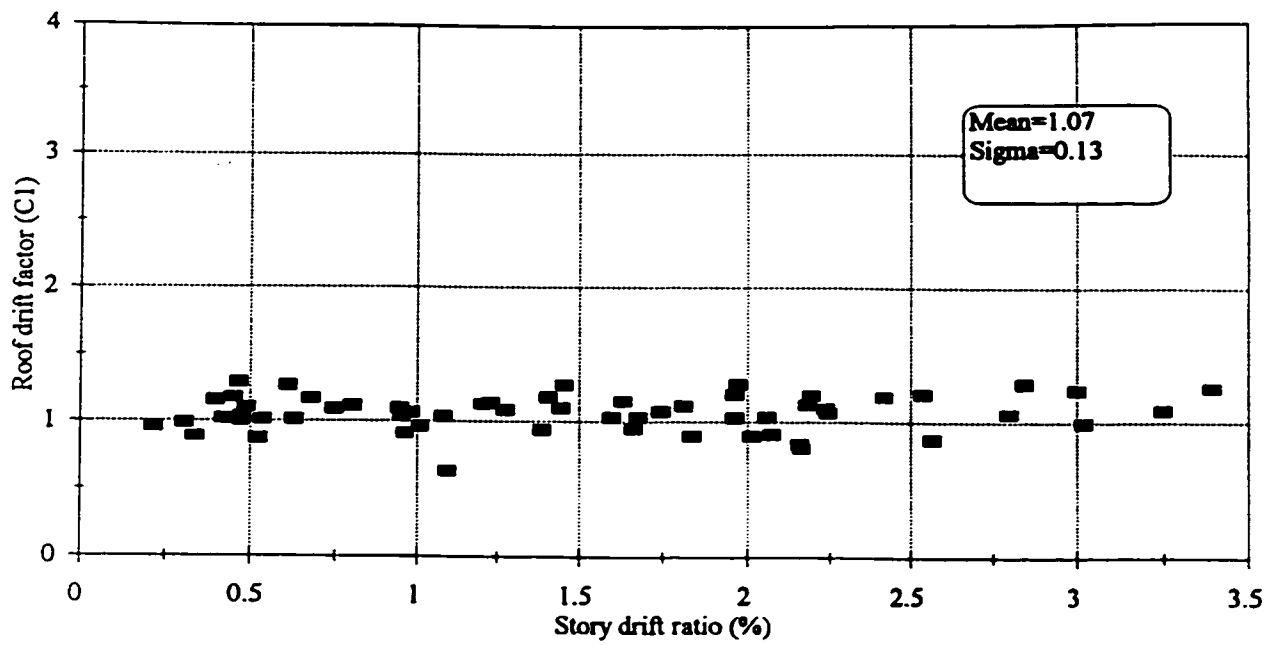
Figure 7.26 Relationship between the story drift ratio and the response factor C_1
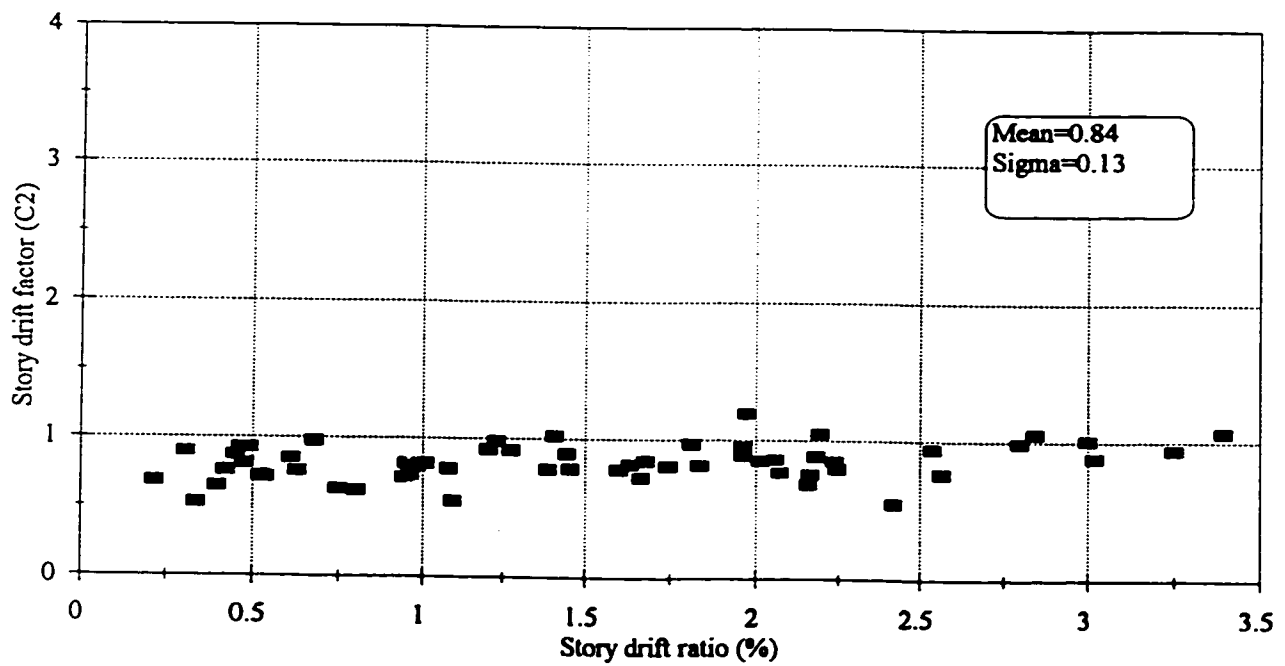
Figure 7.27 Relationship between the story drift ratio and the response factor C_2
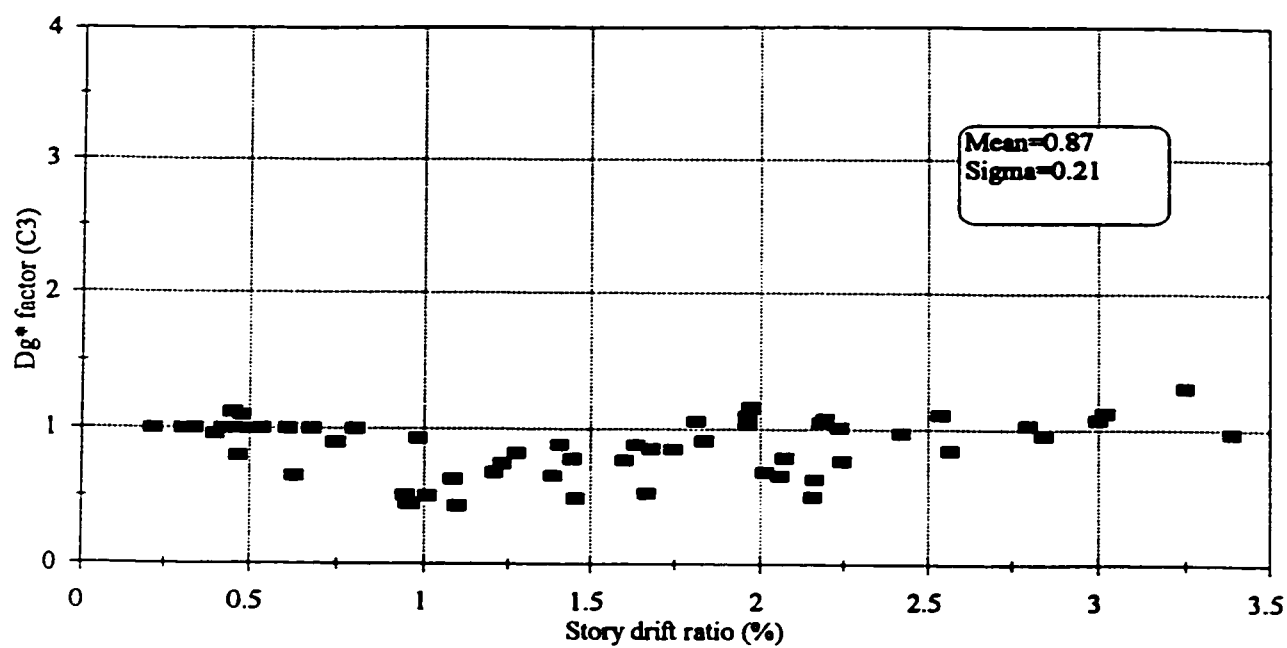
Figure 7.28 Relationship between the story drift ratio and the response factor C₃
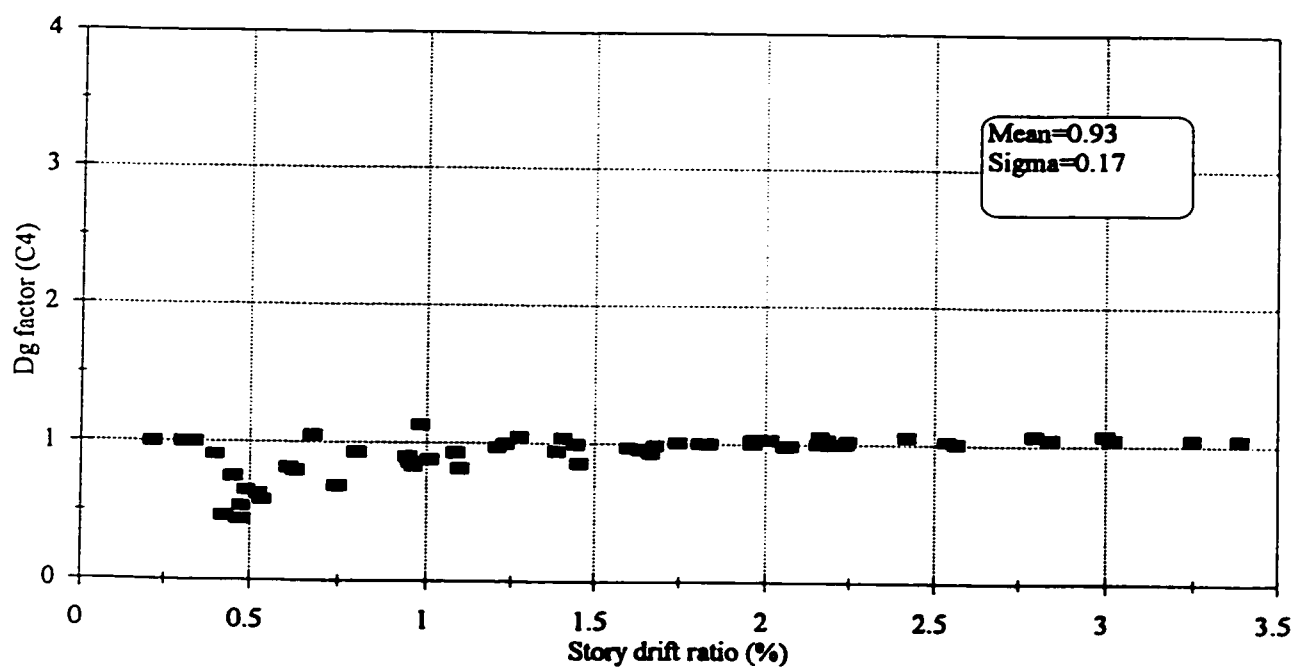
Figure 7.29 Relationship between the story drift ratio and the response factor C4

CHAPTER 8

CONCLUSIONS AND RECOMMENDATIONS FOR FUTURE RESEARCH

8.1 CONCLUSIONS

The conclusions of the current study can be summarized as follows:

1. A beam-column model was developed to represent the seismic response of nonductile structures. The developed model accounted for the strength softening behaviour of nonductile RC members. It also included the effect of the interaction between the axial force and the moment capacity of the RC members. The model was verified using available experimental data. The analytical approach provided a practical and reliable tool to represent the behaviour of nonductile RC buildings beyond its ultimate strength and up to failure. It was found that neglecting the strength softening when modelling nonductile frames leads to significant underestimation of displacements and damage.

2. A new damage evaluation approach was developed for assessing the damage of nonductile RC buildings due to seismic loading. The developed approach provided damage indices for each individual story and for the entire building. The damage indices represented actual measures of stiffness degradation and lateral load carrying capacity deterioration of the nonductile RC buildings. These damage indices

eliminated the need for an averaging or weighting procedure to integrate the damage of the building elements.

3. A parameter v was proposed for evaluating the plastic mechanisms of RC buildings under the effect of lateral loading. The proposed parameter, which varied from 0.0 to 1.0, represented the uniformity of the story drift distribution along the building height. The lower the value of v the more desirable was the developed plastic mechanism of the building.

4. The inelastic dynamic analysis of rehabilitated nonductile low-rise buildings with concentric steel bracing revealed that significant improvement in the response was due to the addition of the bracing members. This improvement was even more enhanced with increasing the amount of bracing regardless of the associated increase of the building stiffness.

5. Several distributions of steel bracing over the building height were examined. Adding uniformly distributed steel bracing did not provide the optimum solution. Buildings with steel bracing distributed over the building height to obtain the smallest value of v exhibited a significant improvement in the seismic performance. Brace distribution along the frame bays affected the response of the rehabilitated building. A brace distribution that avoided concentrating the brace members in one bay reduced the building damage and deformation. The use of concentric steel bracing as a

rehabilitation technique was found to be unsuitable for the selected nine-story building. This was due to the significant increase in the axial forces in the RC columns. A solution for this problem would require increasing the columns axial strength using steel collectors or by replacing the steel bracing scheme by attached steel frames.

6.   An analytical model for vertical shear links was incorporated into the DRAIN-2DX computer program and used to study the performance of nonductile buildings rehabilitated using eccentric steel bracing. These buildings were found to exhibit better ability to dissipate energy under the effect of static cyclic loading as compared to buildings rehabilitated using concentric bracing. The enhancement in the energy dissipation capacity of eccentric bracing, which was attributed to the stable inelastic behaviour of the vertical shear links, led to a significant improvement in the seismic performance of the rehabilitated building. The main disadvantage of eccentric bracing was in the limitations imposed on the building deformation in order to keep the link deformation angle below the allowable levels. The distribution of eccentric bracing along the height of the building was found to have a significant effect on the characteristics of the developed plastic mechanism under the effect of lateral loading. The use of uniform distribution of vertical links along the height did not provide the optimum scheme. Better seismic performance was achieved using vertical link distribution over the height that provided the smallest value of the parameter v.

7. Rehabilitating the nine-story building using steel frames led to an improvement in the seismic performance of the nonductile building as indicated by lower levels of deformation and damage achieved. A major advantage of using steel frame schemes over steel bracing systems was the avoidance of the increase in the axial forces of the RC columns. The braced steel frames attracted more seismic forces than that of moment resisting steel frames. However better improvement in the seismic performance was achieved as compared to the case where flexible moment resisting steel frames was used.

8. Steel systems were found to be more efficient in the rehabilitation of nonductile low-rise buildings as compared to medium-rise buildings. The maximum reduction in the response parameters of the rehabilitated three-story building was much higher than that of the nine-story building.

9. A simplified approach for evaluating the seismic performance of existing and rehabilitated nonductile buildings using SDOF model was proposed. The simplified approach considered the strength softening behaviour in the hysteretic force-displacement relationship and was used to predict an approximate estimate for the strength based and stiffness based damage indices. Results of the simplified approach slightly overestimated the building response parameters of the three story building. For the nine story building, the simplified approach overestimated the roof drift and underestimated the story drift and the damage indices.

8.2 RECOMMENDATIONS FOR FUTURE RESEARCH

1. The statistical analysis performed in the current study is based on the results of only twelve earthquake records. More records are needed to achieve more representative data and lower standard deviations.

2. The analytical models developed in this thesis can be extended for use in 3D application. This will allow the consideration of building irregularities and the effect of bidirectional ground motions. This can also include the damage evaluation of the structures using the proposed strength based and stiffness based damage indices using pushover analysis for 3D modelled structures.

3. The soil structure interaction effects can be included in the developed models. This will allow better representation of the ground conditions which have been assumed to be rigid throughout the analysis. Soil structure interaction effects can affect the vibrational characteristics of the structures and this need to be addressed.

4. Economical aspects of rehabilitation schemes need to be investigated. The economical considerations should be used in conjunction with the technical data to reach a decision on the most effective and economical method for rehabilitating structures in different regions. The economical study should consider the variation in the cost of material and labour form one region to another.

REFERENCES

Aboutaha, R.S. and Jirsa, J.O., 1996, "Seismic Retrofit of R/C Columns Using Steel Jackets". Seismic Rehabilitation of concrete Structures, SP-160, ACI, pp. 59-72.

ACI Committee 318, 1963, Building Code Requirements for Reinforced Concrete (ACI 318-63) and Commentary, American Concrete Institute, Detroit, MI.

Alsiwat J. M. and Saatcioglu, M., 1992, "Reinforcement Anchorage Slip Under Monotonic Loading". Journal of Structural Engineering, ASCE, Vol. 118, No. 9, pp. 2421-2438.

Anderson, J.C., 1989, "Dynamic Response of Buildings", Chapter 3 in the Seismic Design Handbook, edited by Naeim, F., New York: Van Nostrand Reinhold.

Aycardi, L.E., Mander, J.B. and Reinhorn, A.M., 1992, "Seismic Resistance of RC Frame Structures Designed only for Gravity Loads - Part II - Experimental Performance of Subassemblages ". Technical Report NCEER-92-0028, Department of Civil Engineering, State University of New York at Buffalo, Buffalo, New York.

Badoux, M., 1987, "Seismic Retrofitting of Reinforced Concrete Frame Structures with Steel Bracing Systems". Thesis presented to the University of Texas at Austin, Tex., in Partial Fulfilment of the Requirements for the Degree of Doctor of Philosophy.

Biddah, A., 1997, "Seismic Behaviour of Existing and Rehabilitated Reinforced Concrete Frame Connections". Ph. D. Thesis, Department of Civil Eng., McMaster Univ., Canada.

Biddah, A., Ghobarah, A. and Aziz, T. S., 1997, "Upgrading of Nonductile Reinforced Concrete Frame Connections". Journal of Structural Engineering, ASCE, Vol. 123, No. 8, pp. 1001-1010.

Bouadi, A., Engelhardt, M.D., Jirsa, J.O. and Kreger, M.E, 1994, "Eccentrically Braced Frames for Strengthening of R/C Building with Short Columns". Proceeding of the 5th U.S. National Conference on Earthquake Engineering, Chicago, Illinois, Vol. 3., pp. 617-626.

Bracci, J., Reinhorn, A. and Mander, J., 1992, "Seismic Resistance of Reinforced Concrete Frame Structures Designed only for Gravity Loads - Part III - Experimental Performance and Analytical Study of a Structural Model". Technical Report NCEER-92-0029, Department of Civil Engineering, State University of New York at Buffalo, Buffalo, NY.

Canales, M. D. and Briseno de la Vega, R., 1992, "Retrofitting Techniques Used in Telephone Buildings in Mexico". Proceeding of the 10th World Conference on Earthquake Engineering, Madrid, Spain, Vol. 9, pp. 5143-5147.

Chung, Y., Meyer, C. and Shinozuka, M, 1987, "Seismic Damage Assessment of Reinforced

317

Concrete Members". Report No. NCEER-87-0022, National Center for Earthquake Engineering Research, State University of New York at Buffalo, Buffalo, NY.

Chung, Y.S., Shinozuka, M. and Meyer, C., 1988, "Seismic Analysis of Reinforced Concrete Frames (SARCF)-User Guide". Report No. NCEER-88-0044, Department of Civil Engineering and Mechanics, Columbia University, New York.

Collins, K. R. and Foutch, D. A., 1995 "Investigation of Alternative Seismic Design Procedure for Standard Buildings" Structural Research Series No. 600, Department of Civil Engineering, University of Illinois at Urbana-Champaign, Urbana, Illinois.

CSA-S16.1-94, 1994, "Limit State Design of Steel Structures". Canadian Standards Association, Rexdale, Ont., Canada.

DiPasquale, E. and Cakmak, A., 1987, "Detection and Assessment of Seismic Structural Damage". Report NCEER-87, National Center for Earthquake Engineering Research, State University of New York at Buffalo, Buffalo, N.Y.

EERI, HF-96, 1996, "Senario for a Magnitude 7.0 Earthquake On Hayward Fault". Earthquake Engineering Research Institute, Oakland, California.

Eligehausen, R., Popov, E. P. and Bertero, V. V., 1983, "Local bond Stress-Slip Relationship of a Deformed Bar Under Generalized Excitation.". Report No. 83/23, University of California at Berkeley, Berkeley, CA.

Fehling, E., Pauli, W. and Bouwkamp, J.G., 1992, "Use of vertical Shear Links in Eccentrically Braced Frames". The Tenth World Conference on Earthquake Engineering, Vol. 8, pp. 4475-4480.

Fujimoto, M., Wada, A., Shibata, K. and Kosugi, R., 1973, "Nonlinear Analysis of K-Type Braced Steel Frames". Transactions of the Architectural Institute of Japan, no. 209.

Ghobarah, A., Biddah, A. and Mahgoub, M., 1997, "Seismic Retrofit of RC Columns Using Steel Jackets". European Earthquake Engineering Journal, Vol. 15, pp. 1052-1066.

Ghobarah, A., 1998, "Seismic Assessment of Existing RC Structures". Progress in Structural Engineering and Materials, Vol. 2, No. 1.

Goel, S. C. and Lee, H., 1990, "Seismic Strengthening of RC Structures by Ductile Steel Bracing System". Proceeding of the 4th U.S. National Conference on Earthquake Engineering, Palm Springs, California, Vol. 3., pp. 323-331.

Goel, S. C. and Masri, A.C. 1994, "Seismic Strengthening of RC Slab-Column Frames with Steel Frames". Proceeding of the 5[a] U.S. National Conference on Earthquake Engineering, Chicago, Illinois, Vol. 3., pp. 789-798.

Grigoriu, M., 1987 "Damage Models for Seismic Analysis". Report 87-4, Department of Structural Engineering, Cornell University, Ithaca, NY.

Han, S.W. and Wen, Y.K., 1997, "Method of Reliability-Based Seismic Design". Journal of Structural Engineering, ASCE, Vol. 123, No. 3, pp. 256-270.

Hjelmstad, K. and Popov, E.,1983, "Cyclic Behaviour and Design of Link Beams". Journal of the Structural Division, ASCE, Vol. 109, No. 10, pp. 2387-2403.

Ikeda, K., Mahin, S. and Dermitzakis, S., 1984, "Phenomenological Modeling of Steel Braces Under Cyclic Loading". Report No. EERC 84-9, Earthquake Engineering Research Center, University of California, Berkeley, California.

Jain, A. K. and Goel, S.C., 1978, "Hysteresis Models for Steel Members Subjected to cyclic Buckling". Report No. UMEE 78R6, Department of Civil Engineering, University of Michigan, Ann Arbor, Michigan.

Jain, A. K., Goel, S.C. and Hanson, R.D., 1980, "Hysteretic Cycles of Axially Loaded Members". Journal of the Structural Division, ASCE, Vol. 106, No.ST 8, pp.1777-1795.

Jones, T., 1985, "Seismic Strengthening of a RC Frame Using Structural Steel Bracing". Thesis Presented to the University of Texas at Austin, Tex., in Partial Fulfilment of the Requirements for the Degree of Master of Science.

Kang-Ning Li, 1992, "Nonlinear Earthquake Response of R/C Space Frames with Triaxial Interaction". Proceeding of the 10th World Conference on Earthquake Engineering, Madrid, Spain, Vol. 9, pp. 5143-5147.

Kappos, A.J., 1997, "Seismic Damage Indices for RC Buildings -Evaluation of Concepts and Procedures". Progress in Structural Engineering and Materials, Vol. 1, No. 1, pp.78-87.

Kasai, K. and Popov, E., 1986, "A Study of Seismically Resistant Eccentrically Braced Steel Frame Systems". Report No. UCB/EERC-86/01, Earthquake Engineering Research Center, University of California, Berkeley, CA.

Kawamata, S. and Masaki, Q.,1980, "Strengthening Effect of Eccentric Steel Braces to Existing RC Frames". Proceeding of the 7th world Conference on Earthquake Engineering, Istanbul, Turkey, pp. 513-520

Krawinkler, H., 1987, "Performance Assessment of Steel Components". Earthquake Spectra, Vol. 3, No. 1, pp. 27-41.

Krawinkler, H., 1996, "Pushover Analysis: Why, How, When, and When Not to Use It". Proceedings of the 65 Annual Convention of the Structural Engineers Association of California, Maui, Hawaii, October 1-6, 1996, pp.17-36.

Lee, S. and Goel, S., 1987, "Seismic behaviour of Hollow and Concrete-filled Square Tubular Bracing Members". Report No. UMCE 87-11, University of Michigan, Ann Arbor, Michigan.

Lynn, A. C., Moehle J. P. and Mahin, S. A., 1994, "Evaluation of Existing Reinforced Concrete Building Columns". Earthquake Engineering Research Center (EERC) News, Jan., Vol. 15, No 1.

Maheri, M. R. and Sahebi, A., 1995, "Use of Steel Bracing in RC Frames". Engineering Structures Journal, Vol. 19, No. 12, pp. 1018-1024.

Maison, B.F., 1992, "PC-ANSR: A Computer Program for Nonlinear Structural Analysis". University of California, Berkeley, California.

Martin, S., Williams, I.V. and Sexsmith, R.G., 1997, "Evaluation of Seismic Damage Indices for Concrete Elements Loaded in Combined Shear and Flexure". ACI Structural Journal, Vol. 94, No. 3, pp.315-322.

Michael, D. and Popov, E.P., 1989, "Behaviour of Long Links in Eccentrically Braced Frames". Report No. UCB/EERC-89/01, Earthquake Engineering Research Center, University of California, Berkeley, CA.

Miramontes, D., Merabet, O. and Reynouard, M., 1996, "Beam Global Model For Seismic Analysis of RC Frames". Earthquake Engineering and Structural Dynamics, Vol. 25, pp. 671-688.

Miranda, E., 1991, "Seismic Evaluation and upgrading of Existing Buildings". Thesis Presented to the University of California at Berkeley, in Partial Fulfilment of the Requirements for the Degree of Doctor of Philosophy.

Mitchell, D. and Dandurand, A., 1988, "Repair and Upgrading of Concrete Structures in Mexico city after the 1985 Earthquake ". Canadian Journal of Civil Engineering, Vol. 15, pp. 1052-1066.

Mori, Y. and Ellingwood, B.R., 1993, "Reliability Based Service Life Assessment of Aging Concrete Structures". Journal of Structural Engineering, ASCE, Vol. 119, No. 5, pp. 1600-1621.

Nassar, A. A. and Krawinkler, H., 1991, "Seismic Demands for SDOF and MDOF Systems". Report No. 95, Department of Civil Engineering, Stanford University, Stanford, California.

Nateghi, F., 1994, "Seismic Strengthening of 8-Story Reinforced Concrete Building". Proceeding of the 8ª European Conference on Earthquake Engineering, Vienna, Austria, Vol. 3, pp. 2235-2240.

Nateghi, F. and Shahbazian, B., 1992, "Seismic Evaluation, Upgrading and Retrofitting of Structures: Recent Experiences in Iran". Proceeding of the 10ª World Conference on Earthquake Engineering, Madrid, Spain, Vol. 9, pp. 5137-5141.

NBCC, 1995, "National Building Code of Canada". The National Research Council of Canada, Ottawa, Ontario, Canada.

Newmark, N.M. and Rosenblueth, E., 1971, "Fundamentals of Earthquake Engineering". Prentice hall, Inc. Englewood Cliffs, New Jersey.

Otani, S., 1980,"Nonlinear Dynamic Analysis of Reinforced Concrete Building Structures". Canadian Journal of Civil Engineering, vol. 7, pp. 333-344.

Park, Y.J. and Ang, A., 1985, "Mechanistic Seismic Damage Model for Reinforced Concrete". Journal of Structural Engineering, ASCE, Vol. 111, No. ST4, pp. 722-739.

Park, Y.J., Reinhorn, A. and Kunnath, S., 1987, "IDARC: Inelastic Damage Analysis of Frame Shear-Wall Structures". Technical report NCEER-87-0008, Department of Civil Engineering, State University of New York at Buffalo, Buffalo, NY.

Pessiki, S.P., Conley, C.H., Gergely, P. and White, R.N.,1990, "Seismic Behaviour of Lightly-RC Column and Beam-Column Joint". Technical Report NCEER-90-0014, Department of Structural Engineering, Cornell University, Ithaca, New York.

Pincheira, J.A., 1992, "Seismic Strengthening of Reinforced Concrete Frames using post-tensioned Bracing Systems". Thesis presented to the University of Texas at Austin, Tex., in Partial Fulfilment of the Requirements for the Degree of Doctor of Philosophy.

Pincheira, J. A. and Jirsa, J. O., 1995, "Seismic Response of RC Frames Retrofitting with Steel Braces or Walls ". Journal of Structural Engineering, ASCE, Vol. 121, No.8 , pp. 1225-1235.

Popov, E., Engelhardt, M. and Ricles, J.M., 1989,"Eccentrically Braced Frames: U.S. Practice". Engineering Journal, AISC, Second quarter, pp.66-80.

Popov, E.P. and Malley, J.O., 1983, "Design of Links and Beam-to-Column Connections For Eccentrically Braced Steel Frames". Report No. EERC 83-03, Earthquake Engineering Research Center, University of California, Berkeley, California.

Prakash, V. and Powell, G.H., 1993 "DRAIN-2DX - Version 1.02 - User Guide". Report No. UCB/SEMM-93/ 17, Civil Engineering Dept., University of California at Berkeley, Berkeley, California.

Priestley, M. and Seible, F., 1991, "Seismic Assessment and Retrofit of Bridges". Report No. SSRP -91/3, Dept. of Applied Mechanics and Engineering Sciences, University of California, San Diego, CA.

Priestley, M.J., Verma, R. and Xiao, Y., 1994, "Seismic Strength of Reinforced Concrete Columns". Journal of Structural Engineering, ASCE, Vol.120, No. 8, pp. 2310-2329.

Ramadan, T., 1994, "Extended End-Plate Connections For Link-Column Joints Of Eccentrically Braced Frames". Ph.D. Thesis, McMaster University, Hamilton, ON, Canada.

Ramadan, T. and Ghobarah, A., 1995, "Analytical Model for Shear-Link Behavior". Journal of Structural Engineering, ASCE, Vol.121, No. 11, pp. 1574-1580.

Remennikov, A. and Walpole, W., 1995, "Incremental Model for Predicting the Inelastic Hysteretic Behaviour of Steel Bracing Members". Research Report 95-6, Department of Civil Engineering, University of Canterbury, Christchurch, New Zealand.

Ricles, J.M. and Popov, E.P., 1987, "Dynamic Analysis of Seismically Resistant Eccentrically Braced Frames". Report No. UCB/EERC-87/07, Earthquake Engineering Research Center, University of California, Berkeley, CA.

Riddell, R., 1979, "Statistical Analysis of the Response of Nonlinear Systems Subjected to Earthquake". Thesis presented to the University of Illinois, in Partial Fulfilment of the Requirements for the Degree of Doctor of Philosophy.

Robins P. J. and Standish, I. G., 1984, "Influence of Lateral Pressure Upon Anchorage". Magazine of Concrete Research, Vol. 36, No. 129, pp. 195-202.

Roeder, C.W. and Popov, E.P., 1977, "Inelastic Behavior of Eccentrically Braced Frames Under Cyclic Loading". Report No. EERC 77-18, Earthquake Engineering Research Center, University of California, Berkeley, California.

Roufaiel, M.S.L. and Meyer, C., 1987 "Analytical Modeling of Hysteretic Behaviour of R/C Frames". Journal of Structural Engineering, ASCE, Vol. 113, No. 3, pp. 429-444.

Su, Y., Hanson, R.D., 1990, "Comparison of Effective Supplemental Damping Equivalent Viscous and Hysteretic". Proceeding of the 4th U.S. National Conference on Earthquake Engineering, Palm Spring, California, Vol. 3., pp. 507-516.

Sugano, S., 1989, "Study of the Seismic Behaviour of Retrofitted RC Buildings". Seismic Engineering, Research and Practice, Proceedings of the sessions related to Seismic engineering at structures Congress, American Society of Civil Engineering, pp. 517-526.

Takeda,T., Sozen, M. and Nielsen, N., 1970, "Reinforced Concrete Response to Simulated Earthquakes". Journal of the Structural Division, ASCE, Vol. 96, No. ST12, pp. 2557-2573.

Trifunac, M.D. and Brady, A. G., 1975, "A Study on the Duration of Strong Earthquake Ground Motion". Bulletin of the Seismological Society of America, Vol. 65, No. 3, pp. 581-626.

Valles, R.E., Reinhorn, A.M., Kunnath, S.K., Li, C. and Madan, A., 1996, "IDARC2D Ver. 4.0: A Computer Program for the Inelastic Analysis of Buildings". Report No. NCEER-96-0010, State University of New York at Buffalo, New York.

Yamamoto, Y. and Aoyama, H.,1987, "Seismic Behaviour of Existing RC Frame Strengthened with Retrofitting Steel Elements". Proceeding of the Seminar on Repair and Retrofit of Structures, Workshop on Repair and Retrofit of Existing Structures, U.S. Japan Panel on Wind and Seismic Effects, UJNR, Tsukuba, Ibaraki, Japan.

Yamamoto, Y. and Umemura, H., 1992, "Analysis of Reinforced Concrete Frames Retrofitted with Steel Braces". Proceeding of the 10th World Conference on Earthquake Engineering, Madrid, Spain, Vol. 9, pp. 5187-5192.